



UNIVERSIDAD DE MURCIA
ESCUELA INTERNACIONAL DE DOCTORADO
TESIS DOCTORAL

Assessment of Materials for the Support of In Vitro Fertilization

Evaluación de Materiales para el Apoyo de la Fecundación In Vitro

D. RAMSES BELDA PEREZ
2024



UNIVERSIDAD DE MURCIA
ESCUELA INTERNACIONAL DE DOCTORADO
TESIS DOCTORAL

Assessment of Materials for the Support of In Vitro Fertilization

Evaluación de Materiales para el Apoyo de la Fecundación In Vitro

Autor: D. Ramses Belda Perez

Director/es: D. Nicola Bernabò

Dña. María Pilar Coy Fuster



**DECLARACIÓN DE AUTORÍA Y ORIGINALIDAD
DE LA TESIS PRESENTADA PARA OBTENER EL TÍTULO DE DOCTOR**

Aprobado por la Comisión General de Doctorado el 19-10-2022

D./Dña. Ramses Belda Perez

doctorando del Programa de Doctorado en

Biología y tecnología de la salud reproductiva

de la Escuela Internacional de Doctorado de la Universidad Murcia, como autor/a de la tesis presentada para la obtención del título de Doctor y titulada:

Assesment of Material for the Support of In vitro Fertilization

y dirigida por,

D./Dña. Nicola Bernabò

D./Dña. Maria Pilar Coy Fuster

D./Dña.

DECLARO QUE:

La tesis es una obra original que no infringe los derechos de propiedad intelectual ni los derechos de propiedad industrial u otros, de acuerdo con el ordenamiento jurídico vigente, en particular, la Ley de Propiedad Intelectual (R.D. legislativo 1/1996, de 12 de abril, por el que se aprueba el texto refundido de la Ley de Propiedad Intelectual, modificado por la Ley 2/2019, de 1 de marzo, regularizando, aclarando y armonizando las disposiciones legales vigentes sobre la materia), en particular, las disposiciones referidas al derecho de cita, cuando se han utilizado sus resultados o publicaciones.

Si la tesis hubiera sido autorizada como tesis por compendio de publicaciones o incluyese 1 o 2 publicaciones (como prevé el artículo 29.8 del reglamento), declarar que cuenta con:

- La aceptación por escrito de los coautores de las publicaciones de que el doctorando las presente como parte de la tesis.*
- En su caso, la renuncia por escrito de los coautores no doctores de dichos trabajos a presentarlos como parte de otras tesis doctorales en la Universidad de Murcia o en cualquier otra universidad.*

Del mismo modo, asumo ante la Universidad cualquier responsabilidad que pudiera derivarse de la autoría o falta de originalidad del contenido de la tesis presentada, en caso de plagio, de conformidad con el ordenamiento jurídico vigente.

En Murcia, a 04 de Marzo de 2024

Fdo.:

BELDA PEREZ
RAMSES -
48619228B

Firmado digitalmente por
BELDA PEREZ RAMSES -
48619228B
Fecha: 2024.03.04 10:23:09
+01'00'

Esta DECLARACIÓN DE AUTORÍA Y ORIGINALIDAD debe ser insertada en la primera página de la tesis presentada para la obtención del título de Doctor.

Información básica sobre protección de sus datos personales aportados	
Responsable:	Universidad de Murcia. Avenida teniente Flomesta, 5. Edificio de la Convalecencia. 30003; Murcia. Delegado de Protección de Datos: dpd@um.es
Legitimación:	La Universidad de Murcia se encuentra legitimada para el tratamiento de sus datos por ser necesario para el cumplimiento de una obligación legal aplicable al responsable del tratamiento. art. 6.1.c) del Reglamento General de Protección de Datos
Finalidad:	Gestionar su declaración de autoría y originalidad
Destinatarios:	No se prevén comunicaciones de datos
Derechos:	Los interesados pueden ejercer sus derechos de acceso, rectificación, cancelación, oposición, limitación del tratamiento, olvido y portabilidad a través del procedimiento establecido a tal efecto en el Registro Electrónico o mediante la presentación de la correspondiente solicitud en las Oficinas de Asistencia en Materia de Registro de la Universidad de Murcia



UNIVERSIDAD DE
MURCIA

D. Nicola Bernabò, Profesor Titular de Universidad del Área de Anatomía Veterinaria en el Departamento de Bioscience dell'Università degli Studi di Teramo, AUTORIZA:

La presentación de la Tesis Doctoral titulada "Assessment of Materials for the Support of In Vitro Fertilization", realizada por D. Ramsés Belda Pérez, bajo mi inmediata dirección y supervisión, y que presenta para la obtención del grado de Doctor por la Universidad de Murcia.

En Murcia, a de de



Nicola Bernabò
09.02.2024
09:44:39
GMT+01:00



UNIVERSIDAD DE
MURCIA

D. Maria Pilar Coy Fuster, Catedrática de Universidad del Área de Fisiología en el Departamento de Fisiología, AUTORIZA:

La presentación de la Tesis Doctoral titulada "Assessment of Materials for the Support of In Vitro Fertilization", realizada por D. Ramsés Belda Pérez, bajo mi inmediata dirección y supervisión, y que presenta para la obtención del grado de Doctor por la Universidad de Murcia.

En Murcia, a 16 de febrero de 2024

COY FUSTER
MARIA PILAR
- 27449572S

Firmado
digitalmente por
COY FUSTER MARIA
PILAR - 27449572S
Fecha: 2024.02.16
09:59:13 +01'00'



UNIVERSITÀ
DEGLI STUDI
DI TERAMO



UNIVERSIDAD
DE MURCIA

RESEARCH DOCTORATE IN

“CELLULAR AND MOLECULAR BIOTECHNOLOGIES”

DEPARTMENT OF BIOSCIENCES AND AGRO-FOOD AND ENVIRONMENTAL TECHNOLOGIES

CYCLE XXXVI

Assessment of Materials for the Support of *In Vitro* Fertilization

Academic Discipline VET/02

Coordinator:

Professor Valentina Russo

Ph.D. Candidate:

Ramsés Belda Pérez

Tutors:

Professor Nicola Bernabò

Professor Maria Pilar Coy Fuster

Index

RESUMEN	1
SUMMARY	9
INTRODUCTION	
1. Use and problem of the assisted reproductive techniques	16
2. Spermatozoa: a long way until fertilization	19
3. Mimicking the oviduct	23
4. References	30
OBJECTIVES	52
CHAPTER 1. Assessing the Suitability of 3D Printing Materials in the context of <i>In Vitro</i> Fertilization	
Manuscript 1	53
1. Introduction	54
2. Materials and methods	58
2.1. Experimental design	58
2.2. Culture media reagents	60
2.3. 3D Printing materials	60
2.4. Material sterilization	60
2.5. <i>In vitro</i> maturation	60
2.6. <i>In vitro</i> fertilization	62
2.7. Embryo culture	63
2.8. Differential apoptotic staining	63
2.9. Statistical analysis	64
3. Results	65
3.1. Effects of the different materials on cleavage	65
3.2. Effects of the different materials on blastocyst rate at day 7	66
3.3. Effects of the different materials on blastocyst rate at day 8	67
3.4. Principal component analysis of the different materials considering all variables studied	68
4. Discussion	70
5. References	74
CHAPTER 2. Non-physiological materials to support IVF	
Manuscript 2	87
1. Introduction	88
2. Results and discussion	90
2.1. Preparation and characterization of water-phase exfoliated MoS ₂ /CT nanoflakes	90
2.2. MoS ₂ /CT and CT supplementation does not affect the acrosome integrity	93

2.3.	MoS ₂ /CT and CT supplementation does not modify the intracellular calcium concentration, membrane fluidity and mitochondrial activity	94
2.4.	MoS ₂ /CT and CT supplementation does not influence sperm pKa activity and tyrosine phosphorylation patterns	98
2.5.	CT supplementation improves the IVF outcomes.....	100
3.	Materials and Methods	103
3.1.	Chemicals	103
3.2.	MoS ₂ sonochemical exfoliation in water assisted by catechin.....	103
3.3.	Experimental groups.....	104
3.4.	Spermatozoa preparation and incubation	105
3.5.	Monitoring of MoS ₂ /CT toxicity on acrosome integrity.....	106
3.6.	Flow cytometry analysis of intracellular calcium concentration, membrane fluidity and mitochondrial activity.....	106
3.7.	Evaluation of sperm PKA activity and tyrosine phosphorylation pattern (pTyr) by western blot	108
3.8.	<i>In vitro</i> fertilization assay.....	109
3.9.	Statistical analysis	110
4.	Conclusions	111
5.	References	112

CHAPTER 3. Delving into oviduct architecture

Manuscript 3	122
1. Introduction	123
2. Materials and methods	125
2.1. Oviduct selection and collection	125
2.2. MicroCT and image acquisition	126
2.3. Image analysis.....	126
2.4. Two-dimensional image processing	127
2.5. Processing of the three-dimensional model	127
2.6. Calculation of the shape-factor	129
3. Results	130
3.1. Utero-tubal junction	130
3.2. Ampullary-isthmic junction.....	135
3.3. 3-D reconstruction.....	139
4. Discussion	139
5. References	146
CONCLUSIONS	153
SUPPLEMENTARY MATERIALS.....	154

The background of the slide features a series of elegant, flowing, and overlapping lines in various shades of blue and white. These lines create a sense of movement and depth, resembling smoke or liquid in motion. The colors transition from deep blue to light blue and finally to white, giving the design a clean and modern feel.

Resumen

Resumen

Las técnicas de reproducción asistida (TRA) han transformado radicalmente la manera en que abordamos la infertilidad desde el nacimiento de la primera "bebé probeta", Luis Brown, en 1978. La infertilidad afecta a un porcentaje significativo (15-20%) de parejas en edad reproductiva, lo que ha contribuido al constante aumento de la demanda de TRA en el mercado a lo largo de los años.

Si bien en humanos estas técnicas se utilizan principalmente para tratar problemas reproductivos, en el ámbito animal ofrecen aplicaciones valiosas en campos como la edición genética, la selección de reproductores y la creación de modelos animales para su uso en biomedicina. Además, presentan ventajas significativas en la producción animal al reducir costos y disminuir el riesgo de enfermedades, lo que impulsa su adopción en diversas especies animales de manera creciente cada año.

A pesar de las mejoras continuas experimentadas por las TRA desde su creación, siguen existiendo desafíos significativos, ya que no todos los ovocitos logran desarrollarse hasta el estadio de blastocisto *in vitro* y los pocos que lo consiguen no exhiben la misma calidad que sus contrapartes producidas de forma natural *in vivo*. Estas disparidades se atribuyen, entre otras causas, a problemas en la reprogramación epigenética del embrión, un proceso crítico que ocurre en las primeras etapas celulares y puede ser influenciado por diversos factores ambientales.

Entre estos factores, las condiciones no fisiológicas del laboratorio han demostrado tener un impacto significativo en la reprogramación epigenética del embrión, generando consecuencias que, en algunas especies como la porcina, no son subsanadas durante el proceso de crecimiento. Se ha observado que, al replicar los parámetros fisiológicos, como la temperatura y la concentración de oxígeno en los medios de cultivo

en el laboratorio, se logra una mejora notable en el sistema de producción *in vitro* de embriones (PIV). Incluso se ha logrado optimizar el sistema de PIV porcino al agregar fluidos reproductivos como suplemento a los medios de cultivo, lo que ha conducido a una disminución de las diferencias entre embriones *in vitro-in vivo* y a una mejora significativa en el proceso.

En la naturaleza, la fecundación tiene lugar en el oviducto, un órgano tubular que conecta los ovarios con el útero. En ciertas especies, se atribuyen funciones clave al oviducto en la selección y capacitación espermática. Se postula que, en este órgano, tienen lugar procesos de quimiotaxis, reotaxis y quimiotaxis que guían a los espermatozoides hacia el ovocito.

Aunque históricamente se han subestimado las funciones de este órgano, ya que es posible lograr el embarazo sin exponer a los embriones o gametos a este ambiente, recientemente ha surgido un interés creciente en los roles que desempeña. Además de las funciones mencionadas anteriormente, cabe destacar que las células epiteliales del oviducto también crean un entorno propicio para las primeras divisiones embrionarias, que favorece una correcta reprogramación epigenética y un adecuado desarrollo.

A pesar de ello, los estudios *in vitro* de este órgano han empleado tradicionalmente cultivos en monocapa (2D), los cuales en ocasiones no logran replicar de manera precisa la realidad, debido a la disparidad entre el ambiente *in vitro* y el ambiente fisiológico.

Para abordar esta limitación, en los últimos años se ha producido un incremento notable en la cantidad de investigaciones que emplean cultivos 3D en "scaffolds", los cuales permiten a las células mantener un estado funcional y de diferenciación durante más tiempo. Por otro lado, se ha producido un gran desarrollo en el campo de la microfluídica, que permite el control y manipulación de fluidos permitiendo imitar *in*

vitro las dinámicas *in vivo*. Estos scaffolds, combinados con sistemas de microfluidos, posibilitan la creación de los llamados "organ-on-a-chip". Estos dispositivos representan de manera más precisa el entorno fisiológico, demostrando ser herramientas valiosas en la mejora del sistema de PIV. Además, la aplicación de estos dispositivos en la PIV favorece una reprogramación epigenética en los embriones más semejante a la que ocurre en embriones producidos de forma natural *in vivo*.

En este contexto, resulta igualmente interesante considerar la funcionalización de los scaffolds, ya que posibilita su personalización, influyendo en su bioactividad, biocompatibilidad y propiedades mecánicas, incluso cuando los materiales utilizados no son fisiológicos. Algunos de estos materiales, como el óxido de grafeno, han demostrado incluso potenciar el rendimiento en la fecundación *in vitro* (FIV) en varias especies, como la porcina, bovina o murina. La investigación emprendida en esta tesis doctoral se centra específicamente en la identificación de nuevos materiales y en el desarrollo de procedimientos para la creación de dispositivos 3D que contribuyan a perfeccionar el sistema de producción *in vitro*. A la luz de estas razones, aún hay margen suficiente para mejorar las TRA. Identificando nuevos materiales y procedimientos para construir estos dispositivos, la eficiencia del proceso podría mejorar significativamente en la calidad y cantidad de los embriones producidos. Por ello, la presente tesis doctoral tiene la intención de contribuir a estos objetivos.

En el primer capítulo, nuestro objetivo fue evaluar la idoneidad de diferentes procesos de impresión 3D en combinación con un conjunto correspondiente de biomateriales disponibles comercialmente. Para la impresión por extrusión, empleamos ácido poliláctico (PLA) y policaprolactona (PCL), mientras que para la impresión por estereolitografía utilizamos diacrilato de polietilenglicol (PEGDA) en variantes de rigidez (PEGDA500, PEGDA200, PEGDA PhotoInk).

Con el fin de examinar los posibles efectos adversos que estos materiales pudieran tener sobre los embriones cuando están presentes durante la fecundación, llevamos a cabo un "embryo assay", un ensayo aprobado por la "Food and Drug Administration" (FDA) en el modelo murino para evaluar la calidad de productos destinados a FIV. Optamos por utilizar el ganado bovino como modelo animal, aprovechando las ventajas que presenta sobre otros modelos animales como el murino o el pez cebra.

En este estudio, implementamos el sistema convencional de PIV, empleando complejos cúmulo-ovocitos (COCs) recuperados de ovarios de vacas destinadas a matadero. Tras la aspiración y selección, los COCs se sometieron a maduración *in vitro* durante 22 horas. Realizamos ensayos específicos para cada material, dividiendo los embriones en tres grupos: grupo control, grupo "rinse" y grupo "scaffold", definidos según las condiciones de FIV.

En el grupo control, la FIV se realizó utilizando medio fresco, mientras que en el grupo rinse, el medio empleado para la FIV estuvo en contacto con los diferentes materiales durante 24h antes de su uso, con el objetivo de comprobar la posible liberación por parte del material de residuos tóxicos. Finalmente, en el grupo "scaffold", la FIV se realizó en presencia del scaffold. Cada material tuvo su propio grupo "rinse" y grupo "scaffold", compartiendo el grupo control. Utilizamos semen congelado seleccionado por gradientes de densidad para la fecundación.

El cultivo embrionario se llevó a cabo bajo las mismas condiciones para todos los grupos, y solo se consideraron los replicados en los cuales el control mostró una tasa de blastocistos entre el 20% y el 40%, considerada normal en la PIV bovina. Medimos parámetros de división y tasas de blastocistos a los días 7 y 8. Además, fijamos y teñimos los embriones obtenidos utilizando una doble tinción diferencial, midiendo varios

parámetros de calidad embrionaria, como el número de células, la proporción entre trofotodermo y masa celular interna, y la proporción de células apoptóticas.

Observamos un impacto negativo en las tasas de división y blastocistos cuando la FIV se realizó en medios expuestos a la mayoría de los materiales de estereolitografía (PEGDA200, PEGDA500). Este efecto adverso podría estar relacionado posiblemente con compuestos filtrados utilizados para imprimir y estabilizar los scaffolds, aunque este fenómeno no fue tan evidente con PEGDA PhotoInk y solamente la presencia del material PEGDA500 tuvo efectos perjudiciales. Por otro lado, todos los materiales impresos mediante extrusión (PLA y PCL) no generaron ningún efecto adverso en las tasas de división o blastocistos.

El análisis de componentes principales (ACP) revela que los embriones generados en presencia de scaffolds impresos mediante extrusión muestran la mayor similitud con los embriones control al considerar todos los parámetros analizados, incluyendo tasas de división, tasas de blastocisto, número de células, la proporción entre trofotodermo y masa celular interna, así como la proporción de células apoptóticas. No obstante, a pesar de que los embriones producidos en presencia de PLA, o en el medio condicionado por este, no presentaron diferencias significativas en ninguno de los parámetros analizados, el ACP reveló un grado mayor de disparidad en comparación con el grupo control en comparación con la PCL. Por consiguiente, nuestros resultados sugieren que la PCL podría ser la elección óptima para la construcción de nuevos dispositivos de FIV.

En el segundo capítulo, investigamos los impactos de un material no fisiológico, el sulfuro de molibdeno MoS_2 , en el proceso de FIV y en la capacitación espermática. Este compuesto ha sido previamente empleado en la funcionalización de scaffolds,

mejorando sus propiedades y promoviendo el crecimiento celular, al igual que el óxido de grafeno, que ha demostrado incrementar la eficiencia de la FIV en diversas especies.

Aunque el MoS₂ no ha mostrado efectos adversos en otros tipos celulares, su impacto en los gametos, especialmente los espermatozoides, y si podría replicar los beneficios observados con el óxido de grafeno, son desconocidos. En este estudio, para solubilizar el MoS₂, lo conjugamos con catequina, un antioxidante. Evaluamos diversas concentraciones de estos compuestos y conjugados para determinar la óptima. Se emplearon dosis seminales de verraco, centrifugando el semen para eliminar el diluyente, y resuspendiendo los espermatozoides en un medio capacitante suplementado con los compuestos mencionados. Monitorizamos la integridad del acrosoma para detectar posibles efectos tóxicos en los espermatozoides y analizamos indicadores de la capacitación (concentración de calcio intracelular, fluidez de membrana y actividad mitocondrial) mediante citometría de flujo y western blot (fosforilación de proteínas). Finalmente, evaluamos funcionalmente los espermatozoides mediante FIV, utilizando COCs porcinos madurados *in vitro* obtenidos de ovarios de matadero, como en el estudio anterior.

Los resultados indican que el MoS₂ conjugado con catequina (MoS₂/CT) no afectó la integridad del acrosoma. La citometría de flujo no reveló diferencias en la concentración de calcio intracelular, desorden de membrana ni actividad mitocondrial. El western blot tampoco mostró variaciones en la fosforilación de proteínas. Sin embargo, observamos una mayor tasa de penetración y polispermia en la FIV cuando se utilizó solo la catequina, no el complejo MoS₂/CT. Estos hallazgos sugieren que la catequina podría haber tenido un efecto antioxidante, protegiendo a los espermatozoides de especies reactivas de oxígeno y prolongando su viabilidad. Además, notamos que el MoS₂ no tuvo efectos adversos en estos gametos ni en el proceso de capacitación.

En el tercer capítulo de esta tesis, se abordó el estudio de la estructura del oviducto, reconociendo la importancia de comprender la anatomía y morfología de este órgano para imitar y entender su ambiente fisiológico. Tradicionalmente, los estudios de este órgano se han llevado a cabo mediante técnicas de microscopía, que, aunque útiles, pueden presentar limitaciones al permitir el análisis de áreas reducidas y propensas a errores derivados de artefactos durante la reconstrucción.

En la última fase de esta investigación, se procedió a la reconstrucción de secciones de oviducto mediante técnicas de microtomografía computarizada (MicroTC). Esta técnica no destructiva posibilita la obtención de modelos 3D de manera precisa. Se seleccionaron oviductos de tractos genitales obtenidos de matadero y se clasificaron según las diferentes fases del ciclo estral basándonos en la morfología del ovario. Los oviductos se fijaron en paraformaldehído, se incluyeron en bloques de parafina y luego se obtuvieron imágenes mediante MicroTC.

A partir de estas imágenes, se realizaron mediciones detalladas de los pliegues del oviducto, así como análisis de dimensión fractal y lacunaridad. Además, se llevaron a cabo reconstrucciones tridimensionales del oviducto. Hasta la fecha, los scaffolds diseñados para simular el ambiente del oviducto no han tenido en cuenta su compleja arquitectura. Los modelos 3D generados a partir de estas imágenes pueden convertirse en archivos compatibles con la impresión 3D, permitiendo la creación de réplicas exactas. Estas réplicas no solo serían útiles para la creación de dispositivos para la PIV, sino que también podrían emplearse para estudios biofísicos y biomecánicos, aspectos estrechamente vinculados con las funciones desempeñadas por el oviducto.

En resumen, este trabajo establece los cimientos para el desarrollo de un nuevo dispositivo de FIV que imite de manera más precisa la compleja arquitectura del oviducto, abriendo oportunidades para investigaciones más avanzadas en reproducción asistida.

The background of the slide features a series of elegant, flowing, and overlapping lines in various shades of blue and white. These lines create a sense of movement and depth, resembling smoke or liquid in motion. The colors transition from deep blue to light blue and finally to white, giving the design a clean and modern feel.

Summary

Summary

Assisted Reproductive Techniques (ART) have radically transformed the way we approach infertility since the birth of the first "test-tube baby," Louise Brown, in 1978. Infertility affects a significant percentage (15-20%) of couples of reproductive age, which has contributed to the constant increase in demand for ART in the market over the years.

While in humans these techniques are primarily used to treat reproductive problems, in the animal realm, they offer valuable applications in fields such as genetic editing, reproductive selection, and the creation of animal models for use in biomedicine. Additionally, they present significant advantages in animal production by reducing costs and decreasing the risk of diseases, driving their adoption in various animal species increasingly each year.

Despite the continuous improvements experienced by ART since their inception, significant challenges still exist, as not all oocytes manage to develop into the blastocyst stage *in vitro*, and the few that do achieve it do not exhibit the same quality as their counterparts produced naturally *in vivo*. These disparities are attributed, among other causes, to problems in the epigenetic reprogramming of the embryo, a critical process that occurs in the early cellular stages and can be influenced by various environmental factors.

Among these factors, the non-physiological conditions of the laboratory have been shown to have a significant impact on the epigenetic reprogramming of the embryo, generating consequences that, in some species such as pigs, are not remedied during the growth process. It has been observed that by replicating physiological parameters, such as temperature and oxygen concentration in culture media in the laboratory, a notable improvement is achieved in the *in vitro* embryo production (IVP) system. It has even been possible to optimize the porcine IVP system by adding reproductive fluids as supplements

to the culture media, leading to a decrease in the differences between in vitro and in vivo embryos and a significant improvement in the process.

In nature, fertilization takes place in the oviduct, a tubular organ that connects the ovaries to the uterus. In certain species, key functions are attributed to the oviduct in sperm selection and capacitation. It is postulated that in this organ, processes such as chemotaxis, rheotaxis, and thermotaxis take place, guiding the sperm towards the oocyte.

Although historically the functions of this organ have been underestimated, as it is possible to achieve pregnancy without exposing embryos or gametes to this environment, there has recently been a growing interest in the roles it plays. In addition to the functions mentioned above, it is worth noting that the epithelial cells of the oviduct also create a conducive environment for early embryonic divisions, favoring proper epigenetic reprogramming and adequate development.

Nevertheless, in vitro studies of this organ have traditionally employed monolayer cultures (2D), which sometimes fail to accurately replicate reality due to the disparity between the in vitro and physiological environments. To address this limitation, in recent years there has been a notable increase in the amount of research employing 3D cultures on scaffolds, which allow cells to maintain a functional and differentiated state for longer periods. Additionally, significant progress has been made in the field of microfluidics, which allows for the control and manipulation of fluids, enabling the in vitro imitation of in vivo dynamics. These scaffolds, combined with microfluidic systems, enable the creation of so-called "organ-on-a-chip" devices. These devices more accurately represent the physiological environment, proving to be valuable tools in improving the IVP system. Furthermore, the application of these devices in IVP favors epigenetic reprogramming in embryos more similar to that which occurs in embryos produced naturally in vivo.

In this context, it is equally interesting to consider the functionalization of scaffolds, as it allows for their customization, influencing their bioactivity, biocompatibility, and mechanical properties, even when non-physiological materials are used. Some of these materials, such as graphene oxide, have even been shown to enhance *in vitro* fertilization (IVF) performance in various species, such as pigs, cattle, or mice. The research undertaken in this doctoral thesis specifically focuses on the identification of new materials and the development of procedures for creating 3D devices that contribute to perfecting the *in vitro* production system. In light of these reasons, there is still sufficient room for improving ART. By identifying new materials and procedures to build these devices, the efficiency of the process could be significantly improved in the quality and quantity of embryos produced. Therefore, this doctoral thesis aims to contribute to these objectives.

In the first chapter, our aim was to evaluate the suitability of different 3D printing processes in combination with a corresponding set of commercially available biomaterials. For extrusion printing, we used polylactic acid (PLA) and polycaprolactone (PCL), while for stereolithography printing, we used polyethylene glycol diacrylate (PEGDA) in stiffness variants (PEGDA500, PEGDA200, PEGDA PhotoInk).

In order to examine the potential adverse effects these materials might have on embryos when present during fertilization, we conducted an embryo assay, an assay approved by the Food and Drug Administration (FDA) in the murine model to evaluate the quality of products intended for IVF. We chose to use bovine cattle as an animal model, taking advantage of its benefits over other animal models such as murine or zebrafish.

In this study, we implemented the conventional IVP system, using cumulus-oocyte complexes (COCs) recovered from slaughterhouse cow ovaries. After aspiration and selection, COCs were subjected to in vitro maturation for 22 hours. Specific assays were performed for each material, dividing the embryos into three groups: control group, rinse group, and scaffold group, defined according to IVF conditions.

In the control group, IVF was performed using fresh medium, while in the rinse group, the medium used for IVF was in contact with the different materials for 24 hours before use, with the aim of checking for possible release of toxic residues by the material. Finally, in the scaffold group, IVF was performed in the presence of the scaffold. Each material had its own rinse group and scaffold group, sharing the control group. We used frozen semen selected by density gradients for fertilization.

Embryonic culture was carried out under the same conditions for all groups, and only replicates in which the control showed a blastocyst rate between 20% and 40%, considered normal in bovine IVP, were considered. We measured division parameters and blastocyst rates on days 7 and 8. Additionally, we fixed and stained the embryos obtained using a double differential staining, measuring various parameters of embryonic quality, such as the number of cells, the ratio between trophectoderm and inner cell mass, and the proportion of apoptotic cells.

We observed a negative impact on division and blastocyst rates when IVF was performed in media exposed to most stereolithography materials (PEGDA200, PEGDA500). This adverse effect could possibly be related to filtered compounds used to print and stabilize the scaffolds, although this phenomenon was not as evident with PEGDA PhotoInk and only the presence of the PEGDA500 material had detrimental

effects. On the other hand, all materials printed by extrusion (PLA and PCL) did not generate any adverse effects on division or blastocyst rates.

Principal component analysis (PCA) reveals that embryos generated in the presence of extrusion-printed scaffolds show the greatest similarity to control embryos when considering all analyzed parameters, including division rates, blastocyst rates, number of cells, ratio between trophectoderm and inner cell mass, as well as the proportion of apoptotic cells. However, although embryos produced in the presence of PLA, or in medium conditioned by it, did not show significant differences in any of the analyzed parameters, PCA revealed a higher degree of disparity compared to the control group compared to PCL. Therefore, our results suggest that PCL could be the optimal choice for the construction of new IVF devices.

In the second chapter, we investigated the impacts of a non-physiological material, molybdenum disulfide (MoS_2), on the IVF process and sperm capacitation. This compound has previously been used in scaffold functionalization, improving its properties and promoting cell growth, similar to graphene oxide, which has been shown to increase IVF efficiency in various species.

Although MoS_2 has not shown adverse effects on other cell types, its impact on gametes, especially sperm, and whether it could replicate the benefits observed with graphene oxide, are unknown. In this study, to solubilize MoS_2 , we conjugated it with catechin, an antioxidant. We evaluated various concentrations of these compounds and conjugates to determine the optimal one. We used seminal doses from boars, centrifuging the semen to remove the diluent, and resuspending the sperm in capacitating medium supplemented with the mentioned compounds. We monitored acrosome integrity to detect possible toxic effects on sperm and analyzed indicators of capacitation (intracellular

calcium concentration, membrane fluidity, and mitochondrial activity) using flow cytometry and western blot (protein phosphorylation). Finally, we functionally evaluated sperm through IVF, using in vitro matured porcine COCs obtained from slaughterhouse ovaries, as in the previous study.

The results indicate that MoS₂ conjugated with catechin (MoS₂/CT) did not affect acrosome integrity. Flow cytometry did not reveal differences in intracellular calcium concentration, membrane disorder, or mitochondrial activity. Western blot also showed no variations in protein phosphorylation. However, we observed a higher penetration rate and polyspermy in IVF when only catechin was used, not the MoS₂/CT complex. These findings suggest that catechin could have had an antioxidant effect, protecting sperm from reactive oxygen species and prolonging their viability. Additionally, we noted that MoS₂ had no adverse effects on these gametes or on the capacitation process.

In the third chapter of this thesis, we addressed the study of the oviduct structure, recognizing the importance of understanding the anatomy and morphology of this organ to mimic and understand its physiological environment. Traditionally, studies of this organ have been carried out using microscopy techniques, which, although useful, may have limitations in allowing the analysis of reduced and error-prone areas during reconstruction.

In the final phase of this research, sections of the oviduct were reconstructed using computerized microtomography (MicroTC) techniques. This non-destructive technique enables precise 3D model acquisition. Oviducts from genital tracts obtained from the slaughterhouse were selected and classified according to the different phases of the estrous cycle based on ovarian morphology. The oviducts were fixed in paraformaldehyde, embedded in paraffin blocks, and then imaged using MicroTC.

From these images, detailed measurements of the oviduct folds were made, as well as fractal dimension and lacunarity analysis. Additionally, three-dimensional reconstructions of the oviduct were carried out. To date, scaffolds designed to simulate the oviduct environment have not taken into account its complex architecture. The 3D models generated from these images can be converted into files compatible with 3D printing, allowing the creation of exact replicas. These replicas would not only be useful for creating devices for IVF but could also be used for biophysical and biomechanical studies, aspects closely linked to the functions performed by the oviduct.

In summary, this work establishes the foundations for the development of a new IVF device that more accurately mimics the complex architecture of the oviduct, opening up opportunities for more advanced research in assisted reproduction.

The background of the slide features a series of fluid, overlapping, and translucent blue and white lines that create a sense of movement and depth, resembling smoke or liquid waves. These lines are concentrated on the left side and flow towards the right, framing the text.

Introduction

1. Use and problematic of the assisted reproductive techniques.

Since the birth of Louise Brown, the first “test-tube baby” in 1978 (Hilson et al., 1978; Edwards et al., 1980), assisted reproductive techniques (ARTs) have changed the way we face infertility, a problem that currently affects a large number (15-20%) of couples in reproductive age (Cox et al., 2022). This problem is one of the reasons why birth rates are currently below the replacement rate in most European countries, and that has promoted that the use of ARTs rise until more than one million treatment cycles in one year (Gliozheni et al., 2022). This high number of cycles means that, in some countries, the babies born through these techniques represent more than 7% of the national births. For that reason, the value of these technologies in the market was around 26 billion dollars in 2019, and it is expected to reach 45 billion within 2025 (Aderaldo et al., 2023).

However, the use of ARTs in animals has been reported even before, with the earliest recorded instance of embryo transfer dating back to 1890, by Walter Heape (Heape, 1891). The use of these techniques in animals can be an attractive option for transgenesis and medicine, allowing the creation of suitable donors for organ transplantation (Sykes, 2022), or new animal models for human diseases (Navarro-Serna et al., 2022). Furthermore, it's worth highlighting that ARTs offer a range of significant advantages for animal production (Figure 1). These advantages include shortening generational times, reducing the risk of disease transmission, reducing quarantine costs, and enhancing the adaptability of animals in different species (Mapletoft and Hasler, 2005; Martinez et al., 2005; Amiridis and Cseh, 2012). In addition to reducing quarantine costs and the risk of diseases, ARTs significantly ease international trade, since transporting live animals is considerably harder and expensive compared to the transportation of embryos or semen.

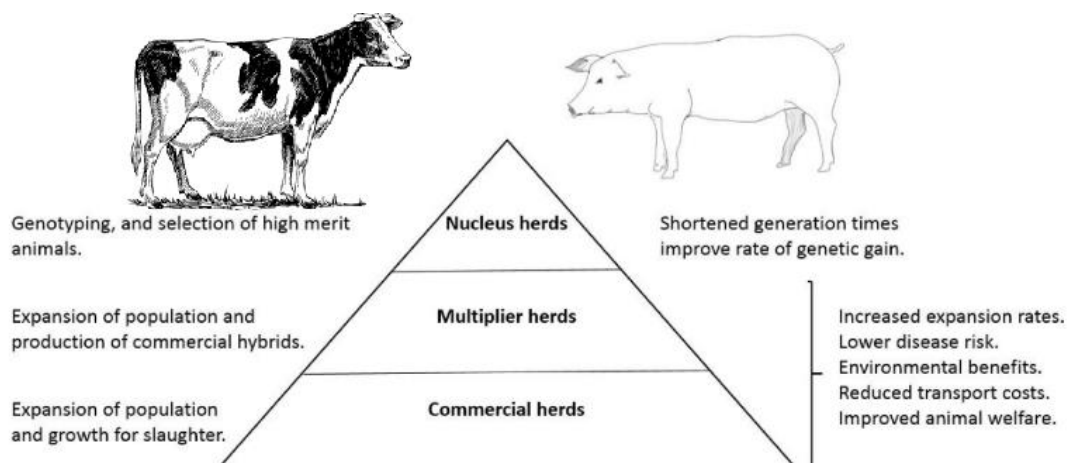


Figure 1. Schematic representation of the possible production gains achieved with ARTs (Modified from Fowler et al., 2018).

Therefore, their use in animals has been growing and continues to rise each year according to the International Embryo Technology Society (IETS) (Viana, 2022). Despite that in some domestic species such as goats or sheep, the embryo *in vitro* production (IVP) grown by more than 150% in just one year, cattle still lead the way with over one million embryos produced and transferred to recipients. One of the reasons, a part from the abovementioned, is that dairy production is inversely correlated with fertility (Hansen, 2000). In addition, ARTs could hold even more significant value in cattle breeding in light of the challenges presented by global warming. Bovine embryos are known to be exceptionally vulnerable to heat stress before reaching the morula stage (Sakatani et al., 2004). The application of these techniques has been proposed as a promising strategy to mitigate the adverse effects of heat stress on early-stage embryos (Sakatani, 2017), since in the laboratory temperature can be controlled, preventing heat-induced stress, and enhancing the pregnancy rate under this condition.

Among the wide array of ARTs, two of them are particularly challenging for the IVP of embryos: the *in vitro* fertilization (IVF) and the so-called

intracytoplasmic-sperm injection (ICSI). During the IVF the oocytes are placed in a culture dish, where they are exposed to sperm. In this case, spermatozoon selection for fertilization occurs naturally since sperm penetrate by itself, without human intervention. On the other hand, ICSI is an invasive technique in which the embryologist selects a spermatozoon and injects it into the ooplasm, overcoming the natural barriers such as the zona pellucida and even the oolemma. The use of ICSI experienced a significant rise and ultimately stabilized in 2006, with its incorporation in 70% of the treatment cycles in humans (Gliozheni et al., 2022), even when there is no indication (Boulet et al., 2015).

Since their creation, ARTs have been subject to continuous improvements and refinements. However, despite the advancements achieved, the ARTs are still suboptimal. Not all oocytes successfully develop into embryos, and the ones that do reach the blastocyst stage may not exhibit the same quality as their *in vivo* counterparts, showing reduced developmental capacity in species such as bovine (Nava-Trujillo and Rivera, 2023) or swine (Romar et al., 2019). This suboptimal quality can primarily be attributed to the epigenetic reprogramming process that occurs during the early stages of mammalian embryo development when they consist of just a few cells (Ishida and Moore, 2013) which renders them susceptible to environmental factors. For instance, maternal malnutrition has been observed to affect imprints on the offspring's epigenome (Begum et al., 2013). Furthermore, this susceptibility to the environment, makes embryos exceptionally vulnerable to suboptimal *in vitro* conditions, which notably differ from the natural conditions of the female reproductive tract. These differences in environmental factors, such as oxygen levels or temperature, can influence the developmental trajectory of embryo (García-Martínez et al., 2018, 2020).

It has been well-known from decades that ARTs cause epigenetic modification of embryo genes (Stojanov and O'Neill, 2001; DeBaun et al., 2003; Lucifero et al., 2006). In addition, it has been suggested that IVF/ICSI can influence perinatal outcomes, increasing the risk of low birth weights or preterm births in humans (Henningsen et al., 2011) or result in lower placental efficiency in pigs (París-Oller et al., 2021). Furthermore, it has been observed that these effects are not consistently rectified during an organism's development, leading to variations between *in vitro* produced and *in vivo derived* offspring growth (París-Oller et al., 2022), as well as differences in the glucose tolerance (Chen et al., 2014).

Numerous studies have shown that when the parameters such oxygen (García-Martínez et al., 2018), temperature (García-Martínez et al., 2020) or pH (Soriano-Úbeda et al., 2017), are adjusted closer to the physiologic ranges, significant improvements occur in the IVP system.

2. Spermatozoa: a long way until fertilization

While after mating, millions of ejaculated sperm can be counted in the vagina or cervix, depending on the species, only a few hundred manage to reach the oviduct, the organ where fertilization takes place (Mburu et al., 1996; Soto-Heras et al., 2023). However, even though the vast majority of sperm are lost during their journey, the few that reach the oviduct are capable of *in vivo* fertilization. Nevertheless, in *in vitro* conditions, we have a different situation since even though the oocytes are exposed to thousands/millions of spermatozoa, fertilization is not always successful. These discrepancies between natural and laboratory environments can be explained by the strong selection that spermatozoa undergo in the female genital tract. For instance, in some species, cervical mucus is

hypothesized to serve as a selective barrier for sperm, as it is highly effective at impeding defective spermatozoa that are unable to swim normally or possess a poor hydrodynamic profile due to morphoanomalies (Barros et al., 1984; Katz et al., 1990), eliminating around 70-85% of the sperm in this step (Kölle, 2022). After overcoming this barrier, spermatozoa enter the uterus, where another portion of the sperm population appears to be attacked by neutrophilic granulocytes, which are present in significant numbers following their post-insemination migration into the uterus (Taylor et al., 2008). Later on, the spermatozoa arrive at the utero tubal junction, the part of the oviduct that connects with the uterus. While in humans this part does not play a significant role in sperm selection due to the strong anatomical continuity between the oviduct and the uterus, in certain species such as ruminants, pigs, rats, hamster or mice, it does indeed play a role in sperm selection, being considered the second main selective barrier that exists after the cervix (Mahé et al., 2021). In those species, the utero tubal junction only allows the pass to live (Baker and Degen, 1972), unreacted (Muro et al., 2016) and motile (Gaddum-Rosse, 1981) spermatozoa. Although the mechanisms of sperm selection at this point are still unknown, it has been suggested a single molecule depending interaction, since the sperm of ADAM3 knockout mice are unable to overcome this point (Yamaguchi et al., 2009).

Finally, after this nightmarish journey, the few fortunate sperm that have overcome all barriers enter the oviduct, where the environment is much more favourable. Here, it seems like there are no leukocytes to attack them (Rodriguez-Martinez et al., 1990). Instead, they bind to the ciliated cells of the oviduct epithelium, forming the sperm reservoir. These ciliated cells “take care” of spermatozoa, delaying the process of sperm capacitation (Rodriguez-Martinez,

2007), and extending their viability from hours to months, depending on the species (Holt, 2011). This process ensures that sperm are ready at the time of ovulation, when they are released, and acquire their fertilization capacity (Boilard et al., 2002; Lamy et al., 2017).

However, when they are free, they need still to navigate through a long and intricate way, overcoming all the folds of the oviduct until they reach the oocyte. For that reason, it has been proposed that the mating of the spermatozoa and the oocyte is not a coincidence (Cerezales et al., 2015). In vitro studies have shown that spermatozoa can respond to temperature gradients. This phenomenon is not limited to a single species; it has been documented in rabbits (Bahat et al., 2003), pigs (Martin-Hidalgo et al., 2018), humans (Bahat et al., 2003, 2012), cattle (Mondal et al., 2017), and horses (Ruiz-Díaz et al., 2020), and is recognized as a common trait among mammalian sperm (Xiao et al., 2022). In conjunction with the finding that after ovulation, in certain animals such as rabbits (David et al., 1972) or pigs (Hunter and Nichol, 1986), the temperature in the fertilization place is higher than in the sperm reservoir, researchers propose that thermotaxis could be one of the mechanisms guiding sperm to the site of fertilization.

On the other hand, it has been shown that spermatozoa are able to align against the fluid flow (Miki and Clapham, 2013), a phenomenon called rheotaxis. As previously, this effect has been observed in several species as mouse (Miki and Clapham, 2013), human (De Martin et al., 2017), boar (Fair and Romero-Aguirregomez, 2019) and bull (Tung et al., 2014; Johnson et al., 2017). For this ability of the sperm together with the fact that there is a current flow that goes from the ovaries to the uterus (Miki and Clapham, 2013; Yoshimoto et al., 2017), rheotaxis has been proposed as another mechanism to guide the spermatozoa until

the oocyte. Lastly, sperm are capable of moving in response to chemical gradients of certain substances. One of the first chemoattractants reported was the follicular fluid in humans (Ralt et al., 1991) and since then, the phenomenon has been observed in species such as mice (Oliveira et al., 1999) or bovine (Dominguez et al., 2018). However, follicular fluid is not the only fluid that could have chemoattractants. The cumulus cells accompanying the oocyte produce progesterone (Bar-Ami et al., 1989), a steroid capable of inducing chemotaxis in humans (Gatica et al., 2013), cattle (Dominguez et al., 2018) and rabbits (Teves et al., 2006), among others (Giojalas and Guidobaldi, 2020).

Although these mechanisms have been heavily criticized because in the *in vivo* oviduct peristaltic movements may play a more significant role (Hino and Yanagimachi, 2019), they have proven to be useful *in vitro*, improving sperm selection and IVP outcome (De Martin et al., 2017; Dominguez et al., 2018; Pérez-Cerezales et al., 2018; Doostabadi et al., 2022; Ruiz-Díaz et al., 2023). In figure 2, a representation of the proposed mechanisms is provided.

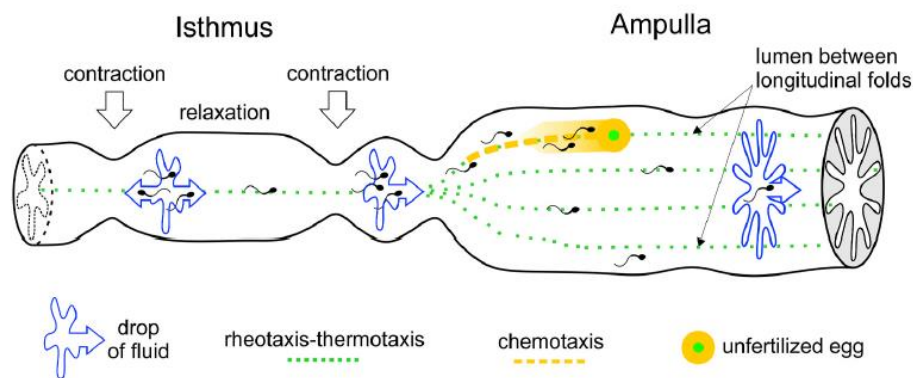


Figure 2. Representation of the theoretical mechanism that guides spermatozoa until the oocyte (Modified from Giojalas and Guidobaldi, 2020)

After fertilization, the first division of the embryos takes place. It has been observed that the presence of the embryo, can induce distinct gene expression

patterns in the epithelial cells (Smits et al., 2016; Hamdi et al., 2019). This diverse gene expression could play essential roles, such as facilitating embryo transport (e.g., ciliary motility) or creating an optimal environment for early embryo development (Maillo et al., 2016). In a bidirectional way, it has been observed that co-culture of embryos with epithelial cells promotes a different gene expression profile of genes involved in embryo quality (Cordova et al., 2014). In fact, when the embryos are produced in oviducts, they have higher quality, even in a heterologous manner (Lazzari et al., 2002; Rizos et al., 2007). The aforementioned effects have been observed in both *in vitro* and *in vivo* experiments in the bovine species.

Traditionally, the oviduct has been regarded as a simple tube, mainly because pregnancy can be achieved without exposing gametes or embryos to the oviduct's environment. However, as we have previously discussed, its functions should not be underestimated, as we are dealing with a highly complex system that is even capable of reacting differently depending on the sperm's sex, since the presence of X or Y-sperm population can change the oviductal transcriptome (Almiñana et al., 2014).

3. Mimicking the oviduct

It's important to highlight that the abovementioned *in vitro* studies have predominantly relied on monolayer cultures. Those standard 2D growth techniques have played an important role in advancing our understanding of how OECs respond to different stimuli. Nevertheless, 2D cell cultures may not always represent the optimal approach for conducting studies, since they fail to closely mimic the physiological conditions. As Watson et al., (2017) said, this kind of *in vitro* studies give us results describing the 2D life, where the cells “talk only to cells of like mind, live in the dark and in their own excrement, and don’t bury their dead”. A solution

for this problem could be to adopt a 3D approach, providing us with a more realistic perspective on how these responses might translate to an *in vivo* environment (Ravi et al., 2015; Watson et al., 2017)

In the last years, several works have been published using the 3D-culture approach to study diverse areas of the female reproductive tract, like the uterus (Wang et al., 2013; Murphy et al., 2019; López-Martínez et al., 2021), oviduct (Eddie et al., 2015; Francés-Herrero et al., 2021) or vagina (Orabi et al., 2017; Jakubowska et al., 2020). Meanwhile, there is a growing interest in the development of microfluidics, a field that focuses on the control and manipulation of fluids at microscopic scales to recreate the dynamic *in vivo* flow (Campo et al., 2023). When that technology has been applied to 3D cultures, it has been even possible to recreate the menstrual cycle *in vitro* (Xiao et al., 2017). By combining both 3D cell cultures and microfluidics technology, it is possible to create the so-called "oviducts on a chip", that represent a significant advancement in improving IVP (Ferraz et al., 2017, 2018). These innovative scaffold devices accurately replicate the physiological conditions of the oviduct, providing a more realistic environment for sperm-egg interaction.

Functionalizing scaffolds is a pivotal aspect of tissue engineering and regenerative medicine, as it enables the customization of biomaterials. The choice of materials for scaffold functionalization is an important decision, since it profoundly influences the scaffold's bioactivity, biocompatibility (Liu et al., 2012), and mechanical properties (Ma et al., 2021), even when they are functionalized with non-physiologic materials (Forero et al., 2017; Hezma et al., 2017; Shimabukuro et al., 2022).

In recent years, there has been a growing utilization of non-physiological materials in biomedicine (Zhou et al., 2020). Graphene oxide is an example of how they can be used in assisted reproduction techniques. When added to the culture medium, graphene oxide significantly improves IVF performance in murine (Bernabò et al., 2020), porcine (Bernabò et al., 2019), and bovine (Ramal-Sanchez et al., 2019) models. Molybdenum disulfide (MoS₂), a substance with a structure similar to graphene and the ability to promote cell differentiation and proliferation, stands out among these non-physiological compounds. MoS₂ is composed of layers that overlap and are kept together by van der Waals forces, and its properties could be particularly interesting to functionalizing the scaffolds. In the last years, this material has been already used in drug delivery and cancer therapy (Wang et al., 2021), and even it has been shown that it can promote cell differentiation and proliferation when it is present in the culture media (Zou et al., 2017), properties that could be useful in a scaffold. In addition, it has been used recently to construct scaffolds together with polycaprolactone (PCL) for bone regeneration and to promote anastomosis, showing itself as a promising tool to prevent anastomosis leakage (Ebrahim Soltani et al., 2023) and demonstrating improved cell growth and osteogenic activity (Ma et al., 2021).

In the light of the above-discussed reasons, there is still ample room for improvement in the ART in general and in the IVF and ICSI procedures in particular. By identifying new materials and new procedures to construct 3D IVF-devices the efficiency of the process could make a significant leap in the quality and quantity of embryos produced. The present PhD thesis intends to contribute to these goals.

To that aim, the next steps were followed:

- **Chapter 1**

In the initial phase of this thesis, our primary objective was to identify appropriate materials for supporting IVF, with the intention of using them in the construction of an IVF device in the near future. To achieve this, we employed various 3D printing methods, each paired with compatible materials tailored to the specific printing technique. Subsequently, our research endeavoured to explore the impact of these materials on IVF assessing the ability of the embryos to develop in their presence.

Animal embryos have played an important role in the development of crucial areas of ARTs like the cryopreservation or formulation of the culture media (Chronopoulou and Harper, 2015), particularly, the use of mouse and rabbit embryos. Actually, the use of mouse embryos, is still important since serves as a quality control in the modern laboratory. In fact, before a culture media or another IVF product is approved for clinical use, the Food and Drug Administration (FDA) mandates rigorous quality control measures. This includes not only assessing parameters such as pH, osmolarity, and endotoxicity but also requiring the performance of a mouse embryo assay (MEA) (Mouse Embryo Assay for Assisted Reproduction Technology Devices, FDA, 2021). Lately, the researchers are using other animal models like zebrafish, in order to avoid the use of mammals embryos (Hoyberghs et al., 2020). However, these types of studies, nonetheless, pose ethical concerns, are expensive, and consume a significant amount of time. In this line, some pharmaceutical and chemical companies have recognized the zebrafish as a potential model for toxicological studies (Hoyberghs et al., 2020). This model has been already used to study the toxic effects of different 3D printing polymers (MacDonald et al., 2016; Oskui et al., 2016). Another plausible option is the bovine model, which

could offer multiple practical benefits for toxicological studies. One of the primary advantages is the ease and affordability of producing *in vitro* embryos. Bovine ovaries can be sourced from local abattoirs, which provides a cost-effective and accessible supply of biological material. Furthermore, obtaining semen is an easy process thanks to the numerous specialized companies dedicated to commercializing it for artificial insemination. In addition, using those sources does not necessitate the establishment of dedicated animal care facilities or the allocation of extra personnel for this purpose, in contrast with the mouse or zebrafish models, where maintaining and monitoring the animals can be a significant logistical and financial burden.

One of the most compelling aspects of using the bovine model for toxicological studies is that these animals are already being sacrificed for the meat industry. This means that utilizing them as a model for scientific research effectively repurposes a resource that would otherwise go to waste. Since the animals are ultimately destined for human consumption, their use in scientific experimentation does not raise significant ethical concerns or pose an ethical dilemma. This sustainable and ethical aspect of the bovine model adds an extra layer of appeal for researchers seeking to conduct cost-effective and responsible toxicological studies. Indeed, some companies like EmbryoCloud (Murcia, Spain) are starting to offer services for the evaluation of culture mediums and medical devices.

For these reasons, in this study, we have chosen to conduct a bovine embryo assay to investigate the compatibility of various materials, without consideration of the final device design. To achieve this, we conducted *in vitro* fertilization procedures in the presence of these materials or their exudates. Subsequently, we assessed key parameters, including cleavage rates and the formation of blastocysts.

Moreover, a double differential staining approach was employed with the objective of shedding more light on embryonic quality.

- **Chapter 2**

As mentioned, the MoS₂ could be an interesting option to functionalize the biomaterials tested in Chapter 1 for a future IVF device. This material is part of the family of inorganic 2D nanomaterials (Lv et al., 2015), a category of layered materials known for their remarkable thinness, planar and anisotropic architecture (Chimene et al., 2015). 2D nanomaterials have a higher specific surface area than 1D or 3D nanomaterials, which means that there are more surface atoms than volume atoms in them (Murali et al., 2021). Thanks to these characteristics, it possesses a significant number of anchoring sites on its surface, enhancing its interaction with biological components, such as cells, cellular structures, and biomolecules (Murali et al., 2021). Moreover, these properties are particularly intriguing from a functionalization perspective, as they offer exceptional versatility in surface modification for a variety of applications (Roy et al., 2022).

Taking into account that MoS₂ has previously shown a lack of adverse effects on other cell types, we have chosen to examine its impact on gametes, specifically spermatozoa, to determine whether it exhibits properties similar to graphene oxide. In this study, we not only observed that MoS₂ and catechins do not have a detrimental effect on spermatozoa but also delved deeper into their influence on sperm capacitation. This investigation aimed to shed light on whether these substances might possess properties similar to graphene oxide. We sought to discern how MoS₂ and catechins could potentially impact the capacitation process of

spermatozoa, offering valuable insights into their functional attributes and the broader implications for reproductive biology and assisted reproductive technologies.

In this context, we functionalized MoS₂ with catechins, a flavonoid with high antioxidant capacity (Bernatoniene and Kopustinskiene, 2018). The amphiphilic nature of catechins (Rojas et al., 2022), combined with MoS₂ ability to readily incorporate hydrophobic molecules (due to its hydrophobic surface) (Roy et al., 2022), facilitates the interaction between the nanomaterial's surface and catechins. Additionally, functionalization with catechins renders MoS₂ soluble, greatly facilitating studies on the material's compatibility with gametes.

In the second chapter, MoS₂ nanoflakes functionalized with CT and CT were employed to investigate their effects on the functional parameters of swine spermatozoa during capacitation. This study not only assessed the absence of adverse effects of the MoS₂/CT and CT complexes on their own but also delved into the potential role of MoS₂ in *in vitro* capacitation, a critical biological event. Different concentrations of MoS₂/CT and CT (10, 1, and 0.1 ppm) were examined using a multi-step approach to evaluate possible effects in terms of acrosome damage, membrane disorder, biochemical patterns, and intracellular calcium.

- **Chapter 3**

Since the understanding of anatomy and morphology is crucial to understand and mimicking physiology processes, it becomes essential to delve into the study of the oviduct's anatomy. This organ has already been described through different techniques such as transvaginal sonohysterography (Deichert et al., 1989) or magnetic resonance (Carrascosa et al., 2016), generating low-resolution images.

With high accuracy, it has been characterized through electronic microscopy (Yániz et al., 2000; Yaniz et al., 2006; Yániz et al., 2014), although it is worth it to acknowledge that it is inherently limited by its ability to study only small areas.

In contrast to the confined capabilities of electronic microscopy, MicroCT provides a non-destructive, three-dimensional imaging approach that enables the examination of larger tissue volumes (Metscher, 2009). Although at the beginning this technique was mainly used for mineralized tissues (Neues et al., 2007; Neues and Eppele, 2008), the progress in the X-ray imaging has allowed the use of MicroCT for soft tissues (Withers et al., 2021; Holliday et al., 2022).

Recently, CT-generated images have been employed to generate a file compatible with 3D printing technology for the production of bone phantoms (Mei et al., 2023). For that, in this chapter, we examine and characterize the internal structure of the oviduct with the aim that, shortly, the data acquired in this investigation can be harnessed to formulate a 3D printable file. We aimed to lay the foundation for the development of a precise oviduct 3D-printed model. This device could serve as a tool to improve in vitro fertilization. Moreover, would serve as a valuable tool for studying the interaction of gametes and embryos with the oviduct.

4. References

- Aderaldo, J. F., de Albuquerque, B. H. D. R., de Oliveira, M. T. F. C., de Medeiros Garcia Torres, M., and Lanza, D. C. F. (2023). Main topics in assisted reproductive market: A scoping review. *PLoS One* 18. doi: 10.1371/JOURNAL.PONE.0284099.
- Almiñana, C., Caballero, I., Heath, P. R., Maleki-Dizaji, S., Parrilla, I., Cuello, C., et al. (2014). The battle of the sexes starts in the oviduct: modulation of

- oviductal transcriptome by X and Y-bearing spermatozoa. *BMC Genomics* 15. doi: 10.1186/1471-2164-15-293.
- Amiridis, G. S., and Cseh, S. (2012). Assisted reproductive technologies in the reproductive management of small ruminants. *Anim Reprod Sci* 130, 152–161. doi: 10.1016/J.ANIREPROSCI.2012.01.009.
- Bahat, A., Caplan, S. R., and Eisenbach, M. (2012). Thermotaxis of Human Sperm Cells in Extraordinarily Shallow Temperature Gradients Over a Wide Range. *PLoS One* 7, 41915. doi: 10.1371/JOURNAL.PONE.0041915.
- Bahat, A., Tur-Kaspa, I., Gakamsky, A., Giojalas, L. C., Breitbart, H., and Eisenbach, M. (2003). Thermotaxis of mammalian sperm cells: A potential navigation mechanism in the female genital tract. *Nature Medicine* 2003 9:2 9, 149–150. doi: 10.1038/nm0203-149.
- Baker, R. D., and Degen, A. A. (1972). Transport of live and dead boar spermatozoa within the reproductive tract of gilts. *J Reprod Fertil* 28, 369–377. doi: 10.1530/JRF.0.0280369.
- Bar-Ami, S., Gitay-Goren, H., and Brandes, J. M. (1989). Different Morphological and Steroidogenic Patterns in Oocyte/Cumulus-Corona Cell Complexes Aspirated at in Vitro Fertilization. *Biol Reprod* 41, 761–770. doi: 10.1095/BIOLREPROD41.4.761.
- Barros, C., Vigil, P., Herrera, E., Arguello, B., and Walker, R. (1984). Selection of morphologically abnormal sperm by human cervical mucus. *Arch Androl* 12 Suppl, 95–107. Available at: <https://europepmc.org/article/med/6535459> [Accessed October 26, 2023].

- Begum, G., Davies, A., Stevens, A., Oliver, M., Jaquier, A., Challis, J., et al. (2013). Maternal undernutrition programs tissue-specific epigenetic changes in the glucocorticoid receptor in adult offspring. *Endocrinology* 154, 4560–4569. doi: 10.1210/EN.2013-1693.
- Bernabò, N., Machado-Simoes, J., Valbonetti, L., Ramal-Sanchez, M., Capacchietti, G., Fontana, A., et al. (2019). Graphene Oxide increases mammalian spermatozoa fertilizing ability by extracting cholesterol from their membranes and promoting capacitation. *Sci Rep* 9. doi: 10.1038/S41598-019-44702-5.
- Bernabò, N., Valbonetti, L., Raspa, M., Fontana, A., Palestini, P., Botto, L., et al. (2020). Graphene Oxide Improves in vitro Fertilization in Mice With No Impact on Embryo Development and Preserves the Membrane Microdomains Architecture. *Front Bioeng Biotechnol* 8. doi: 10.3389/FBIOE.2020.00629.
- Bernatoniene, J., and Kopustinskiene, D. M. (2018). The Role of Catechins in Cellular Responses to Oxidative Stress. *Molecules : A Journal of Synthetic Chemistry and Natural Product Chemistry* 23. doi: 10.3390/MOLECULES23040965.
- Boilard, M., Bailey, J., Collin, S., Dufour, M., and Sirard, M. A. (2002). Effect of bovine oviduct epithelial cell apical plasma membranes on sperm function assessed by a novel flow cytometric approach. *Biol Reprod* 67, 1125–1132. doi: 10.1095/BIOLREPROD67.4.1125.
- Boulet, S. L., Mehta, A., Kissin, D. M., Lee, W., Kawwass, J. F., and Jamieson, D. J. (2015). Trends in Use of and Reproductive Outcomes Associated With Intracytoplasmic Sperm Injection. *JAMA* 313, 255. doi: 10.1001/JAMA.2014.17985.

- Campo, H., Zha, D., Pattarawat, P., Colina, J., Zhang, D., Murphy, A., et al. (2023). A new tissue-agnostic microfluidic device to model physiology and disease: the lattice platform. *Lab Chip*. doi: 10.1039/D3LC00378G.
- Carrascosa, P., Capuñay, C., Vallejos, J., Carpio, J., Baronio, M., and Papier, S. (2016). Two-dimensional and three-dimensional imaging of uterus and fallopian tubes in female infertility. *Fertil Steril* 105, 1403-1420.e7. doi: 10.1016/J.FERTNSTERT.2016.04.016.
- Cerezales, S., Boryshpolets, S., and Eisenbach, M. (2015). Behavioral mechanisms of mammalian sperm guidance. *Asian J Androl* 17, 628. doi: 10.4103/1008-682X.154308.
- Chen, M., Wu, L., Zhao, J., Wu, F., Davies, M. J., Wittert, G. A., et al. (2014). Altered glucose metabolism in mouse and humans conceived by IVF. *Diabetes* 63, 3189–3198. doi: 10.2337/DB14-0103.
- Chimene, D., Alge, D. L., and Gaharwar, A. K. (2015). Two-Dimensional Nanomaterials for Biomedical Applications: Emerging Trends and Future Prospects. *Advanced Materials* 27, 7261–7284. doi: 10.1002/ADMA.201502422.
- Chronopoulou, E., and Harper, J. C. (2015). IVF culture media: past, present and future. *Hum Reprod Update* 21, 39–55. doi: 10.1093/HUMUPD/DMU040.
- Cordova, A., Perreau, C., Uzbekova, S., Ponsart, C., Locatelli, Y., and Mermillod, P. (2014). Development rate and gene expression of IVP bovine embryos cocultured with bovine oviduct epithelial cells at early or late stage of

- preimplantation development. *Theriogenology* 81, 1163–1173. doi: 10.1016/J.THERIOGENOLOGY.2014.01.012.
- Cox, C. M., Thoma, M. E., Tchangalova, N., Mburu, G., Bornstein, M. J., Johnson, C. L., et al. (2022). Infertility prevalence and the methods of estimation from 1990 to 2021: a systematic review and meta-analysis. *Hum Reprod Open* 2022, 1–24. doi: 10.1093/HROPEN/HOAC051.
- David, A., Vilensky, A., and Nathan, H. (1972). Temperature Changes in the Different Parts of the Rabbit's Oviduct. *International Journal of Gynecology & Obstetrics* 10, 52–56. doi: 10.1002/J.1879-3479.1972.TB00818.X.
- De Martin, H., Cocuzza, M. S., Tiseo, B. C., Wood, G. J. A., Miranda, E. P., Monteleone, P. A. A., et al. (2017). Positive rheotaxis extended drop: a one-step procedure to select and recover sperm with mature chromatin for intracytoplasmic sperm injection. *J Assist Reprod Genet* 34, 1699–1708. doi: 10.1007/S10815-017-1024-1.
- DeBaun, M. R., Niemitz, E. L., and Feinberg, A. P. (2003). Association of in vitro fertilization with Beckwith-Wiedemann syndrome and epigenetic alterations of LIT1 and H19. *Am J Hum Genet* 72, 156–160. doi: 10.1086/346031.
- Deichert, U., Schlieff, R., Van De Sandt, M., and Juhnke, I. (1989). Transvaginal hysterosalpingo-contrast-sonography (Hy-Co-Sy) compared with conventional tubal diagnostics. *Hum Reprod* 4, 418–424. doi: 10.1093/OXFORDJOURNALS.HUMREP.A136920.
- Dominguez, E. M., Moreno-Irusta, A., Guidobaldi, H. A., Tribulo, H., and Giojalas, L. C. (2018). Improved bovine in vitro embryo production with sexed and

- unsexed sperm selected by chemotaxis. *Theriogenology* 122, 1–8. doi: 10.1016/J.THERIOGENOLOGY.2018.08.023.
- Doostabadi, M. R., Mangoli, E., Marvast, L. D., Dehghanpour, F., Maleki, B., Torkashvand, H., et al. (2022). Microfluidic devices employing chemo- and thermotaxis for sperm selection can improve sperm parameters and function in patients with high DNA fragmentation. *Andrologia* 54. doi: 10.1111/AND.14623.
- Ebrahim Soltani, Z., Elahi, M., Tashak-Golroudbari, H., Nazari, H., Badripour, A., Heirani-Tabasi, A., et al. (2023). Evaluation of colonic anastomosis healing using hybrid nanosheets containing molybdenum disulfide (MOS₂) scaffold of human placental amniotic membrane and polycaprolactone (PCL) in rat animal model. *Naunyn Schmiedebergs Arch Pharmacol* 396, 1911–1921. doi: 10.1007/S00210-023-02438-0.
- Eddie, S. L., Quartuccio, S. M., Zhu, J., Shepherd, J. A., Kothari, R., Kim, J. J., et al. (2015). Three-dimensional modeling of the human fallopian tube fimbriae. *Gynecol Oncol* 136, 348–354. doi: 10.1016/J.YGYNO.2014.12.015.
- Edwards, R. G., Steptoe, P. C., and Purdy, J. M. (1980). Establishing full-term human pregnancies using cleaving embryos grown in vitro. *Br J Obstet Gynaecol* 87, 737–756. doi: 10.1111/J.1471-0528.1980.TB04610.X.
- Fair, S., and Romero-Aguirregomezcorta, J. (2019). Implications of boar sperm kinematics and rheotaxis for fertility after preservation. *Theriogenology* 137, 15–22. doi: 10.1016/J.THERIOGENOLOGY.2019.05.032.

- Ferraz, M. A. M. M., Henning, H. H. W., Costa, P. F., Malda, J., Melchels, F. P., Wubbolts, R., et al. (2017). Improved bovine embryo production in an oviduct-on-a-chip system: prevention of poly-spermic fertilization and parthenogenic activation. *Lab Chip* 17, 905–916. doi: 10.1039/c6lc01566b.
- Ferraz, M. A. M. M., Rho, H. S., Hemerich, D., Henning, H. H. W., van Tol, H. T. A., Hölker, M., et al. (2018). An oviduct-on-a-chip provides an enhanced in vitro environment for zygote genome reprogramming. *Nat Commun* 9. doi: 10.1038/s41467-018-07119-8.
- Forero, J. C., Roa, E., Reyes, J. G., Acevedo, C., and Osses, N. (2017). Development of Useful Biomaterial for Bone Tissue Engineering by Incorporating Nano-Copper-Zinc Alloy (nCuZn) in Chitosan/Gelatin/Nano-Hydroxyapatite (Ch/G/nHAp) Scaffold. *Materials* 2017, Vol. 10, Page 1177 10, 1177. doi: 10.3390/MA10101177.
- Fowler, K. E., Mandawala, A. A., Griffin, D. K., Walling, G. A., and Harvey, S. C. (2018). The production of pig preimplantation embryos in vitro: Current progress and future prospects. *Reprod Biol* 18, 203–211. doi: 10.1016/J.REPBIO.2018.07.001.
- Francés-Herrero, E., De Miguel-Gómez, L., López-Martínez, S., Campo, H., Garcia-Dominguez, X., Diretto, G., et al. (2021). Development of Decellularized Oviductal Hydrogels as a Support for Rabbit Embryo Culture. *Reproductive Sciences* 28, 1644–1658. doi: 10.1007/S43032-020-00446-6/FIGURES/8.
- Gaddum-Rosse, P. (1981). Some observations on sperm transport through the uterotubal junction of the rat. *Am J Anat* 160, 333–341. doi: 10.1002/AJA.1001600309.

- García-Martínez, S., Hurtado, M. A. S., Gutiérrez, H., Margallo, F. M. S., Romar, R., Latorre, R., et al. (2018). Mimicking physiological O₂ tension in the female reproductive tract improves assisted reproduction outcomes in pig. *Mol Hum Reprod* 24, 260–270. doi: 10.1093/MOLEHR/GAY008.
- García-Martínez, S., Latorre, R., Sánchez-Hurtado, M. A., Sánchez-Margallo, F. M., Bernabò, N., Romar, R., et al. (2020). Mimicking the temperature gradient between the sow's oviduct and uterus improves in vitro embryo culture output. *Mol Hum Reprod* 26, 748–759. doi: 10.1093/MOLEHR/GAAA053.
- Gatica, L. V., Guidobaldi, H. A., Montesinos, M. M., Teves, M. E., Moreno, A. I., Uñates, D. R., et al. (2013). Picomolar gradients of progesterone select functional human sperm even in subfertile samples. *Mol Hum Reprod* 19, 559–569. doi: 10.1093/MOLEHR/GAT037.
- Giojalas, L. C., and Guidobaldi, H. A. (2020). Getting to and away from the egg, an interplay between several sperm transport mechanisms and a complex oviduct physiology. *Mol Cell Endocrinol* 518. doi: 10.1016/J.MCE.2020.110954.
- Glozheni, O., Hambartsoumian, E., Strohmer, H., Petrovskaya, E., Tishkevich, O., de Neubourg, D., et al. (2022). ART in Europe, 2018: results generated from European registries by ESHRE. *Hum Reprod Open* 2022. doi: 10.1093/HROPEN/HOAC022.
- Hamdi, M., Sánchez-Calabuig, M. J., Rodríguez-Alonso, B., Arnal, S. B., Roussi, K., Sturmey, R., et al. (2019). Gene expression and metabolic response of bovine oviduct epithelial cells to the early embryo. *Reproduction* 158, 85–94. doi: 10.1530/REP-18-0561.

- Hansen, L. B. (2000). Consequences of selection for milk yield from a geneticist's viewpoint. *J Dairy Sci* 83, 1145–1150. doi: 10.3168/JDS.S0022-0302(00)74980-0.
- Heape, W. (1891). III. Preliminary note on the transplantation and growth of mammalian ova within a uterine foster-mother. *Proceedings of the Royal Society of London* 48, 457–458. doi: 10.1098/RSPL.1890.0053.
- Henningsen, A. K. A., Pinborg, A., Lidegaard, Ø., Vestergaard, C., Forman, J. L., and Andersen, A. N. (2011). Perinatal outcome of singleton siblings born after assisted reproductive technology and spontaneous conception: Danish national sibling-cohort study. *Fertil Steril* 95, 959–963. doi: 10.1016/J.FERTNSTERT.2010.07.1075.
- Hezma, A. M., EL-Rafei, A. M., El-Bahy, G. S., and Abdelrazzak, A. B. (2017). Electrospun hydroxyapatite containing polyvinyl alcohol nanofibers doped with nanogold for bone tissue engineering. *InterCeram: International Ceramic Review* 66, 96–100. doi: 10.1007/BF03401205/METRICS.
- Hilson, D., Bruce, R. L., and Sims, D. G. (1978). Successful pregnancy following in-vitro fertilisation. *Lancet* 2, 473. doi: 10.1016/S0140-6736(78)91471-X.
- Hino, T., and Yanagimachi, R. (2019). Active peristaltic movements and fluid production of the mouse oviduct: their roles in fluid and sperm transport and fertilization†. *Biol Reprod* 101, 240–249. doi: 10.1093/BIOLRE/IOZ061.
- Holliday, C. M., Sellers, K. C., Lessner, E. J., Middleton, K. M., Cranor, C., Verhulst, C. D., et al. (2022). New frontiers in imaging, anatomy, and

- mechanics of crocodylian jaw muscles. *Anat Rec (Hoboken)* 305, 3016–3030. doi: 10.1002/AR.25011.
- Holt, W. V. (2011). Mechanisms of sperm storage in the female reproductive tract: an interspecies comparison. *Reprod Domest Anim* 46 Suppl 2, 68–74. doi: 10.1111/J.1439-0531.2011.01862.X.
- Hoyberghs, J., Bars, C., Pype, C., Foubert, K., Ayuso Hernando, M., Van Ginneken, C., et al. (2020). Refinement of the zebrafish embryo developmental toxicity assay. *MethodsX* 7. doi: 10.1016/J.MEX.2020.101087.
- Hunter, R. H. F., and Nichol, R. (1986). A preovulatory temperature gradient between the isthmus and ampulla of pig oviducts during the phase of sperm storage. *J Reprod Fertil* 77, 599–606. doi: 10.1530/JRF.0.0770599.
- Ishida, M., and Moore, G. E. (2013). The role of imprinted genes in humans. *Mol Aspects Med* 34, 826–840. doi: 10.1016/J.MAM.2012.06.009.
- Jakubowska, W., Chabaud, S., Saba, I., Galbraith, T., Berthod, F., and Bolduc, S. (2020). Prevascularized Tissue-Engineered Human Vaginal Mucosa: In Vitro Optimization and In Vivo Validation. *Tissue Eng Part A* 26, 811–822. doi: 10.1089/TEN.TEA.2020.0036.
- Johnson, G. P., English, A. M., Cronin, S., Hoey, D. A., Meade, K. G., and Fair, S. (2017). Genomic identification, expression profiling, and functional characterization of CatSper channels in the bovine. *Biol Reprod* 97, 302–312. doi: 10.1093/BIOLRE/IOX082.

- Katz, D. F., Morales, P., Samuels, S. J., and Overstreet, J. W. (1990). Mechanisms of filtration of morphologically abnormal human sperm by cervical mucus. *Fertil Steril* 54, 513–516. doi: 10.1016/S0015-0282(16)53772-8.
- Kölle, S. (2022). Sperm-oviduct interactions: Key factors for sperm survival and maintenance of sperm fertilizing capacity. *Andrology* 10, 837. doi: 10.1111/ANDR.13179.
- Lamy, J., Corbin, E., Blache, M. C., Garanina, A. S., Uzbekov, R., Mermillod, P., et al. (2017). Steroid hormones regulate sperm-oviduct interactions in the bovine. *Reproduction* 154, 497–508. doi: 10.1530/REP-17-0328.
- Lazzari, G., Wrenzycki, C., Herrmann, D., Duchi, R., Kruip, T., Niemann, H., et al. (2002). Cellular and molecular deviations in bovine in vitro-produced embryos are related to the large offspring syndrome. *Biol Reprod* 67, 767–775. doi: 10.1095/BIOLREPROD.102.004481.
- Liu, X., Holzwarth, J. M., and Ma, P. X. (2012). Functionalized Synthetic Biodegradable Polymer Scaffolds for Tissue Engineering. *Macromol Biosci* 12, 911–919. doi: 10.1002/MABI.201100466.
- López-Martínez, S., Rodríguez-Eguren, A., de Miguel-Gómez, L., Francés-Herrero, E., Faus, A., Díaz, A., et al. (2021). Bioengineered endometrial hydrogels with growth factors promote tissue regeneration and restore fertility in murine models. *Acta Biomater* 135, 113–125. doi: 10.1016/J.ACTBIO.2021.08.025.
- Lucifero, D., Suzuki, J., Bordignon, V., Martel, J., Vigneault, C., Therrien, J., et al. (2006). Bovine SNRPN Methylation Imprint in Oocytes and Day 17 In Vitro-

- Produced and Somatic Cell Nuclear Transfer Embryos. *Biol Reprod* 75, 531–538. doi: 10.1095/BIOLREPROD.106.051722.
- Lv, R., Robinson, J. A., Schaak, R. E., Sun, D., Sun, Y., Mallouk, T. E., et al. (2015). Transition metal dichalcogenides and beyond: Synthesis, properties, and applications of single- and few-layer nanosheets. *Acc Chem Res* 48, 56–64. doi: 10.1021/AR5002846/ASSET/IMAGES/MEDIUM/AR-2014-002846_0007.GIF.
- Ma, K., Liao, C., Huang, L., Liang, R., Zhao, J., Zheng, L., et al. (2021). Electrospun PCL/MoS₂ Nanofiber Membranes Combined with NIR-Triggered Photothermal Therapy to Accelerate Bone Regeneration. *Small* 17. doi: 10.1002/SMLL.202104747.
- MacDonald, N. P., Zhu, F., Hall, C. J., Reboud, J., Crosier, P. S., Patton, E. E., et al. (2016). Assessment of biocompatibility of 3D printed photopolymers using zebrafish embryo toxicity assays. *Lab Chip* 16, 291–297. doi: 10.1039/c5lc01374g.
- Mahé, C., Zlotkowska, A. M., Reynaud, K., Tsikis, G., Mermillod, P., Druart, X., et al. (2021). Sperm migration, selection, survival, and fertilizing ability in the mammalian oviduct†. *Biol Reprod* 105, 317–331. doi: 10.1093/BIOLRE/IOAB105.
- Maillo, V., De Frutos, C., O’Gaora, P., Forde, N., Burns, G. W., Spencer, T. E., et al. (2016). Spatial differences in gene expression in the bovine oviduct. *Reproduction* 152, 37–46. doi: 10.1530/REP-16-0074.

- Mapletoft, R. J., and Hasler, J. F. (2005). Assisted reproductive technologies in cattle: A review. *OIE Revue Scientifique et Technique* 24, 393–403. doi: 10.20506/RST.24.1.1582.
- Martinez, E. A., Vazquez, J. M., Roca, J., Cuello, C., Gil, M. A., Parrilla, I., et al. (2005). An update on reproductive technologies with potential short-term application in pig production. *Reprod Domest Anim* 40, 300–309. doi: 10.1111/J.1439-0531.2005.00593.X.
- Martin-Hidalgo, D., Gil, M. C., Llera, A. H. de, Perez, C. J., Bragado, M. J., Garcia-Marin, L. J., et al. (2018). Boar sperm hyperactivated motility is induced by temperature via an intracellular calcium-dependent pathway. *Reprod Fertil Dev* 30, 1462–1471. doi: 10.1071/RD17549.
- Mburu, J. N., Einarsson, S., Lundeheim, N., and Rodriguez-Martinez, H. (1996). Distribution, number and membrane integrity of spermatozoa in the pig oviduct in relation to spontaneous ovulation. *Anim Reprod Sci* 45, 109–121. doi: 10.1016/S0378-4320(96)01566-7.
- Mei, K., Pasyar, P., Geagan, M., Liu, L. P., Shapira, N., Gang, G. J., et al. (2023). Design and fabrication of 3D-printed patient-specific soft tissue and bone phantoms for CT imaging. *Res Sq*. doi: 10.21203/RS.3.RS-2828218/V1.
- Metscher, B. D. (2009). MicroCT for developmental biology: a versatile tool for high-contrast 3D imaging at histological resolutions. *Dev Dyn* 238, 632–640. doi: 10.1002/DVDY.21857.
- Miki, K., and Clapham, D. E. (2013). Rheotaxis guides mammalian sperm. *Current Biology* 23, 443–452. doi: 10.1016/j.cub.2013.02.007.

- Mondal, M. A., Takagi, Y., Baba, S. A., and Hamano, K. I. (2017). Involvement of calcium channels and intracellular calcium in bull sperm thermotaxis. *J Reprod Dev* 63, 143. doi: 10.1262/JRD.2016-107.
- Mouse Embryo Assay for Assisted Reproduction Technology Devices | FDA (2021). *January*. Available at: <https://www.fda.gov/regulatory-information/search-fda-guidance-documents/mouse-embryo-assay-assisted-reproduction-technology-devices> [Accessed October 30, 2023].
- Murali, A., Lokhande, G., Deo, K. A., Brokesh, A., and Gaharwar, A. K. (2021). Emerging 2D nanomaterials for biomedical applications. *Materials Today* 50, 276–302. doi: 10.1016/J.MATTOD.2021.04.020.
- Muro, Y., Hasuwa, H., Isotani, A., Miyata, H., Yamagata, K., Ikawa, M., et al. (2016). Behavior of Mouse Spermatozoa in the Female Reproductive Tract from Soon after Mating to the Beginning of Fertilization. *Biol Reprod* 94. doi: 10.1095/BIOLREPROD.115.135368.
- Murphy, A. R., Wiwatpanit, T., Lu, Z., Davaadelger, B., and Kim, J. J. (2019). Generation of Multicellular Human Primary Endometrial Organoids. *J Vis Exp* 2019. doi: 10.3791/60384.
- Navarro-Serna, S., Dehesa-Etxebeste, M., Piñeiro-Silva, C., Romar, R., Lopes, J. S., López de Munaín, A., et al. (2022). Generation of Calpain-3 knock-out porcine embryos by CRISPR-Cas9 electroporation and intracytoplasmic microinjection of oocytes before insemination. *Theriogenology* 186, 175–184. doi: 10.1016/J.THERIOGENOLOGY.2022.04.012.

- Nava-Trujillo, H., and Rivera, R. M. (2023). Review: Large offspring syndrome in ruminants: current status and prediction during pregnancy. *Animal* 17 Suppl 1. doi: 10.1016/J.ANIMAL.2023.100740.
- Neues, F., and Epple, M. (2008). X-ray microcomputer tomography for the study of biomineralized endo- and exoskeletons of animals. *Chem Rev* 108, 4734–4741. doi: 10.1021/CR078250M.
- Neues, F., Goerlich, R., Renn, J., Beckmann, F., and Epple, M. (2007). Skeletal deformations in medaka (*Oryzias latipes*) visualized by synchrotron radiation micro-computer tomography (SRmicroCT). *J Struct Biol* 160, 236–240. doi: 10.1016/J.JSB.2007.08.010.
- Oliveira, R. G., Tomasi, L., Rovasio, R. A., and Giojalas, L. C. (1999). Increased velocity and induction of chemotactic response in mouse spermatozoa by follicular and oviductal fluids. *Reproduction* 115, 23–27. doi: 10.1530/JRF.0.1150023.
- Orabi, H., Saba, I., Rousseau, A., and Bolduc, S. (2017). Novel three-dimensional autologous tissue-engineered vaginal tissues using the self-assembly technique. *Transl Res* 180, 22–36. doi: 10.1016/J.TRSL.2016.07.019.
- Oskui, S. M., Diamante, G., Liao, C., Shi, W., Gan, J., Schlenk, D., et al. (2016). Assessing and Reducing the Toxicity of 3D-Printed Parts. *Environ Sci Technol Lett* 3, 1–6. doi: 10.1021/ACS.ESTLETT.5B00249/ASSET/IMAGES/MEDIUM/EZ-2015-002497_0006.GIF.

- París-Oller, E., Navarro-Serna, S., Soriano-Úbeda, C., Lopes, J. S., Matás, C., Ruiz, S., et al. (2021). Reproductive fluids, used for the in vitro production of pig embryos, result in healthy offspring and avoid aberrant placental expression of PEG3 and LUM. *J Anim Sci Biotechnol* 12. doi: 10.1186/S40104-020-00544-0.
- París-Oller, E., Soriano-Úbeda, C., Belda-Pérez, R., Sarriás-Gil, L., Lopes, J. S., Canha-Gouveia, A., et al. (2022). Reproductive fluids, added to the culture media, contribute to minimizing phenotypical differences between in vitro-derived and artificial insemination-derived piglets. *J Dev Orig Health Dis*. doi: 10.1017/S2040174421000702.
- Pérez-Cerezales, S., Laguna-Barraza, R., De Castro, A. C., Sánchez-Calabuig, M. J., Cano-Oliva, E., De Castro-Pita, F. J., et al. (2018). Sperm selection by thermotaxis improves ICSI outcome in mice. *Sci Rep* 8. doi: 10.1038/S41598-018-21335-8.
- Ralt, D., Goldenberg, M., Fetterolf, P., Thompson, D., Dor, J., Mashiach, S., et al. (1991). Sperm attraction to a follicular factor(s) correlates with human egg fertilizability. *Proceedings of the National Academy of Sciences* 88, 2840–2844. doi: 10.1073/PNAS.88.7.2840.
- Ramal-Sanchez, M., Valbonetti, L., Tsikis, G., Dubuisson, F., Blache, M. C., Labas, V., et al. (2019). Graphene oxide: A glimmer of hope for Assisted Reproductive Technology. *Carbon N Y* 150, 518–530. doi: 10.1016/J.CARBON.2019.05.055.

- Ravi, M., Paramesh, V., Kaviya, S. R., Anuradha, E., and Paul Solomon, F. D. (2015). 3D cell culture systems: advantages and applications. *J Cell Physiol* 230, 16–26. doi: 10.1002/JCP.24683.
- Rizos, D., Pintado, B., De La Fuente, J., Lonergan, P., and Gutiérrez-Adán, A. (2007). Development and pattern of mRNA relative abundance of bovine embryos cultured in the isolated mouse oviduct in organ culture. *Mol Reprod Dev* 74, 716–723. doi: 10.1002/MRD.20652.
- Rodriguez-Martinez, H. (2007). Role of the oviduct in sperm capacitation. *Theriogenology* 68 Suppl 1. doi: 10.1016/J.THERIOGENOLOGY.2007.03.018.
- Rodriguez-Martinez, H., Nicander, L., Viring, S., Einarsson, S., and Larsson, K. (1990). Ultrastructure of the uterotubal junction in preovulatory pigs. *Anat Histol Embryol* 19, 16–36. doi: 10.1111/J.1439-0264.1990.TB00875.X.
- Rojas, D., Della Pelle, F., Silveri, F., Ferraro, G., Fratini, E., and Compagnone, D. (2022). Phenolic compounds as redox-active exfoliation agents for group VI transition metal dichalcogenides. *Mater Today Chem* 26, 101122. doi: 10.1016/J.MTCHEM.2022.101122.
- Romar, R., Cánovas, S., Matás, C., Gadea, J., and Coy, P. (2019). Pig in vitro fertilization: Where are we and where do we go? *Theriogenology* 137, 113–121. doi: 10.1016/j.theriogenology.2019.05.045.
- Roy, S., Deo, K. A., Singh, K. A., Lee, H. P., Jaiswal, A., and Gaharwar, A. K. (2022). Nano-bio interactions of 2D molybdenum disulfide. *Adv Drug Deliv Rev* 187, 114361. doi: 10.1016/J.ADDR.2022.114361.

- Ruiz-Díaz, S., Mazzarella, R., Navarrete-López, P., Fernández-González, R., de Frutos, C., Maroto, M., et al. (2023). Bull spermatozoa selected by thermotaxis exhibit high DNA integrity, specific head morphometry, and improve ICSI outcome. *J Anim Sci Biotechnol* 14. doi: 10.1186/S40104-022-00810-3.
- Ruiz-Díaz, S., Oseguera-López, I., De La Cuesta-Díaz, D., García-López, B., Serres, C., Sanchez-Calabuig, M. J., et al. (2020). The Presence of D-Penicillamine during the In Vitro Capacitation of Stallion Spermatozoa Prolongs Hyperactive-Like Motility and Allows for Sperm Selection by Thermotaxis. *Animals (Basel)* 10, 1–18. doi: 10.3390/ANI10091467.
- Sakatani, M. (2017). Effects of heat stress on bovine preimplantation embryos produced in vitro. *J Reprod Dev* 63, 347. doi: 10.1262/JRD.2017-045.
- Sakatani, M., Kobayashi, S. I., and Takahashi, M. (2004). Effects of heat shock on in vitro development and intracellular oxidative state of bovine preimplantation embryos. *Mol Reprod Dev* 67, 77–82. doi: 10.1002/MRD.20014.
- Shimabukuro, M., Hayashi, K., Kishida, R., Tsuchiya, A., and Ishikawa, K. (2022). Surface functionalization with copper endows carbonate apatite honeycomb scaffold with antibacterial, proangiogenic, and pro-osteogenic activities. *Biomaterials advances* 135. doi: 10.1016/J.BIOADV.2022.212751.
- Smits, K., De Coninck, D. I. M., Van Nieuwerburgh, F., Govaere, J., Van Poucke, M., Peelman, L., et al. (2016). The Equine Embryo Influences Immune-Related Gene Expression in the Oviduct. *Biol Reprod* 94. doi: 10.1095/BIOLREPROD.115.136432.

- Soriano-Úbeda, C., García-Vázquez, F. A., Romero-Aguirregomezcorta, J., and Matás, C. (2017). Improving porcine in vitro fertilization output by simulating the oviductal environment. *Scientific Reports* 2017 7:1 7, 1–12. doi: 10.1038/srep43616.
- Soto-Heras, S., Sakkas, D., and Miller, D. J. (2023). Sperm selection by the oviduct: perspectives for male fertility and assisted reproductive technologies†. *Biol Reprod* 108, 538–552. doi: 10.1093/BIOLRE/IOAC224.
- Stojanov, T., and O'Neill, C. (2001). In Vitro Fertilization Causes Epigenetic Modifications to the Onset of Gene Expression from the Zygotic Genome in Mice. *Biol Reprod* 64, 696–705. doi: 10.1095/BIOLREPROD64.2.696.
- Sykes, M. (2022). Developing pig-to-human organ transplants: Recent advances raise hope for a promising solution to the transplant organ shortage. *Science* 378, 135. doi: 10.1126/SCIENCE.ABO7935.
- Taylor, U., Rath, D., Zerbe, H., and Schuberth, H. J. (2008). Interaction of intact porcine spermatozoa with epithelial cells and neutrophilic granulocytes during uterine passage. *Reprod Domest Anim* 43, 166–175. doi: 10.1111/J.1439-0531.2007.00872.X.
- Teves, M. E., Barbano, F., Guidobaldi, H. A., Sanchez, R., Miska, W., and Giojalas, L. C. (2006). Progesterone at the picomolar range is a chemoattractant for mammalian spermatozoa. *Fertil Steril* 86, 745–749. doi: 10.1016/j.fertnstert.2006.02.080.
- Tung, C. K., Ardon, F., Fiore, A. G., Suarez, S. S., and Wu, M. (2014). Cooperative roles of biological flow and surface topography in guiding sperm migration

- revealed by a microfluidic model. *Lab Chip* 14, 1348–1356. doi: 10.1039/C3LC51297E.
- Viana, J. H. (2022). 2021 Statistics of embryo production and transfer in domestic farm animals A new milestone has been reached: Transfers of IVP embryos were over one million worldwide. *Embryo Technology Newsletter* 40.
- Wang, F., Lv, F. Y., Liu, K. L., Li, Z. H., Niu, S., Zhang, Y. Y., et al. (2021). Synthesis of MoS₂ nanosheets drug delivery system and its drug release behaviors. *Ferroelectrics* 578, 31–39. doi: 10.1080/00150193.2021.1902761.
- Wang, H., Bocca, S., Anderson, S., Yu, L., Rhavi, B. S., José Horcajadas, et al. (2013). Sex steroids regulate epithelial-stromal cell cross talk and trophoblast attachment invasion in a three-dimensional human endometrial culture system. *Tissue Eng Part C Methods* 19, 676–687. doi: 10.1089/TEN.TEC.2012.0616.
- Watson, D. E., Hunziker, R., and Wikswo, J. P. (2017). Fitting tissue chips and microphysiological systems into the grand scheme of medicine, biology, pharmacology, and toxicology. *Exp Biol Med* 242, 1559. doi: 10.1177/1535370217732765.
- Withers, P. J., Bouman, C., Carmignato, S., Cnudde, V., Grimaldi, D., Hagen, C. K., et al. (2021). X-ray computed tomography. *Nature Reviews Methods Primers* 2021 1:1 1, 1–21. doi: 10.1038/s43586-021-00015-4.
- Xiao, S., Coppeta, J. R., Rogers, H. B., Isenberg, B. C., Zhu, J., Olalekan, S. A., et al. (2017). A microfluidic culture model of the human reproductive tract and 28-day menstrual cycle. *Nat Commun* 8. doi: 10.1038/ncomms14584.

- Xiao, W., Yu, M., Yuan, Y., Liu, X., and Chen, Y. (2022). Thermotaxis of mammalian sperm. *Mol Hum Reprod* 28. doi: 10.1093/MOLEHR/GAAC027.
- Yamaguchi, R., Muro, Y., Isotani, A., Tokuhiko, K., Takumi, K., Adham, I., et al. (2009). Disruption of ADAM3 impairs the migration of sperm into oviduct in mouse. *Biol Reprod* 81, 142–146. doi: 10.1095/BIOLREPROD.108.074021.
- Yániz, J. L., Carretero, T., Recreo, P., Arceiz, E., and Santolaria, P. (2014). Three-dimensional architecture of the ovine oviductal mucosa. *Anat Histol Embryol* 43, 331–340. doi: 10.1111/AHE.12078.
- Yaniz, J. L., Lopez-Gatius, F., and Hunter, R. H. F. (2006). Scanning Electron Microscopic Study of the Functional Anatomy of the Porcine Oviductal Mucosa. *Anat Histol Embryol* 35, 28–34. doi: 10.1111/J.1439-0264.2005.00634.X.
- Yániz, J. L., Lopez-Gatius, F., Santolaria, P., and Mullins, A. K. J. (2000). Study of the Functional Anatomy of Bovine Oviductal Mucosa. *Anat Rec* 260, 268–278. doi: 10.1002/1097-0185.
- Yoshimoto, Y., Nishie, T., Ito, S., Kobayashi, Y., Yamamoto, Y., Okuda, K., et al. (2017). Adrenomedullin regulates the speed of oviductal fluid flow in cattle. *Mol Reprod Dev* 84, 712–718. doi: 10.1002/MRD.22852.
- Zhou, X., Sun, H., and Bai, X. (2020). Two-Dimensional Transition Metal Dichalcogenides: Synthesis, Biomedical Applications and Biosafety Evaluation. *Front Bioeng Biotechnol* 8, 236. doi: 10.3389/FBIOE.2020.00236/XML/NLM.

Zou, W., Zhang, X., Zhao, M., Zhou, Q., and Hu, X. (2017). Cellular proliferation and differentiation induced by single-layer molybdenum disulfide and mediation mechanisms of proteins via the Akt-mTOR-p70S6K signaling pathway. *Nanotoxicology* 11, 781–793. doi: 10.1080/17435390.2017.1357213.

The background of the slide features a series of fluid, overlapping, and translucent blue and white lines that create a sense of motion and depth, resembling smoke or liquid waves. These lines are concentrated on the left side and flow towards the right, framing the text.

Objectives

Objectives

As reviewed in the introduction, the oviduct stands as a crucial organ for successful reproduction. Our overarching goal is to engineer a 3D-printed device capable of mimicking the oviduct's functionality, thereby improving the *in vitro* production. This goal necessitates a systematic approach:

- Firstly, we delve into the assessment of the compatibility of various 3D printing materials with gametes (Chapter I).
- Subsequently, our exploration extends to the evaluation of non-physiological materials that could be employed to functionalize the final device, and their potential on capacitation process (Chapter II).
- Finally, we aim to gathering anatomical data from the oviduct, serving as a crucial reference for the creation of the 3D-printed device, allowing us the mimic as well the architecture of the organ (Chapter III).

The background of the page features abstract, flowing, and overlapping lines in shades of light blue and white, creating a sense of movement and depth. These lines are more prominent on the left side and fade towards the right.

CHAPTER I

Assessing the Suitability of 3D Printing Materials in the Context of In Vitro Fertilization (IVF)

Manuscript 1.

Advancing Bovine In Vitro Fertilization through 3D Printing: the effect of the 3D printed materials.

*Manuscript published in Frontiers in Bioengineering and Biotechnology,
Volume 11, Oct 2023
doi.org/10.3389/FBIOE.2023.1260886*

Ramses Belda-Perez^{1,2}, Sonia Heras², Costanza Cimini¹, Jon Romero-Aguirregomezcorta², Luca Valbonetti^{1,4}, Alessia Colosimo¹, Bianca Maria Colosimo³, Silvia Santoni³, Barbara Barboni¹, Nicola Bernabò^{1,4}, Pilar Coy^{2*}

¹ Department of Biosciences and Technology for Food, Agriculture and Environment, University of Teramo, 64100 Teramo, Italy.

² Physiology of Reproduction Group, Department of Physiology, Faculty of Veterinary Medicine, International Excellence Campus for Higher Education and Research (Campus Mare Nostrum), University of Murcia, 30100 Murcia, Spain.

³ Department of Mechanical Engineering, Politecnico di Milano, Via Privata Giuseppe La Masa, 1, Milano 20156, Italy.

⁴ Institute of Biochemistry and Cell Biology (CNRIBBC/EMMA/Infrafrontier/IMPC), National Research Council, 00015 Rome, Italy.

*** Correspondence: Pilar Coy, pcoy@um.es**

Keywords: IVF, bovine, embryo culture, biomaterials, PCL, PEGDA, PLA.

Abstract

Nowadays there is an increasing demand for assisted reproductive technologies due to the growth of infertility problems. Naturally, fertilization occurs in the oviduct, where the oviductal epithelial cells (OECs) secrete many molecules that affect the embryo's metabolism and protect it from oxidative stress. When the OECs are grown in 3D culture systems, they maintain a great part of their functional characteristics, making them an excellent model for in vitro fertilization (IVF) studies. In this work, we aimed to evaluate the suitability of different 3D-printing processes in conjunction with the

corresponding set of commercially available biomaterials: extrusion-based processing using polylactic acid (PLA) and polycaprolactone (PCL) and stereolithography or digital-light processing using polyethylene-glycol-diacrylate (PEGDA) with different stiffness (PEGDA500, PEGDA200, PEGDA PhotoInk). All the 3D-printed scaffolds were used to support IVF process in a bovine embryo assay. Following fertilization, embryo development and quality were assessed in terms of cleavage, blastocyst rate at days 7 and 8, total cell number (TCN), inner cell mass/trophectoderm ratio (ICN/TE), and apoptotic cell ratio (ACR). We found a detrimental effect on cleavage and blastocyst rates when the IVF was performed on any medium conditioned by most of the materials available for digital-light processing (PEGDA200, PEGDA500). The observed negative effect could be possibly due to some leaked compound used to print and stabilize the scaffolds, which was not so evident however with PEGDA PhotoInk. On the other hand, all the extrusion-based processable materials did not cause any detrimental effect on cleavage or blastocyst rates. The principal component analysis reveals that embryos produced in presence of 3D-printed scaffolds produced via extrusion exhibit the highest similarity with the control embryos considering cleavage, blastocyst rates, TCN, ICN/TE and ACR per embryo. Conversely, all the photo-cross linkable materials or medium conditioned by PLA, lead to the highest dissimilarities. Since the use of PCL scaffolds, as well as its conditioned medium, bring to embryos that are more similar to the control group. Our results suggest that extrusion-based 3D printing of PCL could be the best option to be used for new IVF devices, possibly including the support of OECs, to enhance bovine embryo development.

1. Introduction

In recent years, the demand for artificial reproductive technologies (ARTs) is growing due to an increase in infertility, which already affects 15% of couples of

reproductive age and continues to rise every year (Assidi, 2022). The high number of infertile couples, together with reproductively healthy ones seeking to prevent genetic diseases in their offspring, have contributed to an increase in the proportion of children born through ARTs in Europe, from 2.3% (De Geyter et al., 2020) to 3.5% (Gliozheni et al., 2022) in just three years. In human reproduction, a popular technique is intracytoplasmic sperm microinjection (ICSI) (Haddad et al., 2021), in which a sperm selected by the embryologist is directly injected into the ooplasm. With this technique, positive results are obtained despite the low motility of the sample or immaturity of the sperm (Palermo et al., 1996). However, there are main concerns about ICSI for its invasiveness since it involves the piercing of the membrane. As a result, it could induce spindle damage or the introduction of contaminating external material (Verpoest and Tournaye, 2009). Another option is *in vitro* fertilization (IVF), where the oocyte and sperm are co-cultured in the same plate for a certain period so that penetration occurs without human intervention. Although IVF has been associated with an increased risk of congenital diseases or developmental delay (Waynforth, 2018), this method is considered the most physiological, since the spermatozoa penetrates the oocyte by itself. In addition, the scientific community is increasingly concerned about the potential long-term effects of ARTs (Sunde et al., 2016; Fleming et al., 2018). It is known that suboptimal *in vitro* conditions influence the epigenetic reprogramming of embryos (Canovas et al., 2017; Ferraz et al., 2018b). In humans, it has been suggested that ARTs may be related to a higher risk of imprinting disorders such as Beckwith-Wiedemann (Maher et al., 2003) or Angelman syndrome (Manipalviratn et al., 2009), although in the latter, it is very difficult to understand whether these disorders are related to the couple's infertility-subfertility problems or to ARTs (Pérez-Aytés et al., 2017). Moreover, differences in growth in

ARTs-derived offspring in pig (París-Oller et al., 2022) and human (Ceelen et al., 2009) have also been observed.

All these above-mentioned problems could be solved by mimicking the physiological environment (i.e., the oviduct). In this organ, the oviductal epithelial cells (OECs) produce a large number of molecules that can protect embryos from oxidative stress and modify their metabolism (Ménézo et al., 2015). Indeed, two alternative strategies can be used to replicate natural conditions: i) the use of reproductive fluid as a culture media supplement (Canovas et al., 2017) and ii) co-culture of gametes and embryos with oviductal epithelial cells (OECs) (Ferraz et al., 2018b). Two-D cultures (where cells grow in a monolayer) are the most popular for studying the physiology of the oviduct and have been used in IVF and embryo culture in several species (Kölle et al., 2020), probably due to their high reproducibility, low cost, or ease of handling (Costa et al., 2016). Indeed, when these cultures are used during embryo *in vitro* production (IVP), there is an enhanced developmental rate of bovine embryos (Abe and Hoshi, 1997). However, it has been shown that this 2D culture method is not the best suited for fertilization studies since the cells dedifferentiate and lose their polarity, morphology, secretory capacity, and ciliary activity (Ferraz et al., 2017). On the contrary, when cultured in 3D, these cells retain much of their natural features (Pennarossa et al., 2021), making them a better model by keeping gene and metabolic expression closer to the *in vivo* context than their 2D counterparts (Anton et al., 2015). When the physiological environment is mimicked using microfluidics culture during IVF, it has been shown that the epigenetic reprogramming of bovine embryos is more similar to *in vivo* derived embryos (Ferraz et al., 2018b). All these data are indicators of the limitations of the 2D culture methods, thus encouraging researchers to move towards 3D culture systems to improve the quality of IVP embryos. To achieve this goal, it is crucial to construct a 3D

device in which it is possible to co-culture differentiated OECs with gametes/zygotes. As a matter of fact, despite the well-known relevance the oviduct in gamete maturation/activation, fertilization, and early embryo development, only a few bioengineering studies have been focused on these female reproductive structures, so far (Kessler et al., 2015; Xiao et al., 2017; Ferraz et al., 2018b, 2020; Francés-Herrero et al., 2022).

Nowadays, a great variety of 3D printable biomaterials are commercially available (Santoni et al., 2021). One popular biomaterial is polylactic acid (PLA), a promising biodegradable polymer that can be produced from renewable sources like sugarcane (Li et al., 2020). PLA-scaffolds have excellent biocompatibility (Shilov et al., 2022), and have been used for medical purposes in bone (Diomedea et al., 2018; Velioglu et al., 2019) and cartilage regeneration (Rosenzweig et al., 2015). Together with PLA, polycaprolactone (PCL) is the most common biodegradable synthetic polymer used in tissue engineering (Arif et al., 2022), and it has already been employed for bone (Rumiński et al., 2018), liver (Huang et al., 2007) or skin (Ghosal et al., 2017) regenerative purposes. Similarly, photo-cross-linkable hydrogels are widely used, due to their tunable mechanical properties and to their capability to mimic native extracellular matrix (Lim et al., 2020; Zhang et al., 2022a). In fact, when viscoelasticity and stiffness properties of biomaterials can be tuned, this can represent an additional advantage to create scaffolds mimicking the native tissues with high resolution and complex architecture. Among them, polyethylene glycol diacrylate (PEGDA) is a synthetic polymer approved by the Food and Drug Administration (FDA) (Kim et al., 2022) that has been used in variegate studies, from bone (Rajabi et al., 2023) to cartilage (Zhang et al., 2022b) or muscle (Vannozzi et al., 2018) regeneration. In addition, PEGDA mechanical properties can be modulated by varying the molecular weight of the polymer

(Nguyen et al., 2012) and it can be functionalized with cell binding motifs to enable cell adhesion (Della Sala et al., 2020). Despite the wide range of biomedical applications in which these materials have been used, no studies have been carried out so far to test the feasibility of these materials to construct a 3D-printed device for IVF.

Because of this lack of information, our study aims to evaluate the biocompatibility of different materials (PLA, PCL, PEGDA500, PEGDA200, and PEGDA PhotoInk) to support IVF, using bovine embryo development parameters (cleavage, blastocyst rates at day 7 and 8). In addition, to assess the quality of the *in vitro* produced embryos, we examined three fundamental parameters (Wydooghe et al., 2014) the cell number/embryo (TCN), the inner cell mass/trophectoderm (ICM/TE) ratio, and the apoptotic cell ratio (ACR).

2. Materials and methods

2.1. Experimental design

To evaluate the feasibility of different materials (PLA, PCL, PEGDA500, PEGDA200, and PEGDA PhotoInk) to support IVF and their effects on bovine embryo development, 3 experimental groups were settled for each of the materials tested:

- Control group: the IVF was performed, without having any contact with the materials (Figure 1A).

- Rinse group: to assess if these materials could release some unknown substances that could have adverse effects in IVF or embryo development, the IVF was carried out in a Fert-TALP medium conditioned by the scaffold of each material during 24h (Figure 1B).

- Scaffold group: prior to fertilization, the same scaffold used to condition the IVF media, was transferred to another well with new media and the IVF was performed in the presence of the scaffold (Figure 1C).

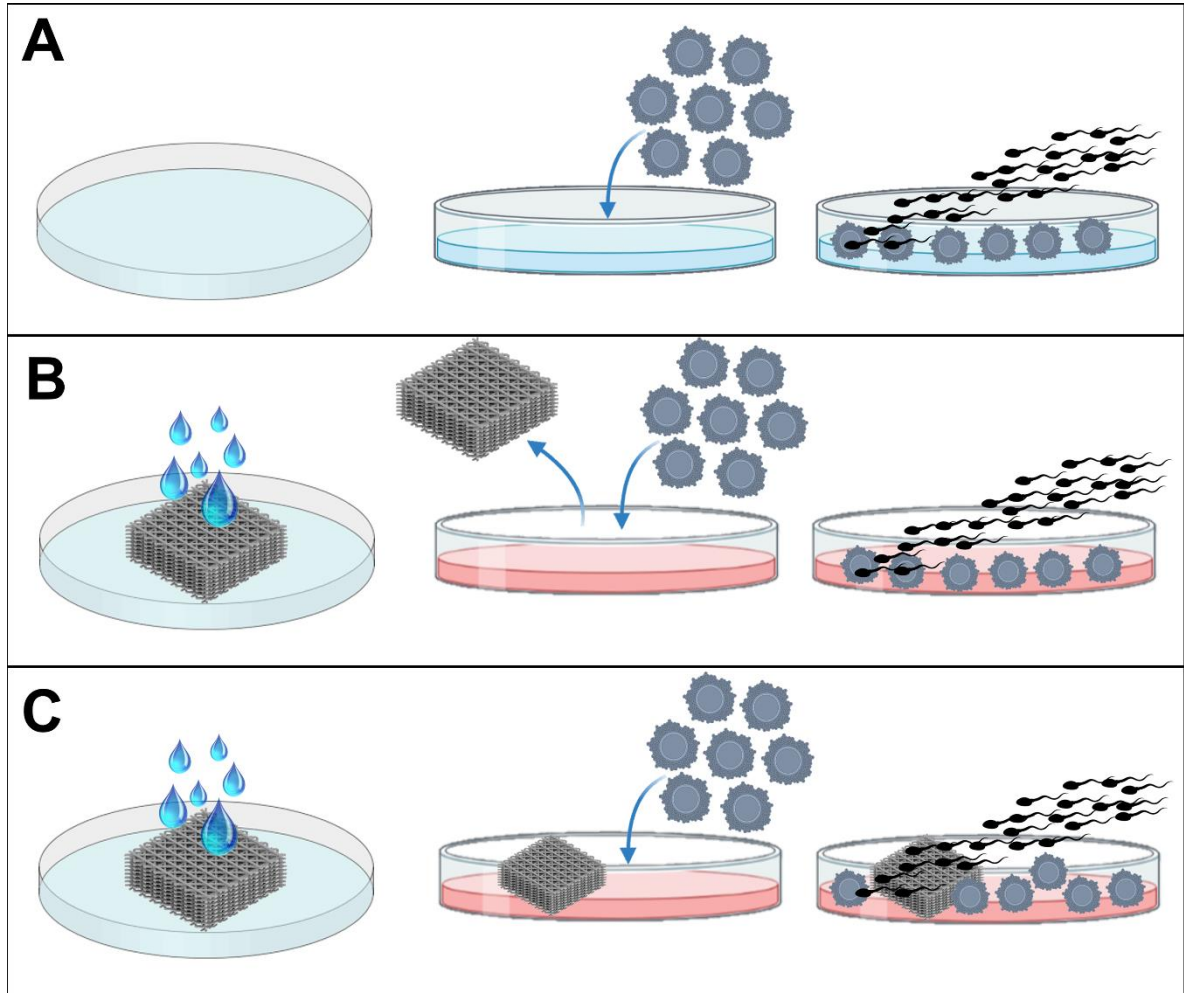


Figure 1. Experimental design. A) IVF in normal Fert-TALP medium, without conditioning or scaffold, B) IVF in Fert-TALP medium conditioned by scaffold for 24h, and C) IVF performed in presence of the rinsed scaffold.

The number of oocytes was $n = 2892$ distributed for each group as follows: $n = 585$ for control, $n = 297$ for scaffold PCL, $n = 293$ for rinse PCL, $n = 196$ for scaffold PLA, $n = 201$ for rinse PLA, $n = 131$ for scaffold PEGDA500, $n = 143$ for rinse PEGDA500, $n = 248$ for scaffold PEGDA200, $n = 256$ for rinse PEGDA200, $n = 269$ for scaffold PEGDA PhotoInk, $n = 273$ for rinse PEGDA PhotoInk. We carried out 11 replicates, the control group was present in every single replicate, while PCL material was present in 6 of them, the PLA

material in 4, the PEGDA500 material in 3, and the PEGDA200 and PEGDA PhotoInk materials were present in 5 replicates.

2.2. Culture media reagents.

All chemicals were purchased from Sigma-Aldrich Quimica, S.A. (Madrid, Spain) unless otherwise indicated.

2.3. 3D Printing Materials

3D printed structures were produced to test the biocompatibility of the material and the effect of the 3D architecture on cells. All structures were designed using SolidWorks software (Dassault Systèmes SE, Vélizy-Villacoublay, France) and exported as an STL file. Depending on the printer used, the STL file was directly loaded on the printer or sliced using PrusaSlicer (Prusa Research, Prague, Czech Republic) to obtain the gcode file.

The 3D models were printed using different materials with different stiffness (Table 1) and 3D printing methods. PLA filaments were purchased from Sharebot, Italy; PCL pellet ($M_n=50.000$ g/mol), PEGDA200, PEGDA500, and PEGDA Photoink were purchased from Cellink, Sweden. PLA filaments were printed via extrusion-based processing (FFF, Fused Filament Fabrication) using a Sharebot 42 3D printer (Sharebot, Italy) with a 0.4 mm diameter nozzle. PCL (CELLINK, Gothenburg, Sweden) structures were 3D printed using a BioX, a pneumatic extrusion-based 3D bioprinter (CELLINK, Gothenburg, Sweden) using a 0.4 mm nozzle, a pressure of 180 kPa, a velocity in a range 15-20 mm/s, and a temperature of 180°C according to suggested printing protocol. PEGDA500 Photoink, PEGDA200 Photoink, and PEGDA Photoink hydrogels (listed in decreasing order of stiffness) were 3D printed using a LumenX bioprinter based on

stereolithography via digital light processing (CELLINK, Gothenburg, Sweden) considering a 50 μm layer height for the slicing and 20 mWatt/cm² power, 3x as first layer time scale factor, and a variable time of 2 s/3 s/12 s depending on the formulation, respectively, according to printing protocol.

Table 1. Hardness of different materials (PLA, PCL, PEGDA500, PEGDA200 and PEGDA PhotoInk) expressed by Young's modulus.

Material	Young modulus	Source
PLA	3000 MPa	Manufacturer (Sharebot)
PCL	370 MPa	Scocozza et al., 2023
PEGDA500	500 KPa	Manufacturer (Cellink)
PEGDA200	200 KPa	Manufacturer (Cellink)
PEGDA PhotoInk	50 KPa	Manufacturer (Cellink)

2.4. Material sterilization

PLA, PCL, PEGDA500, PEGDA200, and PEGDA PhotoInk were sterilized following the manufacturer's instructions. Briefly, they were immersed in 70% ethanol for 5 min, then submerged twice in PBS (30 min each), and finally washed for 24 h with Fert-TALP (Parrish et al., 1986) culture medium supplemented con 175 U/mL heparin, 6 mg/mL BSA, 0.20 mM Na-pyruvate and 50 $\mu\text{g/mL}$ gentamicin. Fert-TALP medium consisted of 114 mM sodium chloride, 3.2 mM potassium chloride, 0.3 Mm sodium phosphate monobasic monohydrate, 10 mM sodium lactate, 2.0 mM calcium chloride dihydrate, 0.5 mM magnesium chloride hexahydrate and 25 mM sodium bicarbonate.

2.5. *in vitro* maturation

Ovaries from one year old cows were transported from the local slaughterhouse to the laboratory in physiological saline solution (0.9% w/vol) supplemented with 100 mg/L kanamycin sulfate at 38.5°C within two hours of slaughter. Once in the laboratory, the ovaries were washed with a 0.04% cetrimide solution and twice with saline. In vitro maturation was performed as previously described (Lopes et al., 2019) with minor

modifications. Briefly, follicles between 2- and 8-mm diameter were aspirated. Only Cumulus-Oocyte Complexes (COCs) with at least 3 cumulus cell layers and with a homogeneous cytoplasm were selected and then washed 3 times in handling medium, consisting of TCM 199 supplemented with 4.2 mM sodium bicarbonate, 10 mM HEPES, 2 mM glutamine, 1% w/v polyvinyl alcohol, 50 IU/mL penicillin and 50 µg/mL streptomycin. Subsequently, COCs were washed once in a maturation medium, consisting of TCM 199 (with Hanks' salts) supplemented with 4.2 mM sodium bicarbonate, 2 mM glutamine, 50 IU/mL gentamicin, 10% v/v of bovine follicular fluid (BFF, NaturARTs-BFF, Embryocloud, Murcia, Spain), 10 IU/mL equine chorionic gonadotropin (Foligon, Intervet International BV, Netherlands) and 10 IU/mL human chorionic gonadotropin (Veterin Corion, Divasa Farmavic, Spain) and incubated in 500 µl of maturation medium in groups of 50-55 COCs in a 4 well dish at 38.5°C with a humidity-saturated atmosphere with 5% CO₂ for 22 h.

2.6. In vitro fertilization

After maturation and 30 min before IVF, the oocytes were washed once in Fert-TALP medium supplemented with 175 U/mL heparin, 6 mg/mL BSA, 0.20 mM Na-pyruvate and 50 µg/mL gentamicin. For fertilization, frozen-thawed semen from three bulls of proven fertility was used. The straw was thawed in a water bath at 38.5°C for 30 sec. Once thawed, a Bovipure gradient (Nidacon, Sweden) was performed, centrifuging at 300 g for 10 min and removing the supernatant. Before insemination, sperm cells were washed once in modified Sperm-TALP medium (Parrish et al., 1988) (114 mM sodium chloride, 3.2 mM potassium chloride, 0.3 Mm sodium phosphate monobasic monohydrate, 10 mM sodium lactate, 2.0 mM calcium chloride dihydrate, 0.5 mM magnesium chloride hexahydrate, 25 mM sodium bicarbonate and 10mM HEPES) supplemented with 6mg/mL BSA, 1.0mM Na-pyruvate and 50 µg/mL gentamicin, by

centrifuging at 300 g during 3 min and removing the supernatant. Insemination was performed in medium conditioned by the scaffold, in the presence of scaffold and in fresh medium, in a final concentration of 1×10^6 spz/mL. Oocytes were coincubated with the spermatozoa for 22h at 38.5°C with a humidity-saturated atmosphere with 5% CO₂.

2.7. Embryo culture

Twenty-two hours after insemination, the presumptive zygotes were moved into a 15 mL Falcon tube with a handling medium and vortexed for 4 min for decumulation. Zygotes were then washed once in Synthetic Oviductal Fluid medium (SOF) (Holm et al., 1999) and transferred into 50 µl microdrops of the same media covered by paraffin oil (Nidoil, Nidacon) in groups of 25 embryos per drop and cultured during 8 days at 38.5°C, 5% CO₂ and 5% O₂. Evaluation of embryo development occurred 48h post insemination as the percentage of cleaved embryos out of presumptive zygotes, and at 7 and 8 days post insemination (dpi). In this study, only embryos with quality 1-2 according to the criteria of the International Embryo Technology Society (IETS) (summarized in Bó and Mapletoft, 2013) have been considered.

2.8. Differential apoptotic staining

To assess the total cell number (TCN), the inner cell mass/trophectoderm ratio (ICM/TE), and the apoptotic cell ratio (ACR), differential staining was performed as described previously (Wydooghe et al., 2011) with minor modifications. Briefly, day 8 blastocysts were fixed in 4% paraformaldehyde for 20 min at RT and conserved in 2% paraformaldehyde at 4°C until the moment of staining. The embryos were permeabilized with 0.5% Triton-X and 0.05% Tween in PBS overnight at 4°C. On the second day, blastocysts were washed 3 times for 10 minutes in PBS containing 0.5% BSA (washing solution). Subsequently, the DNA of the cells was denatured with 2N HCl for 20 minutes followed by 100Mm trisHCL (pH=8.5) for 10min. After denaturation, the embryos were

washed three times in washing solution and transferred to blocking solution (10% goat serum and 0.05% tween in PBS) overnight at 4°C. After blocking, the blastocysts were washed 3 times in washing solution and incubated in ready-to-use mouse anti-CDX2 primary antibody (Biogenex, San Ramon, USA) for overnight at 4°C, while two embryos remained in blocking solution as negative control. After this incubation, test embryos were washed 3 times in washing solution and incubated 1:500 dilution of rabbit anti - active caspase-3 primary antibody (Cell Signaling Technology, Leiden, Netherlands) in blocking solution overnight at 4°C. On the last day, all blastocysts (negative and test) were washed three times for 10 min in washing solution, and incubated with 1:100 goat anti-mouse TRICT (Abcam, Cambridge, UK) in blocking solution for 1 h at RT. After another three-wash step, the embryos were incubated in 1:200 goat anti-rabbit FITC secondary antibody (Abcam, Cambridge, UK) in blocking solution for 1 h at RT. Finally, the blastocysts were washed, stained with Hoechst 33342 for 15 min, washed for the last time, mounted in Dabco (1,4-Diazabicyclo[2.2.2]octane solution), and evaluated under fluorescence microscopy (Eclipse Ti Series, Nikon, Japan). A representative image of embryo was taken using Nikon A1r laser confocal scanning microscope.

2.9. Statistical analysis

For statistical analysis, GraphPad Prism 8 Software (La Jolla, CA, USA) was used. Data were checked for normal distribution with Shapiro-Wilk normality test prior to perform the comparison with parametric tests. In all cases the differences among groups were considered statistically significant when $p < 0.05$.

For Principal Component Analysis, Past 4.13 (Oslo, Norway) was used to evaluate the effect of different materials on Cleavage, blastocyst rate at day 7, blastocyst rate at day 8, TCN, ICM/TE and AC ratio.

3. Results

3.1. Effect of the different materials on cleavage

We observed a significant lower cleavage rate in rinse PEGDA500 ($45\pm15\%$), scaffold PEGDA500 ($50\pm23\%$), and rinse PEGDA200 ($63\pm8\%$) groups vs CTRL group ($84\pm8\%$), while we did not observe any difference between the cleavage rate of rinse PCL ($82\pm10\%$), scaffold PCL ($80\pm10\%$), rinse PLA ($77\pm7\%$), scaffold PLA ($81\pm6\%$), scaffold PEGDA200 ($73\pm11\%$), rinse PEGDA PhotoInk ($71\pm14\%$) or scaffold PEGDA PhotoInk ($77\pm10\%$) compared to the control (Figure 2).

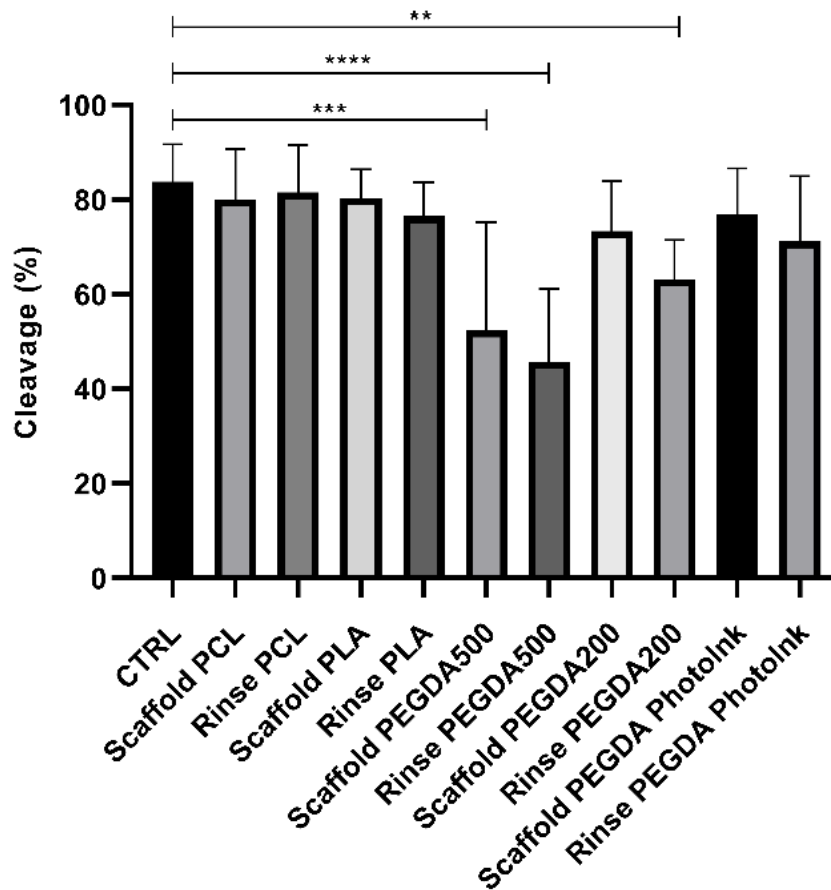


Figure 2. Effect of different materials on the percentage of cleaved embryos. The histograms show the cleavage rate when the IVF was performed with an unconditioned medium (CTRL), with medium conditioned by each material (rinse groups) or when different scaffolds were present (scaffold groups). The data show significant differences ($p<0.05$) in CTRL vs Scaffold PEGDA500, CTRL vs Rinse PEGDA500 and CTRL vs Rinse PEGDA200. The data are presented as the mean \pm SD of 11 independent experiments. Data were analyzed using Dunnett's test. ** $P<0.01$, *** $P<0.005$, **** $P<0.0001$ versus control.

3.2. Effect of the different materials on blastocyst rate at Day 7

Compared to the CTRL group ($23\pm6\%$), blastocyst rates were significantly lower ($p<0.05$) in the rinse PEGDA500 ($4\pm4\%$), scaffold PEGDA500 ($7\pm7\%$), and rinse PEGDA200 ($8\pm7\%$) groups on day 7 (Figure 3). The scaffold PCL group had a $25\pm10\%$ blastocyst yield, which was not statistically different ($p>0.05$) vs the CTRL, while scaffold PLA ($17\pm7\%$), scaffold PEGDA200 ($14\pm7\%$), and scaffold PEGDA PhotoInk ($16\pm4\%$) showed similar blastocyst rates. On the other hand, rinse groups have decreased embryo development compared to control but not significantly less than their scaffold groups, being $18\pm4\%$ for rinse PCL, $13\pm4\%$ for rinse PLA, and $16\pm7\%$ for rinse PEGDA PhotoInk (Figure 3).

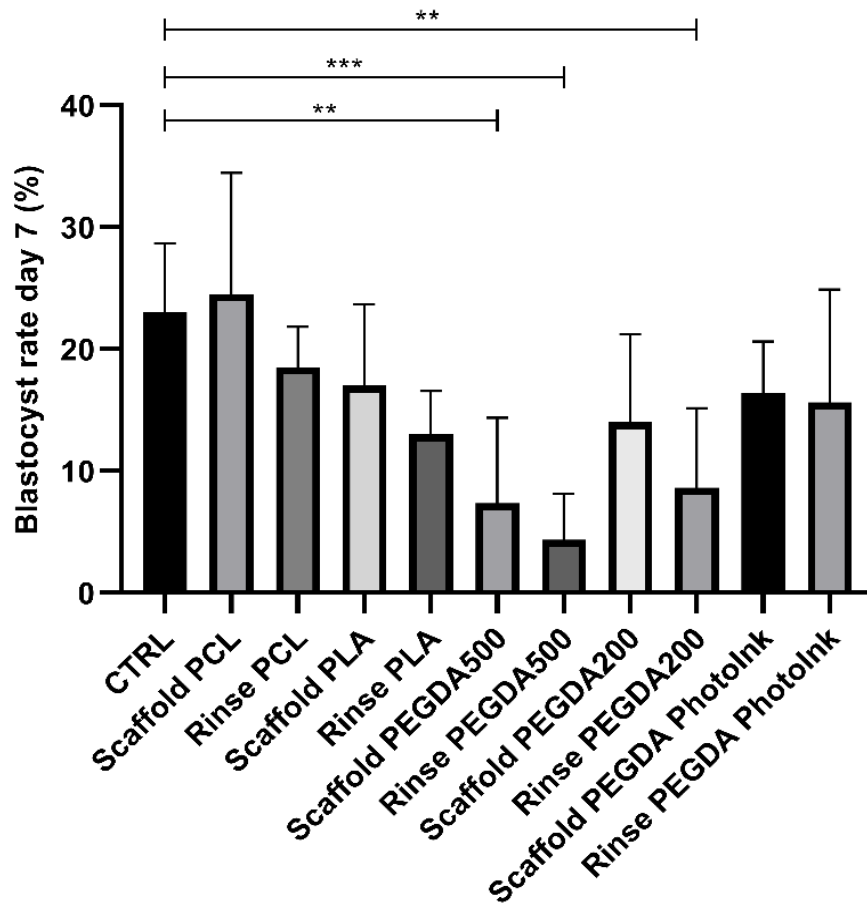


Figure 3. Effect of different materials on blastocyst rate at day 7. The histograms show the blastocyst rate at day 7 when the IVF was performed with unconditioned medium (CTRL), with medium conditioned by each material (rinse groups) or when different scaffolds were present (scaffold groups). The data show significant differences ($p<0.05$) in CTRL vs Scaffold PEGDA500, CTRL vs Rinse PEGDA500 and CTRL vs Rinse PEGDA200. The data are presented as the mean of 11 independent experiments. Data were analyzed using the Dunnett's test. ** $P<0.01$, *** $P<0.005$ versus control.

3.3. Effect of the different materials on blastocyst rate at Day 8

Blastocyst rate at day 8 were significantly lower in rinse PEGDA500 ($6\pm6\%$), scaffold PEGDA500 ($10\pm9\%$), and rinse PEGDA200 ($12\pm9\%$) groups vs CTRL group ($25\pm6\%$). On the scaffold's groups, we had not statistical differences ($p>0.05$) for blastocyst yield in the scaffold PCL group with $29\pm8\%$, while the scaffold PLA ($14\pm2\%$), scaffold PEGDA200 ($20\pm9\%$) and scaffold PhotoInk ($19\pm5\%$) groups showed similar blastocyst rates. In addition, rinse groups did not present significant differences vs the CTRL, being the blastocyst rates $22\pm6\%$ for rinse PCL, $14\pm2\%$ for rinse PLA, and $17\pm11\%$ for rinse PEGDA PhotoInk (Figure 4).

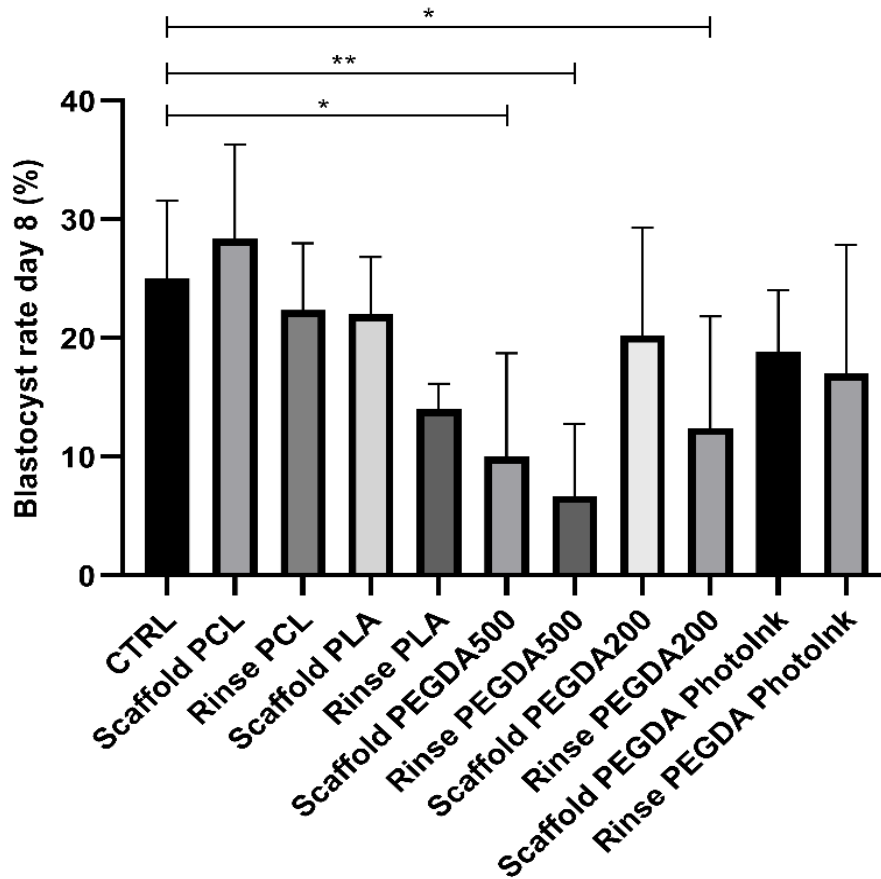


Figure 4. Effect of different materials scaffolds on blastocyst rate at day 8. The histograms show the blastocyst rate at day 8 when the IVF was performed with unconditioned medium (CTRL), with medium conditioned by each material (rinse groups) or when different scaffolds were present (scaffold groups). The data shows significant differences ($p<0.05$) in CTRL vs Scaffold PEGDA500, CTRL vs Rinse PEGDA500 and CTRL vs Rinse PEGDA200. The data are presented as mean of 11 independent experiments. Data were analyzed using the Dunnett's test. * $P<0.05$, ** $P<0.01$ versus control.

3.4. Principal component analysis of the different materials considering all variables studied.

The total cell number, the trophectoderm and the apoptosis were evaluated under fluorescence microscopy (Figure 5) and the ICM/TE ratio and ACR were calculated. Since we studied several biological factors (cleavage, blastocyst rate at day 7 and 8, TCN, ICM/TE ratio and ACR), we used the Principal Component Analysis (PCA) as a multivariable analysis to simplify the data analysis and interpretation by reducing the complexity (Jolliffe and Cadima, 2016). This analysis allows to reduce the amount of information needed since the system works with more compact representation of the data by retaining the relevant information and highlighting the underlying patterns and structures (Jolliffe and Cadima, 2016). PCA showed how the scaffold PCL, rinse PCL, scaffold PLA and control groups were more similar among them than to the other groups (scaffold PEGDA500, rinse PEGDA500, rinse PEGDA200, scaffold PEGDA200, rinse PLA, rinse PhotoInk and scaffold PhotoInk) (Figure 6).

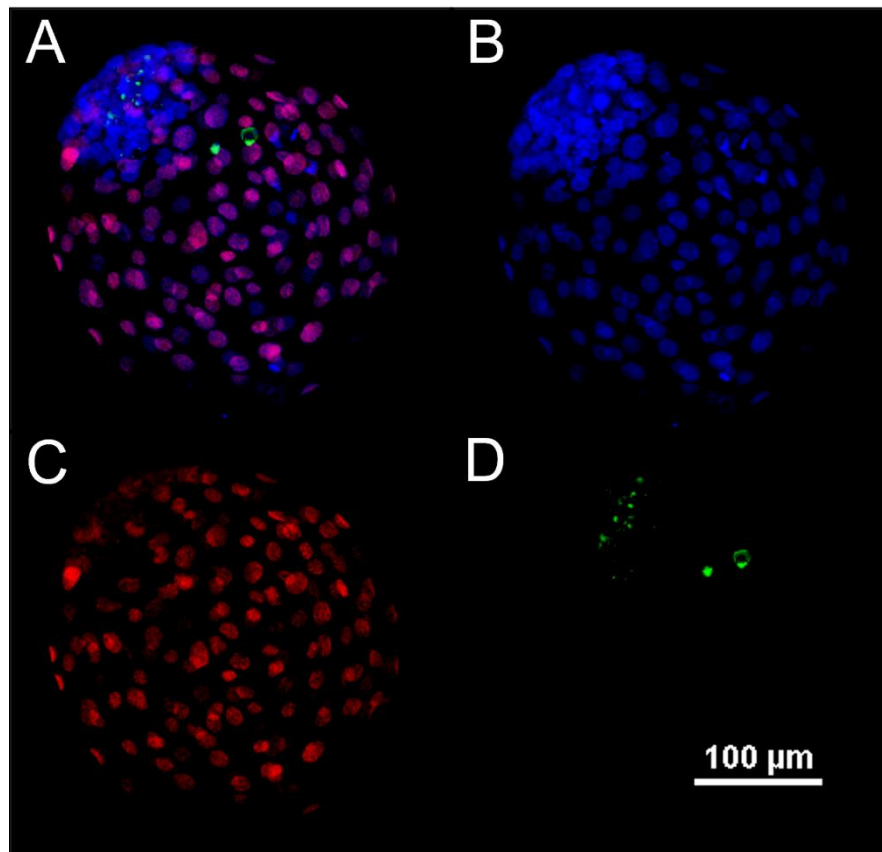


Figure 5. Representative confocal image of blastocyst at day 8. Fluorescent image of differential apoptotic staining (A-D). At day 8, bovine blastocysts were fixed, dyed with Hoechst 33342 for nuclei (B), immune-stained for CDX2 for the trophectoderm (C), and for active caspase-3 for the apoptosis (D). In (A) an overlay (B, C and D) is provided.

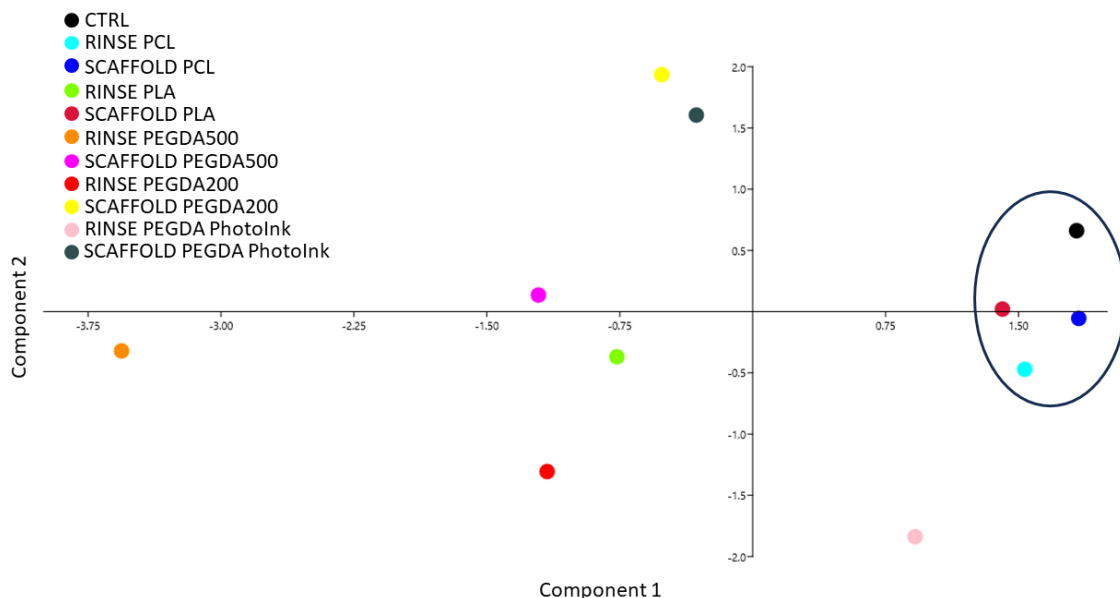


Figure 6. Principal component analysis performed by assessing the different parameters studied (Cleavage, blastocyst rate at days 7 and 8, TCN, ICM/TE and ACR). Principal component analysis shows no separation among groups. However, we observed that the closest groups to control are scaffold PLA, scaffold PCL and rinse PCL.

4. Discussion

In the present study we performed a bovine embryo assay to evaluate the potential toxicity of PLA, PCL, PEGDA500, PEGDA200, and PEGDA PhotoInk biomaterials in the embryo IVP during IVF. In addition, we tested not only different materials but also different printing methods, using for each material the most suitable method for the scaffold construction needs. We chose this animal model since it has already been used for embryo assay (Ieda et al., 2018) and it represents a valuable model for IVF improvement trials (Ménézo and Hérubel, 2002). It is also well-known that IVP produces suboptimal embryos with a lower yield of blastocysts and lower developmental capacity than their *in vivo* counterparts (Heras et al., 2016; Canovas et al., 2017; Ferraz et al., 2018b).

The first step in producing a device that could improve the IVP is the choice of biomaterial. All the materials we propose have been used in cell culture and have shown a good biocompatibility (Eslahi et al., 2013; Biagini et al., 2021; Di Berardino et al., 2022; Testore et al., 2022). However, as the cytotoxicity of the materials such as PLA (Biagini et al., 2021) could be different according to the cell types, the biocompatibility should be tested in regard to gametes, zygotes and embryos.

Our results suggest that the only material that has toxic effects is PEGDA500. This material had detrimental effect on bovine embryo development, promoting lower cleavage and lower blastocyst rate at day 7 and 8. This is an unexpected effect since PEGDA hydrogels have been suggested as effective candidates to carry out studies for embryogenesis and organogenesis due to their low cost, high reproducibility, and ease fabrication (Hribar et al., 2015). This is not the first time that biomaterials have shown unexpected negative effects when in contact with embryos. MacDonald et al. (2016) showed that VisiJet Crystal material (belonging to the strictest class for plastic

biocompatibility) had a detrimental effect on zebrafish embryos (MacDonald et al., 2016). The materials E-shell200 and E-shell300 have also shown a deleterious effect on bovine embryo development, even having been considered biocompatible according to ISO 10993 (Ferraz et al., 2018a). Furthermore, we must take into consideration the eventuality that our materials might not be exactly the same in chemistry as those used in previously works, since the full chemical composition may vary from one company to another. Another plausible factor could be the fact that in the 3D printed scaffolds could be found some residues of toxic compounds that have been used to stabilize and print the devices. Indeed, several studies have observed that different chemical species are leaked by 3D-printed scaffolds (Oskui et al., 2016; Ferraz et al., 2018a).

Additionally, we detected significant differences between the rinse group of PEGDA200 and CTRL group, but no differences when PEGDA200 scaffolds were compared to the controls. This result suggests that the PEGDA200 may require longer washing than the other PEGDA hydrogels, since this type of scaffold had no detrimental effects on embryo development during IVF after being washed for 24 hours and rinsed for another 24 hrs. However, all these hydrogels might not be the best option for the IVF device manufacturing because they were very fragile, and their rupture could be a relevant inconvenience during sterilization and handling.

Conversely, neither PLA nor PCL have shown detrimental effects on cleavage and blastocyst rate parameters. The PLA synthetic polymer has been suggested as an optimal candidate for scaffold fabrication due to its high biocompatibility, low cost, and mechanical properties (Serra et al., 2013; Di Prima et al., 2016). To our knowledge, this is the first study testing those materials to support bovine IVF, showing high biocompatibility. This is an expected result since both PLA and PCL biomaterials have been used in an emerging field called REPROTEN, the discipline that applies tissue

engineering to restore fertility (Amorim, 2017). It has been shown that PLA is a suitable material to create a nanofiber scaffold that enhance the *in vitro* cluster formation of mouse spermatogonia stem cells, allowing their proliferation and differentiation (Eslahi et al., 2013; Ghorbani et al., 2019). As well, PCL has been used to culture spermatogonia stem cells (Talebi et al., 2019; Ghorbani et al., 2022), obtaining the same successful results as PLA. Furthermore, recent works have used PCL scaffolds as devices to carry out folliculogenesis in sheep (Di Berardino et al., 2022) and pig (Liverani et al., 2019).

We observed worse results with the increase of the PEGDA material stiffness (PEGDA Photoink vs. PEGDA200 vs PEGDA500). Previously, it has been shown that the stiffness of different substrates can affect *in vitro* embryo development in mice (Kolahi et al., 2012), but in our case the lower efficiency could be due to the chemistry employed to promote higher stiffness of the material, since even when the scaffold is absent during IVF, the rinse groups showed lower efficiency. One possible explanation for the worse performance of the rinse groups could be that the scaffolds release toxic compounds during the rinse period culture, so when the scaffolds are used during IVF the release of these toxic chemicals is much lower or absent. However, to confirm this hypothesis mass spectrometry analysis should be performed.

Altogether, these data suggest that the materials printed with stereolithography (PEGDAs) are less biocompatible than extrusion-printed materials (PLA and PCL). On the other hand, the TCN, the ICM/TE ratio and the ACR are three important parameters of embryo quality and in recent years, several studies have shown that the rate of ICM/TE is a strong predictor of live birth (Ai et al., 2021; Sivanantham et al., 2022). When we analyzed all these parameters, the principal component analysis (PCA) showed that the embryos produced in presence of PLA and PCL scaffolds are the most comparable to the control group. Regarding the PCL biopolymer, the rinse and the scaffold groups are both

closer to the control ones, in terms of the analyzed parameters. While a different situation using the PLA biomaterial has been observed, since the scaffold group exhibited similar behavior to the control, contrary to the rinse group of the same biopolymer. For this reason, we consider PCL as the most suitable material for *in vitro* bovine embryo production.

Considering that we have not identified any negative effects on bovine embryo development when PCL is present during IVF, its implementation in the construction of a device compatible with microfluidics systems becomes a promising possibility. The combination of these microfluidics systems with the above-mentioned devices could allow the creation of an *in vitro* model of the oviduct (Romar et al., 2019). This innovative application could have a significant impact on the research and understanding of sperm selection by mimicking rheotaxis, chemotaxis and thermotaxis (Pérez-Cerezales et al., 2018; Ramal-Sanchez et al., 2021), fertilization and early development processes, providing a controlled and reproducible environment for experimental studies, without jeopardizing early embryo development.

In conclusion, the utilization of PCL in the construction of an IVF device holds great promise for the improvement of ARTs in the near future. However, further research and development are necessary to test the biocompatibility with OECs, optimize the design and functionality of this PCL-based IVF devices, ensuring their long-term effectiveness and safety. Nonetheless, the outcomes of our study strongly support the potential of the PCL biomaterial and open the way for advancements in the field of ARTs.

Author Contributions: N.B. and P.C conceptualized the study; B.M.C and S. prepared and characterized the scaffolds; R.B-P, S.H and J.R-A performed IVF experiments; L.V. performed all figures; R.B-P, C.C., and N.B analyzed the data; R.B-P

and A.C. prepared the original draft; all authors contributed to the analysis, writing and editing of the manuscript; P.C., B.B., N.B. supervised and funded the research. All authors have read and agreed to the published version of the manuscript.

5. References

- Abe, H., and Hoshi, H. (1997). Bovine oviductal epithelial cells: their cell culture and applications in studies for reproductive biology. *Cytotechnology* 23, 171. doi: 10.1023/A:1007929826186.
- Ai, J., Jin, L., Zheng, Y., Yang, P., Huang, B., and Dong, X. (2021). The Morphology of Inner Cell Mass Is the Strongest Predictor of Live Birth After a Frozen-Thawed Single Embryo Transfer. *Front Endocrinol (Lausanne)* 12, 621221. doi: 10.3389/FENDO.2021.621221/FULL.
- Amorim, C. A. (2017). Special Issue Devoted to a New Field of Regenerative Medicine: Reproductive Tissue Engineering. *Ann Biomed Eng* 45, 1589–1591. doi: 10.1007/S10439-017-1862-0/METRICS.
- Anton, D., Burckel, H., Josset, E., and Noel, G. (2015). Three-dimensional cell culture: A breakthrough in vivo. *Int J Mol Sci* 16, 5517–5527. doi: 10.3390/ijms16035517.
- Arif, Z. U., Khalid, M. Y., Noroozi, R., Sadeghianmaryan, A., Jalalvand, M., and Hossain, M. (2022). Recent advances in 3D-printed polylactide and polycaprolactone-based biomaterials for tissue engineering applications. *Int J Biol Macromol* 218, 930–968. doi: 10.1016/j.ijbiomac.2022.07.140.
- Assidi, M. (2022). Infertility in Men: Advances towards a Comprehensive and Integrative Strategy for Precision Theranostics. *Cells* 11. doi: 10.3390/cells11101711.

- Biagini, G., Senegaglia, A. C., Pereira, T., Berti, L. F., Marcon, B. H., and Stimamiglio, M. A. (2021). 3D Poly(Lactic Acid) Scaffolds Promote Different Behaviors on Endothelial Progenitors and Adipose-Derived Stromal Cells in Comparison With Standard 2D Cultures. *Front Bioeng Biotechnol* 9, 1. doi: 10.3389/FBIOE.2021.700862.
- Bó, G. A., and Mapletoft, R. J. (2013). Evaluation and classification of bovine embryos. *Animal Reproduction (AR)* 10, 344–348.
- Canovas, S., Ivanova, E., Romar, R., García-Martínez, S., Soriano-Úbeda, C., García-Vázquez, F. A., et al. (2017). DNA methylation and gene expression changes derived from assisted reproductive technologies can be decreased by reproductive fluids. *Elife* 6. doi: 10.7554/eLife.23670.
- Ceelen, M., Van Weissenbruch, M. M., Prein, J., Smit, J. J., Vermeiden, J. P. W., Spreeuwenberg, M., et al. (2009). Growth during infancy and early childhood in relation to blood pressure and body fat measures at age 8–18 years of IVF children and spontaneously conceived controls born to subfertile parents. *Human Reproduction* 24, 2788–2795. doi: 10.1093/HUMREP/DEP273.
- Costa, E. C., Moreira, A. F., de Melo-Diogo, D., Gaspar, V. M., Carvalho, M. P., and Correia, I. J. (2016). 3D tumor spheroids: an overview on the tools and techniques used for their analysis. *Biotechnol Adv* 34, 1427–1441. doi: 10.1016/J.BIOTECHADV.2016.11.002.
- De Geyter, C., Calhaz-Jorge, C., Kupka, M. S., Wyns, C., Mocanu, E., Motrenko, T., et al. (2020). ART in Europe, 2015: results generated from European registries by ESHRE. *Hum Reprod Open* 2020. doi: 10.1093/HROPEN/HOZ038.

- Della Sala, F., Biondi, M., Guarnieri, D., Borzacchiello, A., Ambrosio, L., and Mayol, L. (2020). Mechanical behavior of bioactive poly(ethylene glycol) diacrylate matrices for biomedical application. *J Mech Behav Biomed Mater* 110, 103885. doi: 10.1016/J.JMBBM.2020.103885.
- Di Berardino, C., Liverani, L., Peserico, A., Capacchietti, G., Russo, V., Bernabò, N., et al. (2022). When Electrospun Fiber Support Matters: In Vitro Ovine Long-Term Folliculogenesis on Poly (Epsilon Caprolactone) (PCL)-Patterned Fibers. *Cells* 11. doi: 10.3390/CELLS11121968/S1.
- Di Prima, M., Coburn, J., Hwang, D., Kelly, J., Khairuzzaman, A., and Ricles, L. (2016). Additively manufactured medical products - the FDA perspective. *3D Print Med* 2. doi: 10.1186/S41205-016-0005-9.
- Diomedede, F., Gugliandolo, A., Cardelli, P., Merciaro, I., Ettorre, V., Traini, T., et al. (2018). Three-dimensional printed PLA scaffold and human gingival stem cell-derived extracellular vesicles: A new tool for bone defect repair. *Stem Cell Res Ther* 9, 1–21. doi: 10.1186/s13287-018-0850-0.
- Eslahi, N., Hadjighassem, M. R., Joghataei, M. T., Mirzapour, T., Bakhtiyari, M., Shakeri, M., et al. (2013). The effects of poly L-lactic acid nanofiber scaffold on mouse spermatogonial stem cell culture. *Int J Nanomedicine* 8, 4563–4576. doi: 10.2147/IJN.S45535.
- Ferraz, M. A. M. M., Henning, H. H. W., Da Costa, P. F., Malda, J., Le Gac, S., Bray, F., et al. (2018a). Potential Health and Environmental Risks of Three-Dimensional Engineered Polymers. *Environ Sci Technol Lett* 5, 80–85. doi: 10.1021/acs.estlett.7b00495.

- Ferraz, M. A. M. M., Henning, H. H. W., Stout, T. A. E., Vos, P. L. A. M., and Gadella, B. M. (2017). Designing 3-Dimensional In Vitro Oviduct Culture Systems to Study Mammalian Fertilization and Embryo Production. *Ann Biomed Eng* 45, 1731–1744. doi: 10.1007/s10439-016-1760-x.
- Ferraz, M. A. M. M., Nagashima, J. B., Venzac, B., Le Gac, S., and Songsasen, N. (2020). A dog oviduct-on-a-chip model of serous tubal intraepithelial carcinoma. *Sci Rep* 10, 1–11. doi: 10.1038/s41598-020-58507-4.
- Ferraz, M. A. M. M., Rho, H. S., Hemerich, D., Henning, H. H. W., van Tol, H. T. A., Hölker, M., et al. (2018b). An oviduct-on-a-chip provides an enhanced in vitro environment for zygote genome reprogramming. *Nat Commun* 9. doi: 10.1038/s41467-018-07119-8.
- Fleming, T. P., Watkins, A. J., Velazquez, M. A., Mathers, J. C., Prentice, A. M., Stephenson, J., et al. (2018). Origins of lifetime health around the time of conception: causes and consequences. *Lancet* 391, 1842–1852. doi: 10.1016/S0140-6736(18)30312-X.
- Francés-Herrero, E., Lopez, R., Hellström, M., De Miguel-Gómez, L., Herraiz, S., Brännström, M., et al. (2022). Bioengineering trends in female reproduction: a systematic review. *Hum Reprod Update* 28, 798–837. doi: 10.1093/humupd/dmac025.
- Ghorbani, M., Nourani, M. R., Alizadeh, H., and Goodarzi, V. (2022). Evaluation of the Growth and Differentiation of Spermatogonial Stem Cells on a 3D Polycaprolactone/Multi-Walled Carbon Nanotubes-based Microfibrous Scaffold. *Journal of Applied Biotechnology Reports* 9, 846–855. doi: 10.30491/JABR.2022.312357.1463.

- Ghorbani, S., Eyni, H., Khosrowpour, Z., Salari Asl, L., Shabani, R., Nazari, H., et al. (2019). Spermatogenesis induction of spermatogonial stem cells using nanofibrous poly(l-lactic acid)/multi-walled carbon nanotube scaffolds and naringenin. *Polym Adv Technol* 30, 3011–3025. doi: 10.1002/PAT.4733.
- Ghosal, K., Manakhov, A., Zajíčková, L., and Thomas, S. (2017). Structural and Surface Compatibility Study of Modified Electrospun Poly(ϵ -caprolactone) (PCL) Composites for Skin Tissue Engineering. *AAPS PharmSciTech* 18, 72–81. doi: 10.1208/S12249-016-0500-8.
- Glozheni, O., Hambartsoumian, E., Strohmer, H., Petrovskaya, E., Tishkevich, O., de Neubourg, D., et al. (2022). ART in Europe, 2018: results generated from European registries by ESHRE. *Hum Reprod Open* 2022. doi: 10.1093/HROPEN/HOAC022.
- Haddad, M., Stewart, J., Xie, P., Cheung, S., Trout, A., Keating, D., et al. (2021). Thoughts on the popularity of ICSI. *J Assist Reprod Genet* 38, 101–123. doi: 10.1007/S10815-020-01987-0.
- Heras, S., De Coninck, D. I. M., Van Poucke, M., Goossens, K., Bogado Pascottini, O., Van Nieuwerburgh, F., et al. (2016). Suboptimal culture conditions induce more deviations in gene expression in male than female bovine blastocysts. *BMC Genomics* 17. doi: 10.1186/S12864-016-2393-Z.
- Holm, P., Booth, P. J., Schmidt, M. H., Greve, T., and Callesen, H. (1999). High bovine blastocyst development in a static in vitro production system using SOFaa medium supplemented with sodium citrate and myo-inositol with or without serum-proteins. *Theriogenology* 52, 683–700. doi: 10.1016/S0093-691X(99)00162-4.

- Hribar, K. C., Finlay, D., Ma, X., Qu, X., Ondeck, M. G., Chung, P. H., et al. (2015). Nonlinear 3D projection printing of concave hydrogel microstructures for long-term multicellular spheroid and embryoid body culture. *Lab Chip* 15, 2412–2418. doi: 10.1039/c5lc00159e.
- Huang, H., Oizumi, S., Kojima, N., Niino, T., and Sakai, Y. (2007). Avidin-biotin binding-based cell seeding and perfusion culture of liver-derived cells in a porous scaffold with a three-dimensional interconnected flow-channel network. *Biomaterials* 28, 3815–3823. doi: 10.1016/J.BIOMATERIALS.2007.05.004.
- Ieda, S., Akai, T., Sakaguchi, Y., Shimamura, S., Sugawara, A., Kaneda, M., et al. (2018). A microwell culture system that allows group culture and is compatible with human single media. *J Assist Reprod Genet* 35, 1869–1880. doi: 10.1007/s10815-018-1252-z.
- Jolliffe, I. T., and Cadima, J. (2016). Principal component analysis: A review and recent developments. *Philosophical Transactions of the Royal Society A: Mathematical, Physical and Engineering Sciences* 374. doi: 10.1098/rsta.2015.0202.
- Kessler, M., Hoffmann, K., Brinkmann, V., Thieck, O., Jackisch, S., Toelle, B., et al. (2015). The Notch and Wnt pathways regulate stemness and differentiation in human fallopian tube organoids. *Nat Commun* 6. doi: 10.1038/NCOMMS9989.
- Kim, S., Lee, H., Choi, H., Yoo, K. Y., and Yoon, H. (2022). Investigation on photopolymerization of PEGDA to fabricate high-aspect-ratio microneedles. *RSC Adv* 12, 9550–9555. doi: 10.1039/D2RA00189F.

- Kolahi, K. S., Donjacour, A., Liu, X., Lin, W., Simbulan, R. K., Bloise, E., et al. (2012). Effect of substrate stiffness on early mouse embryo development. *PLoS One* 7. doi: 10.1371/JOURNAL.PONE.0041717.
- Kölle, S., Hughes, B., and Steele, H. (2020). Early embryo-maternal communication in the oviduct: A review. *Mol Reprod Dev* 87, 650–662. doi: 10.1002/MRD.23352.
- Li, G., Zhao, M., Xu, F., Yang, B., Li, X., Meng, X., et al. (2020). Synthesis and Biological Application of Polylactic Acid. *Molecules* 25. doi: 10.3390/MOLECULES25215023.
- Lim, K. S., Galarraga, J. H., Cui, X., Lindberg, G. C. J., Burdick, J. A., and Woodfield, T. B. F. (2020). Fundamentals and Applications of Photo-Cross-Linking in Bioprinting. *Chem Rev* 120, 10662–10694. doi: 10.1021/ACS.CHEMREV.9B00812.
- Liverani, L., Raffel, N., Fattahi, A., Preis, A., Hoffmann, I., Boccaccini, A. R., et al. (2019). Electrospun patterned porous scaffolds for the support of ovarian follicles growth: a feasibility study. *Scientific Reports* 2019 9:1 9, 1–14. doi: 10.1038/s41598-018-37640-1.
- Lopes, J. S., Canha-Gouveia, A., París-Oller, E., and Coy, P. (2019). Supplementation of bovine follicular fluid during in vitro maturation increases oocyte cumulus expansion, blastocyst developmental kinetics, and blastocyst cell number. *Theriogenology* 126, 222–229. doi: 10.1016/j.theriogenology.2018.12.010.
- MacDonald, N. P., Zhu, F., Hall, C. J., Reboud, J., Crosier, P. S., Patton, E. E., et al. (2016). Assessment of biocompatibility of 3D printed photopolymers using zebrafish embryo toxicity assays. *Lab Chip* 16, 291–297. doi: 10.1039/c5lc01374g.

- Maier, E. R., Brueton, L. A., Bowdin, S. C., Luharia, A., Cooper, W., Cole, T. R., et al. (2003). Beckwith-Wiedemann syndrome and assisted reproduction technology (ART). *J Med Genet* 40, 62. doi: 10.1136/JMG.40.1.62.
- Manipalviratn, S., DeCherney, A., and Segars, J. (2009). Imprinting disorders and assisted reproductive technology. *Fertil Steril* 91, 305. doi: 10.1016/J.FERTNSTERT.2009.01.002.
- Ménézo, Y., Guérin, P., and Elder, K. (2015). The oviduct: A neglected organ due for re-assessment in IVF. *Reprod Biomed Online* 30, 233–240. doi: 10.1016/j.rbmo.2014.11.011.
- Ménézo, Y. J. R., and Hérubel, F. (2002). Mouse and bovine models for human IVF. *Reprod Biomed Online* 4, 170–175. doi: 10.1016/S1472-6483(10)61936-0.
- Nguyen, Q. T., Hwang, Y., Chen, A. C., Varghese, S., and Sah, R. L. (2012). Cartilage-like mechanical properties of poly (ethylene glycol)-diacrylate hydrogels. *Biomaterials* 33, 6682. doi: 10.1016/J.BIOMATERIALS.2012.06.005.
- Oskui, S. M., Diamante, G., Liao, C., Shi, W., Gan, J., Schlenk, D., et al. (2016). Assessing and Reducing the Toxicity of 3D-Printed Parts. *Environ Sci Technol Lett* 3, 1–6. doi: 10.1021/ACS.ESTLETT.5B00249/ASSET/IMAGES/MEDIUM/EZ-2015-002497_0006.GIF.
- Palermo, G. D., Schlegel, P. N., Colombero, L. T., Zaninovic, N., Moy, F., and Rosenwaks, Z. (1996). Aggressive sperm immobilization prior to intracytoplasmic sperm injection with immature spermatozoa improves fertilization and pregnancy rates. *Hum Reprod* 11, 1023–1029. doi: 10.1093/OXFORDJOURNALS.HUMREP.A019290.

- París-Oller, E., Soriano-Úbeda, C., Belda-Pérez, R., Sarriás-Gil, L., Lopes, J. S., Canha-Gouveia, A., et al. (2022). Reproductive fluids, added to the culture media, contribute to minimizing phenotypical differences between in vitro-derived and artificial insemination-derived piglets. *J Dev Orig Health Dis*. doi: 10.1017/S2040174421000702.
- Parrish, J. J., Susko-Parrish, J. L., Leibfried-Rutledge, M. L., Critser, E. S., Eyestone, W. H., and First, N. L. (1986). Bovine in vitro fertilization with frozen-thawed semen. *Theriogenology* 25, 591–600. doi: 10.1016/0093-691X(86)90143-3.
- Parrish, J. J., Susko-Parrish, J., Winer, M. A., and First, N. L. (1988). Capacitation of bovine sperm by heparin. *Biol Reprod* 38, 1171–1180. doi: 10.1095/biolreprod38.5.1171.
- Pennarossa, G., Arcuri, S., De Iorio, T., Gandolfi, F., and Brevini, T. A. L. (2021). Current Advances in 3D Tissue and Organ Reconstruction. *Int J Mol Sci* 22, 1–26. doi: 10.3390/IJMS22020830.
- Pérez-Aytés, A., Arcos-Machancoses, J. V., Marin Reina, P., Jimenez Busselo, M. T., and Martínez, F. (2017). Artificial reproductive techniques and epigenetic alterations: Additional comments to the article by Arcos-Machancoses et al. (). *Am J Med Genet A* 173, 1983–1984. doi: 10.1002/AJMG.A.38273.
- Pérez-Cerezales, S., Ramos-Ibeas, P., Acuna, O. S., Avilés, M., Coy, P., Rizos, D., et al. (2018). The oviduct: from sperm selection to the epigenetic landscape of the embryo. *Biol Reprod* 98, 262–276. doi: 10.1093/BIOLRE/IOX173.

- Rajabi, M., Cabral, J. D., Saunderson, S., and Ali, M. A. (2023). 3D printing of chitooligosaccharide-polyethylene glycol diacrylate hydrogel inks for bone tissue regeneration. *J Biomed Mater Res A*. doi: 10.1002/JBM.A.37548.
- Ramal-Sanchez, M., Bernabò, N., Valbonetti, L., Cimini, C., Taraschi, A., Capacchietti, G., et al. (2021). Role and Modulation of TRPV1 in Mammalian Spermatozoa: An Updated Review. *Int J Mol Sci* 22. doi: 10.3390/IJMS22094306.
- Romar, R., Cánovas, S., Matás, C., Gadea, J., and Coy, P. (2019). Pig in vitro fertilization: Where are we and where do we go? *Theriogenology* 137, 113–121. doi: 10.1016/j.theriogenology.2019.05.045.
- Rosenzweig, D. H., Carelli, E., Steffen, T., Jarzem, P., and Haglund, L. (2015). 3D-Printed ABS and PLA Scaffolds for Cartilage and Nucleus Pulposus Tissue Regeneration. *Int J Mol Sci* 16, 15118. doi: 10.3390/IJMS160715118.
- Rumiński, S., Ostrowska, B., Jaroszewicz, J., Skirecki, T., Włodarski, K., Świąszkowski, W., et al. (2018). Three-dimensional printed polycaprolactone-based scaffolds provide an advantageous environment for osteogenic differentiation of human adipose-derived stem cells. *J Tissue Eng Regen Med* 12, e473–e485. doi: 10.1002/TERM.2310.
- Santoni, S., Gugliandolo, S. G., Sponchioni, M., Moscatelli, D., and Colosimo, B. M. (2021). 3D bioprinting: current status and trends—a guide to the literature and industrial practice. *Bio-Design and Manufacturing* 2021 5:1 5, 14–42. doi: 10.1007/S42242-021-00165-0.
- Scocozza, F., Di Gravina, G. M., Bari, E., Auricchio, F., Torre, M. L., and Conti, M. (2023). Prediction of the mechanical response of a 3D (bio)printed hybrid scaffold

- for improving bone tissue regeneration by structural finite element analysis. *J Mech Behav Biomed Mater* 142. doi: 10.1016/J.JMBBM.2023.105822.
- Serra, T., Planell, J. A., and Navarro, M. (2013). High-resolution PLA-based composite scaffolds via 3-D printing technology. *Acta Biomater* 9, 5521–5530. doi: 10.1016/J.ACTBIO.2012.10.041.
- Shilov, S. Y., Rozhkova, Y. A., Markova, L. N., Tashkinov, M. A., Vindokurov, I. V, and Silberschmidt, V. V (2022). Biocompatibility of 3D-Printed PLA, PEEK and PETG: Adhesion of Bone Marrow and Peritoneal Lavage Cells. doi: 10.3390/polym14193958.
- Sivanantham, S., Saravanan, M., Sharma, N., Shrinivasan, J., and Raja, R. (2022). Morphology of inner cell mass: a better predictive biomarker of blastocyst viability. *PeerJ* 10. doi: 10.7717/PEERJ.13935/SUPP-3.
- Sunde, A., Brison, D., Dumoulin, J., Harper, J., Lundin, K., Magli, M. C., et al. (2016). Time to take human embryo culture seriously. *Hum Reprod* 31, 2174–2182. doi: 10.1093/HUMREP/DEW157.
- Talebi, A., Sadighi Gilani, M. A., Koruji, M., Ai, J., Rezaie, M. J., Navid, S., et al. (2019). Colonization of Mouse Spermatogonial Cells in Modified Soft Agar Culture System Utilizing Nanofibrous Scaffold: A New Approach. *Galen Medical Journal* 8, 1319. doi: 10.31661/gmj.v8i0.1319.
- Testore, D., Zoso, A., Kortaberria, G., Sangermano, M., and Chiono, V. (2022). Electroconductive Photo-Curable PEGDA-Gelatin/PEDOT:PSS Hydrogels for Prospective Cardiac Tissue Engineering Application. *Front Bioeng Biotechnol* 10. doi: 10.3389/fbioe.2022.897575.

- Vannozzi, L., Yasa, I. C., Ceylan, H., Mencias, A., Ricotti, L., and Sitti, M. (2018). Self-Folded Hydrogel Tubes for Implantable Muscular Tissue Scaffolds. *Macromol Biosci* 18. doi: 10.1002/MABI.201700377.
- Velioglu, Z. B., Pulat, D., Demirbakan, B., Ozcan, B., Bayrak, E., and Eriskin, C. (2019). 3D-printed poly(lactic acid) scaffolds for trabecular bone repair and regeneration: scaffold and native bone characterization. *Connect Tissue Res* 60, 274–282. doi: 10.1080/03008207.2018.1499732.
- Verpoest, W., and Tournaye, H. (2009). ICSI: Hype or hazard? <http://dx.doi.org/10.1080/14647270500422158> 9, 81–92. doi: 10.1080/14647270500422158.
- Waynforth, D. (2018). Focus: Medical Technology: Effects of Conception Using Assisted Reproductive Technologies on Infant Health and Development: An Evolutionary Perspective and Analysis Using UK Millennium Cohort Data. *Yale J Biol Med* 91, 225.
- Wydooghe, E., Heras, S., Dewulf, J., Piepers, S., Van Den Abbeel, E., De Sutter, P., et al. (2014). Replacing serum in culture medium with albumin and insulin, transferrin and selenium is the key to successful bovine embryo development in individual culture. *Reprod Fertil Dev* 26, 717–724. doi: 10.1071/RD13043.
- Wydooghe, E., Vandaele, L., Beek, J., Favoreel, H., Heindryckx, B., De Sutter, P., et al. (2011). Differential apoptotic staining of mammalian blastocysts based on double immunofluorescent CDX2 and active caspase-3 staining. *Anal Biochem* 416, 228–230. doi: 10.1016/J.AB.2011.05.033.

- Xiao, S., Coppeta, J. R., Rogers, H. B., Isenberg, B. C., Zhu, J., Olalekan, S. A., et al. (2017). A microfluidic culture model of the human reproductive tract and 28-day menstrual cycle. *Nat Commun* 8. doi: 10.1038/ncomms14584.
- Zhang, Q., Bei, H. P., Zhao, M., Dong, Z., and Zhao, X. (2022a). Shedding light on 3D printing: Printing photo-crosslinkable constructs for tissue engineering. *Biomaterials* 286. doi: 10.1016/j.biomaterials.2022.121566.
- Zhang, X., Yan, Z., Guan, G., Lu, Z., Yan, S., Du, A., et al. (2022b). Polyethylene glycol diacrylate scaffold filled with cell-laden methacrylamide gelatin/alginate hydrogels used for cartilage repair. *J Biomater Appl* 36, 1019–1032. doi: 10.1177/08853282211044853/ASSET/IMAGES/LARGE/10.1177_08853282211044853-FIG8.JPEG.

The background of the slide features abstract, flowing, translucent blue and white lines that create a sense of movement and depth, resembling smoke or liquid waves. These lines are concentrated on the left side and flow towards the right, framing the text.

CHAPTER II

Non-physiological materials to
support IVF.

Manuscript 2.

Catechin versus MoS₂ nanoflakes functionalized with catechin: improving the sperm fertilizing ability – an in vitro study on swine model.

*Manuscript published in International Journal of Molecular Sciences,
Volume 24, Issue 5, March 2023
doi.org/10.3390/ijms24054788*

Costanza Cimini ¹, Marina Ramal-Sanchez ², Angela Taraschi ¹, Flavio Della Pelle ¹, Annalisa Scroccarello ¹, Ramses Belda-Perez ¹, Luca Valbonetti ^{1,3}, Paola Lanuti ^{4,5}, Marco Marchisio ^{4,5}, Mario D'Atri ^{6,7}, Claudio Ortolani ⁶, Stefano Papa ⁶, Giulia Capacchietti ¹, Nicola Bernabò ^{1,3*}, Dario Compagnone¹, Barbara Barboni ¹

¹Department of Biosciences and Technology for Food, Agriculture and Environment, University of Teramo, 64100 Teramo, Italy.

²Department of Innovative Technologies in Medicine and Dentistry, University of Chieti-Pescara, 66100 Chieti, Italy.

³Institute of Biochemistry and Cell Biology (CNRIBBC/EMMA/Infrafrontier/IMPC), National Research Council, 00015 Rome, Italy.

⁴Department of Medicine and Aging Science, University “G. d’Annunzio” of Chieti-Pescara, 66100 Chieti, Italy

⁵Centre on Aging Sciences and Translational Medicine (Ce.S.I-MeT), University “G. d’Annunzio” of Chieti-Pescara, 66100 Chieti, Italy.

⁶Department of Biomolecular Sciences, University of Urbino “Carlo Bo”, 61029 Pesaro-Urbino, Italy.

⁷Sharp Solutions Software, Udine, Italy.

*Correspondence: nbernabo@unite.it

Abstract: Nowadays, the adoption of In Vitro Fertilization (IVF) techniques is undergoing an impressive increase. In light of this, one of the most promising strategies is the novel use of non-physiological materials and naturally derived compounds for advanced sperm preparation methods. Here, sperm cells were exposed during capacitation to MoS₂/Catechin nanoflakes and catechin (CT), a flavonoid with antioxidant properties, at concentrations of 10, 1, 0.1 ppm. The results showed no significant differences in terms of sperm membrane modifications or biochemical pathways among the groups, allowing the hypothesis that MoS₂/CT nanoflakes do not induce any negative effect on the parameters evaluated related to sperm capacitation. Moreover, the addition of CT alone at a specific concentration (0.1 ppm) increased

the spermatozoa fertilizing ability in an IVF assay by increasing the number of fertilized oocytes with respect to the control group. Our findings open interesting new perspectives regarding the use of catechins and new materials obtained using natural or bio compounds, which could be used to implement the current strategies for sperm capacitation.

Keywords: molybdenum disulfide; catechins; spermatozoa; sperm capacitation; in vitro fertilization

1. Introduction

In vitro fertilization (IVF) is one of the most used assisted reproductive techniques, aimed at overcoming fertility problems, either in zootechnics or for human purposes. In this process, an egg is combined with spermatozoa in vitro, after the acquisition of their fertilizing potential in a process commonly known as capacitation.

Recently, the use of non-physiological materials is gaining ground in the reproductive field as a support for the implementation of IVF techniques. For instance, previous studies demonstrated a significant improvement in the fertility outcomes when sperm cells were exposed to graphene oxide (GO) during capacitation in different animal models such as swine, bovine and mouse. This effect could probably be ascribed to the extraction of cholesterol from the sperm membrane thus inducing an intense lipid membrane remodeling [1–3].

Among non-physiological materials and naturally derived compounds, molybdenum disulfide (MoS_2) and catechin stand out as interesting candidates to characterize the effects of their exposure on reproductive function.

MoS₂ is a member of the transition metal dichalcogenides (TMDs) family, which are layered materials with a structure consisting of overlapped layers held together by Van der Waals forces. Each sheet possesses a wafer-like structure with a central hexagonal layer of metal atoms sandwiched in a double layer of chalcogen atoms [4]. MoS₂ is characterized by both a peculiar nanostructure and chemistry that has commenced to be employed in different fields, including catalysis, electrochemistry and an ever increasing use in biological/biomedical applications [5–7]. TMDs' features are strictly dependent on the nanoscale reduction strategy and despite the impressive advancements achieved during the last years, their use for biological/biomedical applications is often limited by their scarce dispersibility in water and/or the need for toxic or pollutant chemicals for their synthesis. It is noteworthy that MoS₂ is a 2D graphene-like material and, although the potential toxicity of TMDs materials has been studied in embryonated eggs [8] and on human lung carcinoma epithelial cells [9], to the best of our knowledge there are no studies evaluating the potential effects of TMDs on sperm capacitation.

On the other hand, catechin (CT) is a flavonoid characterized by a high antioxidant capacity [10], and it has previously been demonstrated that CT supplementation to sperm storage may have a beneficial effect on sperm motility [11]. Interestingly, CT has proved to be able to assist the stabilization and synthesis of various nanomaterials, remaining firmly anchored on their surface and acting as a functional and stabilizing agent [12,13]. In the nanomaterials domain, the dispersion or exfoliation route represents a challenge to modulate the affinity and dispersibility of the materials in different media, defining the final material features in terms of structure, dimension and solubility and thus conferring additional functionalities [4,14–16].

In the present study, we aimed to study the effects of nanoflakes of MoS₂ functionalized with catechins and catechins on swine spermatozoa functional parameters during capacitation. The term capacitation encompasses a necessary series of events occurring naturally in vivo and by which spermatozoa undergo a functional modification, ultimately acquiring their fertilizing ability. While in vivo, sperm cells are free to migrate through the uterus, bind to the oviductal epithelium and encounter the multiple endocrine stimuli prior to the meeting with the oocyte [17–19]. In order to improve the current strategies for sperm capacitation, different concentrations of MoS₂/CT and CT were evaluated (10, 1, and 0.1 ppm). A multiple-step approach was adopted to evaluate the potential effects of this interaction in terms of: (a) acrosome damage; (b) membrane disorder; (c) biochemical patterns (PKA activity and tyrosine phosphorylation patterns); (d) intracellular calcium concentration; and (e) mitochondrial activity. As a functional test, finally an IVF assay was performed to assess the sperms' fertilizing ability.

2. Results and discussion

Here, the potential effects of MoS₂/CT and CT addition during spermatozoa capacitation were analyzed using a swine in vitro model. The swine model has acquired enormous importance for biomedical research and represents an optimal animal model for the study of human reproductive events [20–22].

2.1. Preparation and Characterization of Water-Phase Exfoliated MoS₂/CT Nanoflakes

As reported in Figure 1, the bulk-MoS₂ sonochemical liquid phase exfoliation assisted by catechin (conducted according to the Section 3 Materials and Methods) allowed a stable colloidal dispersion of MoS₂/CT nanoflakes to be obtained, which was then used for further experiments. As expected, in the bulk form this TMD possesses crystalline

structures characterized by micrometric sides and thickness (Figure 1B); in this conformation, MoS₂ is not dispersible in water. Figure 1 C, D show the SEM micrograph of the MoS₂ after exfoliation assisted by catechin (MoS₂/CT). The CT-assisted exfoliated MoS₂ flakes resulted in being significantly smaller when compared to the bulk MoS₂, proving a noticeable exfoliation success. In this conformation, the MoS₂/CT is a colloid, stable for more than 1 year (Figure 1C, right). In the SEM magnification of Figure 1D, the MoS₂/CT flakes obtained are visible and are characterized by nano sides. The catechin effectiveness in the exfoliation of MoS₂ was proved in our previous work [12], where the exfoliation strategy was proposed, optimized, and the nanoflakes obtained were fully characterized. An average size value of about 153±2 nm was obtained via dynamic light scattering for the MoS₂/CT flakes. It is noteworthy that the same study highlighted an interesting residual antioxidant potential for MoS₂/CT, which was attributed to the MoS₂ surface modification influenced by the catechin, able to bring charges and redox-active moieties.

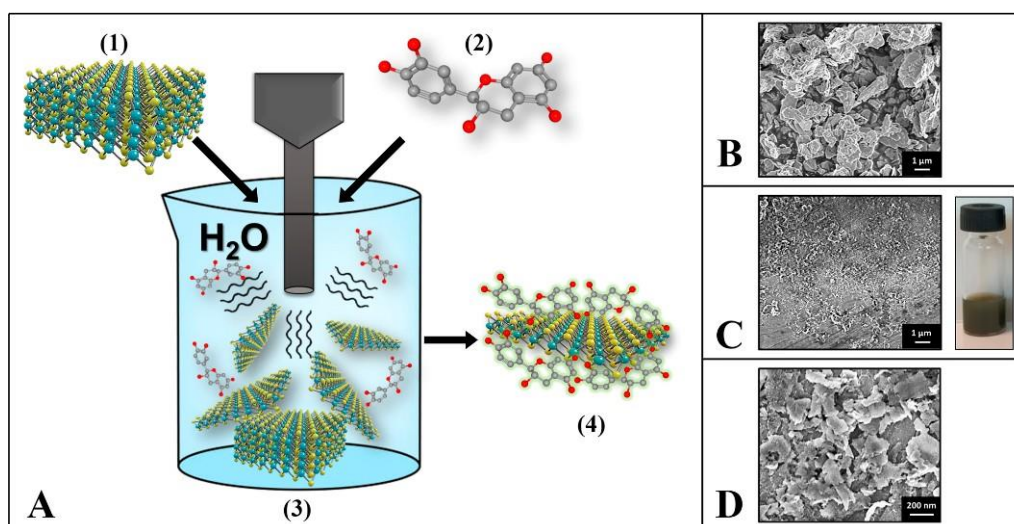


Figure 1. (A) Graphical sketch of the MoS₂ sonochemical exfoliation assisted by catechin. (1) Bulk MoS₂, (2) catechin structure, (3) sonochemical exfoliation process, (4) MoS₂/CT nanoflakes. (B) SEM micrograph of the bulk-MoS₂ (unexfoliated); (C) SEM micrograph of the exfoliated MoS₂/CT (left); picture of the MoS₂-CT colloidal water-dispersion (right). (D) SEM magnification of the MoS₂/CT nanoflakes.

Several exfoliation strategies have been proposed for layered materials. Nevertheless, liquid-phase exfoliation (LPE) has become an affordable and sustainable large-scale strategy to produce water-dispersed 2D nanomaterials. Two-dimensional nano colloids have been obtained in water using LPE by employing different surfactants, polymeric structures and different amphiphilic compounds, which are able to interact with the dispersed/exfoliated nanostructures mainly via non-covalent interactions [23–25]. Recently, our group has demonstrated how naturally-derived polyphenols can assist the graphene and group VI TMDs' exfoliation in water, acting as stabilizing agents and conferring at the same time additional features, partially preserving their antioxidant moieties [12,13].

Catechin is a flavonoid with an amphiphilic structure that is naturally present in different foods, characterized by a high antioxidant capacity and thus associated with several potential biological functions and health benefits [10]. Thanks to its amphiphilic structure, catechin can act as a stabilizing agent for nanomaterials' production and stabilization in water. Catechin has demonstrated an active role in the formation, stabilization and functionalization of metal nanoparticles, graphene, and nanocomposites. Moreover, the catechin adhesion on the formed nanomaterials apports additional electrochemical and antimicrobial features [12,15,26,27], proving to be a useful naturally-derived functional and stabilizing agent.

The sonochemical preparation in water of the MoS₂/CT can be resumed as follow:

- (i) the ultrasound energy allows the layers and dimension number/size reductions of the crystalline bulk-MoS₂; (ii) the stabilization/functionalization of the formed MoS₂ nanoflakes is guaranteed by the catechins' ability to remain attached to the surface of the produce MoS₂ flakes acting as a stabilizing agent. In this case, the catechin carbon skeleton allows π – π interactions with neo-produced MoS₂ flakes, while the CT hydroxyl

groups interact with water via hydrogen bonds allowing the nanoflakes to remain dispersed, ensuring also charge repulsion among flakes and avoiding layer re-stacking. The ability of the compounds containing catechol groups, to allow π – π stacking with other π systems has been already proved by Saiz-Poseu and colleagues (2019) [28] and by Silveri and colleagues (2021) [13] for graphene; on the other hand, electrochemical studies supported the hypothesis that the catechol of catechin is attached to the MoS₂ nanoflakes but has antioxidant moieties free to react [12].

The water-dispersible nature of MoS₂/CT nanoflakes allowed easy nanomaterial handling via differential centrifugation. This important feature enables (i) purifying the exfoliated nanoflakes, (ii) removing the excess supernatant, and (iii) resuspending the MoS₂/CT in the spermatozoa capacitating medium at the desired concentration. This is a challenge for TMDs exfoliated in organic solvents, which are not water dispersible. However, different exfoliation strategies in water imply the use of highly toxic or pollutant chemicals [29]. Unlike the extensively studied graphene oxide, which is naturally dispersible in water, probably the lack of biological studies on spermatozoa with TMDs is attributable to (i) the difficult manipulation of TMDs in aqueous media, (ii) the low-optimal TMDs' exfoliation (studies are often conducted on just roughly dispersed TMDs), (iii) high toxicity materials produced via conventional approaches.

2.2. MoS₂/CT and CT Supplementation Does Not Affect the Acrosome Integrity

The first step to examine the potential impact of MoS₂/CT and CT exposure on spermatozoa was the monitoring of the acrosome damage. Because spermatozoa that have lost their acrosome are unable to fertilize an egg, depending on the species, the acrosome reaction (AR) is one of the most important fertilization mechanisms [30].

Acrosome integrity was evaluated at 0 and 1.5 h after in vitro capacitation. As evidenced in Figure 2, after 1.5 h of capacitation in the presence of MoS₂/CT and CT the proportion of acrosome-reacted spermatozoa was similar among the groups, showing no significant differences ($p > 0.05$). Thus, it is possible to affirm that MoS₂/CT and CT at the different concentrations tested have no statistically significant effect on acrosome integrity.

2.3. MoS₂/CT and CT Supplementation Does Not Modify the Intracellular Calcium Concentration, Membrane Fluidity and Mitochondrial Activity

Flow cytometry analysis was performed to evaluate the effects of MoS₂/CT and CT supplementations in three different events of sperm capacitation after 1.5 h of incubation in capacitating conditions: the increase in the intracellular calcium concentration; the sperm membrane disorder (thus revealing the potential membrane fluidity increase); and the mitochondrial activity. The results showed no differences in terms of intracellular calcium concentration, membrane disorder and mitochondrial activity, as graphically illustrated in Figures 3–5, respectively. Supplementary Materials S1 shows the CTRL group after 0, 1.5 of capacitation.

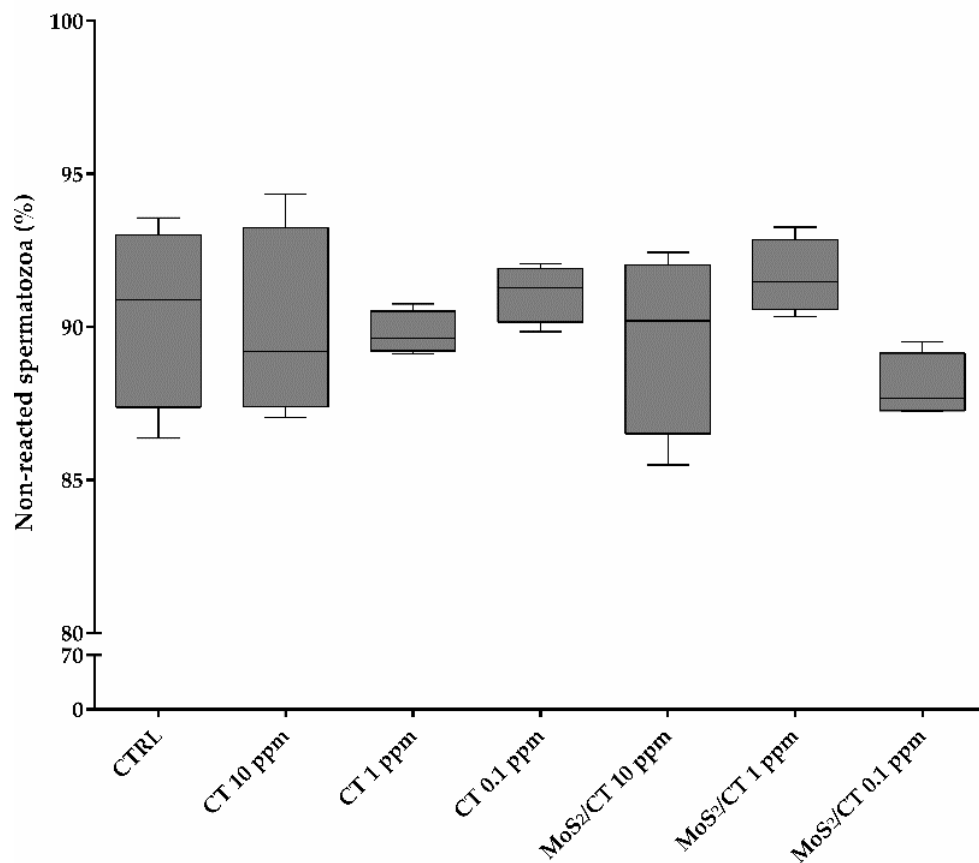


Figure 2. Acrosome integrity. The graph shows the percentage of non-reacted spermatozoa after 1.5 h of capacitation for the different experimental groups: CTRL, CT 10 ppm, CT 1 ppm, CT 0.1, MoS₂/CT 10 ppm, MoS₂/CT 1 ppm and MoS₂/CT 0.1 ppm. A normal acrosome damage rate was obtained, similar to the control (CTRL) group ($p > 0.05$). Three independent technical and biological (from different boars) replicates were performed.

Capacitation status has been associated with changes in the sperm machinery at membrane and cytosolic levels. For instance, the intracellular calcium ($[Ca^{2+}]_i$) homeostasis is a key element in sperm capacitation and acrosome reaction [31]. In resting conditions, the calcium clearance is tightly regulated by Ca^{2+} pumps (Ca^{2+} -ATPases), Na^+/Ca^{2+} -exchangers, and Ca^{2+} -channels in the sperm plasma membrane and in intracellular organelles, including the acrosome, the redundant-nuclear-envelope (RNE) and the mitochondria [32]. A key role is attributed to the Catsper channels, which are directly involved in sperm capacitation producing an influx of Ca^{2+} as a consequence of their stimulation [33,34]. During capacitation, the $[Ca^{2+}]_i$ rises and acts like a second

messenger converting extracellular stimuli into a chemical response involving several molecular systems, such as, protein kinase C (PKC), protein kinase A (PKA), actin, and many others [35]. At the same time, one of most relevant events of AR is the very fast surge of $[Ca^{2+}]^i$, following the spermatozoa's interaction with the oocyte [35]. Thus, Ca^{2+} is not only a homeostatic factor and a second messenger in spermatozoa, but it also controls and modulates the crucial physiological function in a sperm's life, as also happens in excitable cells such as neurons, myocardiocytes, and muscular cells.

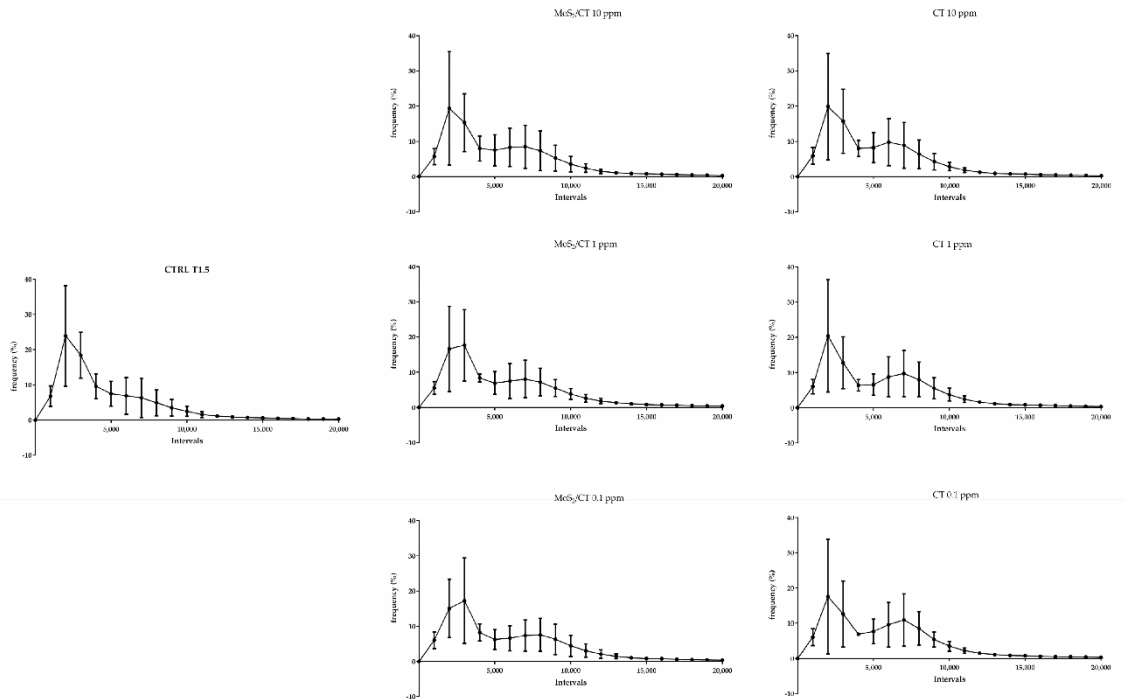


Figure 3. Flow cytometry analysis of intracellular calcium concentration. The graphs show the frequency of spermatozoa emitting a specific fluorescence intensity, which was subdivided into intervals ranging from 0 to 20,000 a.u. Capacitation was performed up to 1.5 h. Fluo 4-AM was used in combination with PI. Three independent technical and biological experiments were performed ($n = 3$).

During sperm capacitation, the membrane physicochemical characteristics change, which is an important aspect to consider since the sperm cytosol is virtually absent, thus implying a direct contact of the sperm plasma membrane with underlying

structures [36]. The sperm head plasma membrane (PM) presents a different composition between the inner and outer leaflets and this asymmetry is established and maintained by several translocating enzymes [36,37]. During capacitation, the phospholipid asymmetry is reduced and the phospholipids move inward and outward according to their concentration gradient [38]. The lipid remodeling allows the removal of cholesterol from extracellular protein, which determines the increase in the ability of the sperm plasma membrane (PM) and the outer acrosome membrane (OAM) to fuse (fusogenicity), a prerequisite for the acrosome reaction [39].

Mitochondrial activity is required for several sperm functions [40]. In addition to contributing to generate ATP, mitochondria act as a hub between the generation of reactive oxygen species (ROS) and the activation of apoptosis-related pathways [41]. The result of the capacitation process is the acquisition of fertilizing ability or activating pro-apoptotic pathways.

Thus, the findings obtained showed no differences in terms of mitochondrial activity, membrane disorder and intracellular calcium concentration, implying that MoS₂/CT and CT do not exert any affect in these events of sperm capacitation in vitro.

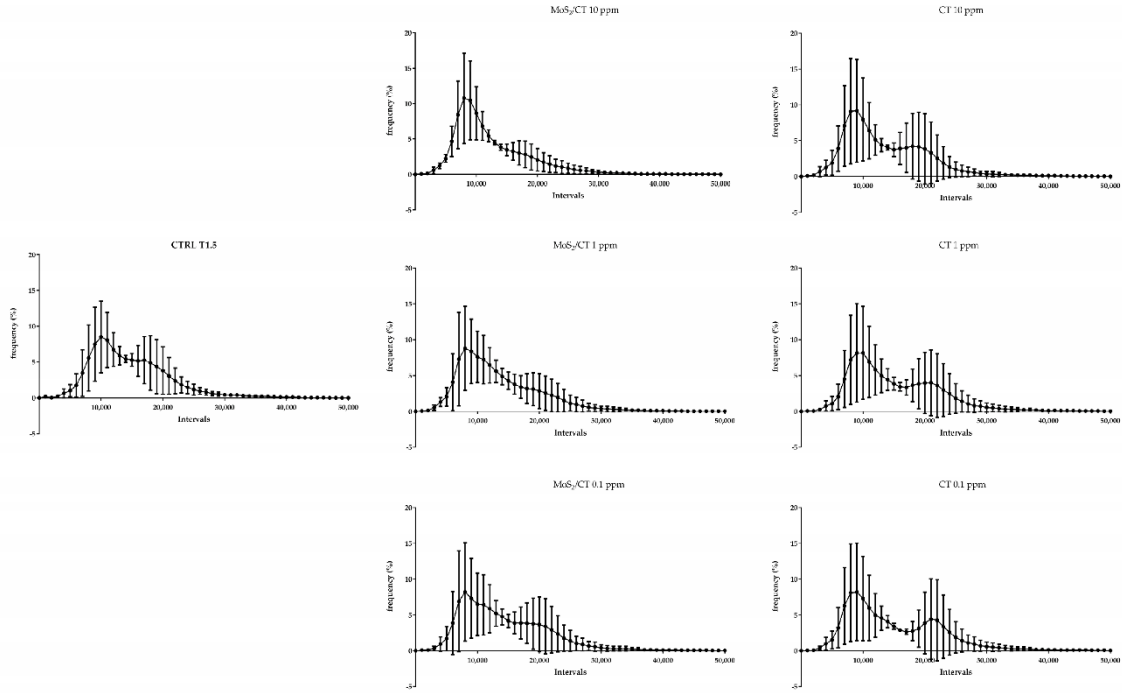


Figure 4. Flow cytometry analysis of membrane disorder and fluidity. The graphs show the frequency of spermatozoa emitting a specific fluorescence intensity, which was subdivided into intervals ranging from 0 to 50,000 a.u. Capacitation was performed up to 1.5 h. DiIC-12 was used as a probe. Three independent technical and biological experiments were performed (n = 3).

2.4. MoS₂/CT and CT Supplementation Does Not Influence Sperm pKa Activity and Tyrosine Phosphorylation Patterns

Flow cytometry was used to analyze the early events of capacitation that lead to PKA activation and the subsequent tyrosine phosphorylation cascade, which were then analyzed by Western blot (WB). Sperm protein soluble adenylyl cyclase (sAC) is activated during capacitation, raising the intracellular pH [42]. As a result, PKA and cAMP levels increase [43] and cAMP binds to the PKA regulatory subunits, allowing the dissociation of the tetramer and the activation of the catalytic subunit and thus initiating a cascade of intracytoplasmic signaling events [44]. Once released, the catalytic subunits continue their function phosphorylating a wide range of substrates on the Ser/Thr residues, activating a variety of protein kinases and/or

inhibiting protein phosphatases to increase the phosphorylation of tyrosine residues either directly or indirectly [30,45] and contributing to reshaping the global protein phosphorylation pattern. This change occurs either in the flagellum or in the sperm head, and it appears to be mandatory for a spermatozoon to reach the ability to fertilize the oocyte [30,45]. While the results show the normal differences between non-capacitated and capacitated spermatozoa in terms of residues' phosphorylation, our results showed no significant differences among the experimental groups. The phosphorylation patterns obtained were similar for MoS₂/CT and CT (10, 1 and 0.1 ppm) with respect to the control group (Figure 6). All full-length membranes and immunoblotting images from three independent experiments were added to Supplementary Materials S2.

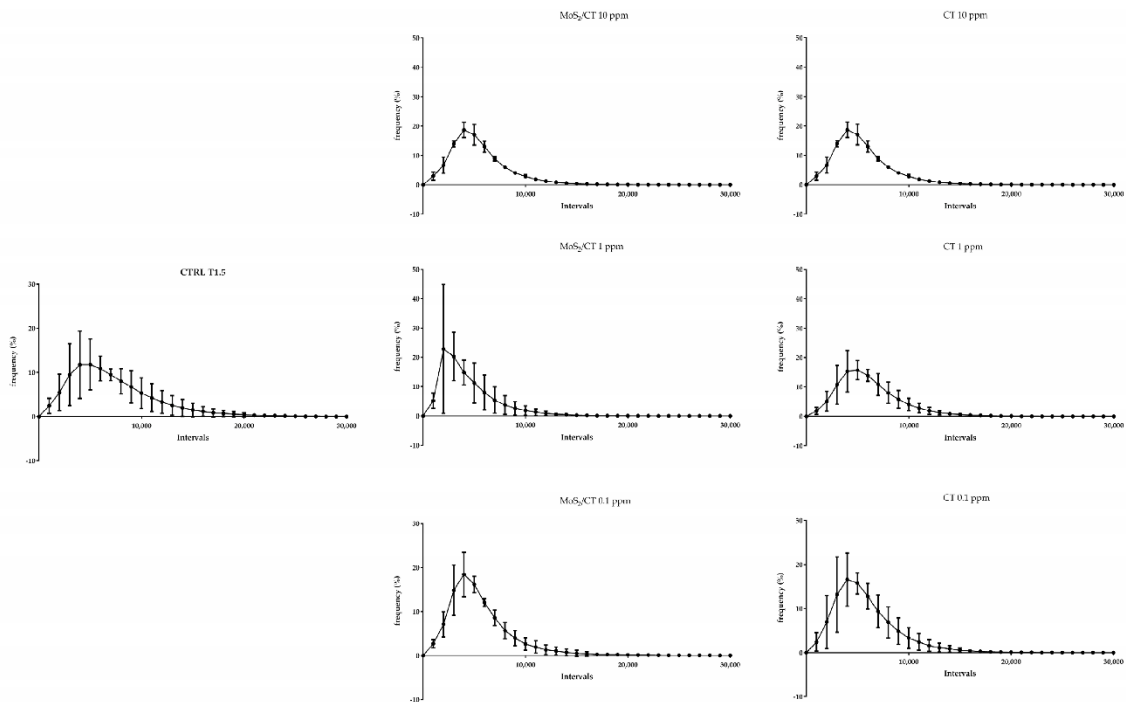


Figure 5. Flow cytometry analysis of mitochondrial activity. The graphs show the frequency of spermatozoa emitting a specific fluorescence intensity, which was subdivided into intervals ranging from 0 to 30,000 a.u. Capacitation was performed up to 1.5 h. Mitotracker Red was used in combination with a near-IR probe. Three independent technical and biological experiments were performed ($n = 3$).

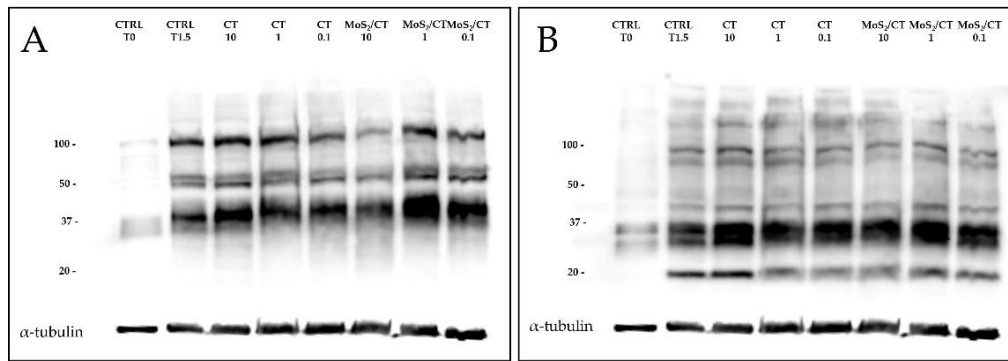


Figure 6. Western blot analysis of PKA activity and tyrosine phosphorylation patterns. The image illustrates (A) the PKA activity and (B) the tyrosine phosphorylation patterns after 1.5 h of incubation under capacitating conditions. Antibodies were incubated on the same blot after membrane stripping and re-blotting. Blots were cut prior to hybridization. α -tubulin was used as a load control. Each of the eight lanes contains 1×10^7 spermatozoa from different animals. At least three independent experiments with different animals were performed.

2.5. CT Supplementation Improves the IVF Outcomes

Finally, IVF was used as a functional test to evaluate the sperms' acquisition of the fertilizing ability after the exposure to MoS₂/CT and CT at selected concentrations. Since the analysis of the PKA activity, phosphorylation patterns, acrosome reaction induction, mitochondrial activity, membrane fluidity and intracellular calcium concentration revealed no differences among the groups treated with different concentrations of MoS₂/CT and CT (10, 1, 0.1 ppm), only the lowest concentrations were selected to perform the IVF assay, in order to minimize any potential risk, as well as the biological material needed.

IVF assays are a valuable tool to assess the sperm fertilizing ability in boar [46,47] due to the fact that the fertilization rates, the number of polyspermic oocytes and number of spermatozoa/polyspermic oocytes are related to the capacitation status and fertility of the semen [48,49]. As observed in Figure 7, the addition of CT alone at a specific concentration (0.1 ppm) during capacitation increases the spermatozoa fertilizing ability, evidenced by the increased number of fertilized oocytes and of polyspermic oocytes with respect to the control group.

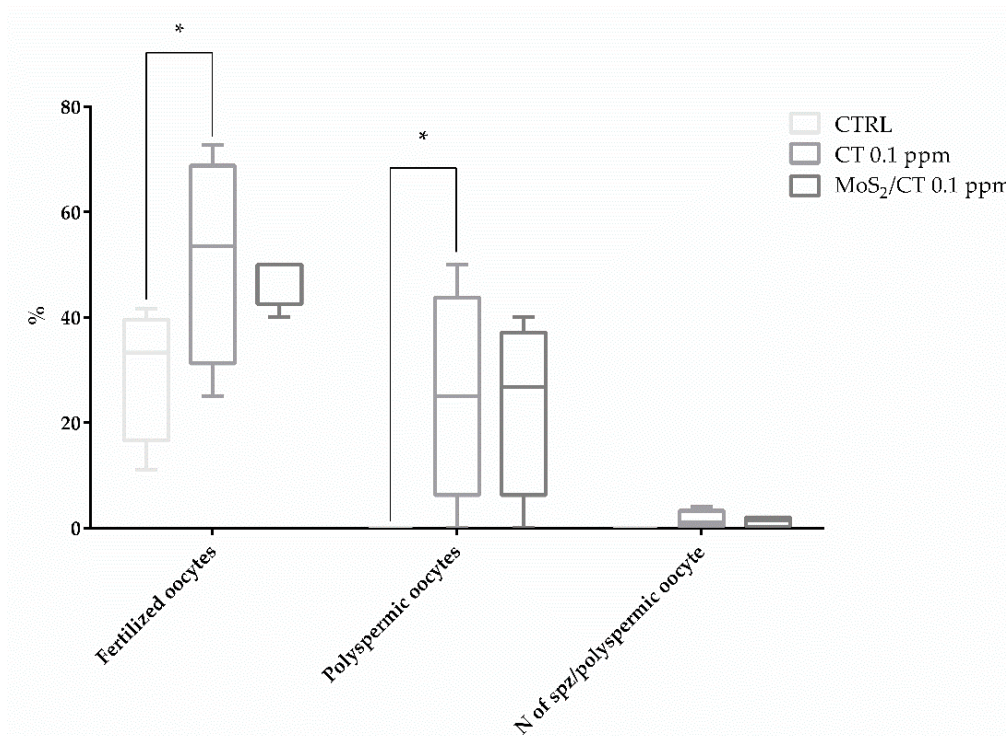


Figure 7. IVF outcomes. Three different groups were subjected to IVF assay: CTRL, CT 0.1 and MoS₂/CT 0.1 ppm. Data are expressed as percentages, showing the number of fertilized oocytes, the number of polyspermic oocytes and the number of spermatozoa per polyspermic oocyte, comparing the groups of spermatozoa capacitated in the presence of MoS₂/CT and CT (0.1 ppm) to the control group. Data were analyzed using Dunnett's test. * $p < 0.05$ versus control. Four independent experiments were performed.

Our findings support the evidence from previous studies showing that the addition of CT to the extender had a positive effect on sperm motility of caprine sperm [11].

This fact allows hypothesizing that the addition of CT might have provided an antioxidant activity, modulating the presence of reactive oxygen species (ROS) in our system. However, further experiments are needed to decipher the lipoperoxidation level and the ROS production, among others. The oxidative stress, observed by the excess of ROS, plays a key role in the life of mammalian sperm. Considering that spermatozoa are very sensitive to oxidative processes and that they are unable to transcribe and synthesize new proteins, with a cytosol virtually absent, preventing or fighting the oxidative stress remains hard to achieve [50]. This situation is aggravated due to the lipid composition of the plasma membrane, where the concentration of polyunsaturated fatty acids (PUFAs)

is higher than in other cell types. PUFAs are the main target of ROS, and their oxidation culminates in the generation of cytotoxic aldehydes. Furthermore, the peroxidation of membrane lipids leads to a loss of motility and flexibility, causing the loss of all membrane-dependent functions [50–52]. The major consequence of oxidative stress is the damage of the sperm's DNA [50,51].

Even if sperm cells are very susceptible to oxidative stress, low levels of ROS contribute to the full maturation of spermatozoa [50], which is necessary for capacitation, hyperactivation, acrosome reaction, oocyte fusion and fertilization [53,54]. Furthermore, there is a leading role in the interaction between ROS and cholesterol, since the oxidation of a part of cholesterol by ROS leads to the formation of oxysterols that facilitate the removal of cholesterol from the sperm plasma membrane to enhance the sperm membrane fluidity [55,56].

This study focused on the effect of an innovative material and a naturally derived compound on the spermatozoa fertilizing ability. Due to the results obtained, it is possible to affirm that nanoflakes of MoS₂/CT at different concentrations (10, 1, 0.1 ppm) do not induce any negative effect on the sperm parameters related to capacitation evaluated here. Moreover, CT alone at a specific concentration (0.1 ppm) acts as a helper of sperm capacitation by improving the IVF results, which could probably be explained by the balance of the ROS levels. These results open encouraging new perspectives for the improvement of Assisted Reproduction Technologies (ART), which has experienced an increase in use during the last decades, both in humans [57] and in animal farming [58]. At the same time, an improvement in these techniques could fight against the ever increasing prevalence of numerous pathologies associated with ART-generated embryos, since ARTs may epigenetically modify gene expression, influencing the long-term development of the embryo by mechanisms that should still be investigated. For instance,

many reports have shown the increasing prevalence of Angelman syndrome (AS), [59,60] and the phenomenon of large offspring syndrome in farm animals [61], with a phenotypic similarity to Beckwith–Wiedemann Syndrome (BWS) in humans [61–63].

3. Materials and Methods

3.1. Chemicals

Unless otherwise stated, all the chemicals were purchased from Sigma-Aldrich (St. Louis, MO, USA). Milli-Q water was purchased from Millipore (Bedford, MA, USA).

3.2. MoS₂ sonochemical exfoliation in water assisted by catechin

MoS₂ exfoliation assisted by catechin (CT) was conducted according to Rojas and colleagues (2022) [12] with some modifications. A total of 0.5 g of bulk MoS₂ powder (<2 μm ; 99% purity) was placed in 50 mL of a 2.5 mg mL⁻¹ (+)-catechin water solution (Milli-Q water) and roughly dispersed using a low-power ultrasonic bath. The dispersion was placed in a steel beaker and subjected to a sonochemical exfoliation treatment using a Branson SFX550 (550 W, 20 kHz) sonifier. The sonication probe employed was a 13 mm \varnothing Branson disruptor horn. Sonochemical exfoliation was conducted at 50% amplitude using a 5 h pulse program (2 s ON and 1 s OFF), maintaining the temperature below 15 °C. The obtained MoS₂/CT dispersion was thus subjected to purification and size selection via differential centrifugation. The MoS₂ not properly exfoliated was precipitated with centrifugation at 250 g (1 h). In this case, the supernatant was recovered, and the formed pellet discarded. The MoS₂/CT size selection and removal of the exfoliation medium containing the residual catechin in solution were conducted on the supernatant of the previous treatment, achieved via a 20,000 g centrifugation (15 min). Then, the supernatant was removed, and the sediment collected and resuspended in water.

The exfoliation yield was estimated via gravimetry, and MoS₂/CT water dispersion and was stored at 4 °C in the dark. MoS₂/CT before use was further purified via a 10,000 x g centrifugation, where the supernatant was discarded, and the sediment was recovered in sterile Dulbecco-PBS to obtain a 200 mg L⁻¹ MoS₂-CT working dispersion.

The pristine and exfoliated MoS₂ was characterized using a high-resolution scanning electron microscopy SIGMA (Carl Zeiss Microscopy GmbH, Munich, Germany). Solutions and materials used for in vitro studies were sterilized before their use and handled under a sterile hood. Catechin solutions were freshly prepared before use.

3.3. Experimental groups

For the present work, a total of seven experimental groups were analyzed. Control group without CT nor MoS₂/CT was included (CTRL). Complexes of MoS₂ functionalized with catechin (MoS₂/CT) were used at three different concentrations: MoS₂/CT 10 ppm; MoS₂/CT 1 ppm; and MoS₂/CT 0.1 ppm. These concentrations were established based on the available literature [33] and the absence of a consensus regarding the use of specific concentrations. As control, catechin alone (CT) was utilized at the same concentrations (CT 10 ppm, CT 1 ppm, CT 0.1 ppm). Finally, Figure 8 schematically illustrates the experimental design, representing the experimental groups and the analyses performed.

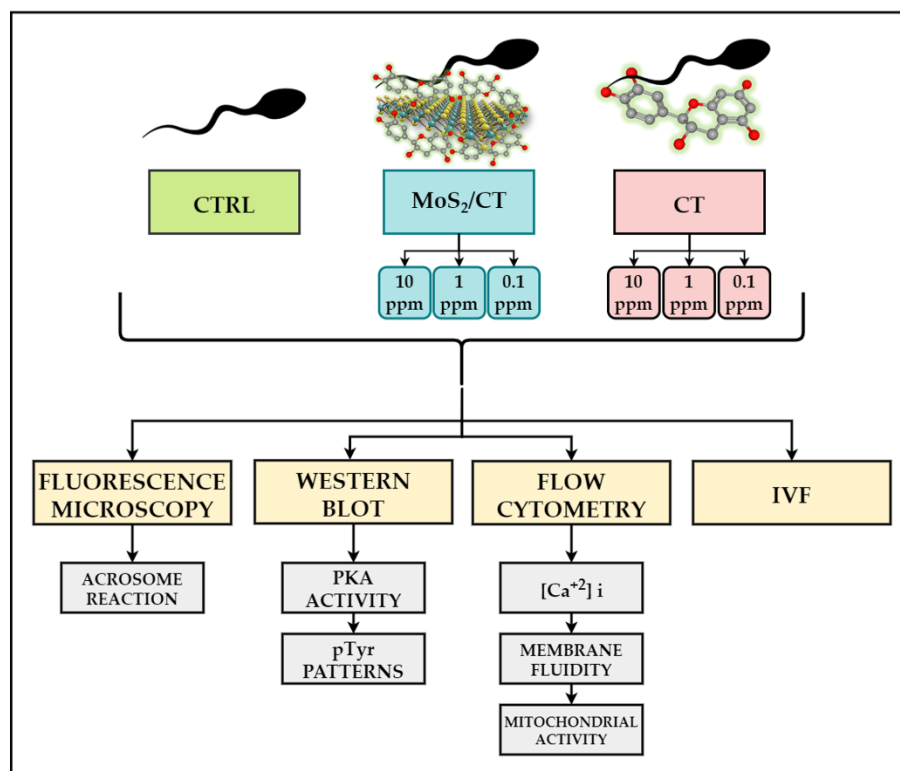


Figure 8. Experimental design. Spermatozoa were exposed to MoS₂ functionalized with catechin at different concentrations (10, 1, 0.1 ppm), catechin alone at the same concentrations (10, 1, 0.1 ppm) for 1.5 h in capacitation medium, a control group (CTRL) was maintained. Different sperm capacitation events were analyzed: acrosome damage, membrane fluidity, mitochondrial activity, intracellular calcium concentration, biochemical phosphorylation patterns and IVF assays.

3.4. Spermatozoa preparation and incubation

Spermatozoa were collected and washed following an already standardized protocol [64]. Briefly, sperm samples purchased from a specialized company (Società Agricola Geneetic S.r.l, Castellazzo, Italy) were incubated in a TCM199 medium supplemented with 13.9 mM glucose, 1.25 mM sodium pyruvate, 2.25 mM calcium lactate and 1 mM caffeine used to induce capacitation in vitro. MoS₂/CT and CT dispersions at different concentrations were added to the capacitating medium to obtain the sample groups: CT 10 ppm, CT 1 ppm, CT 0.1 ppm, MoS₂/CT 10 ppm, MoS₂/CT 1 ppm, and MoS₂/CT 0.1 ppm. Sperm cells were incubated at a final concentration of 1×10^7 cells/mL for 0 or 1.5 h at 38.5 °C in 5% CO₂ and a humidified atmosphere (Heraeus, Hera Cell). Sperm motility was visually estimated before the capacitation by light microscopy before each

experiment and only samples with sperm motility > 90% were considered for further analyses.

3.5. Monitoring of MoS₂/CT toxicity on acrosome integrity.

Acrosome integrity was monitored by using a two stain technique with Hoechst 33258 and FITC-PSA able to identify alive unreacted and reacted spermatozoa [65]. At least 100 cells were assessed by fluorescence microscopy in three independent experiments performed at different capacitation times (T0, T1.5), in the following groups: CTRL, MoS₂/CT, and CT treated spermatozoa (10, 1, 0.1 ppm).

3.6. Flow cytometry analysis of intracellular calcium concentration, membrane fluidity and mitochondrial activity

Flow cytometry analysis was performed to evaluate the differences between the different sperm groups in terms of: (a) intracellular calcium concentration; (b) sperm membrane lipid disorder; and (c) sperm mitochondrial activity. For each experiment and each condition (MoS₂/CT 10 ppm; MoS₂/CT 1 ppm; and MoS₂/CT 0.1 ppm; CT 10 ppm; CT 1 ppm; CT 0.1 ppm; CTRL), three different biological and technical experiments were performed at 0 and 1.5 h of capacitation.

After capacitation, sperm cells were placed in a flow cytometry tube and incubated at RT while gently shaking with: (a) 1 μ M Fluo 4-AM (15 min) to study the intracellular calcium concentration; (b) 1 μ M DilC-12 (15 min) to measure the membrane lipid disorder; and (c) 1 μ M Mitotracker Red (30 min) to check the activation of the mitochondria. To distinguish dead and live spermatozoa, two different stains were used when possible,

depending on the fluorescence emission spectra of the different probes previously stated: 1 μ M PI (5 min) was used in combination with Fluo 4-AM, while 1 μ L LIVE/DEAD™ Fixable Near-IR Dead Cell Stain Kit (Catalog number: L10119, ThermoFisher Scientific, Waltham, MA, USA) (10 min) was combined with Mitotracker Red. After the incubation time, 100,000 events/sample were acquired by flow cytometry (FACSCanto, BD Biosciences, Franklin Lakes, NJ, USA—three laser, eight color configuration). Each reagent was titrated (8-point titration) under assay conditions; dilutions were established based on achieving the highest signal (mean fluorescence intensity, MFI) for the positive population and the lowest signal for the negative population, representing the optimal signal-to-noise ratio, and stain indexes were calculated. Instrument performances, data reproducibility, and fluorescence calibrations were sustained and checked by the Cytometer Setup and Tracking Beads (BD Biosciences). To evaluate non-specific fluorescence, the Fluorescence Minus One (FMO) control was used. Compensation was assessed using CompBeads and FACSsuite FC Beads (BD Biosciences) and single stained fluorescent samples. Data were analyzed first using FACSsuite v 1.0.5 (BD Biosciences) software, and then FcsWizard Software was used to convert .fcs data to .csv format in order to perform an exhaustive analysis of the fluorescence emitted from every single spermatozoon for the various fluorescence probes [66]. To that, the columns “FCS”, “SSC”, “Fluo-4AM”, “PI”, “DiIC12”, “Mito” and “NIR” with the data from the 100,000 events acquired, were selected and filtered following these criteria: forward scatter (FCS) between 35,000 and 135,000 arbitrary units (a.u); side scatter (SSC) between 20,000 and 145,000 a.u; Fluo 3-AM, M540 and Mitotracker Red >0 a.u; PI between 0 and 30,000 a.u; and near infrared between 0 and 20,000 a.u. Then, data were treated and subdivided in intervals of fluorescence intensity as follow: 41 intervals for intracellular calcium (from 0 to 20,000 a.u, 500 a.u range); 101

intervals for membrane disorder (from 0 to 50,000 AU, 500 a.u range); 61 intervals for mitochondrial activity (from 0 to 30,000 a.u, 500 a.u range). At least 98% of the data fitted within this range.

3.7. Evaluation of Sperm PKA Activity and Tyrosine Phosphorylation Patterns (pTyr) by Western Blot

To evaluate protein kinase A (PKA) activity and protein tyrosine phosphorylation pattern (pTyr), at 1.5 h of capacitation, sperm cells were diluted in a sample buffer 5x (5 mM DDT, 2% SDS, 1 M Tris, 10% Glycerol and 0.1% Bromophenol blue), heated (100 °C for 5 min) and centrifuged (15,000 x g for 10 min at 4 °C). Proteins were migrated on an SDS-PAGE 4–15% gradient gel (Mini-PROTEAN® TGX™ Precast Protein Gels, BioRad, Hercules, CA, USA) and blotted on a nitrocellulose membrane using the Trans-Blot® Turbo™ Transfer System (BioRad, Steenvoorde, France). The membranes were stained with Ponceau S solution and scanned, then membranes were blocked for 1 h in 5% (w/v) milk powder diluted in TBS-T and incubated with anti-phospho-pKa antibody (Phospho-pKa Substrate (RRXS*/T*), dilution 1:5000, Rabbit mAb, Cell Signaling, Leiden, The Netherlands) in 5% (w/v) BSA (w/v) in TBS-T (gently shaking, 4 °C, overnight). After washing, membranes were incubated with secondary antibody anti-rabbit HRP (1:10,000, Santa Cruz Technology, Dallas, TX, USA) for 1 h. Peroxidase was revealed using the SuperSignal™ West Pico PLUS Chemiluminescent Substrate (ThermoFisher, Waltham, MA, USA) and the images were digitally captured using an Azure C300 (Chemiluminescent Western Blot Imaging System, Azure Biosystems, Dublin, CA, USA). Tyrosine phosphorylation was assessed on the same membranes by stripping the previous antibodies with Restore™ Western Blot Stripping Buffer (ThermoFisher). After washing, membranes were blocked in 10% (w/v) bovine gelatin (w/v) in TBS-T for 1 h and incubated with

anti-phosphotyrosine antibody (Clone 4G10, dilution 1:10,000, Mouse mAb, Merck Millipore, Burlington, MA, USA) in PBS-T for 1.5 h. After washing, membranes were finally incubated with the secondary anti- Mouse HRP (1:10,000, Santa Cruz Technology) antibody for 1 h and revealed as described previously in this section. At least three biological replicates were performed for each antibody and experimental group.

3.8. *In Vitro* Fertilization Assay

To study the potential effects of MoS₂/CT and CT on spermatozoa fertilizing ability, an in vitro fertilization (IVF) assay was carried out using an already validated protocol [65]. Ovaries from pre-pubertal gilts were collected at a local slaughterhouse and transported to the laboratory within 1 h at 25 °C. After washing, cumulus–oocyte complexes (COCs) were collected by aspirating the follicles that met the requirements (4–5 mm of diameter, translucent appearance, good vascularization and compactness of their granulosa layer and cumulus mass). Maturation was achieved in vitro by culturing the COCs in four-well dishes containing 500 µl of α -MEM medium supplemented with 10% FBS, 1% penicillin/streptomycin, 1% Ultraglutamine, 5 UI/mL hCG and 5 UI/mL PMSG for 44 h at 38.5 °C in a humidified atmosphere with 5% CO₂ (Heraeus, Hera Cell, Hanau, Germany).

Once matured, oocytes were denuded in Dulbecco-PBS with hyaluronidase on a warmed stage at 38.5 °C under a stereomicroscope. Only oocytes presenting the first polar body (MII stage) under the stereomicroscope were used for the IVF assay. Matured oocytes and capacitated sperm cells (1×10^6 cells/mL) from the selected groups (CTRL, CT 0.1 ppm and MoS₂/CT 0.1 ppm) were co-incubated in a fertilization medium (capacitation medium supplemented with 10% FBS). After 3 h

of co-incubation, oocytes were transferred to a fresh medium and maintained in culture for at least 12 h. The penetration rate was evaluated after staining with Hoechst 33342 and assessed under the fluorescence microscope. The IVF outcomes are expressed as fertilization rate (% of penetrated oocytes), incidence of polyspermy (% of polyspermic oocytes) and number of penetrating spermatozoa/polyspermic oocyte according to already published and valuable works [47,65]. A total of four independent experiments were performed, reaching a total number of 104 oocytes (number of fertilized oocytes per group: CTRL, 10 fertilized of 33 total oocytes; CT 0.1 ppm 18 fertilized of 34 total oocytes; MoS₂/CT 0.1 ppm 18 fertilized of 37 total oocytes).

3.9. Statistical analysis

For statistical analysis, GraphPad Prism 6 Software (La Jolla, CA, USA) was used. Data were checked for normal distribution with a D'Agostino and Pearson normality test prior to performing the comparison with parametric or non-parametric tests, as required. In all cases, the differences among groups were considered statistically significant when $p < 0.05$. To normalize the western blot data, Ponceau red staining was used, following a validated protocol [67]. Briefly, the whole lanes were quantified by densitometry and bands were afterwards quantified using ImageQuantTL (GE Healthcare LifeSciences, Barrington, IL, USA). To assess the effect of different treatments on IVF, four independent technical and biological experiments were carried out. An a priori power analysis was performed to establish the number of oocytes with G*Power 3.1.9.7 software, obtaining a final power of our analysis $\geq 95\%$.

4. Conclusions

In conclusion, our study demonstrates that the incubation of spermatozoa in the presence of catechins (0.1 ppm) enhances their fertilizing ability and the incubation with nanoflakes of MoS₂/CT at different concentrations do not induce any negative effect on the sperm parameters related to capacitation. However, further experiments are needed to decipher the exact mechanism by which catechins are able to increase the sperm fertilizing ability and to explore their antioxidant potential on spermatozoa.

The findings open interesting perspectives regarding the use of catechins and new materials obtained using natural or bio compounds, which could be used to implement the current strategies for sperm capacitation.

Supplementary Materials: The following supporting information can be downloaded at: <https://www.mdpi.com/article/10.3390/ijms24054788/s1>.

Author Contributions: N.B. and D.C. conceptualized the study; A.S., F.D.P., C.C., M.R.-S. and A.T. designed the experiments; A.S. and F.D.P. prepared and characterized the molybdenum disulfide and catechins solutions; C.C., M.R.-S. and A.T. performed western blot experiments; C.C., A.T., G.C. and R.B.-P. realized IVF experiments; P.L., M.M. and M.R.-S. performed the flow cytometry experiments; P.L., M.R.-S. and M.D. analyzed the flow cytometry data; M.D., C.O. and S.P. developed the FacsWizard Software L.V. realized all figures; C.C., M.R.-S. and N.B. analyzed the data and prepared the original draft; all authors contributed to the analysis, writing and editing of the manuscript; D.C., B.B. and N.B. supervised and funded the research. All authors have read and agreed to the published version of the manuscript.

Funding: This research received no external funding. Institutional Review Board Statement: Not applicable. Informed Consent Statement: Not applicable.

Data Availability Statement: The original contributions presented in the study are included in the article/Supplementary Materials, further inquiries can be directed to the corresponding author.

Acknowledgments: F.D.P. and D.C. acknowledge the Ministry of Education, University and Research (MIUR) and the European Social Fund (ESF) for the PON R&I 2014–2020 program, action 1.2, and AIM: Attraction and International Mobility (AIM1894039-3).

Conflicts of Interest: The authors declare no conflict of interest.

5. References

1. Bernabò, N.; Fontana, A.; Sanchez, M.R.; Valbonetti, L.; Capacchietti, G.; Zappacosta, R.; Greco, L.; Marchisio, M.; Lanuti, P.; Ercolino, E.; et al. Graphene oxide affects in vitro fertilization outcome by interacting with sperm membrane in an animal model. *Carbon* **2018**, *129*, 428–437. [[CrossRef](#)]
2. Bernabò, N.; Valbonetti, L.; Raspa, M.; Fontana, A.; Palestini, P.; Botto, L.M.; Paoletti, R.; Fray, M.; Allen, S.; Machado- Simoes, J.S.; et al. Graphene Oxide Improves In Vitro Fertilization in Mice with no Impact on Embryo Development and Preserves the Membrane Microdomains Architecture. *Front. Bioeng. Biotechnol.* **2020**, *8*, 629. [[CrossRef](#)]
3. Ramal-Sanchez, M.; Valbonetti, L.; Tsikis, G.; Dubuisson, F.; Blache, M.-C.; Labas, V.; Druart, X.; Fontana, A.; Mermillod, P.; Barboni, B.; et al. Graphene oxide: A glimmer of hope for Assisted Reproductive Technology. *Carbon* **2019**, *150*, 518–530. [[CrossRef](#)]
4. Rojas, D.; Della Pelle, F.; Del Carlo, M.; Compagnone, D.; Escarpa, A. Group VI transition metal dichalcogenides as antifouling transducers for electrochemical oxidation of catechol-containing structures. *Electrochem. Commun.* **2020**, *115*, 106718. [[CrossRef](#)]
5. Zhou, X.; Sun, H.; Bai, X. Two-Dimensional Transition Metal Dichalcogenides: Synthesis, Biomedical Applications and Biosafety Evaluation. *Front. Bioeng. Biotechnol.* **2020**, *8*, 236. [[CrossRef](#)]
6. Della Pelle, F.; Rojas, D.; Silveri, F.; Ferraro, G.; Fratini, E.; Scroccarello, A.; Escarpa, A.; Compagnone, D. Class-selective voltammetric determination of hydroxycinnamic acids structural analogs using a WS₂/catechin-capped

- AuNPs/carbon black–based nanocomposite sensor. *Mikrochim. Acta* **2020**, *187*, 296. [[CrossRef](#)]
7. Agarwal, V.; Chatterjee, K. Recent advances in the field of transition metal dichalcogenides for biomedical applications. *Nanoscale* **2018**, *10*, 16365–16397. [[CrossRef](#)]
 8. Scalisi, E.M.; Salvaggio, A.; Antoci, F.; Messina, A.; Pecoraro, R.; Cantarella, M.; Gorrasi, G.; Impellizzeri, G.; Brundo, M.V. Toxicity assessment of two-dimensional nanomaterials molybdenum disulfide in *Gallus gallus domesticus*. *Ecotoxicol. Environ. Saf.* **2020**, *200*, 110772. [[CrossRef](#)]
 9. Teo, W.Z.; Chng, E.L.K.; Sofer, Z.; Pumera, M. Cytotoxicity of exfoliated transition-metal dichalcogenides (MoS₂, WS₂, and WSe₂) is lower than that of graphene and its analogues. *Chem.-A Eur. J.* **2014**, *20*, 9627–9632. [[CrossRef](#)]
 10. Di Mattia, C.D.; Sacchetti, G.; Mastrocola, D.; Serafini, M. From Cocoa to Chocolate: The Impact of Processing on In Vitro Antioxidant Activity and the Effects of Chocolate on Antioxidant Markers In Vivo. *Front. Immunol.* **2017**, *8*, 1207. [[CrossRef](#)]
 11. Purdy, P.H.; Ericsson, S.A.; Dodson, R.E.; Sternes, K.L.; Garner, D.L. Effects of the flavonoids, silibinin and catechin, on the motility of extended cooled caprine sperm. *Small Rumin. Res.* **2004**, *55*, 239–243. [[CrossRef](#)]
 12. Rojas, D.; Della Pelle, F.; Silveri, F.; Ferraro, G.; Fratini, E.; Compagnone, D. Phenolic compounds as redox-active exfoliation agents for group VI transition metal dichalcogenides. *Mater. Today Chem.* **2022**, *26*, 101122. [[CrossRef](#)]
 13. Silveri, F.; Della Pelle, F.; Rojas, D.; Bukhari, Q.U.A.; Ferraro, G.; Fratini, E.; Compagnone, D. (+)-Catechin-assisted graphene production by sonochemical

exfoliation in water. A new redox-active nanomaterial for electromediated sensing. *Mikrochim. Acta* **2021**, *188*, 369. [[CrossRef](#)]

14. Nguyen, E.P.; Daeneke, T.; Zhuiykov, S.; Kalantar-Zadeh, K. Liquid Exfoliation of Layered Transition Metal Dichalcogenides for Biological Applications. *Curr. Protoc. Chem. Biol.* **2016**, *8*, 97–108. [[CrossRef](#)]
15. Della Pelle, F.; Blandón-Naranjo, L.; Alzate, M.; Del Carlo, M.; Compagnone, D. Cocoa powder and catechins as natural mediators to modify carbon-black based screen-printed electrodes. Application to free and total glutathione detection in blood. *Talanta* **2020**, *207*, 120349. [[CrossRef](#)]
16. Scroccarello, A.; Della Pelle, F.; Ferraro, G.; Fratini, E.; Tempera, F.; Dainese, E.; Compagnone, D. Plasmonic active film integrating gold/silver nanostructures for H₂O₂ readout. *Talanta* **2021**, *222*, 121682. [[CrossRef](#)]
17. Cimini, C.; Moussa, F.; Taraschi, A.; Ramal-Sanchez, M.; Colosimo, A.; Capacchietti, G.; Mokh, S.; Valbonetti, L.; Tagaram, I.; Bernabò, N.; et al. Pre-Treatment of Swine Oviductal Epithelial Cells with Progesterone Increases the Sperm Fertilizing Ability in an IVF Model. *Animal* **2022**, *12*, 1191. [[CrossRef](#)]
18. Ramal-Sanchez, M.; Bernabo, N.; Tsikis, G.; Blache, M.C.; Labas, V.; Druart, X.; Mermillod, P.; Saint-Dizier, M. Progesterone induces sperm release from oviductal epithelial cells by modifying sperm proteomics, lipidomics and membrane fluidity. *Mol. Cell. Endocrinol.* **2020**, *504*, 110723. [[CrossRef](#)]
19. Romero-Aguirregomezcorta, J.; Cronin, S.; Donnellan, E.; Fair, S. Progesterone induces the release of bull spermatozoa from oviductal epithelial cells. *Reprod. Fertil. Dev.* **2019**, *31*, 1463–1472. [[CrossRef](#)]
20. Santos, R.R.; Schoevers, E.J.; Roelen, B.A. Usefulness of bovine and porcine IVM/IVF models for reproductive toxicology. *Reprod. Biol. Endocrinol.* **2014**,

12, 117. [[CrossRef](#)]

21. Swindle, M.M.; Makin, A.; Herron, A.J.; Clubb, F.J.; Frazier, K.S. Swine as Models in Biomedical Research and Toxicology Testing. *Vet. Pathol.* **2012**, *49*, 344–356. [[CrossRef](#)]
22. Walters, E.M.; Prather, R.S. Advancing swine models for human health and diseases. *Mo. Med.* **2013**, *110*, 212–215.
23. Grayfer, E.D.; Kozlova, M.N.; Fedorov, V.E. Colloidal 2D nanosheets of MoS₂ and other transition metal dichalcogenides through liquid-phase exfoliation. *Adv. Colloid Interface Sci.* **2017**, *245*, 40–61. [[CrossRef](#)]
24. Backes, C.; Higgins, T.M.; Kelly, A.; Boland, C.; Harvey, A.; Hanlon, D.; Coleman, J.N. Guidelines for exfoliation, characterization and processing of layered materials produced by liquid exfoliation. *Chem. Mater.* **2017**, *29*, 243–255. [[CrossRef](#)]
25. Bukhari, Q.U.A.; Silveri, F.; Della Pelle, F.; Scroccarello, A.; Zappi, D.; Cozzoni, E.; Compagnone, D. Water-Phase Exfoliated Biochar Nanofibers from Eucalyptus Scraps for Electrode Modification and Conductive Film Fabrication. *ACS Sustain. Chem. Eng.* **2021**, *9*, 13988–13998. [[CrossRef](#)]
26. Scroccarello, A.; Molina-Hernández, B.; Della Pelle, F.; Ciancetta, J.; Ferraro, G.; Fratini, E.; Valbonetti, L.; Chaves Copez, C.; Compagnone, D. Effect of phenolic compounds-capped AgNPs on growth inhibition of *Aspergillus niger*. *Colloids Surf. B. Biointerfaces* **2021**, *199*, 111533. [[CrossRef](#)]
27. Molina-Hernández, J.B.; Scroccarello, A.; Della Pelle, F.; De Flaviis, R.; Compagnone, D.; Del Carlo, M.; Paparella, A.; ChavesLópez, C. Synergistic antifungal activity of catechin and silver nanoparticles on *Aspergillus niger*

- isolated from coffee seeds. *LWT* **2022**, *169*, 113990. [[CrossRef](#)]
28. Saiz-Poseu, J.; Mancebo-Aracil, J.; Nador, F.; Busqué, F.; Ruiz-Molina, D. The Chemistry behind Catechol-Based Adhesion. *Angew. Chem. Int. Ed.* **2019**, *58*, 696–714. [[CrossRef](#)]
29. Samadi, M.; Sarikhani, N.; Zirak, M.; Zhang, H.; Zhang, H.L.; Moshfegh, A.Z. Group 6 transition metal dichalcogenide nanomaterials: Synthesis, applications and future perspectives. *Nanoscale Horiz.* **2018**, *3*, 90–204. [[CrossRef](#)]
30. Ickowicz, D.; Finkelstein, M.; Breitbart, H. Mechanism of sperm capacitation and the acrosome reaction: Role of protein kinases. *Asian J. Androl.* **2012**, *14*, 816–821. [[CrossRef](#)]
31. Bernabò, N.; Mattioli, M.; Barboni, B. The spermatozoa caught in the net: The biological networks to study the male gametes post-ejaculatory life. *BMC Syst. Biol.* **2010**, *4*, 87. [[CrossRef](#)]
32. Finkelstein, M.; Etkovitz, N.; Breitbart, H. Ca^{2+} signaling in mammalian spermatozoa. *Mol. Cell. Endocrinol.* **2020**, *516*, 110953. [[CrossRef](#)]
33. Tvrdá, E.; Benko, F.; Slanina, T.; du Plessis, S.S. The role of selected natural biomolecules in sperm production and functionality. *Molecules* **2021**, *26*, 5196. [[CrossRef](#)]
34. Ded, L.; Hwang, J.Y.; Miki, K.; Shi, H.F.; Chung, J.J. 3D in situ imaging of female reproductive tract reveals molecular signatures of fertilizing spermatozoa in mice. *eLife* **2020**, *9*, e62043. [[CrossRef](#)]
35. Bernabò, N.; Berardinelli, P.; Mauro, A.; Russo, V.; Lucidi, P.; Mattioli, M.;

- Barboni, B. The role of actin in capacitation-related signaling: An in silico and in vitro study. *BMC Syst. Biol.* **2011**, *5*, 47. [[CrossRef](#)]
36. Gadella, B.M.; Tsai, P.; Boerke, A.; Brewis, I.A. Sperm head membrane reorganisation during capacitation. *Int. J. Dev. Biol.* **2008**, *52*, 473–480. [[CrossRef](#)]
37. Hickey, K.D.; Buhr, M.M. Lipid Bilayer Composition Affects Transmembrane Protein Orientation and Function. *J. Lipids* **2011**, *2011*, 208457. [[CrossRef](#)]
38. Bernabò, N.; Greco, L.; Ordinelli, A.; Mattioli, M.; Barboni, B. Capacitation-Related Lipid Remodeling of Mammalian Spermatozoa Membrane Determines the Final Fate of Male Gametes: A Computational Biology Study. *OMICS* **2015**, *19*, 712–721. [[CrossRef](#)]
39. Bernabò, N.; Valbonetti, L.; Greco, L.; Capacchietti, G.; Ramal Sanchez, M.; Palestini, P.; Botto, L.; Mattioli, M.; Barboni, B. Aminopurvalanol A, a Potent, Selective, and Cell Permeable Inhibitor of Cyclins/Cdk Complexes, Causes the Reduction of In Vitro Fertilizing Ability of Boar Spermatozoa, by Negatively Affecting the Capacitation-Dependent Actin Polymerization. *Front. Physiol.* **2017**, *8*, 1097. [[CrossRef](#)]
40. Amaral, A.; Lourenço, B.; Marques, M.; Ramalho-Santos, J. Mitochondria functionality and sperm quality. *Reproduction* **2013**, *146*, R163–R174. [[CrossRef](#)]
41. Amaral, A.; Paiva, C.; Attardo Parrinello, C.; Estanyol, J.M.; Ballescà, J.L.; Ramalho-Santos, J.; Oliva, R. Identification of Proteins Involved in Human Sperm Motility Using High-Throughput Differential Proteomics. *J. Proteome*

Res. **2014**, *13*, 5670–5684. [[CrossRef](#)]

42. Zapata-Carmona, H.; Barón, L.; Zuñiga, L.M.; Díaz, E.S.; Kong, M.; Drobnis, E.Z.; Sutovsky, P.; Morales, P. The activation of the chymotrypsin-like activity of the proteasome is regulated by soluble adenylyl cyclase/cAMP/protein kinase A pathway and required for human sperm capacitation. *Mol. Hum. Reprod.* **2019**, *25*, 587–600. [[CrossRef](#)]
43. Molina, L.C.P.; Luque, G.M.; Balestrini, P.A.; Marín-Briggiler, C.I.; Romarowski, A.; Buffone, M.G. Molecular basis of human sperm capacitation. *Front. Cell Dev. Biol.* **2018**, *6*, 72. [[CrossRef](#)]
44. Balbach, M.; Beckert, V.; Hansen, J.N.; Wachten, D. Shedding light on the role of cAMP in mammalian sperm physiology. *Mol. Cell. Endocrinol.* **2018**, *468*, 111–120. [[CrossRef](#)]
45. Signorelli, J.; Diaz, E.S.; Morales, P. Kinases, phosphatases and proteases during sperm capacitation. *Cell Tissue Res.* **2012**, *349*, 765–782. [[CrossRef](#)]
46. Suzuki, H.; Saito, Y.; Kagawa, N.; Yang, X. In vitro fertilization and polyspermy in the pig: Factors affecting fertilization rates and cytoskeletal reorganization of the oocyte. *Microsc. Res. Tech.* **2003**, *61*, 327–334. [[CrossRef](#)]
47. Abeydeera, L.R.; Day, B.N. Fertilization and subsequent development in vitro of pig oocytes inseminated in a modified Tris-buffered medium with frozen-thawed ejaculated spermatozoa. *Biol. Reprod.* **1997**, *57*, 729–734. [[CrossRef](#)]
48. Abeydeera, L.R.; Funahashi, H.; Kim, N.H.; Day, B.N. Chlortetracycline fluorescence patterns and in vitro fertilisation of frozen-thawed boar spermatozoa incubated under various bicarbonate concentrations. *Zygote* **1997**, *5*, 117–125. [[CrossRef](#)]
49. Hunter, R.H.F.; Nichol, R. Capacitation potential of the fallopian tube: A study

involving surgical insemination and the subsequent incidence of polyspermy.

Gamete Res. **1988**, *21*, 255–266. [[CrossRef](#)]

50. Drevet, J.R.; Aitken, R.J. Oxidation of sperm nucleus in mammals: A physiological necessity to some extent with adverse impacts on oocyte and offspring. *Antioxidants* **2020**, *9*, 95. [[CrossRef](#)]
51. Agarwal, A.; Virk, G.; Ong, C.; du Plessis, S.S. Effect of Oxidative Stress on Male Reproduction. *World J. Mens. Health* **2014**, *32*, 1–17. [[CrossRef](#)]
52. Castellini, C.; D'andrea, S.; Cordeschi, G.; Totaro, M.; Parisi, A.; Di Emidio, G.; Tatone, C.; Francavilla, S.; Barbonetti, A. Pathophysiology of Mitochondrial Dysfunction in Human Spermatozoa: Focus on Energetic Metabolism, Oxidative Stress and Apoptosis. *Antioxidants* **2021**, *10*, 695. [[CrossRef](#)]
53. Sanocka, D.; Kurpisz, M. Reactive oxygen species and sperm cells. *Reprod. Biol. Endocrinol.* **2004**, *2*, 12. [[CrossRef](#)]
54. Kodama, H.; Kuribayashi, Y.; Gagnon, C. Effect of Sperm Lipid Peroxidation on Fertilization. *J. Androl.* **1996**, *17*, 151–157. [[CrossRef](#)]
55. Leahy, T.; Gadella, B.M. New insights into the regulation of cholesterol efflux from the sperm membrane. *Asian J. Androl.* **2015**, *17*, 561–567. [[CrossRef](#)]
56. Aitken, R.J.; Drevet, J.R. The Importance of Oxidative Stress in Determining the Functionality of Mammalian Spermatozoa: A Two-Edged Sword. *Antioxidants* **2020**, *9*, 111. [[CrossRef](#)]
57. Wyns, C.; De Geyter, C.; Calhaz-Jorge, C.; Kupka, M.S.; Motrenko, T.; Smeenk, J.; Bergh, C.; Tandler-Schneider, A.; Rugescu, I.A.; Vidakovic, S.; et al. ART in Europe, 2017: Results generated from European registries by ESHRE. *Hum. Reprod. Open* **2021**, *2021*, hoab026. [[CrossRef](#)]

58. Viana, H.J. 2020 Statistics of embryo production and transfer in domestic farm animals World embryo industry grows despite the Pandemic. *Embryo Technol. Newsl.* **2021**, 39, 4.
59. Ludwig, M.; Katalinic, A.; Groß, S.; Sutcliffe, A.; Varon, R.; Horsthemke, B. Increased prevalence of imprinting defects in patients with Angelman syndrome born to subfertile couples. *J. Med. Genet.* **2005**, 42, 289–291. [[CrossRef](#)]
60. Eroglu, A.; Layman, L.C. Role of ART in Imprinting Disorders. *Semin. Reprod. Med.* **2007**, 83, 255–262. [[CrossRef](#)]
61. Li, Y.; Hagen, D.E.; Ji, T.; Bakhtiarizadeh, M.R.; Frederic, W.M.; Traxler, E.M.; Kalish, J.M.; Rivera, R.M. Altered microRNA expression profiles in large offspring syndrome and Beckwith-Wiedemann syndrome. *Epigenetics* **2019**, 14, 850–876. [[CrossRef](#)]
62. Grace, K.S.; Sinclair, K.D. Assisted reproductive technology, epigenetics, and long-term health: A developmental time bomb still ticking. *Semin. Reprod. Med.* **2009**, 27, 409–416. [[CrossRef](#)]
63. La Rovere, M.; Franzago, M.; Stuppia, L. Epigenetics and Neurological Disorders in ART. *Int. J. Mol. Sci.* **2019**, 20, 4169. [[CrossRef](#)]
64. Maccarrone, M.; Barboni, B.; Paradisi, A.; Bernabò, N.N.; Gasperi, V.; Pistilli, M.G.; Fezza, F.; Lucidi, P.; Mattioli, M. Characterization of the endocannabinoid system in boar spermatozoa and implications for sperm capacitation and acrosome reaction. *J. Cell Sci.* **2005**, 118, 4393–4404. [[CrossRef](#)]
65. Bernabò, N.; Tettamanti, E.; Russo, V.; Martelli, A.; Turriani, M.; Mattoli, M.; Barboni, B. Extremely low frequency electromagnetic field exposure affects

fertilization outcome in swine animal model. *Theriogenology* **2010**, *73*, 1293–1305. [[CrossRef](#)]

66. Raspa, M.; Putti, S.; Paoletti, R.; Barboni, B.; Ramal-Sanchez, M.; Lanuti, P.; Marchisio, M.; D'Atri, M.; Ortolani, C.; Papa, S.; et al. The impact of five years storage/biobanking at 80 °C on mouse spermatozoa fertility, physiology, and function. *Andrology* **2021**, *9*, 989–999. [[CrossRef](#)]
67. Romero-Calvo, I.; Ocón, B.; Martínez-Moya, P.; Suárez, M.D.; Zarzuelo, A.; Martínez-Augustin, O.; de Medina, F.S. Reversible Ponceau staining as a loading control alternative to actin in Western blots. *Anal. Biochem.* **2010**, *401*, 318–320. [[CrossRef](#)]

The background of the slide features abstract, flowing, and overlapping lines in shades of light blue and white, creating a sense of movement and depth. These lines are more concentrated on the left side and fade towards the right.

CHAPTER III

Delving into oviduct architecture

Manuscript 3

Exploring Swine Oviduct Anatomy Through Micro-Computed Tomography: A 3D Modeling Perspective

Manuscript in preparation

Ramses Belda-Perez^{1,2}, Costanza Cimini¹, Tiziana Orsini³ Annunziata D'Elia³, Roberto Massari³, Carlo Di Carlo¹, Alessia Paradiso¹, Seerat Maqsood¹, Marcello Raspa³, Luca Valbonetti^{1,3}, Nicola Bernabò^{1*}, Barbara Barboni¹

¹ Department of Biosciences and Technology for Food, Agriculture and Environment, University of Teramo, 64100 Teramo, Italy.

² Physiology of Reproduction Group, Department of Physiology, Faculty of Veterinary Medicine, International Excellence Campus for Higher Education and Research (Campus Mare Nostrum), University of Murcia, 30100 Murcia, Spain.

³ Institute of Biochemistry and Cell Biology (CNRIBBC/EMMA/Infrafrontier/IMPC), National Research Council, 00015 Rome, Italy.

*** Correspondence:** Nicola Bernabò, nbernabo@unite.it

Keywords: oviduct, MicroCT, 3D-reconstruction, swine

Abstract

The oviduct plays a crucial role in the reproductive process, acting as the conduit for the intricate journey of life initiation in mammals. In this organ, essential processes take place, serving as the stage for fertilization and the early stages of embryonic development. This organ has traditionally been studied through conventional microscopy methods, although such approaches come with inherent limitations, such as the potential for distortions and sample destruction during the preparation process. This study delves into the anatomical intricacies of the oviduct, focusing on two regions, the uterotubal junction (UTJ) and the ampullary-isthmic junction (AIJ) using micro-computed tomography (MicroCT), a non-destructive, high-resolution alternative to explore the 3D anatomy of the UTJ and AIJ regions. In this study, the portions of the UTJ and AIJ of a paraffin-embedded oviduct have been reconstructed using images obtained through MicroCT. Additionally, we have taken measurements of the height and width of the folds within the oviduct, along with assessments of dimension fractal, lacunarity, and shape

factor. Results reveal variations in mucosal folds, with increased size and lumen occupancy towards the ampulla. Additionally, blind sacs or crypts are observed, akin to those found in various species, suggesting potential roles in sperm sequestration or reservoir formation. MicroCT's ability to generate detailed 3D models opens avenues for applications beyond anatomy studies. The obtained data could serve as a basis for creating 3D-printed replicas. In conclusion, this research provides information about the oviduct anatomy, leveraging MicroCT technology for detailed 3D reconstructions, which can significantly contribute to the understanding of geometric-morphological characteristics influencing functional traits.

1. Introduction

The oviduct is the organ that connects the ovaries to the uterus, serving as the site where the journey of life begins for all mammals. Anatomically, this organ is divided into 4 regions, the infundibulum, the ampulla, the isthmus, and the uterotubal junction (Coy et al., 2018). After ovulation, the infundibulum is responsible for collecting the cumulus-oocyte complex, and on the isthmus, the sperm will form the spermathecal reservoir attaching to the epithelial cells, suffering changes in its membrane, and prolonging their viability. During ovulation, sperm will be released from the reservoir and reach the ampulla, where fertilization takes place. On the other hand, the uterine-tubal junction could be considered one of the main selection barriers (Mahé et al., 2021). The epithelium of the oviduct is composed of two types of cells: secretory and ciliated. The secretory cells are responsible for the formation of oviductal fluid (Hugentobler et al., 2010), which plays an important role in creating an appropriate environment for the transport and nourishment of gametes, as well as in protecting the fertilized egg during its journey through the oviduct (Ménézo et al., 2015). Conversely, the ciliated cells possess carbohydrate residues that are recognized by lectin-like proteins on the head of spermatozoa, leading to their binding

and the creation of the previously mentioned sperm reservoir (Talevi and Gualtieri, 2010). The oviduct has a dynamic environment, since its cell proportion and functionality change in response to the hormonal swings that take place throughout the cycle (Steinhauer et al., 2004; Yániz et al., 2000). For instance, during the follicular phase, ciliated cells prevail in the ampulla of the oviduct while during the luteal phase, secretory cells take the forefront in this region (Abe, 1996). By contrast, in other segments of the oviduct, like the isthmus, the proportion of these cell types remains relatively stable with minimal variations throughout the estrus cycle (Abe, 1996).

Understanding the anatomy of the oviduct is important for comprehending the processes that take place within it. However, traditional microscopy methods have their limitations, such as potential distortions and the destruction of samples during preparation (Miranda et al., 2015). In this context, micro-computed tomography (MicroCT) emerges as a promising alternative for anatomical studies of the oviduct and other complex structures. MicroCT offers a powerful and versatile approach to studying anatomical structures like the oviduct. Its non-destructive nature, high resolution, three-dimensional visualization capabilities, and quantitative analysis tools make it an invaluable tool for advancing our understanding of reproductive biology and other fields of biological research.

Exploring the three-dimensional anatomy of the uterotubal junction and the ampullary-isthmic junction using MicroCT technology represents a significant advancement in our understanding of reproductive biology. This innovative approach allows us to delve deep into the intricate structures of the oviducts, shedding light on their morphology and spatial relationships in ways that were previously inaccessible.

By employing MicroCT, it is possible to capture highly detailed and precise images of these anatomical regions, providing a level of insight that traditional two-dimensional imaging methods cannot match. This capability is particularly valuable in the study of the uterotubal junction and the ampullary-isthmic junction, where subtle variations in morphology can have profound implications for reproductive function.

Furthermore, this pilot study serves as an important validation of the utility of MicroCT in anatomical research. By demonstrating its effectiveness in imaging delicate structures like the oviducts, we pave the way for future studies to leverage this technology for a wide range of anatomical investigations. Moreover, the ability to generate detailed three-dimensional models of oviduct anatomy opens up new avenues for research and education. These models could serve as valuable tools for teaching anatomy to medical and veterinary students, as well as for training surgeons in specialized procedures. Additionally, researchers can utilize these models to create 3D-printed scaffolds that precisely mimic the anatomical and physiological conditions of the oviduct. By replicating the intricate structures and microenvironments of the oviducts, these scaffolds hold the potential to advance various fields, including tissue engineering, drug delivery systems, and regenerative medicine. This innovative approach allows for more accurate experimentation and testing, leading to the development of targeted interventions for conditions affecting the oviducts

2. Materials and methods

2.1. Oviduct selection and collection

Genital tracts from sows and gilts were obtained at the local slaughterhouse and transported into the lab within 2 hours of slaughter. Once in the lab, the cycle stage of the tracts was determined based on the ovarian morphology as described previously (Carrasco et al., 2008) and classified into early follicular, late follicular, early luteal, or

late luteal phase. An oviduct was selected for each phase of the reproductive cycle, dissected and divided into segments. The portions corresponding to the isthmus and the uterine-tubal junction were washed in PBS and fixed in 4% paraformaldehyde for 1 hour. Subsequently, the samples underwent dehydration through a series of alcoholic solutions (ranging from 50% to 100%) and soaked in xylene 3 times for 15 minutes each (45 min tot). An incubation step with xylene paraffin (1:1) was carried out for 45 minutes at 56°C before embedding in paraffin wax.

2.2. MicroCT and Image acquisition

MicroCT datasets of swine oviducts at different stages of estrous cycle were acquired by using the high-resolution 3D-imaging system Skyscan 1172G (Bruker, Kontich – Belgium), using an L7901-20 Microfocus X-ray Source (Hamamatsu), with image pixel/size of 7.4 μm , camera binning 2x2, source voltage of 39 kV, source current of 240 μA , exposure time of 500 ms. The reconstructed tomographic volumes of the acquired images were performed using built-in NRecon Skyscan reconstruction software (Version: 1.6.6.0; Skyscan Bruker). 3D-images were generated using 3D-Visualization Software CTvox v. 2.5, while the volume rendering and virtual sectioning views using DataViewer v. 1.4.4 (Skyscan Bruker) and the analysis of the sample was performed using CT-Analyser software version 1.13.

2.3. Histology and Light Microscopy

Paraffin embedded oviducts were microtome-sectioned at 10 μm and stained with Hematoxylin (Sigma-Aldrich, cat. MHS16) - Eosin (Sigma-Aldrich, cat. 109,844) standard protocol to perform histological assay. Images were obtained with the stereomicroscope MZ12 (Leica) equipped with a color camera. The histological analysis highlighted the accuracy and fidelity of the two-dimensional and three-dimensional

images obtained from microtomography, which has the further advantage of guaranteeing the structural integrity of the sample and avoiding distortions and artefacts resulting from the sectioning procedures (Fig.1, 3, 6).

2.4. Image analysis

Using microCT images, measurements of the length and width of the oviduct folds were conducted, as illustrated in Figure 1. The FIJI program (ImageJ 2.0.0-rc-43/1.50e) was employed for this purpose, utilizing its built-in measurement tool to ensure accuracy in anatomical dimensions. Similarly, to calculate the fractal dimension and lacunarity values, we applied the box-counting method using the FracLac plugin in Fiji.

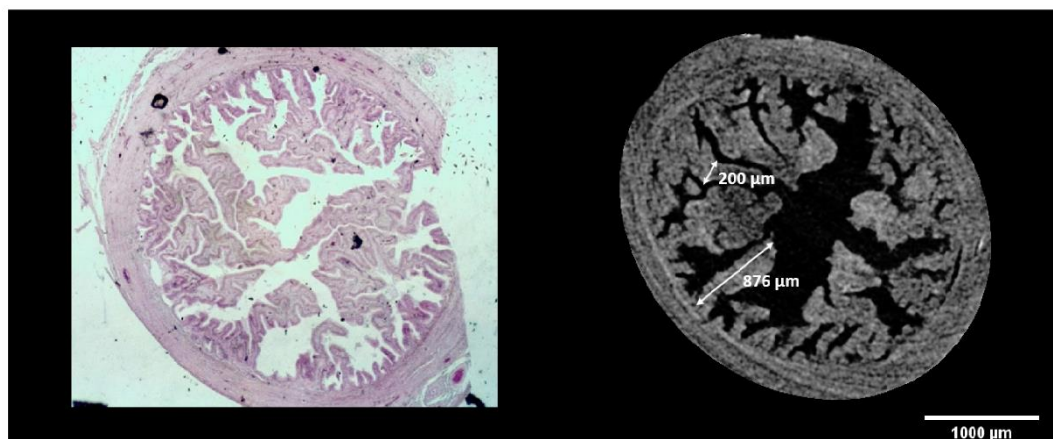


Figure 1. Comparison between virtual and histological oviduct sectioning, with a schematic representation of the measurement method performed.

2.5. Two-dimensional image processing

For the processing of two-dimensional images, the software Mimics from the Belgian company Materialise (Materialise, Leuven, Belgium) and 3Matic (Materialise, Leuven, Belgium) were used. Mimics is the primary software for processing biomedical images in the rapid prototyping sector. Initially, the DICOM files were loaded, and the correct orientation of the images (Top-Bottom, Anterior-Posterior, Right-Left) was set. Once the images were loaded, the software provided their visualization of the three

anatomical planes: transverse/axial, coronal/frontal, and sagittal. It was decided to analyze, in particular, the series of images from the ampullary-isthmus junction (AIJ) and of the utero-tubal junction (UTJ). This approach ensured that images from all phases acquired were available, regardless of their original format. Each image series generated a project within Mimics, i.e., a file in .mcs format. At this point, an initial segmentation was performed on each of the four files by selecting the region of interest through the crop project operation. Specifically, various slices along all three directions (x, y, z) were excluded from the project, retaining only the structures of interest and reducing the number of slices to be analyzed. This helped eliminate the influence of regions not relevant to the study. To achieve this, the position and size of a rectangle were set in all three views (axial, coronal, and sagittal) to delimit the volume of interest in the resulting parallelepiped in the three-dimensional view. After a careful analysis of the images from various contrast phases, the different anatomical structures that would be included in the overall three-dimensional virtual model have been segmented separately: both the external and internal structures of the reference tract (UTJ and AIJ). For each of these structures, it was assessed which image series was most suitable for their segmentation. This decision was based on the presence of enhanced visibility of the mentioned structures in those specific images. Regarding the improvement of image quality, especially in terms of contrast, a point-wise enhancement technique was employed. This involves applying a transformation that maps a small range of grey levels onto the entire possible range, aiming to achieve visual enhancement. Finally, it is specified that the term "mask" refers to a set of pixels that have been grouped together as a result of various operations performed on the three two-dimensional views. Each mask is associated with a specific color, a minimum HU value, and a maximum HU value.

2.6. Processing of the three-dimensional model

Once the segmentation of the different structures has been carried out, it is necessary to process the three-dimensional model by performing a smoothing operation with the appropriate number of iterations. This is done to achieve a virtual model suitable for both three-dimensional visualization and the subsequent potential 3D printing phase. The three-dimensional object calculated from the mask inevitably exhibits a step effect due to the spatial resolution of the images, which is evidently insufficient for our purposes. The edges of the three-dimensional object, reconstructed from the mask, tend to follow individual pixels that have dimensions of approximately 1 mm x 1 mm. This scaling effect can be observed both in the three-dimensional view and on the individual slices for each anatomical structure. The smoothing operation was performed in the Mimics software rather than the modelling software 3-Matic by Materialise, used in the later phase of processing the three-dimensional model and optimizing the mesh. This choice is because, once the smoothing operation with a certain number of iterations is completed in Mimics, it is possible to compare the result with CT images on individual sections (axial, coronal, and sagittal) by visualizing the contours of the obtained three-dimensional object. In general, smoothing operations contribute significantly to enhancing the surface quality of a model. Nevertheless, it is crucial to exercise caution, as an excessively high number of smoothing iterations can lead to alterations in the model, resulting in unexpected outcomes. It is important to keep in mind that real-life organs do not possess perfectly smooth surfaces. The complete virtual model obtained in this way enabled the three-dimensional visualization of various anatomical structures. In this visualization, appropriate degrees of transparency were set for different structures, allowing for the visualization of outer and inner structures as well.

2.7. Processing of the three-dimensional model

The calculation of the shape factor is a procedure used in various contexts, such as physics, engineering, or thermodynamics. The shape factor is a quantity that expresses the geometry of one body in relation to another, often concerning thermal radiation exchange or fluid dynamics. Its mathematical expression can vary depending on the specific context.

In general terms, the shape factor (F) that we used can be calculated using the following simplified formula:

$$F = \frac{S * h}{V}$$

where S and V are respectively the surfaces and volumes of the two bodies under consideration, the UTJ and AIJ, and h is the height of the traits. However, in more complex situations, such as radiation exchange between non-ideal surfaces, the formula can be more intricate and involve angles, distances, and emissivity properties of the surfaces.

3. Results

3.1. Utero tubal junction

In this particular segment of the oviduct, it is noteworthy that there are small folds present, and their dimensions typically fall within the range between 143.88-987.6µm length (Table 1) and 69.81-366.3µm width (Table 2), measurements that are distributed uniformly (Figure 2). These folds don't reach a great percentage of the lumen (Figure 3), an observation that is supported by the high lacunarity value (Table 4).

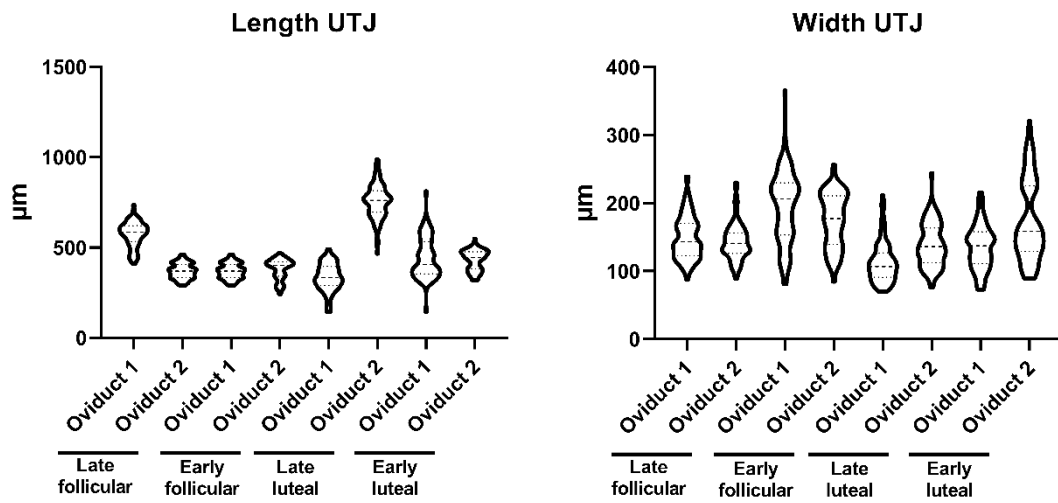


Figure 2. Violin Plot representing the different measurement of length (left) and width (right) of the folds from the UTJ.

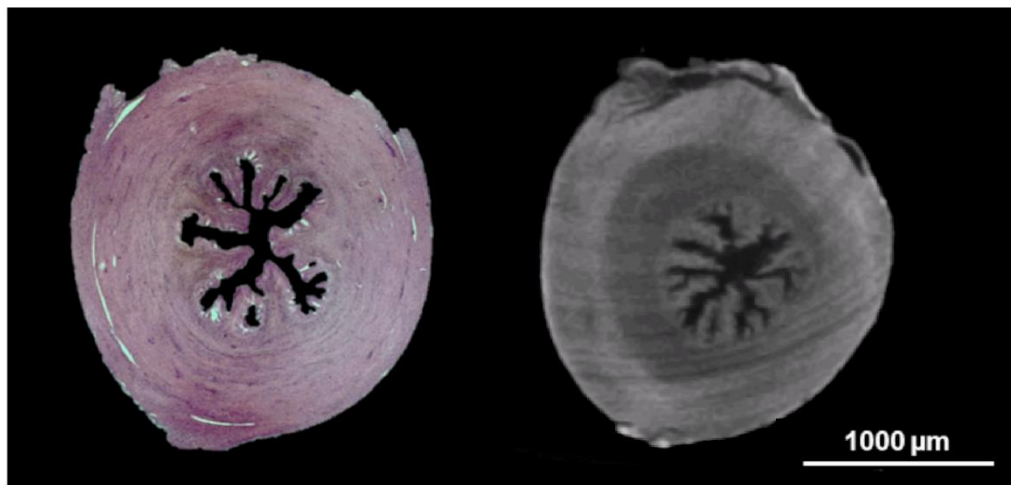


Figure 3. Comparison between histological (left) and virtual (right) oviduct UTJ sectioning.

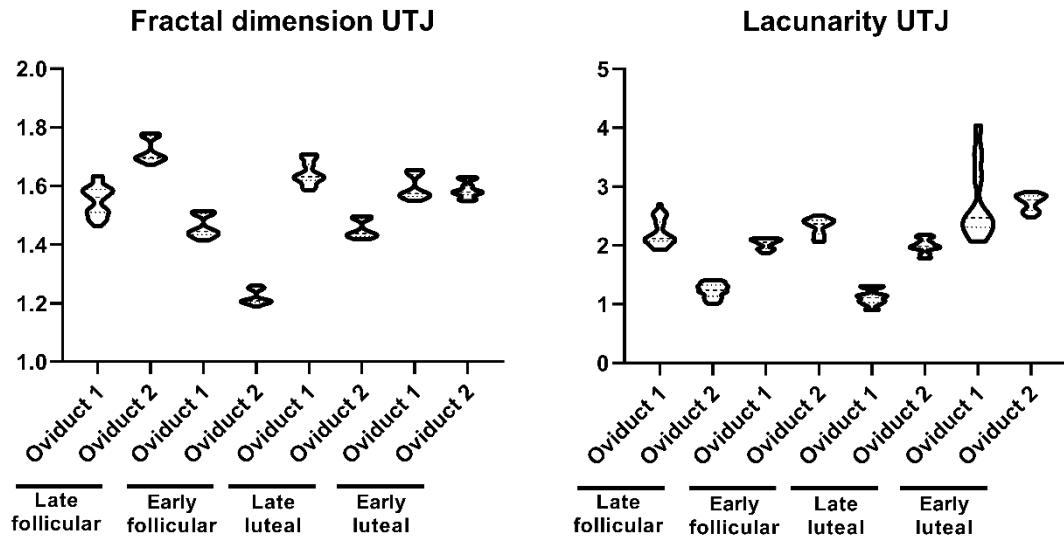


Figure 4. Violin Plot representing the different measurement of fractal dimension (left) and lacunarity (right) of the folds from the UTJ.

On the contrary, the distribution of values for fractal dimension and lacunarity in UTJ is concentrated around a different subpopulation (Figure 4). The fractal dimension encompasses values within the range 1.189-1.1779 (Table 3), while the lacunarity values ranges within 0.901-2.701 (Table 4). On the other hand, the shape factor values of the UTJ external (Table 5) and internal (Table 6) region is provided.

Table 1. Measurements of oviduct folds length (μm) in the UTJ.

	Length (μm)							
	Late follicular		Early Follicular		Late luteal		Early luteal	
	Oviduct 1	Oviduct 2	Oviduct 1	Oviduct 2	Oviduct 1	Oviduct 2	Oviduct 1	Oviduct 2
Median	585.6	369.2	369.2	401.9	332.7	760.9	407.3	444.1
10%	457.0	313.4	313.4	288.2	234.6	639.5	322.0	351.1
Min	410.7	289.0	289.0	241.9	143.88	466.0	143.7	319.0
90%	656.8	426.2	426.2	439.7	436.4	873.2	600.9	493.8
Max	737.1	461.5	461.5	469.0	492.2	987.6	812.9	549.4

Table 2. Measurements of oviduct folds width (μm) in the UTJ.

	Width (μm)							
	Late follicular		Early Follicular		Late luteal		Early luteal	
	Oviduct 1	Oviduct 2	Oviduct 1	Oviduct 2	Oviduct 1	Oviduct 2	Oviduct 1	Oviduct 2
Median	143.2	140.8	206.1	177.3	106.7	136.0	137.1	158.5
10%	114.0	110.2	116.1	115.9	80.0	96.99	93.24	103.8
Min	87.28	89.11	80.91	84.45	69.81	76.45	72.84	89.11
90%	195.0	172.8	255.2	221.9	154.7	182.9	178.2	263.3
Max	239.3	230.5	366.3	256.5	211.9	244.6	215.7	321.3

Table 3. Calculated fractal dimension of UTJ region

	Fractal dimension							
	Late follicular		Early Follicular		Late luteal		Early luteal	
	Oviduct 1	Oviduct 2	Oviduct 1	Oviduct 2	Oviduct 1	Oviduct 2	Oviduct 1	Oviduct 2
Median	1.562	1.697	1.445	1.208	1.631	1.437	1.574	1.579
10%	1.480	1.683	1.421	1.197	1.594	1.422	1.556	1.553
Min	1.464	1.673	1.414	1.189	1.587	1.419	1.551	1.548
90%	1.623	1.777	1.511	1.256	1.706	1.495	1.652	1.627
Max	1.635	1.779	1.514	1.261	1.707	1.497	1.654	1.630

Table 4. Calculated lacunarity for UTJ region

	Lacunarity							
	Late follicular		Early Follicular		Late luteal		Early luteal	
	Oviduct 1	Oviduct 2	Oviduct 1	Oviduct 2	Oviduct 1	Oviduct 2	Oviduct 1	Oviduct 2
Median	2.120	1.238	2.052	2.365	1.109	1.987	2.467	2.774
10%	1.963	1.061	1.895	2.086	0.908	1.787	2.103	2.533
Min	1.928	1.012	1.865	2.061	0.901	1.783	2.071	2.483
90%	2.541	1.386	2.116	2.470	1.310	2.155	3.699	2.872
Max	2.704	1.417	2.127	2.510	1.316	2.181	4.039	2.906

Table 5. Shape factor of the external oviduct in UTJ region

	External shape factor							
	Late follicular		Early Follicular		Late luteal		Early luteal	
	Oviduct 1	Oviduct 2	Oviduct 1	Oviduct 2	Oviduct 1	Oviduct 2	Oviduct 1	Oviduct 2
Volume (mm ³)	66.31	127.71	31.53	26.64	41.55	43.64	84.22	39.80
Surface (mm ²)	234.11	353.68	124.53	109.56	170.13	130.69	268.53	143.59
Height (mm)	4.46	4.46	4.46	4.46	4.46	4.46	4.46	4.46
Shape index	15.75	12.35	17.62	18.34	18.26	13.36	14.22	16.09
shape index (1/mm)	3.53	2.77	3.95	4.11	4.09	2.99	3.19	3.61

Table 6. Shape factor of the internal oviduct in UTJ region

	Internal shape factor							
	Late follicular		Early Follicular		Late luteal		Early luteal	
	Oviduct 1	Oviduct 2	Oviduct 1	Oviduct 2	Oviduct 1	Oviduct 2	Oviduct 1	Oviduct 2
Volume (mm ³)	3.95	3.2	0.52	0.80	1.66	1.58	7.78	2.87
Surface (mm ²)	77.88	50.2	13.83	16.31	30.20	23.92	106.27	30.19
Height (mm)	4.46	4.46	4.46	4.46	4.46	4.46	4.46	4.46
Shape index	87.94	69.97	118.62	90.93	81.14	67.52	60.92	46.92
shape index (1/mm)	19.72	15.69	26.60	20.39	18.19	15.14	13.66	10.52

3.2. Ampullary-isthmic junction

In this section of the oviduct, we not only observe a higher prevalence of folds but also an increase in their individual sizes, ranging between 126-1446 μ m length (Table 7) and 40.02-512 μ m width (Table 8), resulting in a more substantial occupancy within the lumen, reducing the lacunarity (Table 10). In AIJ, distinct subpopulations of folds are discernible, with one set characterized by larger dimensions and another set exhibiting smaller dimensions (Figure 6). By contrast to the width measurements, where the data distribution is not centered around specific values, but rather displays a more homogeneous spread (Figure 5).

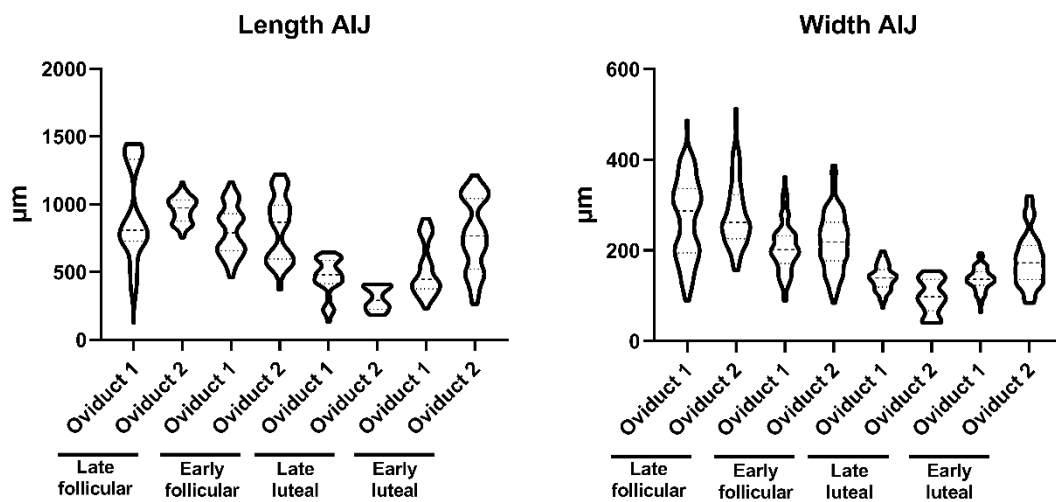


Figure 5. Violin Plot representing the different measurement of length (left) and widths (right) of the folds from the AIJ.

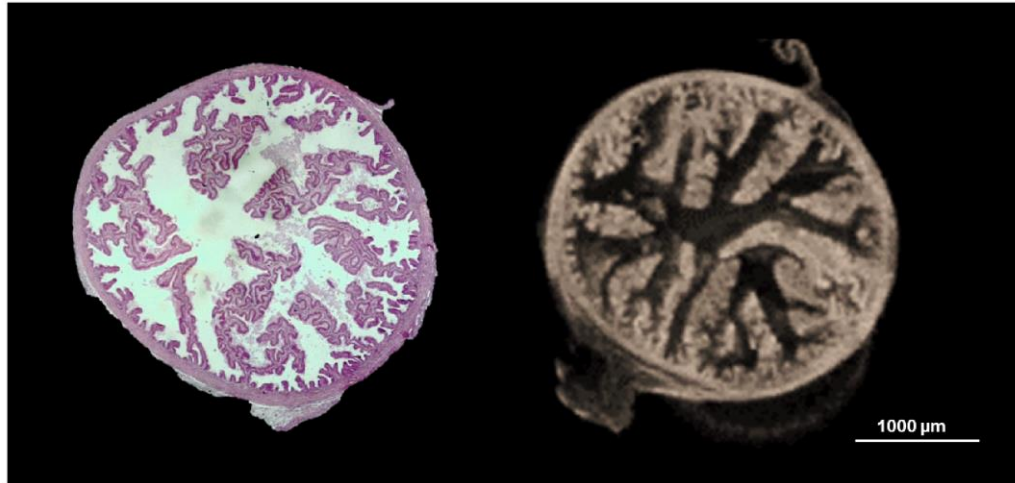


Figure 6. Comparison between histological (left) and virtual (right) oviduct AIJ sectioning

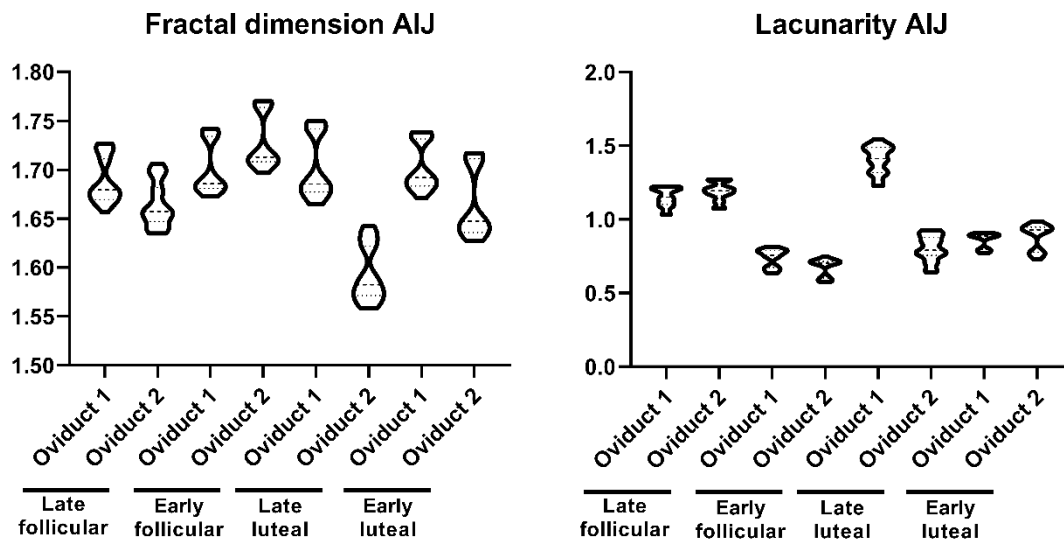


Figure 7. Violin Plot representing the different measurement of fractal dimension (left) and lacunarity (right) of the folds from the UTJ.

Similar to what we observed with the length of the folds, the fractal dimension and lacunarity are also divided into different subpopulation (Figure 7). The fractal dimension encompasses values within the range 1.559-1.770 (Table 9), while the lacunarity values ranges within 0.577-1.544 (Table 10). On the other hand, the shape factor values of the AIJ external (Table 11) and internal (Table 12) region is provided..

Table 7. Measurements of oviduct folds length (μm) in the AIJ region.

	Length (μm)							
	Late follicular		Early Follicular		Late luteal		Early luteal	
	Oviduct 1	Oviduct 2	Oviduct 1	Oviduct 2	Oviduct 1	Oviduct 2	Oviduct 1	Oviduct 2
Median	809.6	972.2	789.6	867.2	480.1	290.1	445.6	766.4
10%	504.9	838.5	584.1	543.0	222.6	189.9	319.5	427.0
Min	126.0	754.7	461.5	369.2	133.6	182.5	232.1	264.8
90%	1415	1072	1046	1154	616.8	407.1	818.5	1109
Max	1446	1161	1166	1220	647.5	410.8	894	1214

Table 8. Measurements of oviduct folds width (μm) in the AIJ.

	Width (μm)							
	Late follicular		Early Follicular		Late luteal		Early luteal	
	Oviduct 1	Oviduct 2	Oviduct 1	Oviduct 2	Oviduct 1	Oviduct 2	Oviduct 1	Oviduct 2
Median	287.3	261.8	201.6	218.5	139.3	97.94	136.4	172.7
10%	148.1	201.7	141.5	139.8	104.6	40.69	101.3	117.2
Min	89.11	156.8	89.42	84.37	73.34	40.02	64.13	84.37
90%	386.3	392.5	279.2	294.6	178.7	149.5	168.5	277.5
Max	486.9	512.7	362.3	387.8	198.8	155.0	193.8	320.3

Table 9. Calculated fractal dimension of AIJ region

	Fractal dimension							
	Late follicular		Early Follicular		Late luteal		Early luteal	
	Oviduct 1	Oviduct 2	Oviduct 1	Oviduct 2	Oviduct 1	Oviduct 2	Oviduct 1	Oviduct 2
Median	1.679	1.657	1.686	1.713	1.686	1.582	1.692	1.647
10%	1.666	1.638	1.677	1.704	1.670	1.561	1.677	1.633
Min	1.656	1.635	1.673	1.697	1.665	1.559	1.671	1.628
90%	1.723	1.701	1.740	1.770	1.746	1.638	1.738	1.715
Max	1.727	1.707	1.742	1.770	1.750	1.642	1.739	1.717

Table 10. Calculated lacunarity for AIJ region

	Lacunarity							
	Late follicular		Early Follicular		Late luteal		Early luteal	
	Oviduct 1	Oviduct 2	Oviduct 1	Oviduct 2	Oviduct 1	Oviduct 2	Oviduct 1	Oviduct 2
Median	1.152	1.195	0.7559	0.7032	1.413	0.7915	0.8870	0.9286
10%	1.042	1.083	0.6469	0.5797	1.250	0.6545	0.7792	0.7584
Min	1.032	1.073	0.6329	0.5770	1.228	0.6418	0.7700	0.7273
90%	1.220	1.270	0.7955	0.7250	1.505	0.9142	0.9007	0.9703
Max	1.223	1.274	0.8141	0.7507	1.544	0.9283	0.9077	0.9879

Table 11. Shape factor of the external oviduct in AIJ region.

	External shape factor							
	Late follicular		Early Follicular		Late luteal		Early luteal	
	Oviduct 1	Oviduct 2	Oviduct 1	Oviduct 2	Oviduct 1	Oviduct 2	Oviduct 1	Oviduct 2
Volume (mm ³)	40.79	44	23.6	26.51	29.83	23.79	35.10	48.41
Surface (mm ²)	226.97	225.73	234.99	286.61	155.14	84.67	166.89	323.40
Height (mm)	4.46	4.46	4.46	4.46	4.46	4.46	4.46	4.46
shape index	24.82	22.88	44.41	48.21	23.20	15.87	21.21	29.79
shape index (1/mm)	5.56	5.13	9.96	10.81	5.20	3.56	4.75	6.68

Table 12. Shape factor of the internal oviduct in AIJ region.

	Shape factor							
	Late follicular		Early Follicular		Late luteal		Early luteal	
	Oviduct 1	Oviduct 2	Oviduct 1	Oviduct 2	Oviduct 1	Oviduct 2	Oviduct 1	Oviduct 2
Volume (mm ³)	4.87	4.32	6.36	5.88	1.99	0.40	0.81	8.34
Surface (mm ²)	66.76	73.22	103.86	141.18	41.52	8.96	18.91	195.45
Height (mm)	4.46	4.46	4.46	4.46	4.46	4.46	4.46	4.46
shape index	61.15	75.59	72.83	107.16	92.96	99.90	104.12	104.56
shape index (1/mm)	13.71	16.95	16.33	24.03	20.84	22.40	23.35	23.44

3.3. 3-D reconstruction

In the 3D reconstruction, the tortuous structure of the AIJ section of the oviduct is represented, offering a detailed view of the high tortuosity it possesses (Figure 8). The visualization also highlights the spatial arrangement of the folds within this section and small blind-ended sacs. On the other hand, in the UTJ of the oviduct, the lumen is narrower and exhibits a less tortuous structure compared to other sections.

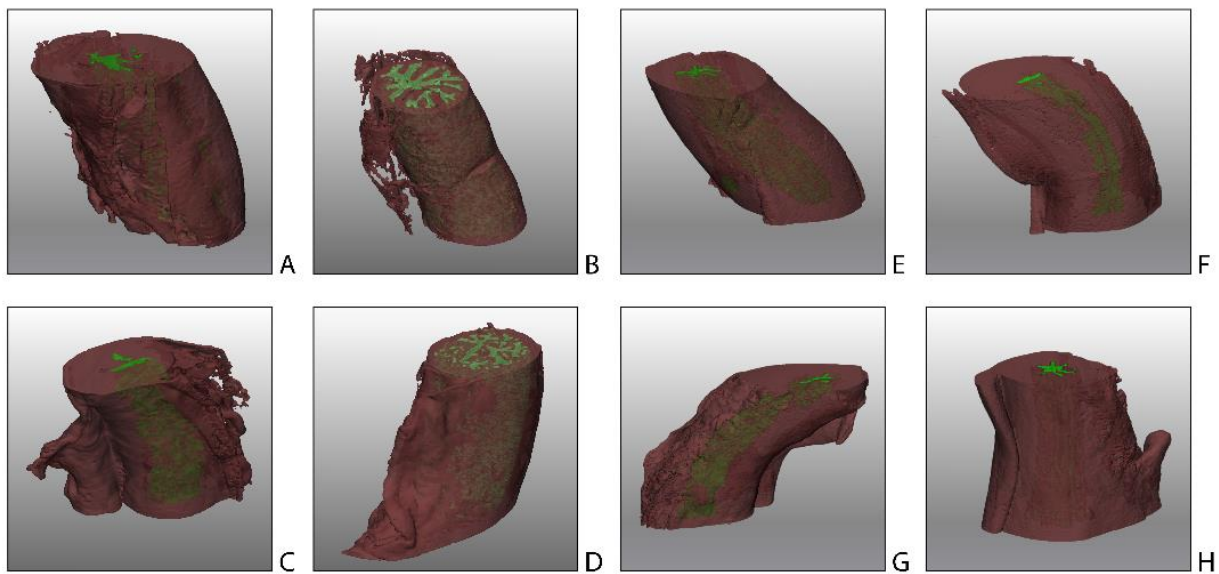


Figure 8. 3D reconstruction of AIJ (A-D) and UTJ (E-H) regions in different phases of the cycle late follicular (A, E), early follicular (B, F) late luteal (C, G) and early luteal (D, H).

4. Discussion

In this study, we have delved into the architectural examination of different segments of the oviduct, attempting to recreate conditions as closely as possible to those encountered in vivo and reporting for the first time parameters such as the shape factor, fractal dimension and lacunarity.

The classical method for reconstructing the oviduct has traditionally involved using histology slides. However, it has been shown that this method may not be the most suitable, as it could result in gaps (Senter-Zapata et al., 2016). Additionally, when using

histology, it can be reconstruction inaccuracies ranging due to deformation or misalignment (Gibson et al., 2013), in particular due to the difficulty of managing three-dimensional orientation. Multiple manual artifacts affect the perfect alignment of the sample in all directions of space. In fact, the positioning procedures of the sample inside the embedding medium, the mounting of the histological specimen on the microtome, the simultaneous three-dimensional angulation of the specimen and the instrument are evident causes of problematic management of the spatial orientation of the specimens. This type of problem is completely overcome in the case of virtual histology that can be performed by microCT, which also becomes the basis of the three-dimensional model perfectly fitting the original sample. MicroCT technique has proven to be a valuable tool for studying mineralized biologic tissues (Neues and Epple, 2008), although its utility in the investigation of soft tissues has been somewhat constrained due to the limited contrast these tissues typically exhibit (Metscher, 2009). Some tries have been made previously to study the internal structure of the oviduct through microCT (Burkitt et al., 2011). Some of them have been made with the oviduct unmodified and without contrast, and other ones fill the oviduct with a strong contrast agent (Burkitt et al., 2011). The initial attempt proved to be unsuccessful as it yielded no discernible internal structures. In contrast, the subsequent approaches provided what could be likened to a photographic "negative" of the oviduct. This effect was achieved due to the significant disparity in clarity between the contrast agent and the surrounding tissue. However, when compared with histology slides, the structure observed was not very detailed. In our work, we employed the paraffin embedding method, a technique that enables us to visualize the high-resolution structure of the oviduct by leveraging its endogenous contrast, as previously described for murine embryos (Ermakova et al., 2018). Although in human the use of MicroCT has

been already used successfully (Castro et al., 2019), to our knowledge, those represent the first data obtained from swine oviducts through microCT.

Similar to what has been observed in humans (Castro et al., 2019; Rocca et al., 1989) or sheep (Yániz et al., 2014), our results show throughout all phases of the cycle, at the UTJ level, mucosal folds are sparse and smaller in size, occupying limited space within the lumen. However, as we move away from the uterus and progress towards the fallopian tubes until the ampulla, a significant increase in the size of these folds and the proportion of space they occupy within the lumen becomes evident. This increase in lumen occupancy is not only apparent from the measurements of the folds in the images but is also corroborated by the decrease in lacunarity. In addition, even though our sample size is relatively small, it is worth noting that the maximum fold amplitude is consistently observed during the follicular phase, as previously described using electronic microscopy (Yaniz et al., 2006). It has been suggested that the folds in the oviduct could play a crucial role in the transport of oocytes and embryos during the fertilization process. These oviductal epithelial folds serve to significantly increase the surface area of the epithelium, thereby enhancing the likelihood of contact between the oocyte/embryo and the ciliated cells within the oviduct (Koyama et al., 2019). Moreover, the specific structure of these folds appears to play a key role in alleviating the pressure difference in the oviductal fluid before and after the passage of the oocyte/embryo (Koyama et al., 2019). It has been observed that the *Celsr1* gene controls the proper formation of these oviductal folds, and *Celsr1*-deficient mice present an altered ciliary beating coordination, and aberrant fold orientation distribution, even leading to infertility (Shi et al., 2014), presumably due to difficulties in the effective transport of oocytes and embryos through the oviduct.

In the 3D reconstruction of the oviduct, we can observe numerous blind sacs or crypts, which are small, pouch-like structures within the oviduct. These anatomical

features have been described in pigs (Yaniz et al., 2006) and in other animal species, including humans (Castro et al., 2019), ovine (Yániz et al., 2014), marsupials (Bedford and Breed, 1994; Rodger and Bedford, 1982), hamster (Smith et al., 1987), bovine (Yániz et al., 2000), and moles (Bedford et al., 1999). In some animals, such as shrews, it has been suggested that the crypts in the oviduct mucosa may serve the function of "sequestering" sperm, thereby preventing polyspermy (Bedford et al., 1997). Meanwhile, in other animals like cows (Yániz et al., 2000) or sows (Yaniz et al., 2006), it has been proposed that these structures could also collaborate to form the sperm reservoir. Even in species like *Sminthopsis crassicaudata*, a notable reduction in flagellar movement has been observed when sperm are within these crypts (Bedford and Breed, 1994). This reduction in flagellar activity may represent a regulatory mechanism that helps maintain sperm viability while they await the opportunity to fertilize the egg.

It is not the first time that microCT has been used to characterize the architecture of organs such as lungs (Scott et al., 2015), tendons or arteries (Shearer et al., 2016), or even to recreate 3D images of breast cancer specimens (DiCorpo et al., 2020). MicroCT can generate 3D models that can then be converted into files suitable for 3D printing, thus enabling the creation of three-dimensional replicas of those organs (Eltorai et al., 2015). This technology has been used to create custom prostheses (Dai et al., 2007), and could be used to create models for surgeon planning (Starosolski et al., 2014) or for educational purposes (Shelmerdine et al., 2018).

The data gleaned from this study possesses significant potential to lay the groundwork for the development of a sophisticated 3D printing model. This model would be meticulously crafted to encompass the intricate architecture of the organ under investigation, such as the oviduct. By meticulously incorporating the detailed structural

nuances revealed by the microCT imaging, this 3D printing file would serve as a blueprint for creating a physical device that faithfully replicates the natural features of the organ.

The process of creating such a device entail translating the intricate anatomical details captured by microCT into a digital format suitable for 3D printing. This involves precisely delineating the various components, such as the mucosal folds, epithelial linings, and vasculature, to ensure an accurate representation of the organ's morphology. Additionally, factors such as tissue density and composition may also be considered to further enhance the realism of the model.

Once the digital model is refined, it can be translated into a format compatible with 3D printing technology. Advanced printing techniques, including additive manufacturing processes, can then be employed to fabricate the physical device layer by layer. This results in a tangible replica of the organ, faithfully reproducing its intricate features and spatial arrangement. The implications of such a 3D-printed device are manifold. From a research standpoint, it provides a valuable tool for conducting in-depth anatomical studies and biomechanical analyses. Researchers can utilize the device to explore various physiological phenomena, simulate pathological conditions, and investigate the efficacy of therapeutic interventions.

The data obtained from this pilot study could potentially serve as a foundation for generating a 3D printing file that considers the organ's intricate architecture, thus enabling the creation of a device that replicates its natural features.

In recent years, the interest in this organ has grown, owing to its involvement in critical processes such as the formation of the sperm reservoir, sperm capacitation, fertilization, and the creation of the optimal environment it provides for the developing embryo (Coy et al., 2012; Li and Winuthayanon, 2017). Furthermore, there have been

efforts to create scaffolds for in vitro construction of this organ (Ferraz et al., 2017a; Ferraz et al., 2020; Xiao et al., 2017), but until now, none have considered its complex architecture, often simplifying to a mere tubular structure.

Recent advancements in 3D printing technology have opened up new possibilities in the field of organ-on-a-chip systems (Ferraz and Ferronato, 2023). These innovative devices, when combined with microfluidic systems, have the potential to replicate the physiology of organs, offering a valuable tool for enhanced studies of organ function and disease (Huh et al., 2011). Notably, in recent years, research has shown that conducting in vitro fertilization processes within devices mimicking the oviduct can yield superior outcomes (Ferraz et al., 2017b; Ferraz et al., 2018). Considering this, the reconstructions obtained in this study hold the promise of serving as the blueprint for a 3D-printed device that accurately reflects this complex architecture. Furthermore, it would enable the conduction of more sophisticated studies on the biophysics of the organ, leading to a deeper understanding of its intricate functions.

The study conducted a comprehensive assessment to determine the most suitable segmentation technique for accurately representing the morphological traits of interest. This evaluation encompassed various segmentation methods, including automatic, interactive, and manual approaches. The challenge of segmentation in biomedical imaging, as highlighted in both the existing literature and this experimental investigation, predominantly arises from the lack of efficient automated tools. While manual segmentation remains a labor-intensive process, particularly in the intricate realm of biomedical imaging, automation offers the potential to streamline and expedite this crucial aspect of analysis.

The complexity of biomedical images, especially when dealing with intricate pathologies and clinical cases, underscores the necessity for robust segmentation techniques. Conventional clinical practices often encounter limitations in conducting thorough diagnostic investigations due to the absence of suitable tools for accurate and efficient segmentation. Therefore, the quest for advanced segmentation methods is paramount to enhance the precision and efficacy of biomedical imaging analyses, ultimately leading to improved diagnostic outcomes and patient care.

Moreover, it is essential to recognize that the processing of biomedical images represents only one facet of a broader continuum in the research and clinical workflow. This continuum begins with the acquisition of diagnostic images from experimental subjects and culminates in the creation of corresponding 3D-printed anatomical models. Here, 3D printing emerges as a transformative technology that bridges the virtual and physical realms, enabling the fabrication of tangible prototypes from digital representations.

In summary, the pursuit of optimal segmentation techniques in biomedical imaging is crucial for advancing both research and clinical practice. By addressing the challenges inherent in segmentation, such as automation and accuracy, researchers and clinicians can harness the full potential of biomedical imaging to enhance diagnostic precision, therapeutic efficacy, and patient outcomes. Additionally, the integration of 3D printing technology further amplifies the impact of biomedical imaging by translating virtual data into tangible assets with diverse applications in research, education, and clinical care. In this context, 3D printing represents a transformative technology that facilitates the conversion of virtual models into physical prototypes. These prototypes, capable of faithfully reproducing even the most intricate shapes and geometric features, serve as a gateway to novel research endeavours grounded in real biomedical images.

5. References

- Abe, H. (1996). The mammalian oviductal epithelium: regional variations in cytological and functional aspects of the oviductal secretory cells. *Histol Histopathol* 11, 743–68.
- Bedford, J. M. and Breed, W. G. (1994). Regulated storage and subsequent transformation of spermatozoa in the fallopian tubes of an Australian marsupial, *Sminthopsis crassicaudata*. *Biol Reprod* 50, 845–854.
- Bedford, J. M., Mock, O. B. and Phillips, D. M. (1997). Unusual ampullary sperm crypts, and behavior and role of the cumulus oophorus, in the oviduct of the least shrew, *Cryptotis parva*. *Biol Reprod* 56, 1255–1267.
- Bedford, J. M., Mock, O. B., Nagdas, S. K., Winfrey, V. P. and Olson, G. E. (1999). Reproductive features of the eastern mole (*Scalopus aquaticus*) and star-nose mole (*Condylura cristata*). *J Reprod Fertil* 117, 345–353.
- Burkitt, M., Walker, D., Romano, D. M. and Fazeli, A. (2011). Computational modelling of maternal interactions with spermatozoa: potentials and prospects. *Reprod Fertil Dev* 23, 976–989.
- Castro, P. T., Aranda, O. L., Matos, A. P. P., Marchiori, E., de Araújo, L. F. B., Alves, H. D. L., Machado, A. S., Lopes, R. T., Werner, H. and Júnior, E. A. (2019). The human endosalpinx: anatomical three-dimensional study and reconstruction using confocal microtomography. *Pol J Radiol* 84, e281–e288.
- Coy, P., García-Vázquez, F. A., Visconti, P. E. and Avilés, M. (2012). Roles of the oviduct in mammalian fertilization. *Reproduction* 144, 649.

Coy, P., Avilés, M. and Latorre, R. (2018). Fallopian tube/Oviduct. In *Encyclopedia of Reproduction* (ed. Skinner, M. A.), p. Academic Press.

Dai, K. R., Yan, M. N., Zhu, Z. A. and Sun, Y. H. (2007). Computer-aided custom-made hemipelvic prosthesis used in extensive pelvic lesions. *J Arthroplasty* 22, 981–986.

DiCorpo, D., Tiwari, A., Tang, R., Griffin, M., Aftreth, O., Bautista, P., Hughes, K., Gershenfeld, N. and Michaelson, J. (2020). The role of Micro-CT in imaging breast cancer specimens. *Breast Cancer Res Treat* 180, 343–357.

Eltorai, A. E. M., Nguyen, E. and Daniels, A. H. (2015). Three-dimensional printing in orthopedic surgery. *Orthopedics* 38, 684–687.

Ermakova, O., Orsini, T., Gambadoro, A., Chiani, F. and Tocchini-Valentini, G. P. (2018). Three-dimensional microCT imaging of murine embryonic development from immediate post-implantation to organogenesis: application for phenotyping analysis of early embryonic lethality in mutant animals. *Mamm Genome* 29, 245–259.

Ferraz, M. de A. M. M. and Ferronato, G. de A. (2023). Opportunities involving microfluidics and 3D culture systems to the in vitro embryo production. *Anim Reprod* 20,.

Ferraz, M. A. M. M., Henning, H. H. W., Stout, T. A. E., Vos, P. L. A. M. and Gadella, B. M. (2017a). Designing 3-Dimensional In Vitro Oviduct Culture Systems to Study Mammalian Fertilization and Embryo Production. *Ann Biomed Eng* 45, 1731–1744.

Ferraz, M. A. M. M., Henning, H. H. W., Costa, P. F., Malda, J., Melchels, F. P., Wubbolts, R., Stout, T. A. E., Vos, P. L. A. M. and Gadella, B. M. (2017b). Improved

bovine embryo production in an oviduct-on-a-chip system: prevention of poly-spermic fertilization and parthenogenic activation. *Lab Chip* 17, 905–916.

Ferraz, M. A. M. M., Rho, H. S., Hemerich, D., Henning, H. H. W., van Tol, H. T. A., Hölker, M., Besenfelder, U., Mokry, M., Vos, P. L. A. M., Stout, T. A. E., et al. (2018). An oviduct-on-a-chip provides an enhanced in vitro environment for zygote genome reprogramming. *Nat Commun* 9,.

Ferraz, M. A. M. M., Nagashima, J. B., Venzac, B., Le Gac, S. and Songsasen, N. (2020). A dog oviduct-on-a-chip model of serous tubal intraepithelial carcinoma. *Sci Rep* 10, 1–11.

Gibson, E., Gaed, M., Gómez, J. A., Moussa, M., Romagnoli, C., Pautler, S., Chin, J. L., Crukley, C., Bauman, G. S., Fenster, A., et al. (2013). 3D prostate histology reconstruction: an evaluation of image-based and fiducial-based algorithms. *Med Phys* 40,.

Hugentobler, S. A., Sreenan, J. M., Humpherson, P. G., Leese, H. J., Diskin, M. G. and Morris, D. G. (2010). Effects of changes in the concentration of systemic progesterone on ions, amino acids and energy substrates in cattle oviduct and uterine fluid and blood. *Reprod Fertil Dev* 22, 684–694.

Huh, D., Hamilton, G. A. and Ingber, D. E. (2011). From Three-Dimensional Cell Culture to Organs-on-Chips. *Trends Cell Biol* 21, 745.

Koyama, H., Shi, D. and Fujimori, T. (2019). Biophysics in oviduct: Planar cell polarity, cilia, epithelial fold and tube morphogenesis, egg dynamics. *Biophys Physicobiol* 16, 89.

Li, S. and Winuthayanon, W. (2017). Oviduct: roles in fertilization and early embryo development. *Journal of Endocrinology* 232, R1–R26.

Mahé, C., Zlotkowska, A. M., Reynaud, K., Tsikis, G., Mermillod, P., Druart, X., Schoen, J. and Saint-Dizier, M. (2021). Sperm migration, selection, survival, and fertilizing ability in the mammalian oviduct†. *Biol Reprod* 105, 317–331.

Ménézo, Y., Guérin, P. and Elder, K. (2015). The oviduct: a neglected organ due for re-assessment in IVF. *Reprod Biomed Online* 30, 233–240.

Metscher, B. D. (2009). MicroCT for comparative morphology: simple staining methods allow high-contrast 3D imaging of diverse non-mineralized animal tissues. *BMC Physiol* 9, 11.

Miranda, K., Girard-Dias, W., Attias, M., de Souza, W. and Ramos, I. (2015). Three dimensional reconstruction by electron microscopy in the life sciences: An introduction for cell and tissue biologists. *Mol Reprod Dev* 82, 530–547.

Neues, F. and Epple, M. (2008). X-ray microcomputer tomography for the study of biomineralized endo- and exoskeletons of animals. *Chem Rev* 108, 4734–4741.

Rocca, M., El Habashy, M., Nayel, S. and Madwar, A. (1989). The intramural segment and the uterotubal junction: an anatomic and histologic study. *Int J Gynaecol Obstet* 28, 343–349.

Rodger, J. C. and Bedford, J. M. (1982). Induction of oestrus, recovery of gametes, and the timing of fertilization events in the opossum, *Didelphis virginiana*. *J Reprod Fertil* 64, 159–169.

Scott, A. E., Vasilescu, D. M., Seal, K. A. D., Keyes, S. D., Mavrogordato, M. N., Hogg, J. C., Sinclair, I., Warner, J. A., Hackett, T. L. and Lackie, P. M. (2015). Three dimensional imaging of paraffin embedded human lung tissue samples by micro-computed tomography. *PLoS One* 10,.

Senter-Zapata, M., Patel, K., Bautista, P. A., Griffin, M., Michaelson, J. and Yagi, Y. (2016). The Role of Micro-CT in 3D Histology Imaging. *Pathobiology* 83, 140–147.

Shearer, T., Bradley, R. S., Hidalgo-Bastida, L. A., Sherratt, M. J. and Cartmell, S. H. (2016). Three-dimensional visualisation of soft biological structures by X-ray computed micro-tomography. *J Cell Sci* 129, 2483–2492.

Shelmerdine, S. C., Simcock, I. C., Hutchinson, J. C., Aughwane, R., Melbourne, A., Nikitichev, D. I., Ong, J. L., Borghi, A., Cole, G., Kingham, E., et al. (2018). 3D printing from microfocus computed tomography (micro-CT) in human specimens: education and future implications. *Br J Radiol* 91,.

Shi, D., Komatsu, K., Hirao, M., Toyooka, Y., Koyama, H., Tissir, F., Goffinet, A. M., Uemura, T. and Fujimori, T. (2014). *Celsr1* is required for the generation of polarity at multiple levels of the mouse oviduct. *Development* 141, 4558–4568.

Smith, T. T., Koyanagi, F. and Yanagimachi, R. (1987). Distribution and Number of Spermatozoa in the Oviduct of the Golden Hamster after Natural Mating and Artificial Insemination. *Biol Reprod* 37, 5–234.

Starosolski, Z. A., Kan, J. H., Rosenfeld, S. D., Krishnamurthy, R. and Annapragada, A. (2014). Application of 3-D printing (rapid prototyping) for creating physical models of pediatric orthopedic disorders. *Pediatr Radiol* 44, 216–221.

Steinhauer, N., Boos, A. and Günzel-Apel, A. R. (2004). Morphological changes and proliferative activity in the oviductal epithelium during hormonally defined stages of the oestrous cycle in the bitch. *Reprod Domest Anim* 39, 110–119.

Talevi, R. and Gualtieri, R. (2010). Molecules involved in sperm-oviduct adhesion and release. *Theriogenology* 73, 796–801.

Xiao, S., Coppeta, J. R., Rogers, H. B., Isenberg, B. C., Zhu, J., Olalekan, S. A., McKinnon, K. E., Dokic, D., Rashedi, A. S., Haisenleder, D. J., et al. (2017). A microfluidic culture model of the human reproductive tract and 28-day menstrual cycle. *Nat Commun* 8,.

Yániz, J. L., Lopez-Gatius, F., Santolaria, P. and Mullins, A. K. J. (2000). Study of the Functional Anatomy of Bovine Oviductal Mucosa. *Anat Rec* 260, 268–278.

Yaniz, J. L., Lopez-Gatius, F. and Hunter, R. H. F. (2006). Scanning electron microscopic study of the functional anatomy of the porcine oviductal mucosa. *Journal of Veterinary Medicine Series C: Anatomia Histologia Embryologia* 35, 28–34.

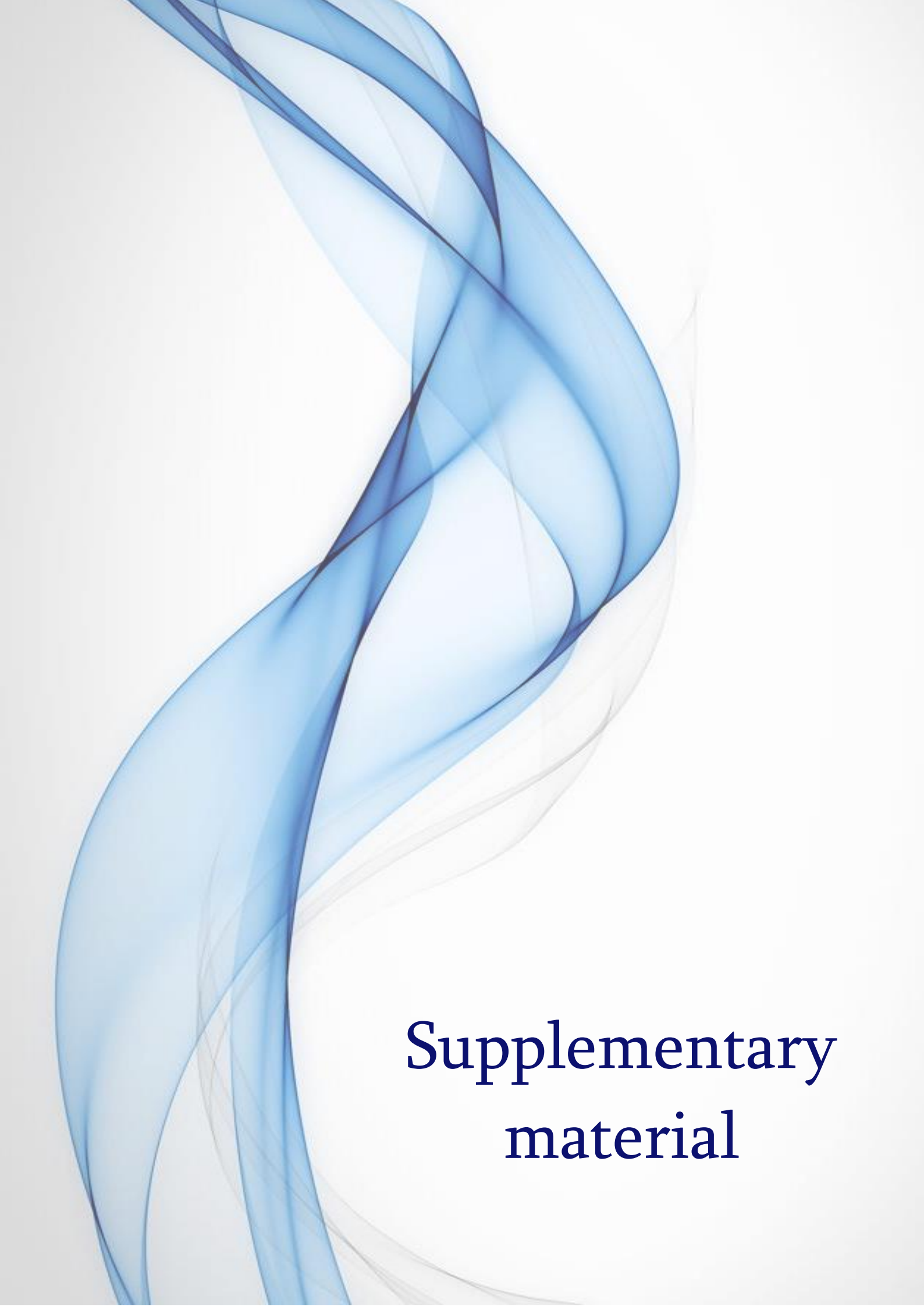
Yániz, J. L., Carretero, T., Recreo, P., Arceiz, E. and Santolaria, P. (2014). Three-dimensional architecture of the ovine oviductal mucosa. *Anat Histol Embryol* 43, 331–340.

The background of the slide features a series of fluid, overlapping, and translucent blue and white lines that create a sense of motion and depth, resembling smoke or liquid waves. These lines are concentrated on the left side and flow towards the right, framing the text.

Conclusions

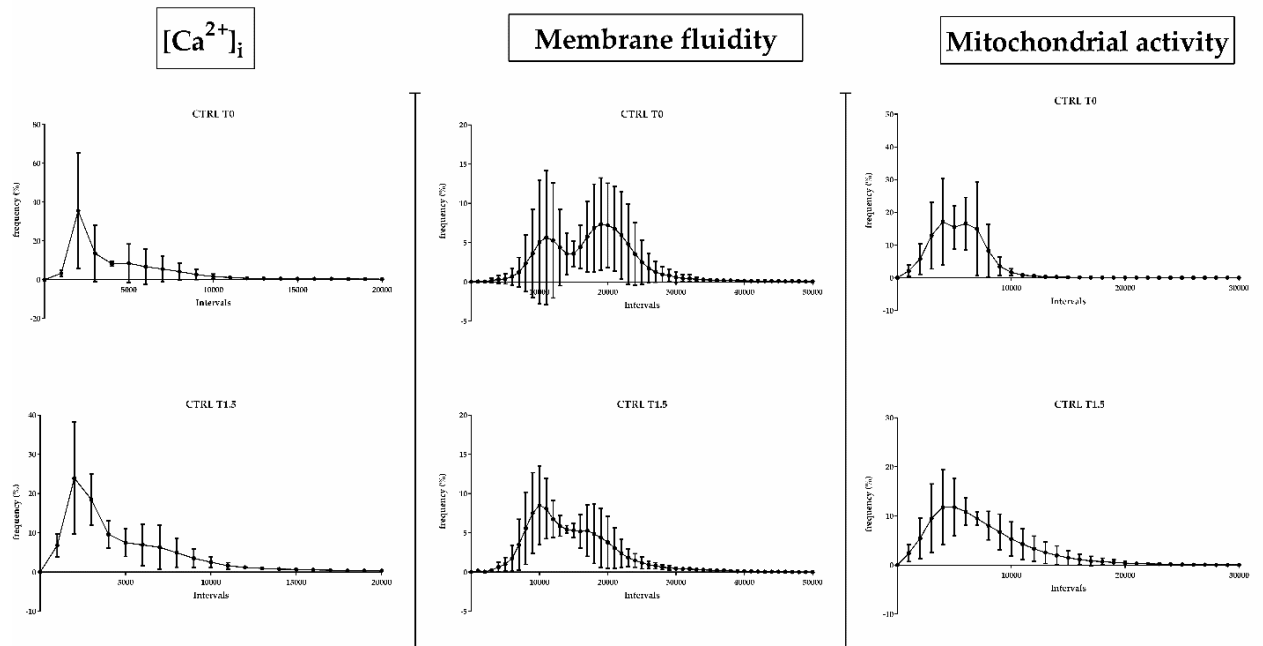
Conclusions

- The presence of PEGDA500 in the culture media or its exudate, as well as the exudate from PEGDA200 material during IVF, has detrimental effects on bovine embryo development.
- Although parameters in embryo development, such as cleavage or blastocyst rate at days 7 and 8, do not seem to be affected when PEGDA PhotoInk or its exudates, PLA or its exudates, PCL or its exudates, or PEGDA200 material are present during in vitro fertilization (IVF), the principal component analysis (PCA) including total cell number (TCN), inner cell mass/trophoblast (ICM/TE), and apoptotic cell rate (ACR), suggests that PCL is the most suitable material for constructing a new 3D printed IVF device. This conclusion is substantiated by the observation that both its rinse group and scaffold group exhibit the closest resemblance to the control group.
- MoS₂/CT nanoflakes at different concentrations do not provoke negative effects on sperm and do not have a negative impact for IVF.
- The presence of CT at 0.1 ppm concentration during capacitation and boost their fertilizing ability.
- MicroCT images has proven to be a useful tool to create 3D reconstruction of paraffin-embedded oviduct. The reconstruction faithfully reflects the anatomical reality, providing a detailed and accurate representation of the oviduct's internal structure. This reconstruction could serve as a solid foundation for the development of a 3D-printed oviduct, ensuring precision and authenticity in replicating the internal architecture of the oviduct.

The background of the slide features a series of fluid, overlapping, and translucent blue and white lines that create a sense of movement and depth, resembling smoke or liquid waves. These lines are concentrated on the left side and flow towards the right, framing the text.

Supplementary material

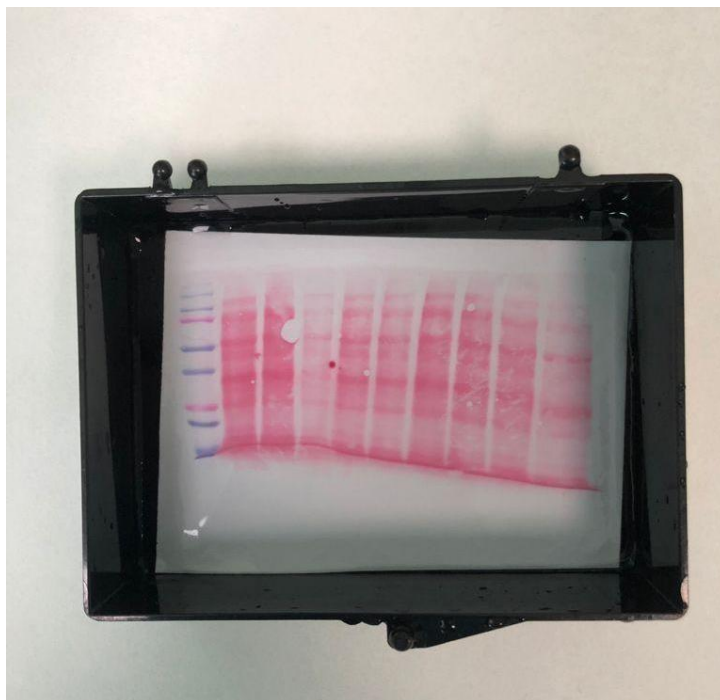
Supplementary Materials Chapter II



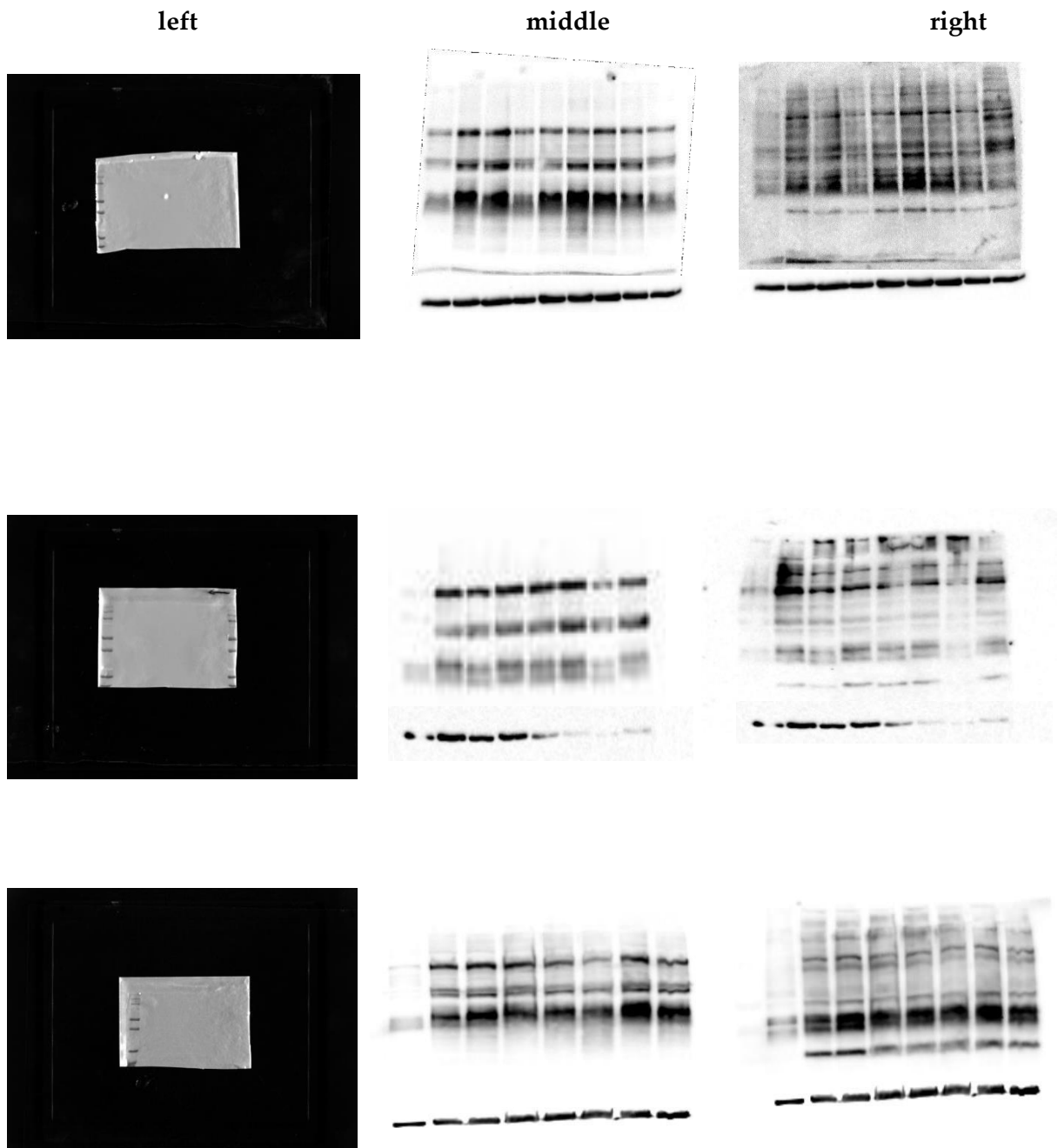
Supplementary Materials S1. CTRL group flow cytometry analysis after 0, 1.5 of capacitation.

Supplementary Materials S

All full-length membranes and immunoblotting images from three independent experiments.



Supplementary Figure S1. Representative image of a membrane prior to hybridization. Blots used were mini size. This figure shows a membrane after Ponceau staining and prior to the incubation with the corresponding antibody



Supplementary Figure S2. Three representative blots with full-length membranes and membrane edges for anti-phospho-pKa antibody (Cell Signaling, Leiden, The Netherlands) and anti-phosphotyrosine antibody (Merck Millipore, USA). Left: molecular weight; middle: PKA activity and right: tyrosine phosphorylation patterns.

The background of the page features a series of elegant, flowing, and overlapping lines in shades of light blue and white. These lines create a sense of movement and depth, resembling smoke or liquid in motion. They are concentrated on the left side and curve towards the right, framing the text.

Acknowledgments

Durante mi doctorado he pensado muchas veces en cómo sería este momento, el toque final a esta tesis que tanto trabajo ha costado. Un día se me pasó por la cabeza la locura de acercarme al mundo de la reproducción y lo que no sabía, es que esa decisión me llevaría a donde estoy ahora. Esto va para largo, pues hay muchas personas que me han acompañado en este capítulo de mi vida a las que agradecerles todo lo que han hecho.

First and foremost, I would like to express my gratitude to my tutors, Pilar Coy and Nicola Bernabò, for their guidance throughout this challenging thesis. I know it has been a very difficult journey, but I hope I have risen to the occasion, at least the major parts of the times. I have learned a lot from both of you, something for which I can never be grateful enough. Pilar, you are an outstanding teacher. I approached you when I was still a lost undergraduate student, unsure of what I wanted to do next, and now, here I am, writing the acknowledgments for a doctoral thesis. I will never forget everything you have taught me, from farm work for a biologist (which I never thought I could do) to laboratory planning. I cannot thank you enough for the opportunities you have given me, from the TFG to the completion of this doctoral thesis. Thank you very much for believing in me and supporting me through the lowest moments. Nicola, thank you very much for giving me the opportunity to do my PhD under your supervision and for guiding me throughout this process. I am grateful for everything you have taught me, not only academically and professionally but also for showing me a more relaxed way of doing things and the valuable life lesson that there is no bureaucratic problem that cannot be solved.

Me faltan palabras para agradecer, a todo el grupo de Fisiología Veterinaria, lo que han hecho por mí. A Joaquín Gadea, por haberme dado la oportunidad de participar en un sinfín de cosas y aprender tantísimo, así como por las cervezas y los consejos que me has dado, científicos y de vida. Al resto de profesores del departamento, Raquel, Carmen, Fran, Sebas, Salvador, ha sido un placer poderme formar y colaborar con

vosotros. Lo puedo decir con la frente bien alta y allá donde vaya, si os puedo ser útil, estaré encantado de ayudar en lo que sea. A Juan, porque sin él todo sería mucho más difícil. Muchas gracias también al resto de doctores que he conocido en este maravilloso sitio, Cristina Soriano, Jordana, Evelyne, Alessia y Gabi, porque también gracias a vosotras he conseguido llegar hasta aquí. Qué decir de la persona con la que hice mi primera FIV, Sergio Navarro, eres un gran científico, pero mejor persona. Gracias por haberme enseñado gran parte de lo que sé, a razonar, como funcionan los grifos de emergencia del laboratorio y, sobre todo, por ser tan buen amigo. Muchas gracias a mi *drama queen sister*, Analuce. Muchas gracias por todos los consejos que me has dado a nivel profesional y de vida. No sé qué habría sido de mí estos últimos meses sin tu apoyo y sin tus mensajes tranquilizadores. Muchas gracias por entenderme como nadie más lo ha hecho. A Chiara, por tu compañía, por la calma que nos transmites a todos, por darnos energía positiva siempre que la necesitamos y, por qué no, por mantenernos al día con todos los cotilleos, eres la mejor vigilante que ha tenido y tendrá el departamento. A Celia, porque desde que hicimos el máster juntos hemos seguido el mismo camino y eres una compañera excepcional. Muchas gracias por estar ahí cuando se necesita una mano, por los cafés, por las pegatinas personalizadas y, sobre todo, por estar presente en los momentos de desahogo en las situaciones más difíciles. A Santa y Paulina, por estar siempre disponibles y ofrecerse siempre a ayudar cuando se necesita. En especial, muchas gracias también a dos de los grandes descubrimientos de este doctorado, Jon y Sonia. Muchas gracias, Jon por acompañarme en los primeros pasos en el laboratorio, por los cafés en el despacho y por el apoyo. Sonia, muchas gracias por enseñarme la importancia de la exactitud, la ayuda en el laboratorio, los protocolos y las risas. Muchas gracias a ambos por las cervezas y los momentos de desconexión fuera del laboratorio.

Además, este es el resultado también del apoyo de mucha gente fuera del laboratorio. Muchas gracias a mi Martu, por darme los consejos más sabios que me han dado nunca y por apoyarme y estar presente en todos y cada uno de los momentos más difíciles de estos años, no existen suficientes palabras para expresarte toda la gratitud que siento. Muchas gracias a la Sevillana y a Miriam por estar siempre presentes y disponibles. Muchas gracias a todos y cada uno de mis fieles rojos campeones, en especial a mi Juanlu, Fran, Papu y Gaspar, porque sin vosotros no habría sido lo mismo. Muchas gracias a uno de los personajes más grandes que he conocido, María súper. Muchas gracias a mi estupenda María Victoria Rosa Silvestre, por escucharme siempre y por animarme con tus grandes dotes irónicas. A Lorena, porque has sido un gran apoyo en muchos momentos. Por último, me gustaría agradecer a mi familia todo lo que ha hecho por mí, porque sin vosotros esto no hubiese sido posible.

Ed è arrivato il momento di ringraziare anche l'itala. Il mio inizio in questo paese è stato piuttosto difficile. Sono arrivato in un momento abbastanza complicato, in piena pandemia COVID, con il coprifuoco e con l'Abruzzo in zona rossa. Tuttavia, sono riuscito a trovare delle persone meravigliose che sono diventate parte della mia famiglia nonostante le difficoltà. Per questo motivo, vorrei ringraziare tantissimo a Sara, perché grazie alle tue lezioni d'italiano sono riuscito a parlare e mi hanno permesso di costruire tutto il resto. Grazie per tutto l'aiuto che mi hai dato, sia quando eravamo coinquilini ma anche dopo. Grazie mille a mia sorellina, Martina, perché senza di te il primo anno non sarebbe stato così meraviglioso. Grazie a Andrea per avermi sempre ascoltato, e scusami per il mio carattere difficile. Tutti voi siete stati i migliori coinquilini che potevo avere.

Grazie a tutti i membri del laboratorio di Fisiologia e Anatomia, specialmente alla Prof. Barbara Barboni, per l'opportunità di collaborazione e di crescita che mi ha offerto in questo posto. Grazie al resto di Prof.; Russo, Mauro, Colosimo e Valbonetti, per essere

stati sempre disponibili quando ho avuto bisogno e per l'alta qualità della formazione percepita. Grazie a tutto il *team* che fa possibile e rende più facile tutto il lavoro, Giulia, Maura, Oriana e Delia.

Grazie a Marina, per il grandissimo sforzo fatto per aiutarmi quando sono appena arrivato. Grazie a tutti i dottorandi, le Chiare, Giuseppe, Alessia, Melissa, Arlette, Adrian, Seerat e Mohammed che, anche se non è più dottorando, lo consideriamo sempre uno di noi. Grazie, Alessia Paradiso, per essere stata una gran integrante dello squadrone di Andrologia e una bellissima scoperta di quest'ultimo anno. È stato un vero piacere lavorare con te. Ci tengo a ringraziare soprattutto a due persone che sono stati molto importanti. Non ci sono abbastanza parole al mondo per ringraziare alla mia capa suprema, la mia *data analyzer*, più conosciuta come "la Coco". Sei una grande ricercatrice e anche una grande persona. Nessuno capisce alle persone come fai tu. Sei sempre stata presente nei momenti più divertenti e anche nei momenti più cupi. Per ultimo, grazie mille a C², perché anche se sei arrivato alla fine, sei diventato una parte molto importante della mia vita. Grazie mille per prendere cura di me quando sono stato "tutto storto e tutto ammalato". Grazie mille per avermi fatto conoscere la cultura e i posti più belli dell'Abruzzo. Per avermi ascoltato e supportato nei momenti difficili e soprattutto per essere stato il primo a festeggiare i miei successi e consolare i miei fallimenti.

Because with you all, the phrase 'standing on the shoulders of giants' has never made so much sense.

The background of the page features a series of fluid, overlapping, and translucent blue and white lines that create a sense of movement and depth, resembling smoke or liquid in motion. These lines are concentrated on the left side and flow towards the right, framing the central text.

Appendix



OPEN ACCESS

EDITED BY

Reza Hedayati,
Delft University of Technology,
Netherlands

REVIEWED BY

Mozhgan Keshavarz,
University of California, Irvine,
United States
Anna Lange-Consiglio,
University of Milan, Italy

*CORRESPONDENCE

Pilar Coy,
✉ pcoy@um.es

RECEIVED 18 July 2023

ACCEPTED 15 September 2023

PUBLISHED 19 October 2023

CITATION

Belda-Perez R, Heras S, Cimini C,
Romero-Aguirregomezcorra J,
Valbonetti L, Colosimo A, Colosimo BM,
Santoni S, Barboni B, Bernabò N and
Coy P (2023), Advancing bovine *in vitro*
fertilization through 3D printing: the
effect of the 3D printed materials.
Front. Bioeng. Biotechnol. 11:1260886.
doi: 10.3389/fbioe.2023.1260886

COPYRIGHT

© 2023 Belda-Perez, Heras, Cimini,
Romero-Aguirregomezcorra, Valbonetti,
Colosimo, Colosimo, Santoni, Barboni,
Bernabò and Coy. This is an open-access
article distributed under the terms of the
[Creative Commons Attribution License](https://creativecommons.org/licenses/by/4.0/)
(CC BY). The use, distribution or
reproduction in other forums is
permitted, provided the original author(s)
and the copyright owner(s) are credited
and that the original publication in this
journal is cited, in accordance with
accepted academic practice. No use,
distribution or reproduction is permitted
which does not comply with these terms.

Advancing bovine *in vitro* fertilization through 3D printing: the effect of the 3D printed materials

Ramses Belda-Perez^{1,2}, Sonia Heras², Costanza Cimini¹,
Jon Romero-Aguirregomezcorra², Luca Valbonetti^{1,3},
Alessia Colosimo¹, Bianca Maria Colosimo⁴, Silvia Santoni⁴,
Barbara Barboni¹, Nicola Bernabò^{1,3} and Pilar Coy^{2*}

¹Department of Biosciences and Technology for Food, Agriculture and Environment, University of Teramo, Teramo, Italy, ²Physiology of Reproduction Group, Department of Physiology, Faculty of Veterinary Medicine, International Excellence Campus for Higher Education and Research (Campus Mare Nostrum), University of Murcia, Murcia, Spain, ³Institute of Biochemistry and Cell Biology (CNRIBBC/EMMA/Infrafrontier/IMPC), National Research Council, Rome, Italy, ⁴Department of Mechanical Engineering, Politecnico di Milano, Milano, Italy

Nowadays there is an increasing demand for assisted reproductive technologies due to the growth of infertility problems. Naturally, fertilization occurs in the oviduct, where the oviductal epithelial cells (OECs) secrete many molecules that affect the embryo's metabolism and protect it from oxidative stress. When the OECs are grown in 3D culture systems, they maintain a great part of their functional characteristics, making them an excellent model for *in vitro* fertilization (IVF) studies. In this work, we aimed to evaluate the suitability of different 3D-printing processes in conjunction with the corresponding set of commercially available biomaterials: extrusion-based processing using polylactic acid (PLA) and polycaprolactone (PCL) and stereolithography or digital-light processing using polyethylene-glycol-diacrylate (PEGDA) with different stiffness (PEGDA500, PEGDA200, PEGDA PhotoInk). All the 3D-printed scaffolds were used to support IVF process in a bovine embryo assay. Following fertilization, embryo development and quality were assessed in terms of cleavage, blastocyst rate at days 7 and 8, total cell number (TCN), inner cell mass/trophectoderm ratio (ICN/TE), and apoptotic cell ratio (ACR). We found a detrimental effect on cleavage and blastocyst rates when the IVF was performed on any medium conditioned by most of the materials available for digital-light processing (PEGDA200, PEGDA500). The observed negative effect could be possibly due to some leaked compound used to print and stabilize the scaffolds, which was not so evident however with PEGDA PhotoInk. On the other hand, all the extrusion-based processable materials did not cause any detrimental effect on cleavage or blastocyst rates. The principal component analysis reveals that embryos produced in presence of 3D-printed scaffolds produced via extrusion exhibit the highest similarity with the control embryos considering cleavage, blastocyst rates, TCN, ICN/TE and ACR per embryo. Conversely, all the photo-cross linkable materials or medium conditioned by PLA, lead to the highest dissimilarities. Since the use of PCL scaffolds, as well as its conditioned medium, bring to embryos that are more similar to the control group. Our results suggest

that extrusion-based 3D printing of PCL could be the best option to be used for new IVF devices, possibly including the support of OECs, to enhance bovine embryo development.

KEYWORDS

IVF, bovine, embryo culture, biomaterials, PCL, PEGDA, PLA

1 Introduction

In recent years, the demand for artificial reproductive technologies (ARTs) is growing due to an increase in infertility, which already affects 15% of couples of reproductive age and continues to rise every year (Assidi, 2022). The high number of infertile couples, together with reproductively healthy ones seeking to prevent genetic diseases in their offspring, have contributed to an increase in the proportion of children born through ARTs in Europe, from 2.3% (De Geyter et al., 2020) to 3.5% (Gliozheni et al., 2022) in just 3 years. In human reproduction, a popular technique is intracytoplasmic sperm microinjection (ICSI) (Haddad et al., 2021), in which a sperm selected by the embryologist is directly injected into the ooplasm. With this technique, positive results are obtained despite the low motility of the sample or immaturity of the sperm (Palermo et al., 1996). However, there are main concerns about ICSI for its invasiveness since it involves the piercing of the membrane. As a result, it could induce spindle damage or the introduction of contaminating external material (Verpoest and Tournaye, 2009). Another option is *in vitro* fertilization (IVF), where the oocyte and sperm are co-cultured in the same plate for a certain period so that penetration occurs without human intervention. Although IVF has been associated with an increased risk of congenital diseases or developmental delay (Waynforth, 2018), this method is considered the most physiological, since the spermatozoa penetrates the oocyte by itself. In addition, the scientific community is increasingly concerned about the potential long-term effects of ARTs (Sunde et al., 2016; Fleming et al., 2018). It is known that suboptimal *in vitro* conditions influence the epigenetic reprogramming of embryos (Canovas et al., 2017; Ferraz et al., 2018b). In humans, it has been suggested that ARTs may be related to a higher risk of imprinting disorders such as Beckwith-Wiedemann (Maher et al., 2003) or Angelman syndrome (Manipalviratn et al., 2009), although in the latter, it is very difficult to understand whether these disorders are related to the couple's infertility-subfertility problems or to ARTs (Pérez-Aytés et al., 2017). Moreover, differences in growth in ARTs-derived offspring in pig (París-Oller et al., 2022) and human (Ceelen et al., 2009) have also been observed.

All these above-mentioned problems could be solved by mimicking the physiological environment (i.e., the oviduct). In this organ, the oviductal epithelial cells (OECs) produce a large number of molecules that can protect embryos from oxidative stress and modify their metabolism (Ménézo et al., 2015). Indeed, two alternative strategies can be used to replicate natural conditions: 1) the use of reproductive fluid as a culture media supplement (Canovas et al., 2017) and 2) co-culture of gametes and embryos with oviductal epithelial cells (OECs) (Ferraz et al., 2018b). Two-D cultures (where cells grow in a monolayer) are the

most popular for studying the physiology of the oviduct and have been used in IVF and embryo culture in several species (Kölle et al., 2020), probably due to their high reproducibility, low cost, or ease of handling (Costa et al., 2016). Indeed, when these cultures are used during embryo *in vitro* production (IVP), there is an enhanced developmental rate of bovine embryos (Abe and Hoshi, 1997). However, it has been shown that this 2D culture method is not the best suited for fertilization studies since the cells dedifferentiate and lose their polarity, morphology, secretory capacity, and ciliary activity (Ferraz et al., 2017). On the contrary, when cultured in 3D, these cells retain much of their natural features (Pennarossa et al., 2021), making them a better model by keeping gene and metabolic expression closer to the *in vivo* context than their 2D counterparts (Anton et al., 2015). When the physiological environment is mimicked using microfluidics culture during IVF, it has been shown that the epigenetic reprogramming of bovine embryos is more similar to *in vivo* derived embryos (Ferraz et al., 2018b). All these data are indicators of the limitations of the 2D culture methods, thus encouraging researchers to move towards 3D culture systems to improve the quality of IVP embryos. To achieve this goal, it is crucial to construct a 3D device in which it is possible to co-culture differentiated OECs with gametes/zygotes. As a matter of fact, despite the well-known relevance the oviduct in gamete maturation/activation, fertilization, and early embryo development, only a few bioengineering studies have been focused on these female reproductive structures, so far (Kessler et al., 2015; Xiao et al., 2017; Ferraz et al., 2018b; Ferraz et al., 2020; Francés-Herrero et al., 2022).

Nowadays, a great variety of 3D printable biomaterials are commercially available (Santoni et al., 2021). One popular biomaterial is polylactic acid (PLA), a promising biodegradable polymer that can be produced from renewable sources like sugarcane (Li et al., 2020). PLA-scaffolds have excellent biocompatibility (Shilov et al., 2022), and have been used for medical purposes in bone (Diomedea et al., 2018; Velioglu et al., 2019) and cartilage regeneration (Rosenzweig et al., 2015). Together with PLA, polycaprolactone (PCL) is the most common biodegradable synthetic polymer used in tissue engineering (Arif et al., 2022), and it has already been employed for bone (Rumiński et al., 2018), liver (Huang et al., 2007) or skin (Ghosal et al., 2017) regenerative purposes. Similarly, photo-cross-linkable hydrogels are widely used, due to their tunable mechanical properties and to their capability to mimic native extracellular matrix (Lim et al., 2020; Zhang et al., 2022a). In fact, when viscoelasticity and stiffness properties of biomaterials can be tuned, this can represent an additional advantage to create scaffolds mimicking the native tissues with high resolution and complex architecture. Among them, polyethylene-glycol-diacylate (PEGDA) is a synthetic polymer approved by the Food and Drug Administration (FDA) (Kim et al., 2022) that has been used in variegated studies, from bone

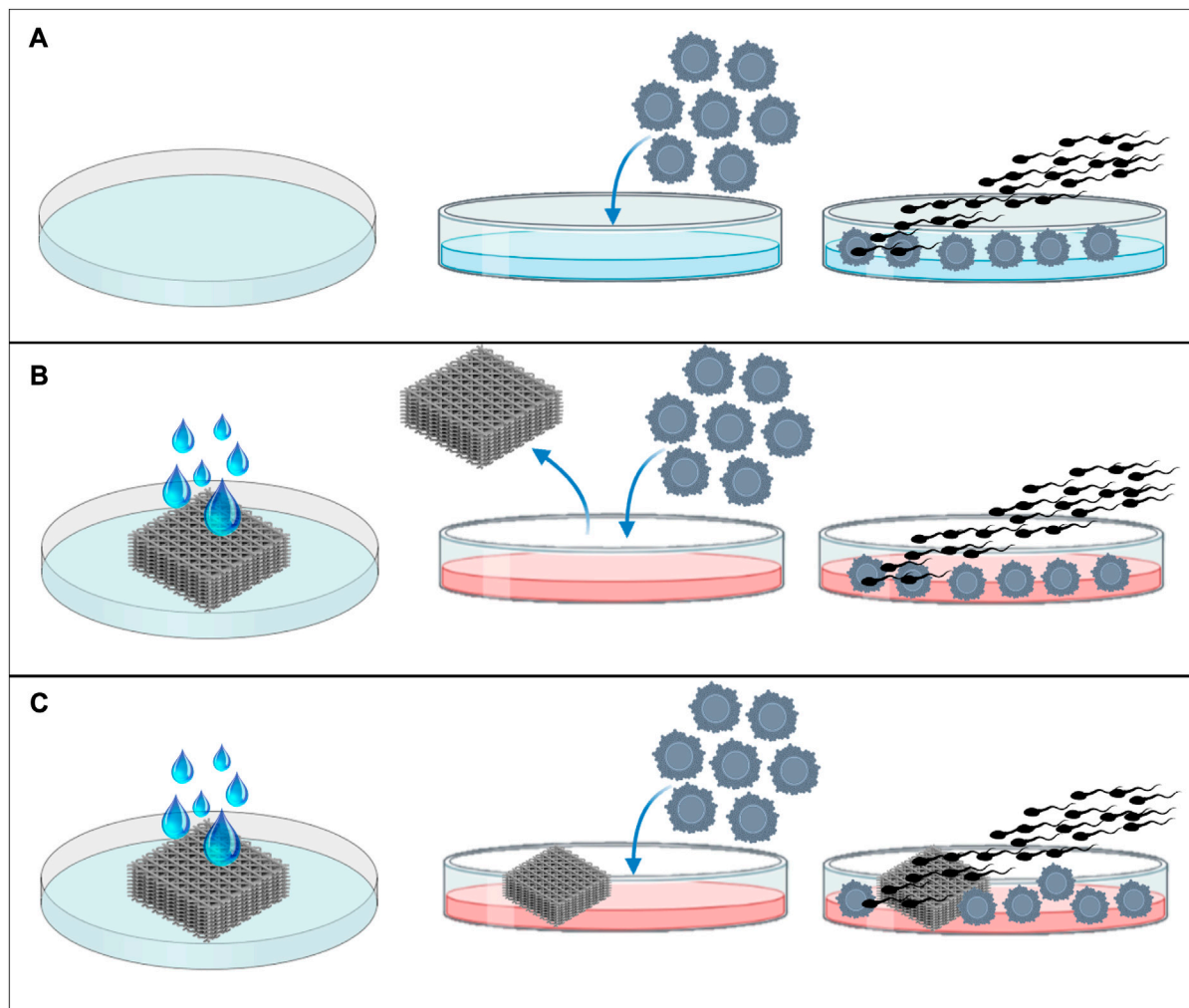


FIGURE 1

Experimental design. **(A)** IVF in normal Fert-TALP medium, without conditioning or scaffold, **(B)** IVF in Fert-TALP medium conditioned by scaffold for 24 h, and **(C)** IVF performed in presence of the rinsed scaffold.

(Rajabi et al., 2023) to cartilage (Zhang et al., 2022b) or muscle (Vannozzi et al., 2018) regeneration. In addition, PEGDA mechanical properties can be modulated by varying the molecular weight of the polymer (Nguyen et al., 2012) and it can be functionalized with cell binding motifs to enable cell adhesion (Della Sala et al., 2020). Despite the wide range of biomedical applications in which these materials have been used, no studies have been carried out so far to test the feasibility of these materials to construct a 3D-printed device for IVF.

Because of this lack of information, our study aims to evaluate the biocompatibility of different materials (PLA, PCL, PEGDA500, PEGDA200, and PEGDA PhotoInk) to support IVF, using bovine embryo development parameters (cleavage, blastocyst rates at day 7 and 8). In addition, to assess the quality of the *in vitro* produced embryos, we examined three fundamental parameters (Wydooghe et al., 2014) the cell number/embryo (TCN), the inner cell mass/trophoblast (ICM/TE) ratio, and the apoptotic cell ratio (ACR).

2 Materials and methods

2.1 Experimental design

To evaluate the feasibility of different materials (PLA, PCL, PEGDA500, PEGDA200, and PEGDA PhotoInk) to support IVF and their effects on bovine embryo development, three experimental groups were settled for each of the materials tested:

- Control group: the IVF was performed, without having any contact with the materials (Figure 1A).
- Rinse group: to assess if these materials could release some unknown substances that could have adverse effects in IVF or embryo development, the IVF was carried out in a Fert-TALP medium conditioned by the scaffold of each material during 24 h (Figure 1B).
- Scaffold group: prior to fertilization, the same scaffold used to condition the IVF media, was transferred to another well with

TABLE 1 Hardness of different materials (PLA, PCL, PEGDA500, PEGDA200, and PEGDA PhotoInk) expressed by Young's modulus.

Material	Young modulus	Source
PLA	3,000 MPa	Manufacturer (Sharebot)
PCL	370 MPa	Scocozza et al. (2023)
PEGDA500	500 KPa	Manufacturer (Cellink)
PEGDA200	200 KPa	Manufacturer (Cellink)
PEGDA PhotoInk	50 KPa	Manufacturer (Cellink)

new media and the IVF was performed in the presence of the scaffold (Figure 1C).

The number of oocytes was $n = 2892$ distributed for each group as follows: $n = 585$ for control, $n = 297$ for scaffold PCL, $n = 293$ for rinse PCL, $n = 196$ for scaffold PLA, $n = 201$ for rinse PLA, $n = 131$ for scaffold PEGDA500, $n = 143$ for rinse PEGDA500, $n = 248$ for scaffold PEGDA200, $n = 256$ for rinse PEGDA200, $n = 269$ for scaffold PEGDA PhotoInk, $n = 273$ for rinse PEGDA PhotoInk. We carried out 11 replicates, the control group was present in every single replicate, while PCL material was present in 6 of them, the PLA material in 4, the PEGDA500 material in 3, and the PEGDA200 and PEGDA PhotoInk materials were present in 5 replicates.

2.2 Culture media reagents.

All chemicals were purchased from Sigma-Aldrich Quimica, S.A. (Madrid, Spain) unless otherwise indicated.

2.3 3D printing materials

3D printed structures were produced to test the biocompatibility of the material and the effect of the 3D architecture on cells. All structures were designed using SolidWorks software (Dassault Systèmes SE, Vélizy-Villacoublay, France) and exported as an STL file. Depending on the printer used, the STL file was directly loaded on the printer or sliced using PrusaSlicer (Prusa Research, Prague, Czech Republic) to obtain the gcode file.

The 3D models were printed using different materials with different stiffness (Table 1) and 3D printing methods. PLA filaments were purchased from Sharebot, Italy; PCL pellet ($M_n = 50,000$ g/mol), PEGDA200, PEGDA500, and PEGDA Photoink were purchased from Cellink, Sweden. PLA filaments were printed via extrusion-based processing (FFF, Fused Filament Fabrication) using a Sharebot 42 3D printer (Sharebot, Italy) with a 0.4 mm diameter nozzle. PCL (CELLINK, Gothenburg, Sweden) structures were 3D printed using a BioX, a pneumatic extrusion-based 3D bioprinter (CELLINK, Gothenburg, Sweden) using a 0.4 mm nozzle, a pressure of 180 kPa, a velocity in a range 15–20 mm/s, and a temperature of 180°C according to suggested printing protocol. PEGDA500 Photoink, PEGDA200 Photoink, and PEGDA Photoink hydrogels (listed in decreasing order of stiffness) were 3D printed using a LumenX bioprinter based on

stereolithography via digital light processing (CELLINK, Gothenburg, Sweden) considering a 50 μ m layer height for the slicing and 20 mWatt/cm² power, 3x as first layer time scale factor, and a variable time of 2/3/12 s depending on the formulation, respectively, according to printing protocol.

2.4 Material sterilization

PLA, PCL, PEGDA500, PEGDA200, and PEGDA PhotoInk were sterilized following the manufacturer's instructions. Briefly, they were immersed in 70% ethanol for 5 min, then submerged twice in PBS (30 min each), and finally washed for 24 h with Fert-TALP (Parrish et al., 1986) culture medium supplemented con 175 U/mL heparin, 6 mg/mL BSA, 0.20 mM Na-pyruvate and 50 μ g/mL gentamicin. Fert-TALP medium consisted of 114 mM sodium chloride, 3.2 mM potassium chloride, 0.3 Mm sodium phosphate monobasic monohydrate, 10 mM sodium lactate, 2.0 mM calcium chloride dihydrate, 0.5 mM magnesium chloride hexahydrate and 25 mM sodium bicarbonate.

2.5 In vitro maturation

Ovaries from 1 year old cows were transported from the local slaughterhouse to the laboratory in physiological saline solution (0.9% w/vol) supplemented with 100 mg/L kanamycin sulfate at 38.5°C within two hours of slaughter. Once in the laboratory, the ovaries were washed with a 0.04% cetrimide solution and twice with saline. *In vitro* maturation was performed as previously described (Lopes et al., 2019) with minor modifications. Briefly, follicles between 2- and 8-mm diameter were aspirated. Only Cumulus-Oocyte Complexes (COCs) with at least three cumulus cell layers and with a homogeneous cytoplasm were selected and then washed three times in handling medium, consisting of TCM 199 supplemented with 4.2 mM sodium bicarbonate, 10 mM HEPES, 2 mM glutamine, 1% w/v polyvinyl alcohol, 50 IU/mL penicillin and 50 μ g/mL streptomycin. Subsequently, COCs were washed once in a maturation medium, consisting of TCM 199 (with Hanks' salts) supplemented with 4.2 mM sodium bicarbonate, 2 mM glutamine, 50 IU/mL gentamicin, 10% v/v of bovine follicular fluid (BFF, NaturARTs-BFF, Embryocloud, Murcia, Spain), 10 IU/mL equine chorionic gonadotropin (Foligon, Intervet International BV, Netherlands) and 10 IU/mL human chorionic gonadotropin (Veterin Corion, Divasa Farmavic, Spain) and incubated in 500 μ L of maturation medium in groups of 50–55 COCs in a four well dish at 38.5°C with a humidity-saturated atmosphere with 5% CO₂ for 22 h.

2.6 In vitro fertilization

After maturation and 30 min before IVF, the oocytes were washed once in Fert-TALP medium supplemented con 175 U/mL heparin, 6 mg/mL BSA, 0.20 mM Na-pyruvate and 50 μ g/mL gentamicin. For fertilization, frozen-thawed semen from three

bulls of proven fertility was used. The straw was thawed in a water bath at 38.5°C for 30 s. Once thawed, a Bovipure gradient (Nidacon, Sweden) was performed, centrifuging at 300 g for 10 min and removing the supernatant. Before insemination, sperm cells were washed once in modified Sperm-TALP medium (Parrish et al., 1988) (114 mM sodium chloride, 3.2 mM potassium chloride, 0.3 Mm sodium phosphate monobasic monohydrate, 10 mM sodium lactate, 2.0 mM calcium chloride dihydrate, 0.5 mM magnesium chloride hexahydrate, 25 mM sodium bicarbonate and 10 mM HEPES) supplemented with 6 mg/mL BSA, 1.0 mM Na-pyruvate and 50 µg/mL gentamicin, by centrifuging at 300 g during 3 min and removing the supernatant. Insemination was performed in medium conditioned by the scaffold, in the presence of scaffold and in fresh medium, in a final concentration of 1×10^6 spz/mL. Oocytes were coincubated with the spermatozoa for 22 h at 38.5°C with a humidity-saturated atmosphere with 5% CO₂.

2.7 Embryo culture

Twenty-two hours after insemination, the presumptive zygotes were moved into a 15 mL Falcon tube with a handling medium and vortexed for 4 min for decumulation. Zygotes were then washed once in Synthetic Oviductal Fluid medium (SOF) (Holm et al., 1999) and transferred into 50 µL microdrops of the same media covered by paraffin oil (Nidoil, Nidacon) in groups of 25 embryos per drop and cultured during 8 days at 38.5°C, 5% CO₂ and 5% O₂. Evaluation of embryo development occurred 48 h post insemination as the percentage of cleaved embryos out of presumptive zygotes, and at 7 and 8 days post insemination (dpi). In this study, only embryos with quality 1–2 according to the criteria of the International Embryo Technology Society (IETS) (summarized in Bó and Mapletoft, 2013) have been considered.

2.8 Differential apoptotic staining

To assess the total cell number (TCN), the inner cell mass/trophoblast ratio (ICM/TE), and the apoptotic cell ratio (ACR), differential staining was performed as described previously (Wydooghe et al., 2011) with minor modifications. Briefly, day 8 blastocysts were fixed in 4% paraformaldehyde for 20 min at RT and conserved in 2% paraformaldehyde at 4°C until the moment of staining. The embryos were permeabilized with 0.5% Triton-X and 0.05% Tween in PBS overnight at 4°C. On the second day, blastocysts were washed three times for 10 min in PBS containing 0.5% BSA (washing solution). Subsequently, the DNA of the cells was denatured with 2N HCl for 20 min followed by 100 Mm trisHCl (pH = 8.5) for 10 min. After denaturation, the embryos were washed three times in washing solution and transferred to blocking solution (10% goat serum and 0.05% tween in PBS) overnight at 4°C. After blocking, the blastocysts were washed three times in washing solution and incubated in ready-to-use mouse anti-CDX2 primary antibody (Biogenex, San Ramon, United States) for overnight at 4°C, while two embryos remained in blocking solution as negative control. After this incubation, test embryos were washed three times in washing solution and incubated 1:500 dilution of rabbit anti-active caspase-3 primary antibody (Cell Signaling Technology, Leiden, Netherlands) in

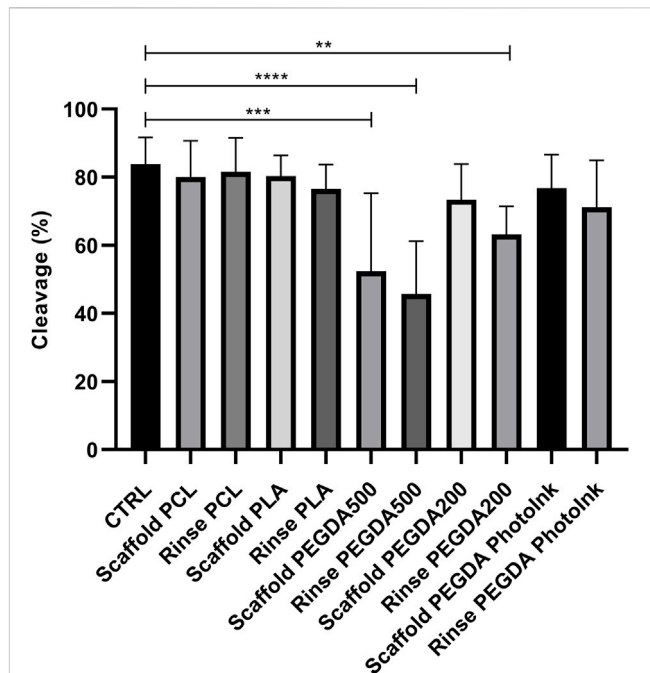


FIGURE 2

Effect of different materials on the percentage of cleaved embryos. The histograms show the cleavage rate when the IVF was performed with an unconditioned medium (CTRL), with medium conditioned by each material (rinse groups) or when different scaffolds were present (scaffold groups). The data show significant differences ($p < 0.05$) in CTRL vs. Scaffold PEGDA500, CTRL vs. Rinse PEGDA500 and CTRL vs. Rinse PEGDA200. The data are presented as the mean \pm SD of 11 independent experiments. Data were analyzed using Dunnett's test. ** $p < 0.01$, *** $p < 0.005$, **** $p < 0.0001$ versus control.

blocking solution overnight at 4°C. On the last day, all blastocysts (negative and test) were washed three times for 10 min in washing solution, and incubated with 1:100 goat anti-mouse TRICT (Abcam, Cambridge, United Kingdom) in blocking solution for 1 h at RT. After another three-wash step, the embryos were incubated in 1:200 goat anti-rabbit FITC secondary antibody (Abcam, Cambridge, United Kingdom) in blocking solution for 1 h at RT. Finally, the blastocysts were washed, stained with Hoechst 33342 for 15 min, washed for the last time, mounted in Dabco (1,4-Diazabicyclo[2.2.2]octane solution), and evaluated under fluorescence microscopy (Eclipse Ti Series, Nikon, Japan). A representative image of embryo was taken using Nikon A1r laser confocal scanning microscope.

2.9 Statistical analysis

For statistical analysis, GraphPad Prism 8 Software (La Jolla, CA, United States) was used. Data were checked for normal distribution with Shapiro-Wilk normality test prior to perform the comparison with parametric tests. In all cases the differences among groups were considered statistically significant when $p < 0.05$.

For Principal Component Analysis, Past 4.13 (Oslo, Norway) was used to evaluate the effect of different materials on Cleavage, blastocyst rate at day 7, blastocyst rate at day 8, TCN, ICM/TE and AC ratio.

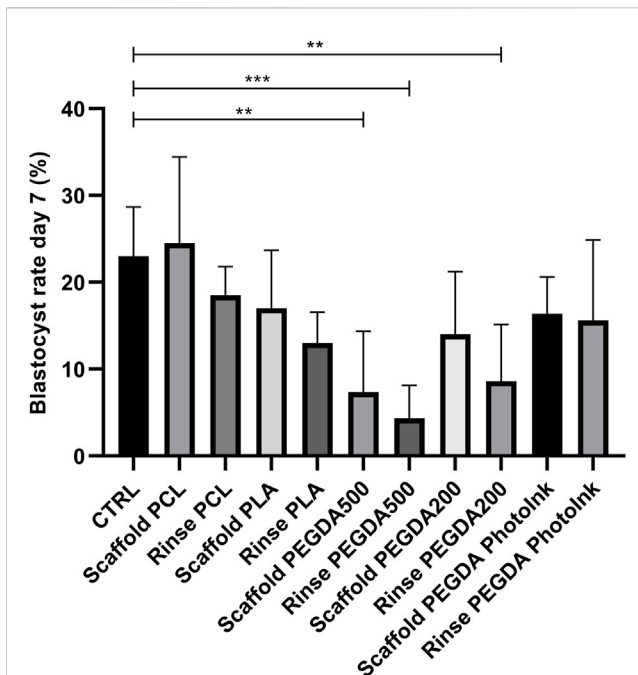


FIGURE 3

Effect of different materials on blastocyst rate at day 7. The histograms show the blastocyst rate at day 7 when the IVF was performed with unconditioned medium (CTRL), with medium conditioned by each material (rinse groups) or when different scaffolds were present (scaffold groups). The data show significant differences ($p < 0.05$) in CTRL vs. Scaffold PEGDA500, CTRL vs. Rinse PEGDA500 and CTRL vs. Rinse PEGDA200. The data are presented as the mean of 11 independent experiments. Data were analyzed using the Dunnett's test. ** $p < 0.01$, *** $p < 0.005$ versus control.

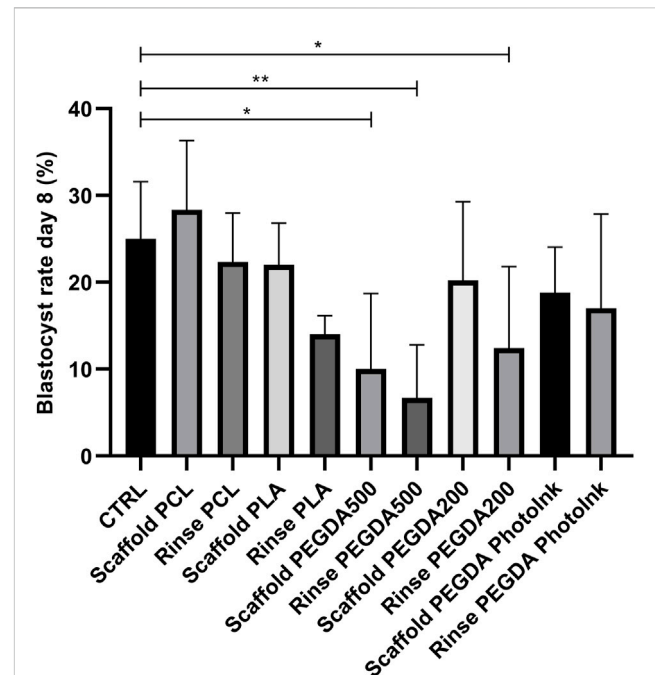


FIGURE 4

Effect of different materials scaffolds on blastocyst rate at day 8. The histograms show the blastocyst rate at day 8 when the IVF was performed with unconditioned medium (CTRL), with medium conditioned by each material (rinse groups) or when different scaffolds were present (scaffold groups). The data shows significant differences ($p < 0.05$) in CTRL vs. Scaffold PEGDA500, CTRL vs. Rinse PEGDA500 and CTRL vs. Rinse PEGDA200. The data are presented as mean of 11 independent experiments. Data were analyzed using the Dunnett's test. * $p < 0.05$, ** $p < 0.01$ versus control.

3 Results

3.1 Effect of the different materials on cleavage

We observed a significant lower cleavage rate in rinse PEGDA500 ($45\% \pm 15\%$), scaffold PEGDA500 ($50\% \pm 23\%$), and rinse PEGDA200 ($63\% \pm 8\%$) groups vs. CTRL group ($84\% \pm 8\%$), while we did not observe any difference between the cleavage rate of rinse PCL ($82\% \pm 10\%$), scaffold PCL ($80\% \pm 10\%$), rinse PLA ($77\% \pm 7\%$), scaffold PLA ($81\% \pm 6\%$), scaffold PEGDA200 ($73\% \pm 11\%$), rinse PEGDA PhotoInk ($71\% \pm 14\%$) or scaffold PEGDA PhotoInk ($77\% \pm 10\%$) compared to the control (Figure 2).

3.2 Effect of the different materials on blastocyst rate at day 7

Compared to the CTRL group ($23\% \pm 6\%$), blastocyst rates were significantly lower ($p < 0.05$) in the rinse PEGDA500 ($4\% \pm 4\%$), scaffold PEGDA500 ($7\% \pm 7\%$), and rinse PEGDA200 ($8\% \pm 7\%$) groups on day 7 (Figure 3). The scaffold PCL group had a $25\% \pm 10\%$ blastocyst yield, which was not statistically different ($p > 0.05$) vs. the CTRL, while scaffold PLA ($17\% \pm 7\%$), scaffold PEGDA200 ($14\% \pm 7\%$), and scaffold PEGDA PhotoInk ($16\% \pm 4\%$) showed similar blastocyst rates. On the other hand, rinse groups have decreased

embryo development compared to control but not significantly less than their scaffold groups, being $18\% \pm 4\%$ for rinse PCL, $13\% \pm 4\%$ for rinse PLA, and $16\% \pm 7\%$ for rinse PEGDA PhotoInk (Figure 3).

3.3 Effect of the different materials on blastocyst rate at day 8

Blastocyst rate at day 8 were significantly lower in rinse PEGDA500 ($6\% \pm 6\%$), scaffold PEGDA500 ($10\% \pm 9\%$), and rinse PEGDA200 ($12\% \pm 9\%$) groups vs. CTRL group ($25\% \pm 6\%$). On the scaffold's groups, we had not statistical differences ($p > 0.05$) for blastocyst yield in the scaffold PCL group with $29\% \pm 8\%$, while the scaffold PLA ($14\% \pm 2\%$), scaffold PEGDA200 ($20\% \pm 9\%$) and scaffold PhotoInk ($19\% \pm 5\%$) groups showed similar blastocyst rates. In addition, rinse groups did not present significant differences vs. the CTRL, being the blastocyst rates $22\% \pm 6\%$ for rinse PCL, $14\% \pm 2\%$ for rinse PLA, and $17\% \pm 11\%$ for rinse PEGDA PhotoInk (Figure 4).

3.4 Principal component analysis of the different materials considering all variables studied

The total cell number, the trophectoderm and the apoptosis were evaluated under fluorescence microscopy (Figure 5) and the

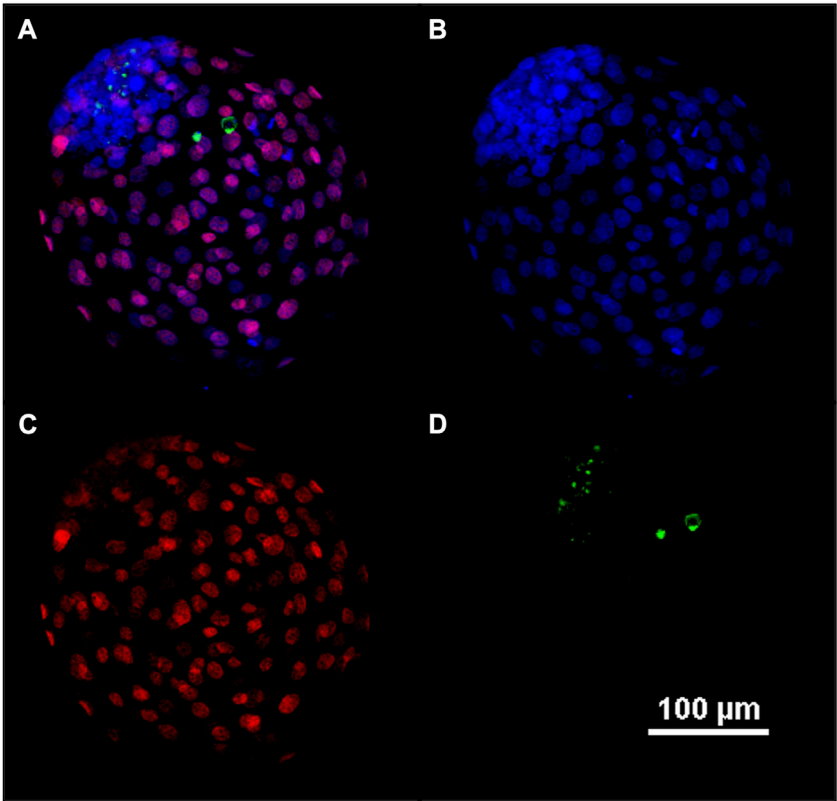


FIGURE 5
Representative confocal image of blastocyst at day 8. Fluorescent image of differential apoptotic staining (A–D). At day 8, bovine blastocysts were fixed, dyed with Hoechst 33342 for nuclei (B), immune-stained for CDX2 for the trophectoderm (C), and for active caspase-3 for the apoptosis (D). In (A) an overlay (B–D) is provided.

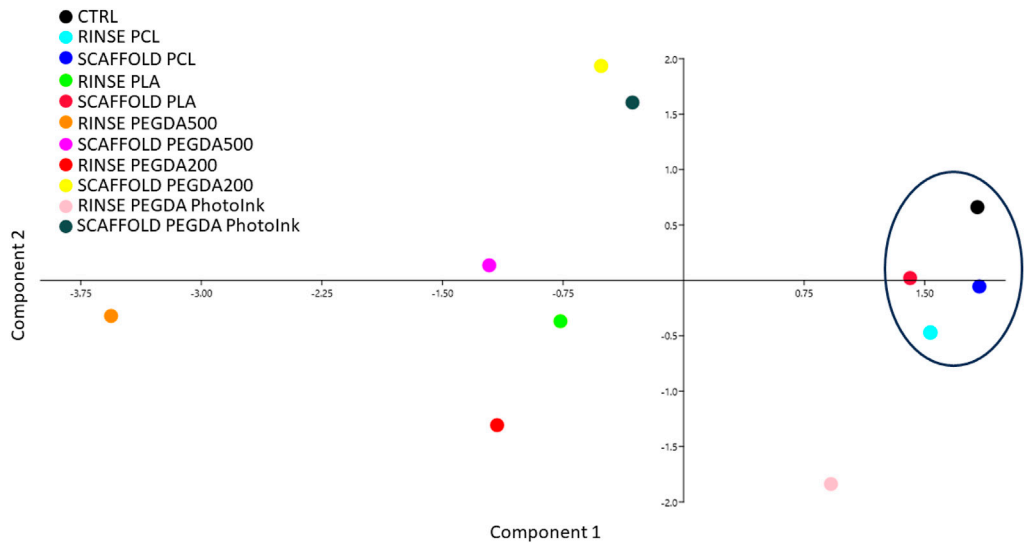


FIGURE 6
Principal component analysis performed by assessing the different parameters studied (Cleavage, blastocyst rate at days 7 and 8, TCN, ICM/TE and ACR). Principal component analysis shows no separation among groups. However, we observed that the closest groups to control are scaffold PLA, scaffold PCL and rinse PCL.

ICM/TE ratio and ACR were calculated. Since we studied several biological factors (cleavage, blastocyst rate at day 7 and 8, TCN, ICM/TE ratio and ACR), we used the Principal Component Analysis (PCA) as a multivariable analysis to simplify the data analysis and interpretation by reducing the complexity (Jolliffe and Cadima, 2016a). This analysis allows to reduce the amount of information needed since the system works with more compact representation of the data by retaining the relevant information and highlighting the underlying patterns and structures (Jolliffe and Cadima, 2016b). PCA showed how the scaffold PCL, rinse PCL, scaffold PLA and control groups were more similar among them than to the other groups (scaffold PEGDA500, rinse PEGDA500, rinse PEGDA200, scaffold PEGDA200, rinse PLA, rinse PhotoInk and scaffold PhotoInk) (Figure 6).

4 Discussion

In the present study we performed a bovine embryo assay to evaluate the potential toxicity of PLA, PCL, PEGDA500, PEGDA200, and PEGDA PhotoInk biomaterials in the embryo IVP during IVF. In addition, we tested not only different materials but also different printing methods, using for each material the most suitable method for the scaffold construction needs. We chose this animal model since it has already been used for embryo assay (Ieda et al., 2018) and it represents a valuable model for IVF improvement trials (Ménézo and Hérubel, 2002). It is also well-known that IVP produces suboptimal embryos with a lower yield of blastocysts and lower developmental capacity than their *in vivo* counterparts (Heras et al., 2016; Canovas et al., 2017; Ferraz et al., 2018b).

The first step in producing a device that could improve the IVP is the choice of biomaterial. All the materials we propose have been used in cell culture and have shown a good biocompatibility (Eslahi et al., 2013; Biagini et al., 2021; Di Berardino et al., 2022; Testore et al., 2022). However, as the cytotoxicity of the materials such as PLA (Biagini et al., 2021) could be different according to the cell types, the biocompatibility should be tested in regard to gametes, zygotes and embryos.

Our results suggest that the only material that has toxic effects is PEGDA500. This material had detrimental effect on bovine embryo development, promoting lower cleavage and lower blastocyst rate at day 7 and 8. This is an unexpected effect since PEGDA hydrogels have been suggested as effective candidates to carry out studies for embryogenesis and organogenesis due to their low cost, high reproducibility, and ease fabrication (Hribar et al., 2015). This is not the first time that biomaterials have shown unexpected negative effects when in contact with embryos. MacDonald et al. (2016) showed that VisiJet Crystal material (belonging to the strictest class for plastic biocompatibility) had a detrimental effect on zebrafish embryos (MacDonald et al., 2016). The materials E-shell200 and E-shell300 have also shown a deleterious effect on bovine embryo development, even having been considered biocompatible according to ISO 10993 (Ferraz et al., 2018a). Furthermore, we must take into consideration the eventuality that our materials might not be exactly the same in chemistry as those used in previously works, since the full chemical composition may vary from one company to another. Another plausible factor could be the fact that in the 3D printed

scaffolds could be found some residues of toxic compounds that have been used to stabilize and print the devices. Indeed, several studies have observed that different chemical species are leaked by 3D-printed scaffolds (Oskui et al., 2016; Ferraz et al., 2018a).

Additionally, we detected significant differences between the rinse group of PEGDA200 and CTRL group, but no differences when PEGDA200 scaffolds were compared to the controls. This result suggests that the PEGDA200 may require longer washing than the other PEGDA hydrogels, since this type of scaffold had no detrimental effects on embryo development during IVF after being washed for 24 h and rinsed for another 24 h. However, all these hydrogels might not be the best option for the IVF device manufacturing because they were very fragile, and their rupture could be a relevant inconvenience during sterilization and handling.

Conversely, neither PLA nor PCL have shown detrimental effects on cleavage and blastocyst rate parameters. The PLA synthetic polymer has been suggested as an optimal candidate for scaffold fabrication due to its high biocompatibility, low cost, and mechanical properties (Serra et al., 2013; Di Prima et al., 2016). To our knowledge, this is the first study testing those materials to support bovine IVF, showing high biocompatibility. This is an expected result since both PLA and PCL biomaterials have been used in an emerging field called REPROTEN, the discipline that applies tissue engineering to restore fertility (Amorim, 2017). It has been shown that PLA is a suitable material to create a nanofiber scaffold that enhance the *in vitro* cluster formation of mouse spermatogonia stem cells, allowing their proliferation and differentiation (Eslahi et al., 2013; Ghorbani et al., 2019). As well, PCL has been used to culture spermatogonia stem cells (Talebi et al., 2019; Ghorbani et al., 2022), obtaining the same successful results as PLA. Furthermore, recent works have used PCL scaffolds as devices to carry out folliculogenesis in sheep (Di Berardino et al., 2022) and pig (Liverani et al., 2019).

We observed worse results with the increase of the PEGDA material stiffness (PEGDA Photoink vs PEGDA200 vs. PEGDA500). Previously, it has been shown that the stiffness of different substrates can affect *in vitro* embryo development in mice (Kolahi et al., 2012), but in our case the lower efficiency could be due to the chemistry employed to promote higher stiffness of the material, since even when the scaffold is absent during IVF, the rinse groups showed lower efficiency. One possible explanation for the worse performance of the rinse groups could be that the scaffolds release toxic compounds during the rinse period culture, so when the scaffolds are used during IVF the release of these toxic chemicals is much lower or absent. However, to confirm this hypothesis mass spectrometry analysis should be performed.

Altogether, these data suggest that the materials printed with stereolithography (PEGDAs) are less biocompatible than extrusion-printed materials (PLA and PCL). On the other hand, the TCN, the ICM/TE ratio and the ACR are three important parameters of embryo quality and in recent years, several studies have shown that the rate of ICM/TE is a strong predictor of live birth (Ai et al., 2021; Sivanantham et al., 2022). When we analyzed all these parameters, the principal component analysis (PCA) showed that the embryos produced in presence of PLA and PCL scaffolds are the most comparable to the control group. Regarding the PCL biopolymer, the rinse and the scaffold groups are both closer to the control ones, in terms of the analyzed parameters. While a

different situation using the PLA biomaterial has been observed, since the scaffold group exhibited similar behavior to the control, contrary to the rinse group of the same biopolymer. For this reason, we consider PCL as the most suitable material for *in vitro* bovine embryo production.

Considering that we have not identified any negative effects on bovine embryo development when PCL is present during IVF, its implementation in the construction of a device compatible with microfluidics systems becomes a promising possibility. The combination of these microfluidics systems with the above-mentioned devices could allow the creation of an *in vitro* model of the oviduct (Romar et al., 2019). This innovative application could have a significant impact on the research and understanding of sperm selection by mimicking rheotaxis, chemotaxis and thermotaxis (Pérez-Cerezales et al., 2018; Ramal-Sanchez et al., 2021), fertilization and early development processes, providing a controlled and reproducible environment for experimental studies, without jeopardizing early embryo development.

In conclusion, the utilization of PCL in the construction of an IVF device holds great promise for the improvement of ARTs in the near future. However, further research and development are necessary to test the biocompatibility with OECs, optimize the design and functionality of this PCL-based IVF devices, ensuring their long-term effectiveness and safety. Nonetheless, the outcomes of our study strongly support the potential of the PCL biomaterial and open the way for advancements in the field of ARTs.

Data availability statement

The original contributions presented in the study are included in the article/Supplementary Material, further inquiries can be directed to the corresponding author.

Ethics statement

Ethical approval was not required for the studies involving animals in accordance with the local legislation and institutional requirements because the ovaries were collected from cows slaughtered for feed purposes. Written informed consent was

obtained from the owners for the participation of their animals in this study.

Author contributions

RB-P: Data curation, Formal Analysis, Methodology, Writing—original draft, Writing—review and editing. SH: Methodology, Writing—review and editing. CC: Data curation, Formal Analysis, Writing—review and editing. JR-A: Methodology, Writing—review and editing. LV: Writing—review and editing. AC: Writing—review and editing. BC: Methodology, Writing—review and editing. SS: Methodology, Writing—review and editing. BB: Funding acquisition, Supervision, Writing—review and editing. NB: Conceptualization, Data curation, Formal Analysis, Funding acquisition, Supervision, Writing—review and editing. PC: Conceptualization, Funding acquisition, Supervision, Writing—review and editing.

Funding

The author(s) declare that no financial support was received for the research, authorship, and/or publication of this article.

Conflict of interest

The authors declare that the research was conducted in the absence of any commercial or financial relationships that could be construed as a potential conflict of interest.

Publisher's note

All claims expressed in this article are solely those of the authors and do not necessarily represent those of their affiliated organizations, or those of the publisher, the editors and the reviewers. Any product that may be evaluated in this article, or claim that may be made by its manufacturer, is not guaranteed or endorsed by the publisher.

References

- Abe, H., and Hoshi, H. (1997). Bovine oviductal epithelial cells: their cell culture and applications in studies for reproductive biology. *Cytotechnology* 23, 171–183. doi:10.1023/A:1007929826186
- Ai, J., Jin, L., Zheng, Y., Yang, P., Huang, B., and Dong, X. (2021). The morphology of inner cell mass is the strongest predictor of live birth after a frozen-thawed single embryo transfer. *Front. Endocrinol. (Lausanne)* 12, 621221. doi:10.3389/fendo.2021.621221
- Amorim, C. A. (2017). Special issue devoted to a new field of regenerative medicine: reproductive tissue engineering. *Ann. Biomed. Eng.* 45, 1589–1591. doi:10.1007/s10439-017-1862-0
- Anton, D., Burckel, H., Josset, E., and Noel, G. (2015). Three-dimensional cell culture: A breakthrough *in vivo*. *Int. J. Mol. Sci.* 16, 5517–5527. doi:10.3390/ijms16035517
- Arif, Z. U., Khalid, M. Y., Noroozi, R., Sadeghianmaryan, A., Jalalvand, M., and Hossain, M. (2022). Recent advances in 3D-printed polylactide and polycaprolactone-based biomaterials for tissue engineering applications. *Int. J. Biol. Macromol.* 218, 930–968. doi:10.1016/j.ijbiomac.2022.07.140
- Assidi, M. (2022). Infertility in men: advances towards a comprehensive and integrative strategy for precision therapeutics. *Cells* 11, 1711. doi:10.3390/cells11101711
- Biagini, G., Senegaglia, A. C., Pereira, T., Berti, L. F., Marcon, B. H., and Stimamiglio, M. A. (2021). 3D poly(lactic acid) scaffolds promote different behaviors on endothelial progenitors and adipose-derived stromal cells in comparison with standard 2D cultures. *Front. Bioeng. Biotechnol.* 9, 700862. doi:10.3389/fbioe.2021.700862
- Bó, G. A., and Mapletto, R. J. (2013). Evaluation and classification of bovine embryos. *Anim. Reprod. Ar.* 10, 344–348.
- Canovas, S., Ivanova, E., Romar, R., García-Martínez, S., Soriano-Úbeda, C., García-Vázquez, F. A., et al. (2017). DNA methylation and gene expression changes derived from assisted reproductive technologies can be decreased by reproductive fluids. *Elife* 6, e23670. doi:10.7554/eLife.23670
- Ceelen, M., Van Weissenbruch, M. M., Prein, J., Smit, J. J., Vermeiden, J. P. W., Spreuwenberg, M., et al. (2009). Growth during infancy and early childhood in relation to blood pressure and body fat measures at age 8–18 years of IVF children and

spontaneously conceived controls born to subfertile parents. *Hum. Reprod.* 24, 2788–2795. doi:10.1093/HUMREP/DEP273

Costa, E. C., Moreira, A. F., de Melo-Diogo, D., Gaspar, V. M., Carvalho, M. P., and Correia, I. J. (2016). 3D tumor spheroids: an overview on the tools and techniques used for their analysis. *Biotechnol. Adv.* 34, 1427–1441. doi:10.1016/J.BIOTECHADV.2016.11.002

De Geyter, C., Calhaz-Jorge, C., Kupka, M. S., Wyns, C., Mocanu, E., Motrenko, T., et al. (2020). ART in Europe, 2015: results generated from european registries by eshre. *Hum. Reprod. Open* 2020, hoz038. doi:10.1093/HROPEN/HOZ038

Della Sala, F., Biondi, M., Guarnieri, D., Borzacchiello, A., Ambrosio, L., and Mayol, L. (2020). Mechanical behavior of bioactive poly(ethylene glycol) diacrylate matrices for biomedical application. *J. Mech. Behav. Biomed. Mater.* 110, 103885. doi:10.1016/J.JMBBM.2020.103885

Di Berardino, C., Liverani, L., Peserico, A., Capacchietti, G., Russo, V., Bernabò, N., et al. (2022). When electrospun fiber support matters: *in vitro* ovine long-term folliculogenesis on poly (epsilon caprolactone) (pcl)-patterned fibers. *Cells* 11, 1968. doi:10.3390/cells11121968

Di Prima, M., Coburn, J., Hwang, D., Kelly, J., Khairuzzaman, A., and Ricles, L. (2016). Additively manufactured medical products - the FDA perspective. *3D Print Med.* 2, 1. doi:10.1186/S41205-016-0005-9

Diomedea, F., Gugliandolo, A., Cardelli, P., Merciaro, I., Ettore, V., Traini, T., et al. (2018). Three-dimensional printed PLA scaffold and human gingival stem cell-derived extracellular vesicles: A new tool for bone defect repair. *Stem Cell Res. Ther.* 9, 104–121. doi:10.1186/s13287-018-0850-0

Eslahi, N., Hadjighassem, M. R., Joghataei, M. T., Mirzapour, T., Bakhtiyari, M., Shakeri, M., et al. (2013). The effects of poly L-lactic acid nanofiber scaffold on mouse spermatogonial stem cell culture. *Int. J. Nanomedicine* 8, 4563–4576. doi:10.2147/IJN.S45535

Ferraz, M. A. M. M., Henning, H. H. W., Da Costa, P. F., Malda, J., Le Gac, S., Bray, F., et al. (2018a). Potential health and environmental risks of three-dimensional engineered polymers. *Environ. Sci. Technol. Lett.* 5, 80–85. doi:10.1021/acs.estlett.7b00495

Ferraz, M. A. M. M., Henning, H. H. W., Stout, T. A. E., Vos, P. L. A. M., and Gadella, B. M. (2017). Designing 3-dimensional *in vitro* oviduct culture systems to study mammalian fertilization and embryo production. *Ann. Biomed. Eng.* 45, 1731–1744. doi:10.1007/s10439-016-1760-x

Ferraz, M. A. M. M., Nagashima, J. B., Venzac, B., Le Gac, S., and Songsasen, N. (2020). A dog oviduct-on-a-chip model of serous tubal intraepithelial carcinoma. *Sci. Rep.* 10, 1–11. doi:10.1038/s41598-020-58507-4

Ferraz, M. A. M. M., Rho, H. S., Hemerich, D., Henning, H. H. W., van Tol, H. T. A., Hölker, M., et al. (2018b). An oviduct-on-a-chip provides an enhanced *in vitro* environment for zygote genome reprogramming. *Nat. Commun.* 9, 4934. doi:10.1038/s41467-018-07119-8

Fleming, T. P., Watkins, A. J., Velazquez, M. A., Mathers, J. C., Prentice, A. M., Stephenson, J., et al. (2018). Origins of lifetime health around the time of conception: causes and consequences. *Lancet* 391, 1842–1852. doi:10.1016/S0140-6736(18)30312-X

Francés-Herrero, E., Lopez, R., Hellström, M., De Miguel-Gómez, L., Herraiz, S., Brännström, M., et al. (2022). Bioengineering trends in female reproduction: A systematic review. *Hum. Reprod. Update* 28, 798–837. doi:10.1093/humupd/dmac025

Ghorbani, M., Nourani, M. R., Alizadeh, H., and Goodarzi, V. (2022). Evaluation of the growth and differentiation of spermatogonial stem cells on a 3D polycaprolactone/multi-walled carbon nanotubes-based microfibrous scaffold. *J. Appl. Biotechnol. Rep.* 9, 846–855. doi:10.30491/JABR.2022.312357.1463

Ghorbani, S., Eyni, H., Khosrowpour, Z., Salari Asl, L., Shabani, R., Nazari, H., et al. (2019). Spermatogenesis induction of spermatogonial stem cells using nanofibrous poly(L-lactic acid)/multi-walled carbon nanotube scaffolds and naringenin. *Polym. Adv. Technol.* 30, 3011–3025. doi:10.1002/PAT.4733

Ghosal, K., Manakhov, A., Zajíčková, L., and Thomas, S. (2017). Structural and surface compatibility study of modified electrospun poly(epsilon-caprolactone) (PCL) composites for skin tissue engineering. *AAPS PharmSciTech* 18, 72–81. doi:10.1208/S12249-016-0500-8

Gliozheni, O., Hambartsumian, E., Strohmmer, H., Petrovskaya, E., Tishkevich, O., de Neubourg, D., et al. (2022). ART in Europe, 2018: results generated from european registries by eshre. *Hum. Reprod. Open* 2022, hoac022. doi:10.1093/HROPEN/HOAC022

Haddad, M., Stewart, J., Xie, P., Cheung, S., Trout, A., Keating, D., et al. (2021). Thoughts on the popularity of ICSI. *J. Assist. Reprod. Genet.* 38, 101–123. doi:10.1007/S10815-020-01987-0

Heras, S., De Coninck, D. I. M., Van Poucke, M., Goossens, K., Bogado Pascottini, O., Van Nieuwerburgh, F., et al. (2016). Suboptimal culture conditions induce more deviations in gene expression in male than female bovine blastocysts. *BMC Genomics* 17, 72. doi:10.1186/S12864-016-2393-Z

Holm, P., Booth, P. J., Schmidt, M. H., Greve, T., and Callesen, H. (1999). High bovine blastocyst development in a static *in vitro* production system using SOFaa medium supplemented with sodium citrate and myo-inositol with or without serum-proteins. *Theriogenology* 52, 683–700. doi:10.1016/S0093-691X(99)00162-4

Hribar, K. C., Finlay, D., Ma, X., Qu, X., Ondeck, M. G., Chung, P. H., et al. (2015). Nonlinear 3D projection printing of concave hydrogel microstructures for long-term multicellular spheroid and embryoid body culture. *Lab. Chip* 15, 2412–2418. doi:10.1039/c5lc00159e

Huang, H., Oizumi, S., Kojima, N., Niino, T., and Sakai, Y. (2007). Avidin-biotin binding-based cell seeding and perfusion culture of liver-derived cells in a porous scaffold with a three-dimensional interconnected flow-channel network. *Biomaterials* 28, 3815–3823. doi:10.1016/J.BIOMATERIALS.2007.05.004

Ieda, S., Akai, T., Sakaguchi, Y., Shimamura, S., Sugawara, A., Kaneda, M., et al. (2018). A microwell culture system that allows group culture and is compatible with human single media. *J. Assist. Reprod. Genet.* 35, 1869–1880. doi:10.1007/s10815-018-1252-z

Jolliffe, I. T., and Cadima, J. (2016a). Principal component analysis: A review and recent developments. *Philosophical Trans. R. Soc. A Math. Phys. Eng. Sci.* 374, 20150202. doi:10.1098/rsta.2015.0202

Jolliffe, I. T., and Cadima, J. (2016b). Principal component analysis: A review and recent developments. *Philosophical Trans. R. Soc. A Math. Phys. Eng. Sci.* 374, 20150202. doi:10.1098/rsta.2015.0202

Kessler, M., Hoffmann, K., Brinkmann, V., Thieck, O., Jackisch, S., Toelle, B., et al. (2015). The Notch and Wnt pathways regulate stemness and differentiation in human fallopian tube organoids. *Nat. Commun.* 6, 8989. doi:10.1038/NCOMMS9989

Kim, S., Lee, H., Choi, H., Yoo, K. Y., and Yoon, H. (2022). Investigation on photopolymerization of PEGDA to fabricate high-aspect-ratio microneedles. *RSC Adv.* 12, 9550–9555. doi:10.1039/D2RA00189F

Kolahi, K. S., Donjacour, A., Liu, X., Lin, W., Simbulan, R. K., Bloise, E., et al. (2012). Effect of substrate stiffness on early mouse embryo development. *PLoS One* 7, e41717. doi:10.1371/JOURNAL.PONE.0041717

Kölle, S., Hughes, B., and Steele, H. (2020). Early embryo-maternal communication in the oviduct: A review. *Mol. Reprod. Dev.* 87, 650–662. doi:10.1002/MRD.23352

Li, G., Zhao, M., Xu, F., Yang, B., Li, X., Meng, X., et al. (2020). Synthesis and biological application of polylactic acid. *Molecules* 25, 5023. doi:10.3390/MOLECULES25215023

Lim, K. S., Galarraga, J. H., Cui, X., Lindberg, G. C. J., Burdick, J. A., and Woodfield, T. B. F. (2020). Fundamentals and applications of photo-cross-linking in bioprinting. *Chem. Rev.* 120, 10662–10694. doi:10.1021/ACS.CHEMREV.9B00812

Liverani, L., Raffel, N., Fattahi, A., Preis, A., Hoffmann, I., Boccaccini, A. R., et al. (2019). Electrospun patterned porous scaffolds for the support of ovarian follicles growth: A feasibility study. *Sci. Rep.* 9 (19), 1150–1214. doi:10.1038/s41598-018-37640-1

Lopes, J. S., Canha-Gouveia, A., Paris-Oller, E., and Coy, P. (2019). Supplementation of bovine follicular fluid during *in vitro* maturation increases oocyte cumulus expansion, blastocyst developmental kinetics, and blastocyst cell number. *Theriogenology* 126, 222–229. doi:10.1016/j.theriogenology.2018.12.010

MacDonald, N. P., Zhu, F., Hall, C. J., Reboud, J., Crosier, P. S., Patton, E. E., et al. (2016). Assessment of biocompatibility of 3D printed photopolymers using zebrafish embryo toxicity assays. *Lab. Chip* 16, 291–297. doi:10.1039/c5lc01374g

Maher, E. R., Brueton, L. A., Bowdin, S. C., Luharia, A., Cooper, W., Cole, T. R., et al. (2003). Beckwith-Wiedemann syndrome and assisted reproduction technology (ART). *J. Med. Genet.* 40, 62–64. doi:10.1136/JMG.40.1.62

Manipalviratn, S., DeCherney, A., and Segars, J. (2009). Imprinting disorders and assisted reproductive technology. *Fertil. Steril.* 91, 305–315. doi:10.1016/J.FERTNSTERT.2009.01.002

Ménézo, Y., Guérin, P., and Elder, K. (2015). The oviduct: A neglected organ due for re-assessment in IVF. *Reprod. Biomed. Online* 30, 233–240. doi:10.1016/j.rbmo.2014.11.011

Ménézo, Y. J. R., and Hérubel, F. (2002). Mouse and bovine models for human IVF. *Reprod. Biomed. Online* 4, 170–175. doi:10.1016/S1472-6483(10)61936-0

Nguyen, Q. T., Hwang, Y., Chen, A. C., Varghese, S., and Sah, R. L. (2012). Cartilage-like mechanical properties of poly (ethylene glycol)-diacrylate hydrogels. *Biomaterials* 33, 6682–6690. doi:10.1016/J.BIOMATERIALS.2012.06.005

Oskui, S. M., Diamante, G., Liao, C., Shi, W., Gan, J., Schlenk, D., et al. (2016). Assessing and reducing the toxicity of 3D-printed parts. *Environ. Sci. Technol. Lett.* 3, 1–6. doi:10.1021/acs.estlett.5b00249

Palermo, G. D., Schlegel, P. N., Colombero, L. T., Zaninovic, N., Moy, F., and Rosenwaks, Z. (1996). Aggressive sperm immobilization prior to intracytoplasmic sperm injection with immature spermatozoa improves fertilization and pregnancy rates. *Hum. Reprod.* 11, 1023–1029. doi:10.1093/OXFORDJOURNALS.HUMREP.A019290

Paris-Oller, E., Soriano-Úbeda, C., Belda-Pérez, R., Sarriás-Gil, L., Lopes, J. S., Canha-Gouveia, A., et al. (2022). Reproductive fluids, added to the culture media, contribute to minimizing phenotypic differences between *in vitro*-derived and artificial insemination-derived piglets. *J. Dev. Orig. Health Dis.* 13, 593–605. doi:10.1017/S2040174421000702

Parrish, J. J., Susko-Parrish, J. L., Leibfried-Rutledge, M. L., Critser, E. S., Eyestone, W. H., and First, N. L. (1986). Bovine *in vitro* fertilization with frozen-thawed semen. *Theriogenology* 25, 591–600. doi:10.1016/0093-691X(86)90143-3

- Parrish, J. J., Susko-Parrish, J., Winer, M. A., and First, N. L. (1988). Capacitation of bovine sperm by heparin. *Biol. Reprod.* 38, 1171–1180. doi:10.1095/biolreprod38.5.1171
- Pennarossa, G., Arcuri, S., De Iorio, T., Gandolfi, F., and Brevini, T. A. L. (2021). Current advances in 3D tissue and organ reconstruction. *Int. J. Mol. Sci.* 22, 830–926. doi:10.3390/IJMS22020830
- Pérez-Aytés, A., Arcos-Machancoses, J. V., Marin Reina, P., Jimenez Busselo, M. T., and Martínez, F. (2017). Artificial reproductive techniques and epigenetic alterations: additional comments to the article by arcos-machancoses et al. *Am. J. Med. Genet. A* 173, 1983–1984. doi:10.1002/AJMG.A.38273
- Pérez-Cereales, S., Ramos-Ibeas, P., Acuna, O. S., Avilés, M., Coy, P., Rizo, D., et al. (2018). The oviduct: from sperm selection to the epigenetic landscape of the embryo. *Biol. Reprod.* 98, 262–276. doi:10.1093/BiolRe/IOX173
- Rajabi, M., Cabral, J. D., Saunderson, S., and Ali, M. A. (2023). 3D printing of chitosan oligosaccharide-polyethylene glycol diacrylate hydrogel inks for bone tissue regeneration. *J. Biomed. Mater. Res. A* 111, 1468–1481. doi:10.1002/JBM.A.37548
- Ramal-Sanchez, M., Bernabò, N., Valbonetti, L., Cimini, C., Taraschi, A., Capacchietti, G., et al. (2021). Role and modulation of TRPV1 in mammalian spermatozoa: an updated review. *Int. J. Mol. Sci.* 22, 4306. doi:10.3390/IJMS22094306
- Romar, R., Cánovas, S., Matás, C., Gadea, J., and Coy, P. (2019). Pig *in vitro* fertilization: where are we and where do we go? *Theriogenology* 137, 113–121. doi:10.1016/j.theriogenology.2019.05.045
- Rosenzweig, D. H., Carelli, E., Steffen, T., Jarzem, P., and Haglund, L. (2015). 3D-Printed ABS and PLA scaffolds for cartilage and nucleus pulposus tissue regeneration. *Int. J. Mol. Sci.* 16, 15118–15135. doi:10.3390/IJMS160715118
- Rumiński, S., Ostrowska, B., Jaroszewicz, J., Skirecki, T., Włodarski, K., Świążkowski, W., et al. (2018). Three-dimensional printed polycaprolactone-based scaffolds provide an advantageous environment for osteogenic differentiation of human adipose-derived stem cells. *J. Tissue Eng. Regen. Med.* 12, e473–e485. doi:10.1002/TERM.2310
- Santoni, S., Gugliandolo, S. G., Sponchioni, M., Moscatelli, D., and Colosimo, B. M. (2021). 3D bioprinting: current status and trends—a guide to the literature and industrial practice. *Bio-Design Manuf.* 5 (15), 14–42. doi:10.1007/S42242-021-00165-0
- Scocozza, F., Di Gravina, G. M., Bari, E., Auricchio, F., Torre, M. L., and Conti, M. (2023). Prediction of the mechanical response of a 3D (bio)printed hybrid scaffold for improving bone tissue regeneration by structural finite element analysis. *J. Mech. Behav. Biomed. Mater.* 142, 105822. doi:10.1016/J.JMBBM.2023.105822
- Serra, T., Planell, J. A., and Navarro, M. (2013). High-resolution PLA-based composite scaffolds via 3-D printing technology. *Acta Biomater.* 9, 5521–5530. doi:10.1016/J.ACTBIO.2012.10.041
- Shilov, S. Y., Rozhkova, Y. A., Markova, L. N., Tashkinov, M. A., Vindokurov, I. V., and Silberschmidt, V. V. (2022). Biocompatibility of 3D-printed PLA, PEEK and PETG: adhesion of bone marrow and peritoneal lavage cells. *Adhesion Bone Marrow Perit. Lavage Cells* 14, 3958. doi:10.3390/polym14193958
- Sivanantham, S., Saravanan, M., Sharma, N., Shrinivasan, J., and Raja, R. (2022). Morphology of inner cell mass: A better predictive biomarker of blastocyst viability. *PeerJ* 10, e13935. doi:10.7717/peerj.13935
- Sunde, A., Brison, D., Dumoulin, J., Harper, J., Lundin, K., Magli, M. C., et al. (2016). Time to take human embryo culture seriously: table i. *Hum. Reprod.* 31, 2174–2182. doi:10.1093/HUMREP/DEW157
- Talebi, A., Sadighi Gilani, M. A., Koruji, M., Ai, J., Rezaie, M. J., Navid, S., et al. (2019). Colonization of mouse spermatogonial cells in modified soft agar culture system utilizing nanofibrous scaffold: A new approach. *Galen Med. J.* 8, 1319. doi:10.31661/gmj.v8i0.1319
- Testore, D., Zoso, A., Kortaberria, G., Sangermano, M., and Chiono, V. (2022). Electroconductive photo-curable PEGDA-gelatin/PEDOT:PSS hydrogels for prospective cardiac tissue engineering application. *Front. Bioeng. Biotechnol.* 10, 897575. doi:10.3389/fbioe.2022.897575
- Vannozzi, L., Yasa, I. C., Ceylan, H., Mencias, A., Ricotti, L., and Sitti, M. (2018). Self-folded hydrogel tubes for implantable muscular tissue scaffolds. *Macromol. Biosci.* 18, 1700377. doi:10.1002/MAB.201700377
- Velioglu, Z. B., Pulat, D., Demirbakan, B., Ozcan, B., Bayrak, E., and Eriskin, C. (2019). 3D-printed poly(lactic acid) scaffolds for trabecular bone repair and regeneration: scaffold and native bone characterization. *Connect. Tissue Res.* 60, 274–282. doi:10.1080/03008207.2018.1499732
- Verpoest, W., and Tournaye, H. (2009). ICSI: hype or hazard? *Hum. Fertil. (Camb)* 9, 81–92. doi:10.1080/14647270500422158
- Waynforth, D. (2018). Effects of conception using assisted reproductive technologies on infant health and development: an evolutionary perspective and analysis using uk millennium cohort data. *Yale J. Biol. Med.* 91, 225–235.
- Wydooghe, E., Heras, S., Dewulf, J., Piepers, S., Van Den Abbeel, E., De Sutter, P., et al. (2014). Replacing serum in culture medium with albumin and insulin, transferrin and selenium is the key to successful bovine embryo development in individual culture. *Reprod. Fertil. Dev.* 26, 717–724. doi:10.1071/RD13043
- Wydooghe, E., Vandaele, L., Beek, J., Favoreel, H., Heindryckx, B., De Sutter, P., et al. (2011). Differential apoptotic staining of mammalian blastocysts based on double immunofluorescent CDX2 and active caspase-3 staining. *Anal. Biochem.* 416, 228–230. doi:10.1016/J.AB.2011.05.033
- Xiao, S., Coppeta, J. R., Rogers, H. B., Isenberg, B. C., Zhu, J., Olalekan, S. A., et al. (2017). A microfluidic culture model of the human reproductive tract and 28-day menstrual cycle. *Nat. Commun.* 8, 14584. doi:10.1038/ncomms14584
- Zhang, Q., Bei, H. P., Zhao, M., Dong, Z., and Zhao, X. (2022a). Shedding light on 3D printing: printing photo-crosslinkable constructs for tissue engineering. *Biomaterials* 286, 121566. doi:10.1016/j.biomaterials.2022.121566
- Zhang, X., Yan, Z., Guan, G., Lu, Z., Yan, S., Du, A., et al. (2022b). Polyethylene glycol diacrylate scaffold filled with cell-laden methacrylamide gelatin/alginate hydrogels used for cartilage repair. *J. Biomater. Appl.* 36, 1019–1032. doi:10.1177/08853282211044853



Article

Catechin versus MoS₂ Nanoflakes Functionalized with Catechin: Improving the Sperm Fertilizing Ability—An In Vitro Study in a Swine Model

Costanza Cimini ¹, Marina Ramal-Sanchez ² , Angela Taraschi ¹, Flavio Della Pelle ¹ , Annalisa Scroccarello ¹, Ramses Belda-Perez ¹, Luca Valbonetti ^{1,3} , Paola Lanuti ^{4,5} , Marco Marchisio ^{4,5} , Mario D'Atri ^{6,7}, Claudio Ortolani ⁶ , Stefano Papa ⁶ , Giulia Capacchietti ¹, Nicola Bernabò ^{1,3,*} , Dario Compagnone ¹ and Barbara Barboni ¹

¹ Department of Biosciences and Technology for Food, Agriculture and Environment, University of Teramo, 64100 Teramo, Italy

² Department of Innovative Technologies in Medicine and Dentistry, University of Chieti-Pescara, 66100 Chieti, Italy

³ Institute of Biochemistry and Cell Biology (CNRIBBC/EMMA/Infrafrontier/IMPC), National Research Council, 00015 Rome, Italy

⁴ Department of Medicine and Aging Science, University "G. d'Annunzio" of Chieti-Pescara, 66100 Chieti, Italy

⁵ Centre on Aging Sciences and Translational Medicine (Ce.S.I-MeT), University "G. d'Annunzio" of Chieti-Pescara, 66100 Chieti, Italy

⁶ Department of Biomolecular Sciences, University of Urbino "Carlo Bo", 61029 Urbino, Italy

⁷ Sharp Solutions Software di D'Atri Mario, Via Udine, 2, Buttrio, 33042 Udine, Italy

* Correspondence: nbernabo@unite.it



Citation: Cimini, C.; Ramal-Sanchez, M.; Taraschi, A.; Della Pelle, F.; Scroccarello, A.; Belda-Perez, R.; Valbonetti, L.; Lanuti, P.; Marchisio, M.; D'Atri, M.; et al. Catechin versus MoS₂ Nanoflakes Functionalized with Catechin: Improving the Sperm Fertilizing Ability—An In Vitro Study in a Swine Model. *Int. J. Mol. Sci.* **2023**, *24*, 4788. <https://doi.org/10.3390/ijms24054788>

Academic Editors: Giovanni Pallio and Letteria Minutoli

Received: 11 January 2023

Revised: 22 February 2023

Accepted: 22 February 2023

Published: 1 March 2023



Copyright: © 2023 by the authors. Licensee MDPI, Basel, Switzerland. This article is an open access article distributed under the terms and conditions of the Creative Commons Attribution (CC BY) license (<https://creativecommons.org/licenses/by/4.0/>).

Abstract: Nowadays, the adoption of In Vitro Fertilization (IVF) techniques is undergoing an impressive increase. In light of this, one of the most promising strategies is the novel use of non-physiological materials and naturally derived compounds for advanced sperm preparation methods. Here, sperm cells were exposed during capacitation to MoS₂/Catechin nanoflakes and catechin (CT), a flavonoid with antioxidant properties, at concentrations of 10, 1, 0.1 ppm. The results showed no significant differences in terms of sperm membrane modifications or biochemical pathways among the groups, allowing the hypothesis that MoS₂/CT nanoflakes do not induce any negative effect on the parameters evaluated related to sperm capacitation. Moreover, the addition of CT alone at a specific concentration (0.1 ppm) increased the spermatozoa fertilizing ability in an IVF assay by increasing the number of fertilized oocytes with respect to the control group. Our findings open interesting new perspectives regarding the use of catechins and new materials obtained using natural or bio compounds, which could be used to implement the current strategies for sperm capacitation.

Keywords: molybdenum disulfide; catechins; spermatozoa; sperm capacitation; in vitro fertilization

1. Introduction

In vitro fertilization (IVF) is one of the most used assisted reproductive techniques, aimed at overcoming fertility problems, either in zootechnics or for human purposes. In this process, an egg is combined with spermatozoa in vitro, after the acquisition of their fertilizing potential in a process commonly known as capacitation.

Recently, the use of non-physiological materials is gaining ground in the reproductive field as a support for the implementation of IVF techniques. For instance, previous studies demonstrated a significant improvement in the fertility outcomes when sperm cells were exposed to graphene oxide (GO) during capacitation in different animal models such as swine, bovine and mouse. This effect could probably be ascribed to the extraction of cholesterol from the sperm membrane thus inducing an intense lipid membrane remodeling [1–3].

Among non-physiological materials and naturally derived compounds, molybdenum disulfide (MoS_2) and catechin stand out as interesting candidates to characterize the effects of their exposure on reproductive function.

MoS_2 is a member of the transition metal dichalcogenides (TMDs) family, which are layered materials with a structure consisting of overlapped layers held together by Van der Waals forces. Each sheet possesses a wafer-like structure with a central hexagonal layer of metal atoms sandwiched in a double layer of chalcogen atoms [4]. MoS_2 is characterized by both a peculiar nanostructure and chemistry that has commenced to be employed in different fields, including catalysis, electrochemistry and an ever increasing use in biological/biomedical applications [5–7]. TMDs' features are strictly dependent on the nanoscale reduction strategy and despite the impressive advancements achieved during the last years, their use for biological/biomedical applications is often limited by their scarce dispersibility in water and/or the need for toxic or pollutant chemicals for their synthesis. It is noteworthy that MoS_2 is a 2D graphene-like material and, although the potential toxicity of TMDs materials has been studied in embryonated eggs [8] and on human lung carcinoma epithelial cells [9], to the best of our knowledge there are no studies evaluating the potential effects of TMDs on sperm capacitation.

On the other hand, catechin (CT) is a flavonoid characterized by a high antioxidant capacity [10], and it has previously been demonstrated that CT supplementation to sperm storage may have a beneficial effect on sperm motility [11]. Interestingly, CT has proved to be able to assist the stabilization and synthesis of various nanomaterials, remaining firmly anchored on their surface and acting as a functional and stabilizing agent [12,13]. In the nanomaterials domain, the dispersion or exfoliation route represents a challenge to modulate the affinity and dispersibility of the materials in different media, defining the final material features in terms of structure, dimension and solubility and thus conferring additional functionalities [4,14–16].

In the present study, we aimed to study the effects of nanoflakes of MoS_2 functionalized with catechins and catechins on swine spermatozoa functional parameters during capacitation. The term capacitation encompasses a necessary series of events occurring naturally in vivo and by which spermatozoa undergo a functional modification, ultimately acquiring their fertilizing ability. While in vivo, sperm cells are free to migrate through the uterus, bind to the oviductal epithelium and encounter the multiple endocrine stimuli prior to the meeting with the oocyte [17–19]. In order to improve the current strategies for sperm capacitation, different concentrations of MoS_2 /CT and CT were evaluated (10, 1, and 0.1 ppm). A multiple-step approach was adopted to evaluate the potential effects of this interaction in terms of: (a) acrosome damage; (b) membrane disorder; (c) biochemical patterns (PKA activity and tyrosine phosphorylation patterns); (d) intracellular calcium concentration; and (e) mitochondrial activity. As a functional test, finally an IVF assay was performed to assess the sperms' fertilizing ability.

2. Results and Discussion

Here, the potential effects of MoS_2 /CT and CT addition during spermatozoa capacitation were analyzed using a swine in vitro model. The swine model has acquired enormous importance for biomedical research and represents an optimal animal model for the study of human reproductive events [20–22].

2.1. Preparation and Characterization of Water-Phase Exfoliated MoS_2 /CT Nanoflakes

As reported in Figure 1, the bulk- MoS_2 sonochemical liquid phase exfoliation assisted by catechin (conducted according to the Section 3 Materials and Methods) allowed a stable colloidal dispersion of MoS_2 /CT nanoflakes to be obtained, which was then used for further experiments. As expected, in the bulk form this TMD possesses crystalline structures characterized by micrometric sides and thickness (Figure 1B); in this conformation, MoS_2 is not dispersible in water. Figure 1C,D show the SEM micrograph of the MoS_2 after exfoliation assisted by catechin (MoS_2 /CT). The CT-assisted exfoliated MoS_2 flakes resulted

in being significantly smaller when compared to the bulk MoS₂, proving a noticeable exfoliation success. In this conformation, the MoS₂/CT is a colloid, stable for more than 1 year (Figure 1C, right). In the SEM magnification of Figure 1D, the MoS₂/CT flakes obtained are visible and are characterized by nano sides. The catechin effectiveness in the exfoliation of MoS₂ was proved in our previous work [12], where the exfoliation strategy was proposed, optimized, and the nanoflakes obtained were fully characterized. An average size value of about 153 ± 2 nm was obtained via dynamic light scattering for the MoS₂/CT flakes. It is noteworthy that the same study highlighted an interesting residual antioxidant potential for MoS₂/CT, which was attributed to the MoS₂ surface modification influenced by the catechin, able to bring charges and redox-active moieties.

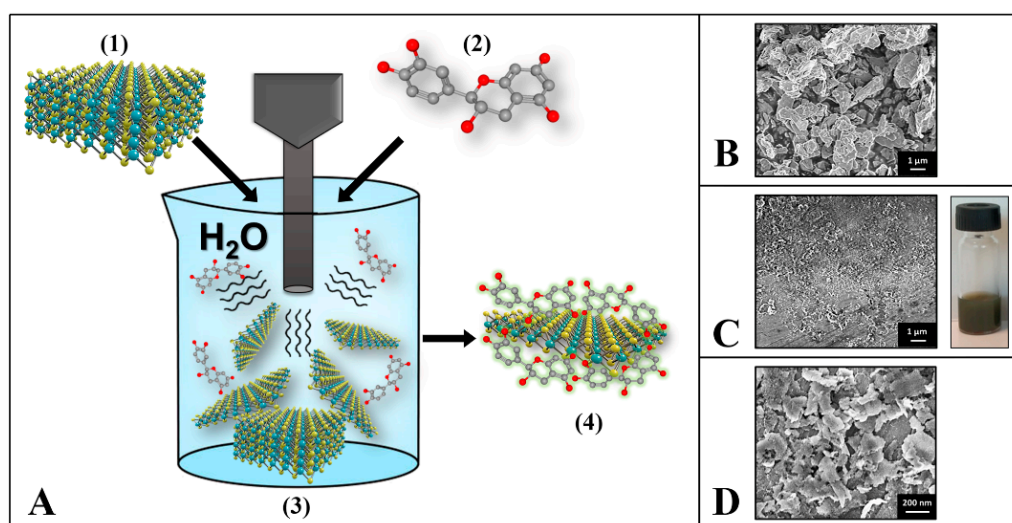


Figure 1. (A) Graphical sketch of the MoS₂ sonochemical exfoliation assisted by catechin. (1) Bulk MoS₂, (2) catechin structure, (3) sonochemical exfoliation process, (4) MoS₂/CT nanoflakes. (B) SEM micrograph of the bulk-MoS₂ (unexfoliated); (C) SEM micrograph of the exfoliated MoS₂/CT (left); picture of the MoS₂-CT colloidal water-dispersion (right). (D) SEM magnification of the MoS₂/CT nanoflakes.

Several exfoliation strategies have been proposed for layered materials. Nevertheless, liquid-phase exfoliation (LPE) has become an affordable and sustainable large-scale strategy to produce water-dispersed 2D nanomaterials. Two-dimensional nano colloids have been obtained in water using LPE by employing different surfactants, polymeric structures and different amphiphilic compounds, which are able to interact with the dispersed/exfoliated nanostructures mainly via non-covalent interactions [23–25]. Recently, our group has demonstrated how naturally-derived polyphenols can assist the graphene and group VI TMDs' exfoliation in water, acting as stabilizing agents and conferring at the same time additional features, partially preserving their antioxidant moieties [12,13].

Catechin is a flavonoid with an amphiphilic structure that is naturally present in different foods, characterized by a high antioxidant capacity and thus associated with several potential biological functions and health benefits [10]. Thanks to its amphiphilic structure, catechin can act as a stabilizing agent for nanomaterials' production and stabilization in water. Catechin has demonstrated an active role in the formation, stabilization and functionalization of metal nanoparticles, graphene, and nanocomposites. Moreover, the catechin adhesion on the formed nanomaterials apportos additional electrochemical and antimicrobial features [12,15,26,27], proving to be a useful naturally-derived functional and stabilizing agent.

The sonochemical preparation in water of the MoS₂/CT can be resumed as follow: (i) the ultrasound energy allows the layers and dimension number/size reductions of the crystalline bulk-MoS₂; (ii) the stabilization/functionalization of the formed MoS₂

nanoflakes is guaranteed by the catechins' ability to remain attached to the surface of the produce MoS₂ flakes acting as a stabilizing agent. In this case, the catechin carbon skeleton allows π - π interactions with neo-produced MoS₂ flakes, while the CT hydroxyl groups interact with water via hydrogen bonds allowing the nanoflakes to remain dispersed, ensuring also charge repulsion among flakes and avoiding layer re-stacking. The ability of the compounds containing catechol groups, to allow π - π stacking with other π systems has been already proved by Saiz-Poseu and colleagues (2019) [28] and by Silveri and colleagues (2021) [13] for graphene; on the other hand, electrochemical studies supported the hypothesis that the catechol of catechin is attached to the MoS₂ nanoflakes but has antioxidant moieties free to react [12].

The water-dispersible nature of MoS₂/CT nanoflakes allowed easy nanomaterial handling via differential centrifugation. This important feature enables (i) purifying the exfoliated nanoflakes, (ii) removing the excess supernatant, and (iii) resuspending the MoS₂/CT in the spermatozoa capacitating medium at the desired concentration. This is a challenge for TMDs exfoliated in organic solvents, which are not water dispersible. However, different exfoliation strategies in water imply the use of highly toxic or pollutant chemicals [29]. Unlike the extensively studied graphene oxide, which is naturally dispersible in water, probably the lack of biological studies on spermatozoa with TMDs is attributable to (i) the difficult manipulation of TMDs in aqueous media, (ii) the low-optimal TMDs' exfoliation (studies are often conducted on just roughly dispersed TMDs), (iii) high toxicity materials produced via conventional approaches.

2.2. MoS₂/CT and CT Supplementation Does Not Affect the Acrosome Integrity

The first step to examine the potential impact of MoS₂/CT and CT exposure on spermatozoa was the monitoring of the acrosome damage. Because spermatozoa that have lost their acrosome are unable to fertilize an egg, depending on the species, the acrosome reaction (AR) is one of the most important fertilization mechanisms [30].

Acrosome integrity was evaluated at 0 and 1.5 h after in vitro capacitation. As evidenced in Figure 2, after 1.5 h of capacitation in the presence of MoS₂/CT and CT the proportion of acrosome-reacted spermatozoa was similar among the groups, showing no significant differences ($p > 0.05$). Thus, it is possible to affirm that MoS₂/CT and CT at the different concentrations tested have no statistically significant effect on acrosome integrity.

2.3. MoS₂/CT and CT Supplementation Does Not Modify the Intracellular Calcium Concentration, Membrane Fluidity and Mitochondrial Activity

Flow cytometry analysis was performed to evaluate the effects of MoS₂/CT and CT supplementations in three different events of sperm capacitation after 1.5 h of incubation in capacitating conditions: the increase in the intracellular calcium concentration; the sperm membrane disorder (thus revealing the potential membrane fluidity increase); and the mitochondrial activity. The results showed no differences in terms of intracellular calcium concentration, membrane disorder and mitochondrial activity, as graphically illustrated in Figures 3–5, respectively. Supplementary Materials S1 shows the CTRL group after 0, 1.5 of capacitation.

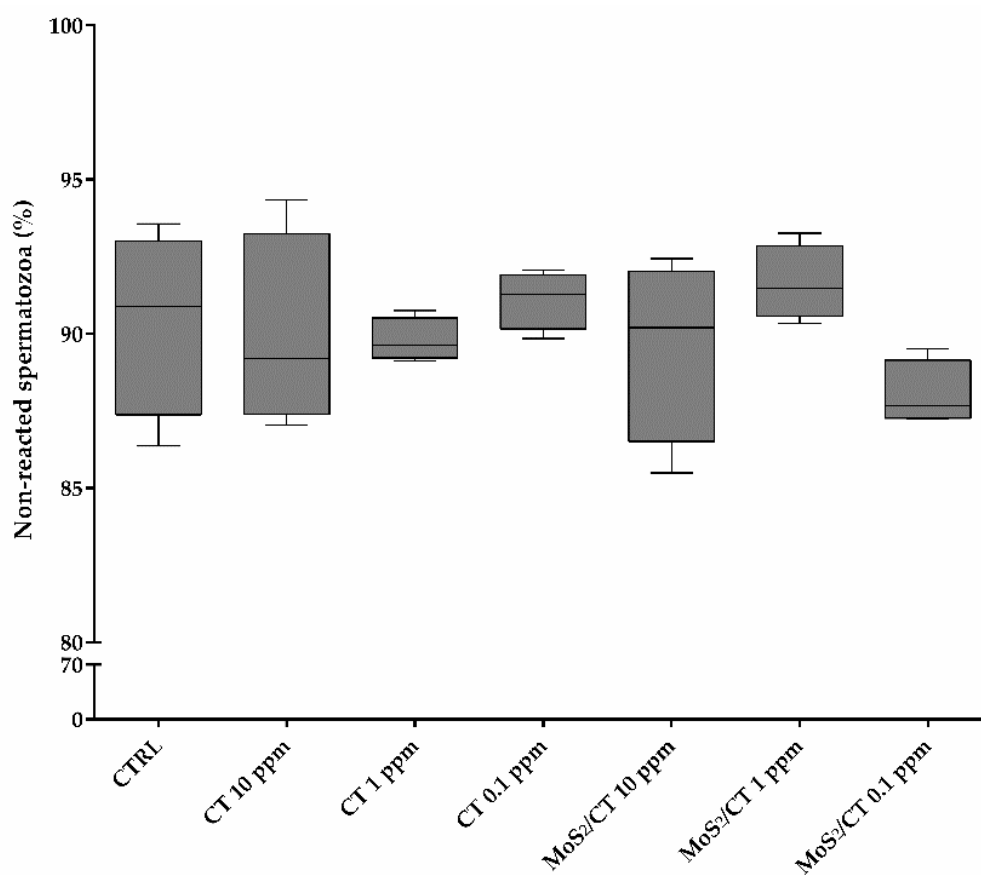


Figure 2. Acrosome integrity. The graph shows the percentage of non-reacted spermatozoa after 1.5 h of capacitation for the different experimental groups: CTRL, CT 10 ppm, CT 1 ppm, CT 0.1, MoS₂/CT 10 ppm, MoS₂/CT 1 ppm and MoS₂/CT 0.1 ppm. A normal acrosome damage rate was obtained, similar to the control (CTRL) group ($p > 0.05$). Three independent technical and biological (from different boars) replicates were performed.

Capacitation status has been associated with changes in the sperm machinery at membrane and cytosolic levels. For instance, the intracellular calcium ($[Ca^{2+}]_i$) homeostasis is a key element in sperm capacitation and acrosome reaction [31]. In resting conditions, the calcium clearance is tightly regulated by Ca^{2+} pumps (Ca^{2+} -ATPases), Na^+/Ca^{2+} -exchangers, and Ca^{2+} -channels in the sperm plasma membrane and in intracellular organelles, including the acrosome, the redundant-nuclear-envelope (RNE) and the mitochondria [32]. A key role is attributed to the Catsper channels, which are directly involved in sperm capacitation producing an influx of Ca^{2+} as a consequence of their stimulation [33,34]. During capacitation, the $[Ca^{2+}]_i$ rises and acts like a second messenger converting extracellular stimuli into a chemical response involving several molecular systems, such as, protein kinase C (PKC), protein kinase A (PKA), actin, and many others [35]. At the same time, one of most relevant events of AR is the very fast surge of $[Ca^{2+}]_i$, following the spermatozoa's interaction with the oocyte [35]. Thus, Ca^{2+} is not only a homeostatic factor and a second messenger in spermatozoa, but it also controls and modulates the crucial physiological function in a sperm's life, as also happens in excitable cells such as neurons, myocardiocytes, and muscular cells.

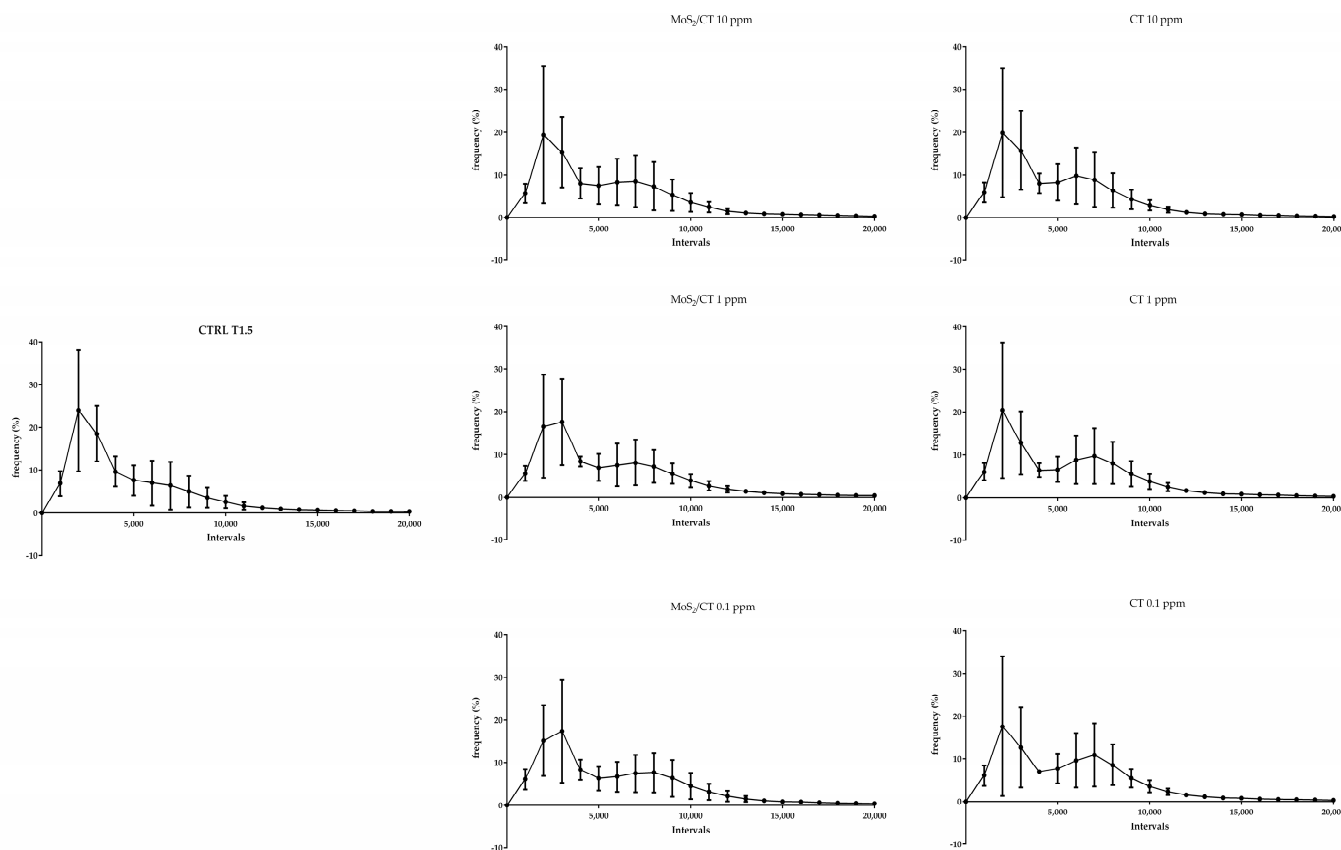


Figure 3. Flow cytometry analysis of intracellular calcium concentration. The graphs show the frequency of spermatozoa emitting a specific fluorescence intensity, which was subdivided into intervals ranging from 0 to 20,000 a.u. Capacitation was performed up to 1.5 h. Fluo 4-AM was used in combination with PI. Three independent technical and biological experiments were performed ($n = 3$).

During sperm capacitation, the membrane physicochemical characteristics change, which is an important aspect to consider since the sperm cytosol is virtually absent, thus implying a direct contact of the sperm plasma membrane with underlying structures [36]. The sperm head plasma membrane (PM) presents a different composition between the inner and outer leaflets and this asymmetry is established and maintained by several translocating enzymes [36,37]. During capacitation, the phospholipid asymmetry is reduced and the phospholipids move inward and outward according to their concentration gradient [38]. The lipid remodeling allows the removal of cholesterol from extracellular protein, which determines the increase in the ability of the sperm plasma membrane (PM) and the outer acrosome membrane (OAM) to fuse (fusogenicity), a prerequisite for the acrosome reaction [39].

Mitochondrial activity is required for several sperm functions [40]. In addition to contributing to generate ATP, mitochondria act as a hub between the generation of reactive oxygen species (ROS) and the activation of apoptosis-related pathways [41]. The result of the capacitation process is the acquisition of fertilizing ability or activating pro-apoptotic pathways.

Thus, the findings obtained showed no differences in terms of mitochondrial activity, membrane disorder and intracellular calcium concentration, implying that MoS₂/CT and CT do not exert any effect in these events of sperm capacitation *in vitro*.

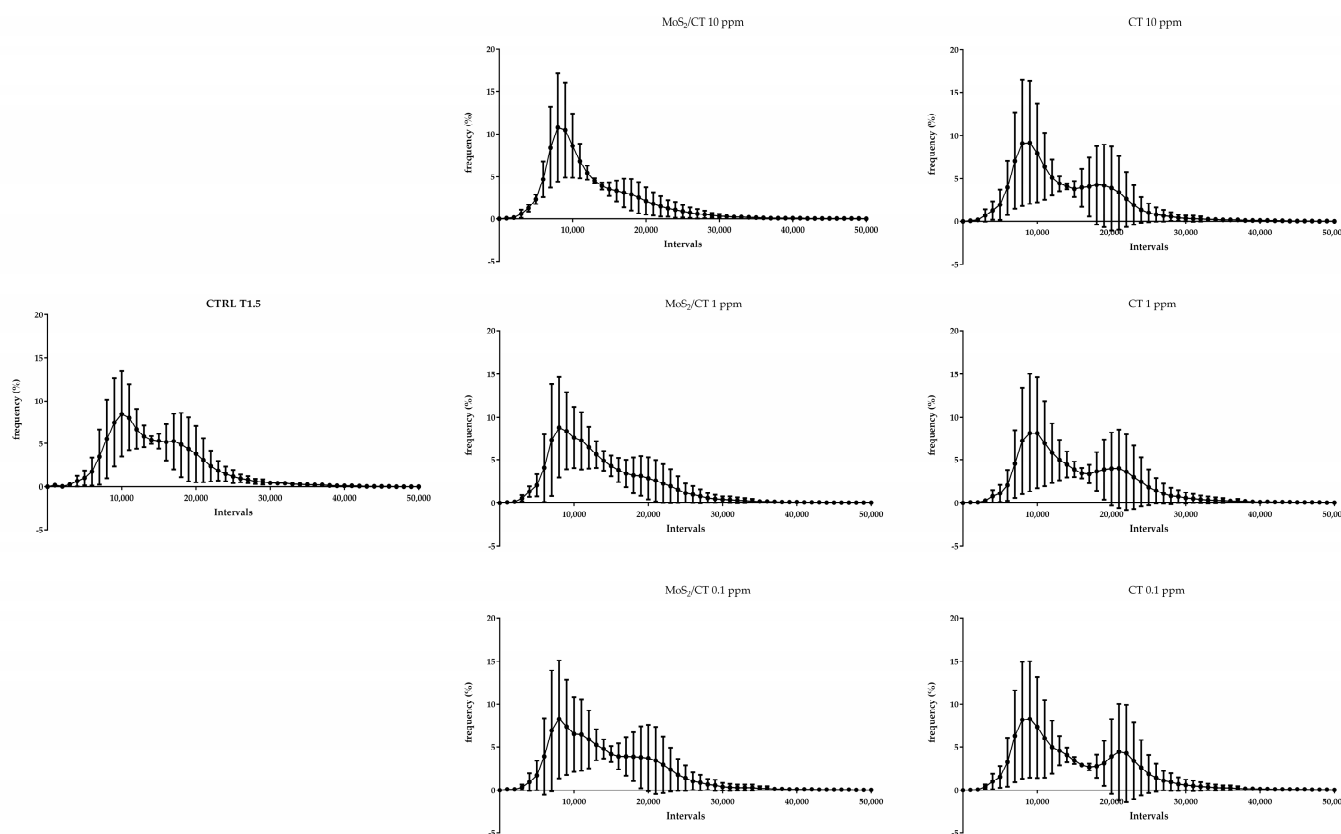


Figure 4. Flow cytometry analysis of membrane disorder and fluidity. The graphs show the frequency of spermatozoa emitting a specific fluorescence intensity, which was subdivided into intervals ranging from 0 to 50,000 a.u. Capacitation was performed up to 1.5 h. DiIC-12 was used as a probe. Three independent technical and biological experiments were performed ($n = 3$).

2.4. MoS_2/CT and CT Supplementation Does Not Influence Sperm pKa Activity and Tyrosine Phosphorylation Patterns

Flow cytometry was used to analyze the early events of capacitation that lead to PKA activation and the subsequent tyrosine phosphorylation cascade, which were then analyzed by Western blot (WB). Sperm protein soluble adenylyl cyclase (sAC) is activated during capacitation, raising the intracellular pH [42]. As a result, PKA and cAMP levels increase [43] and cAMP binds to the PKA regulatory subunits, allowing the dissociation of the tetramer and the activation of the catalytic subunit and thus initiating a cascade of intracytoplasmic signaling events [44]. Once released, the catalytic subunits continue their function phosphorylating a wide range of substrates on the Ser/Thr residues, activating a variety of protein kinases and/or inhibiting protein phosphatases to increase the phosphorylation of tyrosine residues either directly or indirectly [30,45] and contributing to reshaping the global protein phosphorylation pattern. This change occurs either in the flagellum or in the sperm head, and it appears to be mandatory for a spermatozoon to reach the ability to fertilize the oocyte [30,45]. While the results show the normal differences between non-capacitated and capacitated spermatozoa in terms of residues' phosphorylation, our results showed no significant differences among the experimental groups. The phosphorylation patterns obtained were similar for MoS_2/CT and CT (10, 1 and 0.1 ppm) with respect to the control group (Figure 6). All full-length membranes and immunoblotting images from three independent experiments were added to Supplementary Materials S2.

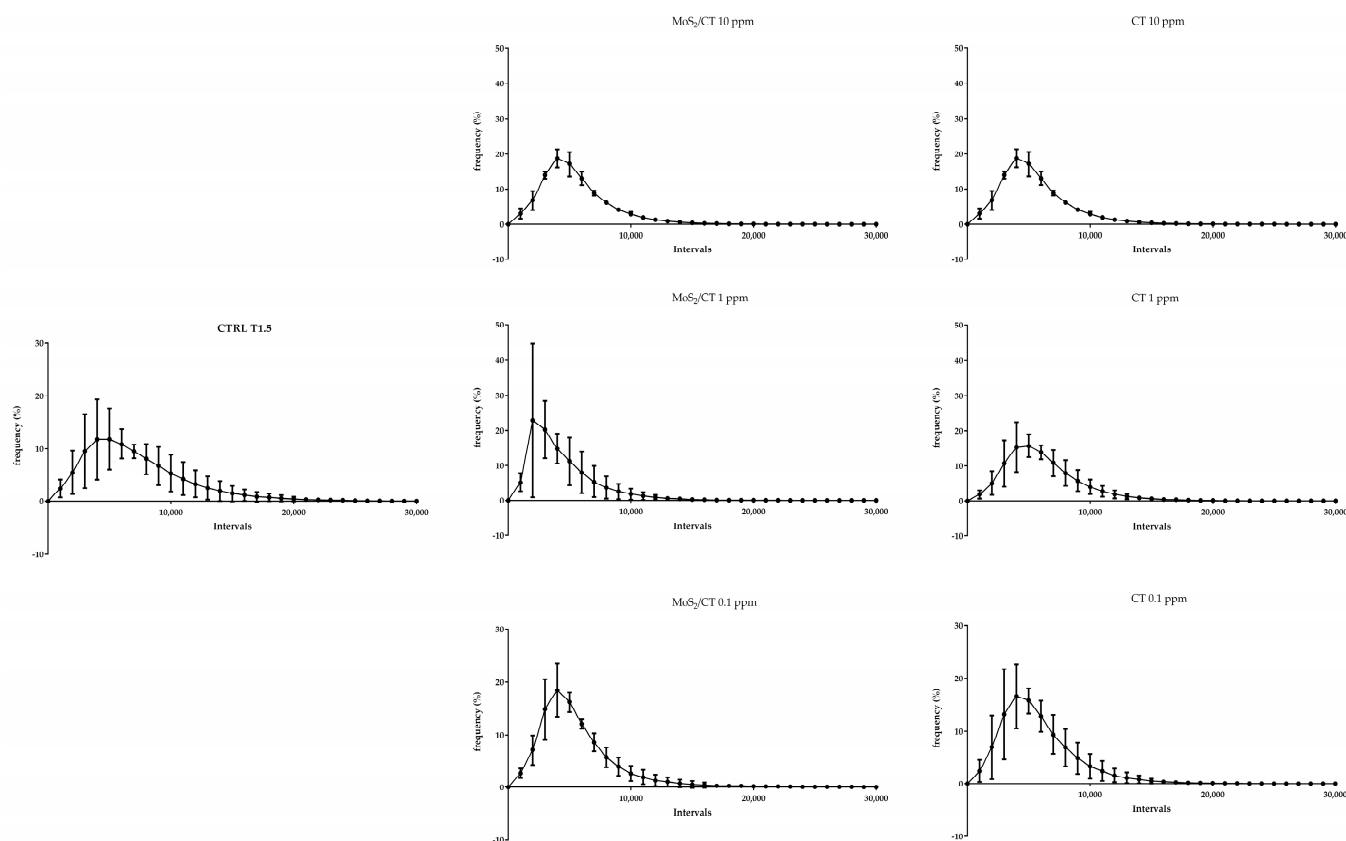


Figure 5. Flow cytometry analysis of mitochondrial activity. The graphs show the frequency of spermatozoa emitting a specific fluorescence intensity, which was subdivided into intervals ranging from 0 to 30,000 a.u. Capacitation was performed up to 1.5 h. Mitotracker Red was used in combination with a near-IR probe. Three independent technical and biological experiments were performed ($n = 3$).

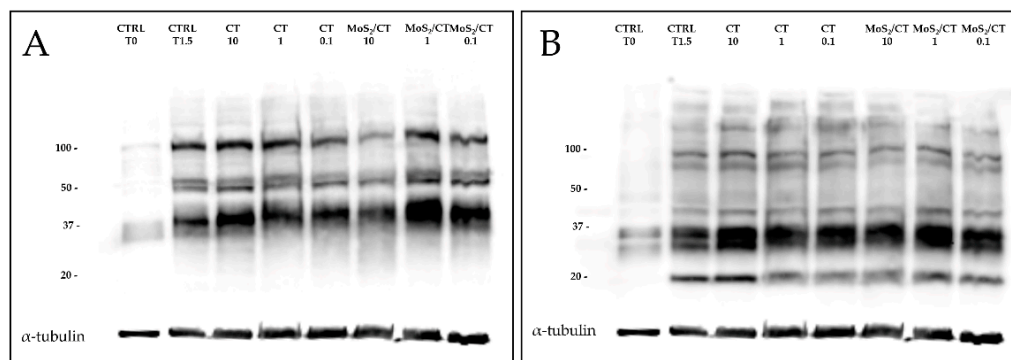


Figure 6. Western blot analysis of PKA activity and tyrosine phosphorylation patterns. The image illustrates (A) the PKA activity and (B) the tyrosine phosphorylation patterns after 1.5 h of incubation under capacitating conditions. Antibodies were incubated on the same blot after membrane stripping and re-blotting. Blots were cut prior to hybridization. α -tubulin was used as a load control. Each of the eight lanes contains 1×10^7 spermatozoa from different animals. At least three independent experiments with different animals were performed.

2.5. CT Supplementation Improves the IVF Outcomes

Finally, IVF was used as a functional test to evaluate the sperms' acquisition of the fertilizing ability after the exposure to MoS_2/CT and CT at selected concentrations. Since the analysis of the PKA activity, phosphorylation patterns, acrosome reaction induction,

mitochondrial activity, membrane fluidity and intracellular calcium concentration revealed no differences among the groups treated with different concentrations of MoS₂/CT and CT (10, 1, 0.1 ppm), only the lowest concentrations were selected to perform the IVF assay, in order to minimize any potential risk, as well as the biological material needed.

IVF assays are a valuable tool to assess the sperm fertilizing ability in boar [46,47] due to the fact that the fertilization rates, the number of polyspermic oocytes and number of spermatozoa/polyspermic oocytes are related to the capacitation status and fertility of the semen [48,49]. As observed in Figure 7, the addition of CT alone at a specific concentration (0.1 ppm) during capacitation increases the spermatozoa fertilizing ability, evidenced by the increased number of fertilized oocytes and of polyspermic oocytes with respect to the control group.

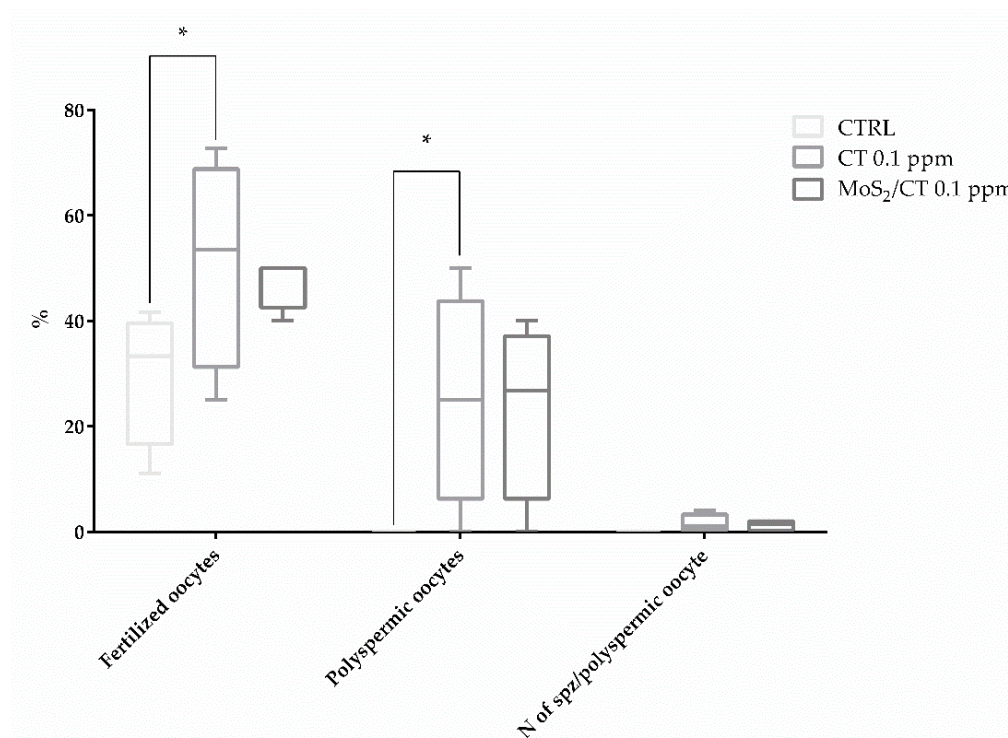


Figure 7. IVF outcomes. Three different groups were subjected to IVF assay: CTRL, CT 0.1 and MoS₂/CT 0.1 ppm. Data are expressed as percentages, showing the number of fertilized oocytes, the number of polyspermic oocytes and the number of spermatozoa per polyspermic oocyte, comparing the groups of spermatozoa capacitated in the presence of MoS₂/CT and CT (0.1 ppm) to the control group. Data were analyzed using Dunnett's test. * $p < 0.05$ versus control. Four independent experiments were performed.

Our findings support the evidence from previous studies showing that the addition of CT to the extender had a positive effect on sperm motility of caprine sperm [11].

This fact allows hypothesizing that the addition of CT might have provided an antioxidant activity, modulating the presence of reactive oxygen species (ROS) in our system. However, further experiments are needed to decipher the lipoperoxidation level and the ROS production, among others. The oxidative stress, observed by the excess of ROS, plays a key role in the life of mammalian sperm. Considering that spermatozoa are very sensitive to oxidative processes and that they are unable to transcribe and synthesize new proteins, with a cytosol virtually absent, preventing or fighting the oxidative stress remains hard to achieve [50]. This situation is aggravated due to the lipid composition of the plasma membrane, where the concentration of polyunsaturated fatty acids (PUFAs) is higher than in other cell types. PUFAs are the main target of ROS, and their oxidation culminates in the generation of cytotoxic aldehydes. Furthermore, the peroxidation of membrane

lipids leads to a loss of motility and flexibility, causing the loss of all membrane-dependent functions [50–52]. The major consequence of oxidative stress is the damage of the sperm's DNA [50,51].

Even if sperm cells are very susceptible to oxidative stress, low levels of ROS contribute to the full maturation of spermatozoa [50], which is necessary for capacitation, hyperactivation, acrosome reaction, oocyte fusion and fertilization [53,54]. Furthermore, there is a leading role in the interaction between ROS and cholesterol, since the oxidation of a part of cholesterol by ROS leads to the formation of oxysterols that facilitate the removal of cholesterol from the sperm plasma membrane to enhance the sperm membrane fluidity [55,56].

This study focused on the effect of an innovative material and a naturally derived compound on the spermatozoa fertilizing ability. Due to the results obtained, it is possible to affirm that nanoflakes of MoS₂/CT at different concentrations (10, 1, 0.1 ppm) do not induce any negative effect on the sperm parameters related to capacitation evaluated here. Moreover, CT alone at a specific concentration (0.1 ppm) acts as a helper of sperm capacitation by improving the IVF results, which could probably be explained by the balance of the ROS levels. These results open encouraging new perspectives for the improvement of Assisted Reproduction Technologies (ART), which has experienced an increase in use during the last decades, both in humans [57] and in animal farming [58]. At the same time, an improvement in these techniques could fight against the ever increasing prevalence of numerous pathologies associated with ART-generated embryos, since ARTs may epigenetically modify gene expression, influencing the long-term development of the embryo by mechanisms that should still be investigated. For instance, many reports have shown the increasing prevalence of Angelman syndrome (AS), [59,60] and the phenomenon of large offspring syndrome in farm animals [61], with a phenotypic similarity to Beckwith–Wiedemann Syndrome (BWS) in humans [61–63].

3. Materials and Methods

3.1. Chemicals

Unless otherwise stated, all the chemicals were purchased from Sigma-Aldrich (St. Louis, MO, USA). Milli-Q water was purchased from Millipore (Bedford, MA, USA).

3.2. MoS₂ Sonochemical Exfoliation in Water Assisted by Catechin

MoS₂ exfoliation assisted by catechin (CT) was conducted according to Rojas and colleagues (2022) [12] with some modifications. A total of 0.5 g of bulk MoS₂ powder (<2 µm; 99% purity) was placed in 50 mL of a 2.5 mg mL^{−1} (+)-catechin water solution (Milli-Q water) and roughly dispersed using a low-power ultrasonic bath. The dispersion was placed in a steel beaker and subjected to a sonochemical exfoliation treatment using a Branson SFX550 (550 W, 20 kHz) sonifier. The sonication probe employed was a 13 mm Ø Branson disruptor horn. Sonochemical exfoliation was conducted at 50% amplitude using a 5 h pulse program (2 s ON and 1 s OFF), maintaining the temperature below 15 °C. The obtained MoS₂/CT dispersion was thus subjected to purification and size selection via differential centrifugation. The MoS₂ not properly exfoliated was precipitated with centrifugation at 250 × g (1 h). In this case, the supernatant was recovered, and the formed pellet discarded. The MoS₂/CT size selection and removal of the exfoliation medium containing the residual catechin in solution were conducted on the supernatant of the previous treatment, achieved via a 20,000 × g centrifugation (15 min). Then, the supernatant was removed, and the sediment collected and resuspended in water. The exfoliation yield was estimated via gravimetry, and MoS₂/CT water dispersion and was stored at 4 °C in the dark. MoS₂/CT before use was further purified via a 10,000 × g centrifugation, where the supernatant was discarded, and the sediment was recovered in sterile Dulbecco-PBS to obtain a 200 mg L^{−1} MoS₂-CT working dispersion.

The pristine and exfoliated MoS₂ was characterized using a high-resolution scanning electron microscopy SIGMA (Carl Zeiss Microscopy GmbH, Munich, Germany). Solutions

and materials used for in vitro studies were sterilized before their use and handled under a sterile hood. Catechin solutions were freshly prepared before use.

3.3. Experimental Groups

For the present work, a total of seven experimental groups were analyzed. Control group without CT nor MoS₂/CT was included (CTRL). Complexes of MoS₂ functionalized with catechin (MoS₂/CT) were used at three different concentrations: MoS₂/CT 10 ppm; MoS₂/CT 1 ppm; and MoS₂/CT 0.1 ppm. These concentrations were established based on the available literature [33] and the absence of a consensus regarding the use of specific concentrations. As control, catechin alone (CT) was utilized at the same concentrations (CT 10 ppm, CT 1 ppm, CT 0.1 ppm). Finally, Figure 8 schematically illustrates the experimental design, representing the experimental groups and the analyses performed.

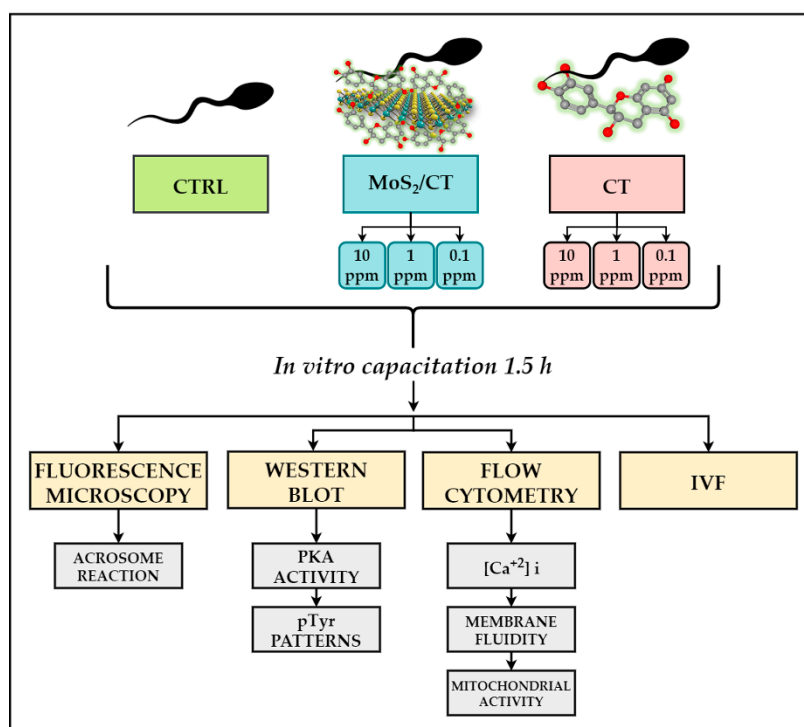


Figure 8. Experimental design. Spermatozoa were exposed to MoS₂ functionalized with catechin at different concentrations (10, 1, 0.1 ppm), catechin alone at the same concentrations (10, 1, 0.1 ppm) for 1.5 h in capacitation medium, a control group (CTRL) was maintained. Different sperm capacitation events were analyzed: acrosome damage, membrane fluidity, mitochondrial activity, intracellular calcium concentration, biochemical phosphorylation patterns and IVF assays.

3.4. Spermatozoa Preparation and Incubation

Spermatozoa were collected and washed following an already standardized protocol [64]. Briefly, sperm samples purchased from a specialized company (Società Agricola Geneetic S.r.l, Castellazzo, Italy) were incubated in a TCM199 medium supplemented with 13.9 mM glucose, 1.25 mM sodium pyruvate, 2.25 mM calcium lactate and 1 mM caffeine used to induce capacitation in vitro. MoS₂/CT and CT dispersions at different concentrations were added to the capacitating medium to obtain the sample groups: CT 10 ppm, CT 1 ppm, CT 0.1 ppm, MoS₂/CT 10 ppm, MoS₂/CT 1 ppm, and MoS₂/CT 0.1 ppm. Sperm cells were incubated at a final concentration of 1×10^7 cells/mL for 0 or 1.5 h at 38.5 °C in 5% CO₂ and a humidified atmosphere (Heraeus, Hera Cell). Sperm motility was visually estimated before the capacitation by light microscopy before each experiment and only samples with sperm motility > 90% were considered for further analyses.

3.5. Monitoring MoS₂/CT Toxicity on Acrosome Integrity

Acrosome integrity was monitored by using a two stain technique with Hoechst 33,258 and FITC-PSA able to identify alive unreacted and reacted spermatozoa [65]. At least 100 cells were assessed by fluorescence microscopy in three independent experiments performed at different capacitation times (T0, T1.5), in the following groups: CTRL, MoS₂/CT, and CT treated spermatozoa (10, 1, 0.1 ppm).

3.6. Flow Cytometry Analysis of Intracellular Calcium Concentration, Membrane Fluidity and Mitochondrial Activity

Flow cytometry analysis was performed to evaluate the differences between the different sperm groups in terms of: (a) intracellular calcium concentration; (b) sperm membrane lipid disorder; and (c) sperm mitochondrial activity. For each experiment and each condition (MoS₂/CT 10 ppm; MoS₂/CT 1 ppm; and MoS₂/CT 0.1 ppm; CT 10 ppm; CT 1 ppm; CT 0.1 ppm; CTRL), three different biological and technical experiments were performed at 0 and 1.5 h of capacitation.

After capacitation, sperm cells were placed in a flow cytometry tube and incubated at RT while gently shaking with: (a) 1 μ M Fluo 4-AM (15 min) to study the intracellular calcium concentration; (b) 1 μ M DiIc-12 (15 min) to measure the membrane lipid disorder; and (c) 1 μ M Mitotracker Red (30 min) to check the activation of the mitochondria. To distinguish dead and live spermatozoa, two different stains were used when possible, depending on the fluorescence emission spectra of the different probes previously stated: 1 μ M PI (5 min) was used in combination with Fluo 4-AM, while 1 μ L LIVE/DEAD™ Fixable Near-IR Dead Cell Stain Kit (Catalog number: L10119, ThermoFisher Scientific, Waltham, MA, USA) (10 min) was combined with Mitotracker Red. After the incubation time, 100,000 events/sample were acquired by flow cytometry (FACSCanto, BD Biosciences, Franklin Lakes, NJ, USA—three laser, eight color configuration). Each reagent was titrated (8-point titration) under assay conditions; dilutions were established based on achieving the highest signal (mean fluorescence intensity, MFI) for the positive population and the lowest signal for the negative population, representing the optimal signal-to-noise ratio, and stain indexes were calculated. Instrument performances, data reproducibility, and fluorescence calibrations were sustained and checked by the Cytometer Setup and Tracking Beads (BD Biosciences). To evaluate non-specific fluorescence, the Fluorescence Minus One (FMO) control was used. Compensation was assessed using CompBeads and FACSuite FC Beads (BD Biosciences) and single stained fluorescent samples. Data were analyzed first using FACSuite v 1.0.5 (BD Biosciences) software, and then FcsWizard Software was used to convert .fcs data to .csv format in order to perform an exhaustive analysis of the fluorescence emitted from every single spermatozoon for the various fluorescence probes [66]. To that, the columns “FCS”, “SSC”, “Fluo-4AM”, “PI”, “DiIc12”, “Mito” and “NIR” with the data from the 100,000 events acquired, were selected and filtered following these criteria: forward scatter (FCS) between 35,000 and 135,000 arbitrary units (a.u); side scatter (SSC) between 20,000 and 145,000 a.u; Fluo 3-AM, M540 and Mitotracker Red >0 a.u; PI between 0 and 30,000 a.u; and near infrared between 0 and 20,000 a.u. Then, data were treated and subdivided in intervals of fluorescence intensity as follow: 41 intervals for intracellular calcium (from 0 to 20,000 a.u, 500 a.u range); 101 intervals for membrane disorder (from 0 to 50,000 AU, 500 a.u range); 61 intervals for mitochondrial activity (from 0 to 30,000 a.u, 500 a.u range). At least 98% of the data fitted within this range.

3.7. Evaluation of Sperm PKA Activity and Tyrosine Phosphorylation Patterns (pTyr) by Western Blot

To evaluate protein kinase A (PKA) activity and protein tyrosine phosphorylation pattern (pTyr), at 1.5 h of capacitation, sperm cells were diluted in a sample buffer 5 \times (5 mM DDT, 2% SDS, 1 M Tris, 10% Glycerol and 0.1% Bromophenol blue), heated (100 °C for 5 min) and centrifuged (15,000 \times g for 10 min at 4 °C). Proteins were migrated on an SDS-PAGE 4–15% gradient gel (Mini-PROTEAN® TGX™ Precast Protein Gels, BioRad, Hercules, CA,

USA) and blotted on a nitrocellulose membrane using the Trans-Blot[®] Turbo[™] Transfer System (BioRad, Steenvoorde, France). The membranes were stained with Ponceau S solution and scanned, then membranes were blocked for 1 h in 5% (*w/v*) milk powder diluted in TBS-T and incubated with anti-phospho-pKa antibody (Phospho-pKa Substrate (RRXS*/T*), dilution 1:5000, Rabbit mAb, Cell Signaling, Leiden, The Netherlands) in 5% (*w/v*) BSA (*w/v*) in TBS-T (gently shaking, 4 °C, overnight). After washing, membranes were incubated with secondary antibody anti-rabbit HRP (1:10,000, Santa Cruz Technology, Dallas, TX, USA) for 1 h. Peroxidase was revealed using the SuperSignal[™] West Pico PLUS Chemiluminescent Substrate (ThermoFisher, Waltham, MA, USA) and the images were digitally captured using an Azure C300 (Chemiluminescent Western Blot Imaging System, Azure Biosystems, Dublin, CA, USA). Tyrosine phosphorylation was assessed on the same membranes by stripping the previous antibodies with Restore[™] Western Blot Stripping Buffer (ThermoFisher). After washing, membranes were blocked in 10% (*w/v*) bovine gelatin (*w/v*) in TBS-T for 1 h and incubated with anti-phosphotyrosine antibody (Clone 4G10, dilution 1:10,000, Mouse mAb, Merck Millipore, Burlington, MA, USA) in PBS-T for 1.5 h. After washing, membranes were finally incubated with the secondary anti-Mouse HRP (1:10,000, Santa Cruz Technology) antibody for 1 h and revealed as described previously in this section. At least three biological replicates were performed for each antibody and experimental group.

3.8. In Vitro Fertilization Assay

To study the potential effects of MoS₂/CT and CT on spermatozoa fertilizing ability, an in vitro fertilization (IVF) assay was carried out using an already validated protocol [65]. Ovaries from pre-pubertal gilts were collected at a local slaughterhouse and transported to the laboratory within 1 h at 25 °C. After washing, cumulus–oocyte complexes (COCs) were collected by aspirating the follicles that met the requirements (4–5 mm of diameter, translucent appearance, good vascularization and compactness of their granulosa layer and cumulus mass). Maturation was achieved in vitro by culturing the COCs in four-well dishes containing 500 µl of α -MEM medium supplemented with 10% FBS, 1% penicillin/streptomycin, 1% Ultraglutamine, 5 UI/mL hCG and 5 UI/mL PMSG for 44 h at 38.5 °C in a humidified atmosphere with 5% CO₂ (Heraeus, Hera Cell, Hanau, Germany).

Once matured, oocytes were denuded in Dulbecco-PBS with hyaluronidase on a warmed stage at 38.5 °C under a stereomicroscope. Only oocytes presenting the first polar body (MII stage) under the stereomicroscope were used for the IVF assay. Matured oocytes and capacitated sperm cells (1×10^6 cells/mL) from the selected groups (CTRL, CT 0.1 ppm and MoS₂/CT 0.1 ppm) were co-incubated in a fertilization medium (capacitation medium supplemented with 10% FBS). After 3 h of co-incubation, oocytes were transferred to a fresh medium and maintained in culture for at least 12 h. The penetration rate was evaluated after staining with Hoechst 33,342 and assessed under the fluorescence microscope. The IVF outcomes are expressed as fertilization rate (% of penetrated oocytes), incidence of polyspermy (% of polyspermic oocytes) and number of penetrating spermatozoa/polyspermic oocyte according to already published and valuable works [47,65]. A total of four independent experiments were performed, reaching a total number of 104 oocytes (number of fertilized oocytes per group: CTRL, 10 fertilized of 33 total oocytes; CT 0.1 ppm 18 fertilized of 34 total oocytes; MoS₂/CT 0.1 ppm 18 fertilized of 37 total oocytes).

3.9. Statistical Analysis

For statistical analysis, GraphPad Prism 6 Software (La Jolla, CA, USA) was used. Data were checked for normal distribution with a D'Agostino and Pearson normality test prior to performing the comparison with parametric or non-parametric tests, as required. In all cases, the differences among groups were considered statistically significant when $p < 0.05$. To normalize the western blot data, Ponceau red staining was used, following a validated protocol [67]. Briefly, the whole lanes were quantified by densitometry and bands were afterwards quantified using ImageQuantTL (GE Healthcare LifeSciences, Barrington,

IL, USA). To assess the effect of different treatments on IVF, four independent technical and biological experiments were carried out. An a priori power analysis was performed to establish the number of oocytes with G*Power 3.1.9.7 software, obtaining a final power of our analysis $\geq 95\%$.

4. Conclusions

In conclusion, our study demonstrates that the incubation of spermatozoa in the presence of catechins (0.1 ppm) enhances their fertilizing ability and the incubation with nanoflakes of MoS₂/CT at different concentrations do not induce any negative effect on the sperm parameters related to capacitation. However, further experiments are needed to decipher the exact mechanism by which catechins are able to increase the sperm fertilizing ability and to explore their antioxidant potential on spermatozoa.

The findings open interesting perspectives regarding the use of catechins and new materials obtained using natural or bio compounds, which could be used to implement the current strategies for sperm capacitation.

Supplementary Materials: The following supporting information can be downloaded at: <https://www.mdpi.com/article/10.3390/ijms24054788/s1>.

Author Contributions: N.B. and D.C. conceptualized the study; A.S., F.D.P., C.C., M.R.-S. and A.T. designed the experiments; A.S. and F.D.P. prepared and characterized the molybdenum disulfide and catechins solutions; C.C., M.R.-S. and A.T. performed western blot experiments; C.C., A.T., G.C. and R.B.-P. realized IVF experiments; P.L., M.M. and M.R.-S. performed the flow cytometry experiments; P.L., M.R.-S. and M.D. analyzed the flow cytometry data; M.D., C.O. and S.P. developed the FacsWizard Software L.V. realized all figures; C.C., M.R.-S. and N.B. analyzed the data and prepared the original draft; all authors contributed to the analysis, writing and editing of the manuscript; D.C., B.B. and N.B. supervised and funded the research. All authors have read and agreed to the published version of the manuscript.

Funding: This research received no external funding.

Institutional Review Board Statement: Not applicable.

Informed Consent Statement: Not applicable.

Data Availability Statement: The original contributions presented in the study are included in the article/Supplementary Materials, further inquiries can be directed to the corresponding author.

Acknowledgments: F.D.P. and D.C. acknowledge the Ministry of Education, University and Research (MIUR) and the European Social Fund (ESF) for the PON R&I 2014–2020 program, action 1.2, and AIM: Attraction and International Mobility (AIM1894039-3).

Conflicts of Interest: The authors declare no conflict of interest.

References

1. Bernabò, N.; Fontana, A.; Sanchez, M.R.; Valbonetti, L.; Capacchietti, G.; Zappacosta, R.; Greco, L.; Marchisio, M.; Lanuti, P.; Ercolino, E.; et al. Graphene oxide affects in vitro fertilization outcome by interacting with sperm membrane in an animal model. *Carbon* **2018**, *129*, 428–437. [CrossRef]
2. Bernabò, N.; Valbonetti, L.; Raspa, M.; Fontana, A.; Palestini, P.; Botto, L.M.; Paoletti, R.; Fray, M.; Allen, S.; Machado-Simoes, J.S.; et al. Graphene Oxide Improves In Vitro Fertilization in Mice with no Impact on Embryo Development and Preserves the Membrane Microdomains Architecture. *Front. Bioeng. Biotechnol.* **2020**, *8*, 629. [CrossRef]
3. Ramal-Sanchez, M.; Valbonetti, L.; Tsikis, G.; Dubuisson, F.; Blache, M.-C.; Labas, V.; Druart, X.; Fontana, A.; Mermillod, P.; Barboni, B.; et al. Graphene oxide: A glimmer of hope for Assisted Reproductive Technology. *Carbon* **2019**, *150*, 518–530. [CrossRef]
4. Rojas, D.; Della Pelle, F.; Del Carlo, M.; Compagnone, D.; Escarpa, A. Group VI transition metal dichalcogenides as antifouling transducers for electrochemical oxidation of catechol-containing structures. *Electrochem. Commun.* **2020**, *115*, 106718. [CrossRef]
5. Zhou, X.; Sun, H.; Bai, X. Two-Dimensional Transition Metal Dichalcogenides: Synthesis, Biomedical Applications and Biosafety Evaluation. *Front. Bioeng. Biotechnol.* **2020**, *8*, 236. [CrossRef]

6. Della Pelle, F.; Rojas, D.; Silveri, F.; Ferraro, G.; Fratini, E.; Scroccarello, A.; Escarpa, A.; Compagnone, D. Class-selective voltammetric determination of hydroxycinnamic acids structural analogs using a WS₂/catechin-capped AuNPs/carbon black-based nanocomposite sensor. *Mikrochim. Acta* **2020**, *187*, 296. [\[CrossRef\]](#)
7. Agarwal, V.; Chatterjee, K. Recent advances in the field of transition metal dichalcogenides for biomedical applications. *Nanoscale* **2018**, *10*, 16365–16397. [\[CrossRef\]](#)
8. Scalisi, E.M.; Salvaggio, A.; Antoci, F.; Messina, A.; Pecoraro, R.; Cantarella, M.; Gorrasi, G.; Impellizzeri, G.; Brundo, M.V. Toxicity assessment of two-dimensional nanomaterials molybdenum disulfide in *Gallus gallus domesticus*. *Ecotoxicol. Environ. Saf.* **2020**, *200*, 110772. [\[CrossRef\]](#)
9. Teo, W.Z.; Chng, E.L.K.; Sofer, Z.; Pumera, M. Cytotoxicity of exfoliated transition-metal dichalcogenides (MoS₂, WS₂, and WSe₂) is lower than that of graphene and its analogues. *Chem.-A Eur. J.* **2014**, *20*, 9627–9632. [\[CrossRef\]](#)
10. Di Mattia, C.D.; Sacchetti, G.; Mastrocola, D.; Serafini, M. From Cocoa to Chocolate: The Impact of Processing on In Vitro Antioxidant Activity and the Effects of Chocolate on Antioxidant Markers In Vivo. *Front. Immunol.* **2017**, *8*, 1207. [\[CrossRef\]](#)
11. Purdy, P.H.; Ericsson, S.A.; Dodson, R.E.; Sternes, K.L.; Garner, D.L. Effects of the flavonoids, silibinin and catechin, on the motility of extended cooled caprine sperm. *Small Rumin. Res.* **2004**, *55*, 239–243. [\[CrossRef\]](#)
12. Rojas, D.; Della Pelle, F.; Silveri, F.; Ferraro, G.; Fratini, E.; Compagnone, D. Phenolic compounds as redox-active exfoliation agents for group VI transition metal dichalcogenides. *Mater. Today Chem.* **2022**, *26*, 101122. [\[CrossRef\]](#)
13. Silveri, F.; Della Pelle, F.; Rojas, D.; Bukhari, Q.U.A.; Ferraro, G.; Fratini, E.; Compagnone, D. (+)-Catechin-assisted graphene production by sonochemical exfoliation in water. A new redox-active nanomaterial for electromediated sensing. *Mikrochim. Acta* **2021**, *188*, 369. [\[CrossRef\]](#)
14. Nguyen, E.P.; Daeneke, T.; Zhuiykov, S.; Kalantar-Zadeh, K. Liquid Exfoliation of Layered Transition Metal Dichalcogenides for Biological Applications. *Curr. Protoc. Chem. Biol.* **2016**, *8*, 97–108. [\[CrossRef\]](#)
15. Della Pelle, F.; Blandón-Naranjo, L.; Alzate, M.; Del Carlo, M.; Compagnone, D. Cocoa powder and catechins as natural mediators to modify carbon-black based screen-printed electrodes. Application to free and total glutathione detection in blood. *Talanta* **2020**, *207*, 120349. [\[CrossRef\]](#)
16. Scroccarello, A.; Della Pelle, F.; Ferraro, G.; Fratini, E.; Tempera, F.; Dainese, E.; Compagnone, D. Plasmonic active film integrating gold/silver nanostructures for H₂O₂ readout. *Talanta* **2021**, *222*, 121682. [\[CrossRef\]](#)
17. Cimini, C.; Moussa, F.; Taraschi, A.; Ramal-Sanchez, M.; Colosimo, A.; Capacchietti, G.; Mokh, S.; Valbonetti, L.; Tagaram, I.; Bernabò, N.; et al. Pre-Treatment of Swine Oviductal Epithelial Cells with Progesterone Increases the Sperm Fertilizing Ability in an IVF Model. *Animal* **2022**, *12*, 1191. [\[CrossRef\]](#)
18. Ramal-Sanchez, M.; Bernabo, N.; Tsikis, G.; Blache, M.C.; Labas, V.; Druart, X.; Mermillod, P.; Saint-Dizier, M. Progesterone induces sperm release from oviductal epithelial cells by modifying sperm proteomics, lipidomics and membrane fluidity. *Mol. Cell. Endocrinol.* **2020**, *504*, 110723. [\[CrossRef\]](#)
19. Romero-Aguirregomez, J.; Cronin, S.; Donnellan, E.; Fair, S. Progesterone induces the release of bull spermatozoa from oviductal epithelial cells. *Reprod. Fertil. Dev.* **2019**, *31*, 1463–1472. [\[CrossRef\]](#)
20. Santos, R.R.; Schoevers, E.J.; Roelen, B.A. Usefulness of bovine and porcine IVM/IVF models for reproductive toxicology. *Reprod. Biol. Endocrinol.* **2014**, *12*, 117. [\[CrossRef\]](#)
21. Swindle, M.M.; Makin, A.; Herron, A.J.; Clubb, F.J.; Frazier, K.S. Swine as Models in Biomedical Research and Toxicology Testing. *Vet. Pathol.* **2012**, *49*, 344–356. [\[CrossRef\]](#)
22. Walters, E.M.; Prather, R.S. Advancing swine models for human health and diseases. *Mo. Med.* **2013**, *110*, 212–215.
23. Grayfer, E.D.; Kozlova, M.N.; Fedorov, V.E. Colloidal 2D nanosheets of MoS₂ and other transition metal dichalcogenides through liquid-phase exfoliation. *Adv. Colloid Interface Sci.* **2017**, *245*, 40–61. [\[CrossRef\]](#)
24. Backes, C.; Higgins, T.M.; Kelly, A.; Boland, C.; Harvey, A.; Hanlon, D.; Coleman, J.N. Guidelines for exfoliation, characterization and processing of layered materials produced by liquid exfoliation. *Chem. Mater.* **2017**, *29*, 243–255. [\[CrossRef\]](#)
25. Bukhari, Q.U.A.; Silveri, F.; Della Pelle, F.; Scroccarello, A.; Zappi, D.; Cozzoni, E.; Compagnone, D. Water-Phase Exfoliated Biochar Nanofibers from Eucalyptus Scraps for Electrode Modification and Conductive Film Fabrication. *ACS Sustain. Chem. Eng.* **2021**, *9*, 13988–13998. [\[CrossRef\]](#)
26. Scroccarello, A.; Molina-Hernández, B.; Della Pelle, F.; Ciantetta, J.; Ferraro, G.; Fratini, E.; Valbonetti, L.; Chaves Copez, C.; Compagnone, D. Effect of phenolic compounds-capped AgNPs on growth inhibition of *Aspergillus niger*. *Colloids Surf. B. Biointerfaces* **2021**, *199*, 111533. [\[CrossRef\]](#)
27. Molina-Hernández, J.B.; Scroccarello, A.; Della Pelle, F.; De Flaviis, R.; Compagnone, D.; Del Carlo, M.; Paparella, A.; Chaves López, C. Synergistic antifungal activity of catechin and silver nanoparticles on *Aspergillus niger* isolated from coffee seeds. *LWT* **2022**, *169*, 113990. [\[CrossRef\]](#)
28. Saiz-Poseu, J.; Mancebo-Aracil, J.; Nador, F.; Busqué, F.; Ruiz-Molina, D. The Chemistry behind Catechol-Based Adhesion. *Angew. Chem. Int. Ed.* **2019**, *58*, 696–714. [\[CrossRef\]](#)
29. Samadi, M.; Sarikhani, N.; Zirak, M.; Zhang, H.; Zhang, H.L.; Moshfegh, A.Z. Group 6 transition metal dichalcogenide nanomaterials: Synthesis, applications and future perspectives. *Nanoscale Horiz.* **2018**, *3*, 90–204. [\[CrossRef\]](#)
30. Ickowicz, D.; Finkelstein, M.; Breitbart, H. Mechanism of sperm capacitation and the acrosome reaction: Role of protein kinases. *Asian J. Androl.* **2012**, *14*, 816–821. [\[CrossRef\]](#)

31. Bernabò, N.; Mattioli, M.; Barboni, B. The spermatozoa caught in the net: The biological networks to study the male gametes post-ejaculatory life. *BMC Syst. Biol.* **2010**, *4*, 87. [\[CrossRef\]](#)
32. Finkelstein, M.; Etkovitz, N.; Breitbart, H. Ca^{2+} signaling in mammalian spermatozoa. *Mol. Cell. Endocrinol.* **2020**, *516*, 110953. [\[CrossRef\]](#)
33. Tvrdá, E.; Benko, F.; Slanina, T.; du Plessis, S.S. The role of selected natural biomolecules in sperm production and functionality. *Molecules* **2021**, *26*, 5196. [\[CrossRef\]](#)
34. Ded, L.; Hwang, J.Y.; Miki, K.; Shi, H.F.; Chung, J.J. 3D in situ imaging of female reproductive tract reveals molecular signatures of fertilizing spermatozoa in mice. *eLife* **2020**, *9*, e62043. [\[CrossRef\]](#)
35. Bernabò, N.; Berardinelli, P.; Mauro, A.; Russo, V.; Lucidi, P.; Mattioli, M.; Barboni, B. The role of actin in capacitation-related signaling: An in silico and in vitro study. *BMC Syst. Biol.* **2011**, *5*, 47. [\[CrossRef\]](#)
36. Gadella, B.M.; Tsai, P.; Boerke, A.; Brewis, I.A. Sperm head membrane reorganisation during capacitation. *Int. J. Dev. Biol.* **2008**, *52*, 473–480. [\[CrossRef\]](#)
37. Hickey, K.D.; Buhr, M.M. Lipid Bilayer Composition Affects Transmembrane Protein Orientation and Function. *J. Lipids* **2011**, *2011*, 208457. [\[CrossRef\]](#)
38. Bernabò, N.; Greco, L.; Ordinelli, A.; Mattioli, M.; Barboni, B. Capacitation-Related Lipid Remodeling of Mammalian Spermatozoa Membrane Determines the Final Fate of Male Gametes: A Computational Biology Study. *OMICS* **2015**, *19*, 712–721. [\[CrossRef\]](#)
39. Bernabò, N.; Valbonetti, L.; Greco, L.; Capacchietti, G.; Ramal Sanchez, M.; Palestini, P.; Botto, L.; Mattioli, M.; Barboni, B. Aminopurvalanol A, a Potent, Selective, and Cell Permeable Inhibitor of Cyclins/Cdk Complexes, Causes the Reduction of In Vitro Fertilizing Ability of Boar Spermatozoa, by Negatively Affecting the Capacitation-Dependent Actin Polymerization. *Front. Physiol.* **2017**, *8*, 1097. [\[CrossRef\]](#)
40. Amaral, A.; Lourenço, B.; Marques, M.; Ramalho-Santos, J. Mitochondria functionality and sperm quality. *Reproduction* **2013**, *146*, R163–R174. [\[CrossRef\]](#)
41. Amaral, A.; Paiva, C.; Attardo Parrinello, C.; Estanyol, J.M.; Ballescà, J.L.; Ramalho-Santos, J.; Oliva, R. Identification of Proteins Involved in Human Sperm Motility Using High-Throughput Differential Proteomics. *J. Proteome Res.* **2014**, *13*, 5670–5684. [\[CrossRef\]](#)
42. Zapata-Carmona, H.; Barón, L.; Zuñiga, L.M.; Díaz, E.S.; Kong, M.; Drobnis, E.Z.; Sutovsky, P.; Morales, P. The activation of the chymotrypsin-like activity of the proteasome is regulated by soluble adenylyl cyclase/cAMP/protein kinase A pathway and required for human sperm capacitation. *Mol. Hum. Reprod.* **2019**, *25*, 587–600. [\[CrossRef\]](#)
43. Molina, L.C.P.; Luque, G.M.; Balestrini, P.A.; Marín-Briggiler, C.I.; Romarowski, A.; Buffone, M.G. Molecular basis of human sperm capacitation. *Front. Cell Dev. Biol.* **2018**, *6*, 72. [\[CrossRef\]](#)
44. Balbach, M.; Beckert, V.; Hansen, J.N.; Wachten, D. Shedding light on the role of cAMP in mammalian sperm physiology. *Mol. Cell. Endocrinol.* **2018**, *468*, 111–120. [\[CrossRef\]](#)
45. Signorelli, J.; Diaz, E.S.; Morales, P. Kinases, phosphatases and proteases during sperm capacitation. *Cell Tissue Res.* **2012**, *349*, 765–782. [\[CrossRef\]](#)
46. Suzuki, H.; Saito, Y.; Kagawa, N.; Yang, X. In vitro fertilization and polyspermy in the pig: Factors affecting fertilization rates and cytoskeletal reorganization of the oocyte. *Microsc. Res. Tech.* **2003**, *61*, 327–334. [\[CrossRef\]](#)
47. Abeydeera, L.R.; Day, B.N. Fertilization and subsequent development in vitro of pig oocytes inseminated in a modified Tris-buffered medium with frozen-thawed ejaculated spermatozoa. *Biol. Reprod.* **1997**, *57*, 729–734. [\[CrossRef\]](#)
48. Abeydeera, L.R.; Funahashi, H.; Kim, N.H.; Day, B.N. Chlorotetracycline fluorescence patterns and in vitro fertilisation of frozen-thawed boar spermatozoa incubated under various bicarbonate concentrations. *Zygote* **1997**, *5*, 117–125. [\[CrossRef\]](#)
49. Hunter, R.H.F.; Nichol, R. Capacitation potential of the fallopian tube: A study involving surgical insemination and the subsequent incidence of polyspermy. *Gamete Res.* **1988**, *21*, 255–266. [\[CrossRef\]](#)
50. Drevet, J.R.; Aitken, R.J. Oxidation of sperm nucleus in mammals: A physiological necessity to some extent with adverse impacts on oocyte and offspring. *Antioxidants* **2020**, *9*, 95. [\[CrossRef\]](#)
51. Agarwal, A.; Virk, G.; Ong, C.; du Plessis, S.S. Effect of Oxidative Stress on Male Reproduction. *World J. Mens. Health* **2014**, *32*, 1–17. [\[CrossRef\]](#)
52. Castellini, C.; D'andrea, S.; Cordeschi, G.; Totaro, M.; Parisi, A.; Di Emidio, G.; Tatone, C.; Francavilla, S.; Barbonetti, A. Pathophysiology of Mitochondrial Dysfunction in Human Spermatozoa: Focus on Energetic Metabolism, Oxidative Stress and Apoptosis. *Antioxidants* **2021**, *10*, 695. [\[CrossRef\]](#)
53. Sanocka, D.; Kurpisz, M. Reactive oxygen species and sperm cells. *Reprod. Biol. Endocrinol.* **2004**, *2*, 12. [\[CrossRef\]](#)
54. Kodama, H.; Kuribayashi, Y.; Gagnon, C. Effect of Sperm Lipid Peroxidation on Fertilization. *J. Androl.* **1996**, *17*, 151–157. [\[CrossRef\]](#)
55. Leahy, T.; Gadella, B.M. New insights into the regulation of cholesterol efflux from the sperm membrane. *Asian J. Androl.* **2015**, *17*, 561–567. [\[CrossRef\]](#)
56. Aitken, R.J.; Drevet, J.R. The Importance of Oxidative Stress in Determining the Functionality of Mammalian Spermatozoa: A Two-Edged Sword. *Antioxidants* **2020**, *9*, 111. [\[CrossRef\]](#)
57. Wyns, C.; De Geyter, C.; Calhaz-Jorge, C.; Kupka, M.S.; Motrenko, T.; Smeenk, J.; Bergh, C.; Tandler-Schneider, A.; Rugescu, I.A.; Vidakovic, S.; et al. ART in Europe, 2017: Results generated from European registries by ESHRE. *Hum. Reprod. Open* **2021**, *2021*, hoab026. [\[CrossRef\]](#)

58. Viana, H.J. 2020 Statistics of embryo production and transfer in domestic farm animals World embryo industry grows despite the Pandemic. *Embryo Technol. Newsl.* **2021**, *39*, 4.
59. Ludwig, M.; Katalinic, A.; Groß, S.; Sutcliffe, A.; Varon, R.; Horsthemke, B. Increased prevalence of imprinting defects in patients with Angelman syndrome born to subfertile couples. *J. Med. Genet.* **2005**, *42*, 289–291. [[CrossRef](#)]
60. Eroglu, A.; Layman, L.C. Role of ART in Imprinting Disorders. *Semin. Reprod. Med.* **2007**, *83*, 255–262. [[CrossRef](#)]
61. Li, Y.; Hagen, D.E.; Ji, T.; Bakhtiarizadeh, M.R.; Frederic, W.M.; Traxler, E.M.; Kalish, J.M.; Rivera, R.M. Altered microRNA expression profiles in large offspring syndrome and Beckwith-Wiedemann syndrome. *Epigenetics* **2019**, *14*, 850–876. [[CrossRef](#)]
62. Grace, K.S.; Sinclair, K.D. Assisted reproductive technology, epigenetics, and long-term health: A developmental time bomb still ticking. *Semin. Reprod. Med.* **2009**, *27*, 409–416. [[CrossRef](#)]
63. La Rovere, M.; Franzago, M.; Stuppia, L. Epigenetics and Neurological Disorders in ART. *Int. J. Mol. Sci.* **2019**, *20*, 4169. [[CrossRef](#)]
64. Maccarrone, M.; Barboni, B.; Paradisi, A.; Bernabò, N.N.; Gasperi, V.; Pistilli, M.G.; Fezza, F.; Lucidi, P.; Mattioli, M. Characterization of the endocannabinoid system in boar spermatozoa and implications for sperm capacitation and acrosome reaction. *J. Cell Sci.* **2005**, *118*, 4393–4404. [[CrossRef](#)]
65. Bernabò, N.; Tettamanti, E.; Russo, V.; Martelli, A.; Turriani, M.; Mattoli, M.; Barboni, B. Extremely low frequency electromagnetic field exposure affects fertilization outcome in swine animal model. *Theriogenology* **2010**, *73*, 1293–1305. [[CrossRef](#)]
66. Raspa, M.; Putti, S.; Paoletti, R.; Barboni, B.; Ramal-Sanchez, M.; Lanuti, P.; Marchisio, M.; D’Atri, M.; Ortolani, C.; Papa, S.; et al. The impact of five years storage/biobanking at -80°C on mouse spermatozoa fertility, physiology, and function. *Andrology* **2021**, *9*, 989–999. [[CrossRef](#)]
67. Romero-Calvo, I.; Ocón, B.; Martínez-Moya, P.; Suárez, M.D.; Zarzuelo, A.; Martínez-Augustin, O.; de Medina, F.S. Reversible Ponceau staining as a loading control alternative to actin in Western blots. *Anal. Biochem.* **2010**, *401*, 318–320. [[CrossRef](#)]

Disclaimer/Publisher’s Note: The statements, opinions and data contained in all publications are solely those of the individual author(s) and contributor(s) and not of MDPI and/or the editor(s). MDPI and/or the editor(s) disclaim responsibility for any injury to people or property resulting from any ideas, methods, instructions or products referred to in the content.